NASA CR-167874

NASA

National Aeronautics and
Space Administration

EQUIVALENT DAMAGE - A CRITICAL ASSESSMENT

November 1982

by

J.H. Laflen
T.S. Cook

GENERAL ELECTRIC COMPANY

Prepared for

National Aeronautics and Space Administration

LEWIS RESEARCH CENTER
Contract NAS3-22534

1. Report No.	2. Government Accession No.	3. Recipient's Catalog No.
CR167874		

4. Title and Subtitle	5. Report Date
Equivalent Damage - A Critical Assessment	November 1982
	6. Performing Organization Code
7. Author(s)	8. Performing Organization Report No.
J.R. Laflen & T.S. Cook	R82AEG533
	10. Work Unit No.
9. Performing Organization Name and Address	11. Contract or Grant No.
General Electric Company Aircraft Engine Business Group Cincinnati, Ohio 45215	NAS3-22534
	13. Type of Report and Period Covered
12. Sponsoring Agency Name and Address	Final - 8/80 thru 12/81
National Aeronautics and Space Administration Lewis Research Center Cleveland, Ohio 44135	14. Sponsoring Agency Code

15. Supplementary Notes

NASA Project Manager - Dr. G.R. Halford
Structures and Mechanical Technologies Division
NASA Lewis Research Center

16. Abstract

Concepts in equivalent damage were evaluated to determine their applicability to the life prediction of hot path components of aircraft gas turbine engines. For the purposes of this study equivalent damage was defined as being those effects which influence the crack initiation life-time beyond the damage that is measured in uniaxial, fully-reversed sinusoidal and isothermal experiments at low homologous temperatures. Three areas of equivalent damage were examined: mean stress, cumulative damage, and multiaxiality. For each area, a literature survey was conducted to aid in selecting the most appropriate theories. Where possible, data correlations were also used in the evaluation process. A set of criteria was developed for ranking the theories in each equivalent damage regime. These criteria considered aspects of engine utilization as well as the theoretical basis and correlative ability of each theory. In addition, consideration was given to the complex nature of the loading cycle at fatigue critical locations of hot path components; this loading includes non-proportional multiaxial stressing, combined temperature and strain fluctuations, and general creep-fatigue interactions. Through applications of selected equivalent damage theories to some suitable data sets it was found that there is insufficient data to allow specific recommendations of preferred theories for general applications. Nevertheless, general guidelines could be drawn which should provide assistance to those involved in life predictions of aircraft gas turbine engine components. To aid future researchers, a series of experiments and areas of further investigations were identified.

17. Key Words (Suggested by Author(s))	18. Distribution Statement
Equivalent Damage, Mean Stress, Cumulative Damage, Multiaxiality, Literature Review, Thermal Mechanical Fatigue, Creep-Fatigue Damage, Nickel-Base Alloys	Distribution Unlimited

19. Security Classif. (of this report)	20. Security Classif. (of this page)	21. No. of Pages	22. Price*
Unclassified	Unclassified	194	

* For sale by the National Technical Information Service, Springfield, Virginia 22161

N83-17542#

TABLE OF CONTENTS

TABLE OF CONTENTS (Concluded)

LIST OF ILLUSTRATIONS

LIST OF ILLUSTRATIONS (Continued)

LIST OF ILLUSTRATIONS (Continued)

LIST OF ILLUSTRATIONS (Concluded)

LIST OF TABLES

1.0 SUMMARY

This report presents the results of an 18-month study of the utility of equivalent damage concepts for application to hot section components of aircraft engines. Specifically, the topics studied were mean stress, cumulative damage, and multiaxiality. Other factors inherently linked to this study were the basic formulation of damage parameters at elevated temperatures and the fact that hot section components experience severe temperature fluctuations throughout their service lifetime. Both of these considerations placed constraints on the level of confidence with which recommendations regarding specific equivalent damage criteria could be made since most such criteria were developed for use at lower temperatures. Despite this limitation, the study yielded useful results, both from the point of view of data consolidation techniques under isothermal conditions and in producing concepts that will be useful in future studies.

Through a literature review of the three areas of interest, the most promising techniques were extracted for further study. In the case of mean stress techniques, statistical evaluations of suggested approaches were made by comparing each technique to various isothermal data sets. Similiarly, a combined literature review and isothermal data analysis technique was used to determine the most appropriate cumulative damage approach. In the case of multiaxiality, this decision process rested solely on the basis of the literature review. Following the initial screening, both the mean stress techniques and the cumulative damage concepts were tested against data sets involving either time dependent aspects of damage and/or varying temperature.

As a part of this approach, several criteria for theory selection were developed. These criteria considered both general concepts and aspects of hot section component usage. While these criteria were thought to accurately portray realistic considerations, in the final analysis they were not particularly useful since much of the data needed to evaluate specific points is lacking for many materials and conditions. More importantly, the need to clearly identify the basic damage mechanisms and damage parameters for thermal mechanical fatigue must come before these criteria can be conclusively applied. Thus they may prove useful in follow-on studies in the HOST program and other efforts.

Final conclusions were drawn with respect to each of the three damage concepts. With respect to mean stress, this study indicated a mathematical formulation which appears most useful to aircraft engine alloys. It appears that mean stress criteria should, in general, add conservatism when applied on an isothermal basis to hot path components which experience typical thermal histories. One particular cumulative damage approach was identified as being most appealing. In this case, a series of experiments is described which could produce meaningful concepts for this application. For multiaxiality, all of the foregoing concerns were magnified. However, through the literature survey, relevant concepts were identified which should be useful in practical applications. In this case, more experimental data would be very useful in scoping the applicability of the recommendations.

2.0 INTRODUCTION

The overall goal of achieving improved life cycle management of aircraft engine, gas turbine components is a major industry thrust. Low cycle fatigue (LCF) crack initiation prediction, an important element of life cycle management, as traditionally applied, may be overly conservative in estimating total cyclic life capability. Consequently, there is increasing pressure to improve predictive methods both for crack initiation and for subsequent crack propagation. This increased emphasis is the result of significantly higher component replacement costs as a consequence of more complex designs coupled with advanced materials and processing techniques. Moreover, despite added strength, the increased performance demands placed on engine components to achieve higher engine thrust-to-weight ratio have resulted in decreased cyclic lives. It is apparent, therefore, that significant cost savings can be realized through improved accuracy in high temperature, LCF crack initiation prediction.

In practical applications, engine components generally undergo very complex cycles of multiaxial strain, temperature, and dwell time, all of which magnify the complexity of life prediction. During the process of designing and analytically evaluating the lifetime of gas turbine engine components, it is necessary to simplify many of these complexities to make the problem tractable. Nevertheless, there remain several important questions which can be answered through the study of generalized theories that are less dependent on the specifics at hand. Among these are how to address the problems of multiaxial loading, cumulative damage, and mean stress effects, and how they influence fatigue crack initiation life. A significant amount of research has already been devoted to developing methods of addressing these questions. However, these models often were developed for the broad high temperature, LCF problem using materials significantly more ductile than the nickel-base superalloys commonly used in gas turbines. Consequently, the methods have not enjoyed widespread application in predicting the high temperature, low cycle fatigue crack initiation lifetimes of aircraft gas turbine engine (AGTE) components.

It was the purpose of this program to overcome this difficulty by specifically:

- Assessing the applicability of multiaxiality concepts, cumulative fatigue damage theories, and mean stress equations to the design and life evaluation of aeronautical gas turbine engine hot section components
- Determining which approaches offer the greatest potential for further development
- Suggesting research studies that would further develop and verify method usefulness for the design process.

This objective was accomplished in a paper study involving no experimental work and consisting of a four-phase effort. (The study was able to draw on experimental data generated by other research programs.) The first task selected criteria for judging the potential usefulness of the various theories. These criteria were based on the rationale used in the design and life evaluation of hot section components of AGTE. The criteria established in Task I (and approved by NASA) were used in a generic sense in three parallel studies of the effects on fatigue crack initiation behavior of metallic materials of multiaxial stress-strain (Task II), cumulative damage (Task III), and mean stress (Task IV). Each of the three latter tasks involved a comprehensive literature review and a critical engineering assessment of the respective theories.

This report is organized as follows. Section 3.0 deals with current concepts in micro and macroscopic aspects of elevated temperature damage. Section 4.0 presents criteria for selecting equivalent damage measures for AGTE hot path components. In the appendices, the literature reviews and most of the more simple data analyses are presented. These appendices are abstracted in Section 5.0 of the main text. In Section 6.0, there is an examination of the utility of equivalent damage criteria in the context of more complicated conditions; this discussion is an abstract of Appendix E. In Sections 7.0 and 8.0, the results are discussed, conclusions drawn, and recommendations are made.

3.0 ALTERNATIVE DEFINITIONS OF DAMAGE

A critical assessment of equivalent damage measures can be conveniently separated into two areas. The first of these is the character of the equivalent damage measure; the second consideration is the application of equivalent damage concepts to an engineering structure. Included in the former are the actual damage mechanisms, the macroparameters used to describe the damage, e.g. plastic strain, damage theories and models, etc. The application phase is more concerned with the level of analysis and expertise required, extent of data required, design criteria, etc. Clearly, both considerations are important, but this report is primarily concerned with the damage measures themselves. While ease of application is constantly measured, the fact that applications require individual consideration make it difficult to be as general as is possible when considering the damage measures themselves. Generic problems with gas turbine engines are the touchstones for the damage parameters throughout the report, but the emphasis is on the parameters themselves, their physical interpretation, models, etc.

In this portion of this report, a brief description is given of potential definitions of damage for hot section component materials. First, a brief review is given of some of the pertinent literature on the micromechanistic aspects of failure in nickel-base superalloys. This discussion is followed by a discussion of proposed macroscopic damage parameters and their connection with a definition of equivalent damage.

3.1 MECHANISTIC LITERATURE REVIEW

In reviewing the literature on high temperature behavior of superalloys, a confusing picture is presented. There have been studies on creep, fatigue, and crack growth under a number of different frequencies, temperatures, and environments. These studies have been done on a number of different superalloys in a number of different forms; because of this multiplicity of materials and test conditions, the experimental results are not always consistent. Moreover, the interpretation of these results has normally been done by concept rather than evidence. That is, the results are normally explained in terms of the experience set that the researcher brings to the project, rather than upon the development of the complete description of the event. For example, an author may suggest that the experimental evidence supports a model of crack advance through an oxidized zone. However, it is often the case that a number of other models could also be suggested to explain the same results. The discovery of fundamental mechanisms is an extremely difficult undertaking; and generally requires a team with broad analytical and experimental tools to perform the work. However, some workers do tend to extrapolate a model much farther than a set of data can support; these researchers need to be more aware of the limitations of their work.

As an example of the problems that arise, consider Figure 1. This figure compares fatigue crack growth rate curves at 649° C (1200° F) for Inconel 718 from four different laboratories (References 1 through 4). These materials are from different heats but all have undergone the same standard heat treatment, ASTM 637, they are all low R-ratio, and all are compact tension specimens. From this figure, it might be concluded that fatigue crack growth at this temperature is extremely sensitive to frequency. However, it is generally conceded that, at least for $0.1 < \nu < 1.0$ Hz, the superalloys are not particularly frequency sensitive. In fact, some current work at this temperature in a powder metallurgy superalloy using compact tension specimens removed from the same turbine disk shows no difference in growth rate for the three frequencies 0.33, 0.50, and 1.0 Hz (Reference 5). The point is, if a model involving frequency was developed and used all the data of Figure 1, the conclusions reached might be different than those reached using a subset of the data.

As would be expected upon examination of the literature to discern trends of mechanisms, the situation is clouded. For example, Runkle and Pelloux (Reference 6) state, "Regardless of the mode of cracking, the air environment accelerates the crack initiation and propagation rates." There seems to be universal agreement that oxidation is a major factor in decreasing the life of a superalloy component, primarily through grain boundary attack. However, Scarlin (Reference 7) found that for the coarse grained cast alloy, Inconel 738LC, crack growth in vacuum was faster than in air. While this is a single result, it indicates that broad generalizations may be difficult to obtain.

The literature does seem to be consistent in the result that, for wrought alloys, air, and particularly oxygen, is an aggressive medium but there are a number of possible modes of damage. Intergranular crack initiation can be by selective oxidation of the chemically segregated species at the grain boundaries. In the case of Stage I initiation, oxidation can play the role of preventing slip reversal and allowing cracks to form at the bottom of the ledges. Both intergranular and transgranular processes are affected by temperature and test frequency (Reference 8). If oxidation "seals" the grain boundary crack or is sufficient to prevent slip from continuing on planes intersecting the surface, than crack initiation will be moved beneath the surface. This results in air and vacuum lives being the same.

One area of oxidation effects that continues to puzzle researchers is the mechanism by which oxygen produces the observed changes. If it is accepted that oxygen accelerates the cracking process, then the question must be, "How are the effects produced?" Is oxidation attack the result of bulk diffusion, of selective diffusion along grain boundaries or slip planes, migration to cavities and grain boundaries or does it merely affect the reversibility of the surface slip? Swanson and Marcus (Reference 9) observed crack growth rates in Monel 404 that were 5.5 times higher in air than vacuum. They suggested that oxygen is swept in ahead of the crack by mobile dislocations. This required that they assume a much higher diffusivity than the bulk parameter.

Duquette and Gell (Reference 10) argued that, in their single crystal Mar-M-200, oxygen absorbed on the crack surface limited the slip reversibility to produce a higher growth rate. In air, the absorbed oxygen lowers the surface energy and produces the cleavage observed on the fracture surface.

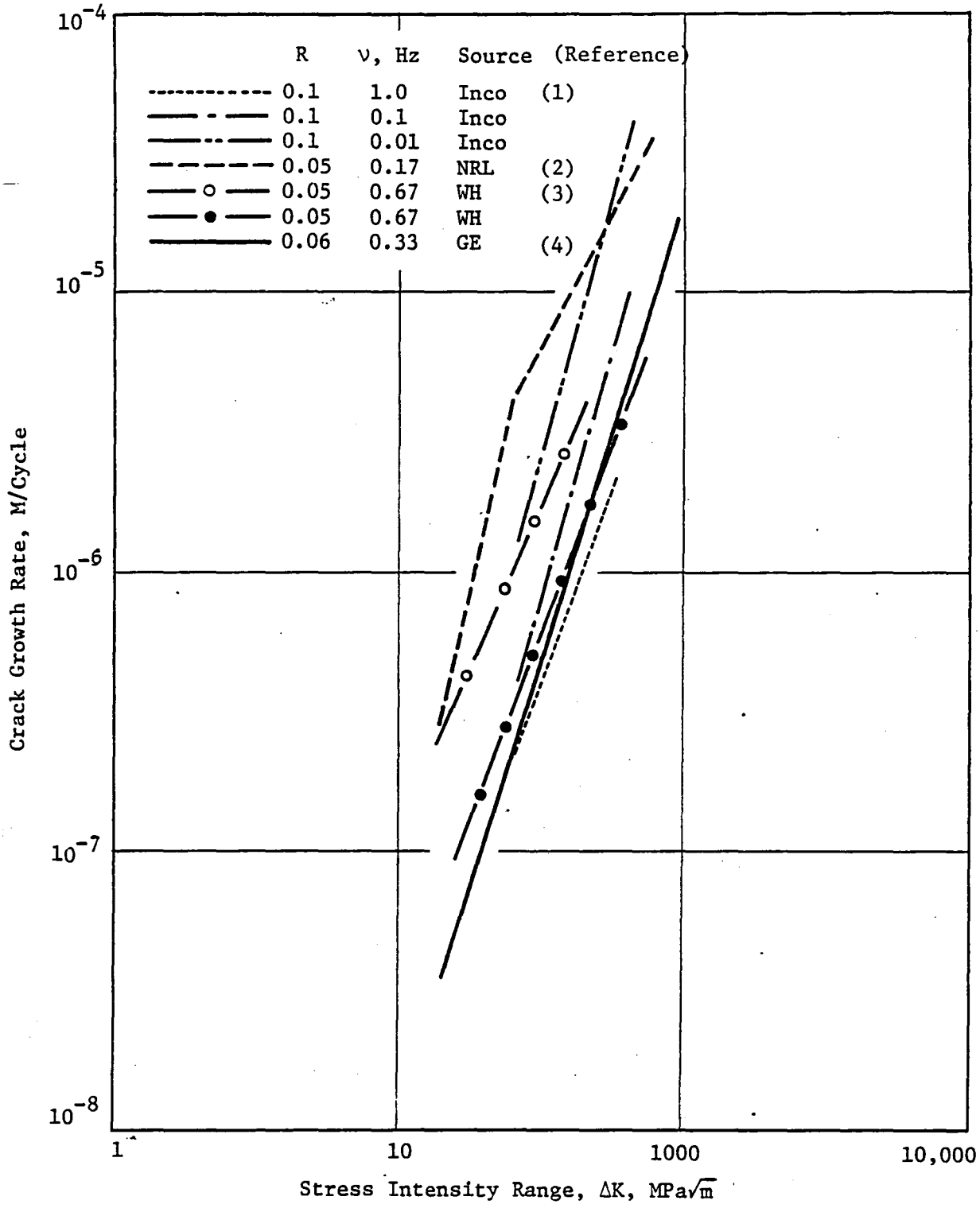

Figure 1. Comparison of Crack Growth Rate Data for Inconel 718 at 649° C from Various Sources.

At temperatures above 0.5 T_m, the usual mode of cracking is intergranular. Runkle and Pelloux (Reference 6) hold that at low crack growth rates, the mechanism is primarily oxidation since the time exists for oxidation damage. At higher growth rates, the mechanism is one of cavitation along the grain boundary. While this provides a simple, conceptual framework, the details are less than clear. Reference 7 suggests that oxygen penetrates along grain boundaries and persistent-slip bands and at the crack tip to enhance Stage II intergranular growth. Sidey and Coffin (Reference 11) suggest that this oxygen penetration can also affect cavitation. Woodford (Reference 12) has found voids beneath the oxide scale in Inconel 738 but did not find the voids extending nearly as deep as the known depth of damage. He attributes the primary effect of oxygen to suppression of grain growth. In fact, Woodford interprets his results principally in terms of metallurgical changes at the grain boundaries.

In terms of crack initiation and propagation, the complicated nature of the nickel-base superalloys presents some real challenges. The metallurgical structure of this alloy system is very complex, and it appears that the microstructure can play a significant role in the cracking process. As noted above, Woodford (Reference 12) interprets much of his data in terms of metallurgical variables. Another pair of examples is cited by Scarlin (Reference 13). In cast Inconel 738, he observed large, coarse γ' along the grain boundaries; this led to intergranular fracture and low threshold stress intensity level, ΔK_{TH}. The large γ' was not found in Nimonic 105, but the growth of the oxide layer on the Nimonic led to dissolution of the γ' in the surrounding matrix. Scarlin interpreted this as yielding a lower yield stress near the crack tip, a blunter crack, and a higher threshold stress intensity factor.

Other observations on the interplay of microstructure and crack growth have appeared in the past few years. Lawless, et al. (Reference 14) studied the microstructural features that promoted planar slip and produced lower crack growth rates. Mills and James (Reference 15) related various fatigue crack growth rates to crack growth mechanisms through detailed observations of the fracture surface. In addition to the many investigations of fatigue behavior, the elevated temperature use of these alloys has led to examinations of the creep crack growth behavior. Crack growth under creep and fatigue has been studied by Sadananda and Shahinian (Reference 16), Floreen (Reference 17), and Cowles, et al. (Reference 18). While the latter paper primarily presents crack growth data for five alloys, the former papers are more concerned with interplay of microstructure and cracking. Reference 16 suggests creep cracking results from a balance of two competing processes, diffusion of point defects, and creep deformation. These efforts are being aided by new models of high temperature superalloy behavior, particularly void growth (Reference 19).

The object of these few citations was to give some indication of the complexity of material behavior during high temperature, low cycle fatigue, and crack growth. The multiplicity of microstructures and product forms means that what is true for a large grain cast material may not be true for a fine-grained wrought material. This situation indicates the difficulty of developing one single parameter or technique describing all elevated temperature damage.

This point should be remembered since many of the comparisons described in this report have used one alloy, Inconel 718, under relatively simple load conditions. This should reduce some of the above-noted complexities in sorting out the important factors affecting life; but conversely, by restricting detailed analyses to one alloy, a limitation of the generality of the conclusions results.

3.2 MACROSCOPIC DAMAGE MEASURES

Perhaps the two most competitive and currently advocated phenomenological crack initiation life prediction methods for elevated temperature applications are strain-range partitioning (References 20 to 23) and frequency modified fatigue life (References 23 to 27). These methods differ radically in terms of their mechanistic interpretations and mathematical formulations (Reference 23). Frequency modified fatigue life is presented as being based on environmental factors, such as oxidation, while strain-range partitioning is founded on the premise that damage is controlled by the amount and sequence of creep and plastic strains. Actually, the mathematical formulation of the frequency modified fatigue life approach is based on early empirical expressions for time-dependent fatigue (Reference 28) where little, if any, consideration of the mechanism was involved in the mathematical formulation. Since the mathematical relationships are expressed in terms of frequency (or the inverse of time) and oxidation has been shown to be a primary mechanism of fatigue failure in certain materials (References 23, 24, and 25), the phenomenological equations have been explained in environmental terms. The strain-range partitioning method has a more direct mechanistic interpretation, although the plastic and the creep strains are not related to the specific micromechanisms such as those portrayed by Ashby's deformation maps (Reference 29). However, both wave shape (as measured by creep and plastic strains) and oxidation are important as can be demonstrated by comparing experimental results obtained in an air and a vacuum environment (Reference 30).

When interpreted in this manner, these two models emphasize the mode of deformation and role of oxidation in their formulation; and, as stated above, both concepts have their regions of applicability. There are also several other models (e.g. References 31 to 36) available which emphasize crack growth either explicitly or implicitly in their formulation. Undoubtedly, all three ideas are important for various materials tested at different homologous temperatures or in various environments.

Regardless of the physical mechanisms involved in the macroscopic damage process, it must be remembered that many gas turbine components operate with a coating to prevent environmental attack. The behavior of the coatings is heavily dependent on the particular coating/substrate combination; the material combination also dominates crack initiation in the substrate. However, it appears that the initiation event usually occurs in the coating. This suggests that for coated components the emphasis in fatigue life prediction should be placed on models of coating crack initiation and propagation. Interestingly, there has been relatively little work performed on coating crack models. The

coating models described in References 37 to 45 all have limitations, but they do incorporate some of the key ideas, namely, coating thickness and properties, substrate properties, and the calculation of a crack driving force. The efficacy of such an approach will have to await key experiments; it may well be that certain temperatures, strain ranges, and materials will require coating models while other situations will not, just as certain initiation models will do better in certain regimes. This is a situation where the mechanical approach will be dictated by the experimental evidence.

Throughout these discussions, it must be borne in mind that the present state of development of equivalent damage theories results from a lack of understanding of microcrack formation and propagation. The inability to predict the occurrence of such defects means that damage models are empirical in nature and are not yet mechanism based. Futhermore, the models are based on some mechanical measure of damage, e.g., inelastic strain range, for convenience in applying the model to an engineering structure. This emphasis on mechanical measures of damage will continue for the foreseeable future, although advances in crack initiation technology are being made. In the meantime, the use of mechanical damage models must be done with the application in mind. For example, the original work on strain-range partitioning employed a fairly ductile steel (e.g. Reference 23). The materials used in gas turbine engines are much higher in strength and lower in ductility, making the partitioning of the strain range a much more difficult task. In the case of the superalloy René 95, it was pointed out (Reference 46) that the use of plastic strain range is questionable as a measure of damage because the inelastic strain ranges are so small that accurate measurement of them is difficult.

What must be emphasized in model selection for a particular application is the use of the "proper" combination of these mechanical measures of damage. This proper set of mechanical measures should reflect the influence of the active mechanisms that cause damage. The above discussion of the myriad of models and the variety of proposed mechanisms strongly suggests that such a selection is not straightforward.

3.3 EQUIVALENT DAMAGE

Modern, low cycle fatigue design philosophy is based on the assumption of similitude between a smooth LCF specimen and the material in a critical location of a component. This so called local stress-strain approach requires detailed aerodynamic, heat transfer, and stress analysis of critical parts. These analyses result in the definition of the stress/strain/time/temperature histories for the material in critical engine locations. These complex response histories are then combined with equivalent damage criteria to predict the component fatigue lives from constant amplitude, isothermal, fully reversed, smooth bar LCF tests.

For time-independent low cycle fatigue, the time and temperature response histories do not affect the development of fatigue damage. For these conditions, the cyclic inelastic strain range is commonly viewed as the primary

factor governing low cycle fatigue. Basic, smooth bar LCF data are, therefore, generated under strain-controlled, fully reversed conditions to define the basic relationship between plastic strain range and fatigue life. Life predictions for components which undergo complex multiaxial stress histories are performed using equivalent damage models to relate these complex histories to the uniaxial, fully reversed LCF data. These equivalent damage models include techniques to account for mean stress and multiaxial stress cycles, and damage accumulation models which prescribe the way spectrum loading accumulates LCF damage.

When the situation involves elevated temperatures, the application of such a simple, conceptual model of equivalent damage is less justified. In this program, three types of equivalent damage measures were evaluated: mean stress, cumulative damage, and multiaxiality, all of which fit neatly into the classical view of equivalent damage. The ambiguities that arise in the elevated temperature case are easily illustrated in the concept of cumulative damage. For example, if creep and fatigue are viewed as separate, independent mechanisms producing damage in hot section components, then a linear summation of time and cycle fractions becomes a cumulative damage model. On the other hand, when a sophisticated model like strain-range partitioning is used to describe the interaction of creep and fatigue, the cumulative damage model would be used to describe the accumulation of the effects of different duty cycles. In considering mean stress, it should be noted that mean stress criteria are often included in the basic damage parameter, e.g. in the Ostergren model (Reference 31). In addition, mean stress plays an integral part in thermal-mechanical fatigue; and it must be consistently factored into the multiaxial criterion. Quite clearly, given all of these theoretical uncertainties, it is impossible in one 18-month period to answer all of these questions for even one alloy or component.

In most of this work, the classical view of these three equivalent damage concepts has been preserved, partially for reasons of convenience. This perception of the classical views suggests that mean stress refers to the influence on the fatigue life of the average (or often maximum) stress in a low cycle (as opposed to high cycle) fatigue environment; cumulative damage refers to the effect of stress- (or strain-) range magnitude and the sequence of application (e.g., high/low or low/high stress cycles); multiaxiality refers simply to approaches of mapping biaxial or triaxial states of cyclic stresses into a fatigue law which is based on uniaxial fatigue experiments. The basic approach was to review the literature and apply some of these theories to an internally available set of isothermal mean stress and two-step data. The more successful approaches were then applied to other data sets which involved various combinations of temperature changes and time-dependent effects. A set of criteria was developed for selecting the most viable approaches, and conclusions and recommendation were made.

4.0 THEORY SELECTION CRITERIA

In this section, a set of criteria is established for selecting the best equivalent damage theories for aircraft gas turbine engine application. First, several aspects of the problem are discussed, followed by the criteria in which a numerical scoring system is mentioned. This scoring system was not used in the final summary, but it is thought to be indicative of the weighting that should be considered in the theory selection process.

The design of hot section components requires consideration of the flight profile, local temperatures, and the selection of the appropriate damage theories, each of which involves uncertainties. Obviously, knowledge of the first two (the flight profile and local temperatures) is required in order to apply a deterministic damage theory. Throughout the design phase, it is not known how a specific engine will be used by a specific user, and so a design profile is selected to represent a spectrum of conditions (contractually, a military profile is much more specific than a commercial one). In addition, detailed determination of the local temperature of certain hot path components (e.g., blades) is very difficult due to the need of establishing the appropriate heat transfer coefficients. Given these uncertainties, it is worthwhile to consider how precise an equivalent damage theory must be in order to be operational in the design and life management process. To aid in this consideration, the scope of this investigation has been reduced to two generic components: (1) blades, vanes and combustor liners, and (2) disks. These two components represent diverse considerations which should include virtually all combinations of damaging events which should be included in a viable equivalent damage theory.

To aid in addressing the engine-related requirements for equivalent change theories, several key design engineers were contacted and interviewed. In almost every case, these engineers agreed that the goals of the current program were needed to improve the life methodology, particularly in the life management process where more advanced design analysis methods, such as inelastic stress analysis, were more likely to be utilized. The reasons for this attitude varied depending upon the component. In the case of blades where the predominate design analysis tool was a one-dimensional inelastic computer program based on beam theory, an improved damage theory was viewed as eliminating one of several important unknown factors which would increase the viability of the overall life analysis methodology. In this case, due in part to the high temperatures and large creep stress, the life analysis process was more of a correlation than a prediction, and was strongly based on experience. Better definition of what constitutes equivalent damage was viewed as a strong plus in improving this correlation. Similiar comments apply to vanes and combustor liners where three-dimensional stress analysis methods are required, and the dominant stresses are thermally induced.

With respect to disks, life management programs are actively pursuing more detailed information with respect to temperatures and actual mission profiles.

The current research is viewed as being required to improve the reliability of life predictions for actual field conditions. One important application of cumulative damage is in the life management process where field-returned disks are cut up into simple specimen configurations and tested to determine the life used during field exposure. This aspect of the problem is detailed later in this report.

With respect to the required precision, a factor of 2 (viewed as an acceptable scatter in low cycle fatigue) was generally perceived as adequate. However, the method should also be capable of predicting the central tendency with high accuracy (within 5% to 25%) with a minimum of layering. Obviously, these are strong requirements that are probably unrealistic in hot section components.

At the same time, an attempt was made to determine if the stress or strain histories of these components yield peculiar states of stress, levels of mean strain, or particular cycle combinations which could be used to eliminate broad requirements on equivalent damage theories. In detail, this goal could not be achieved; generality is required when considering all potentially critical locations of these components. However, broad statements can be made:

1. Disks will generally have:
    - Positive mean stresses
    - Two equivalent cycles (commercial applications only)
    - Elastic strain ranges
    - Smaller effect of variable temperature
    - Less creep considerations (except at the rim).
2. Blades will generally exhibit:
    - Compressive creep at critical (hot) locations
    - Predominately uniaxial behavior.

A view of the general complexity encountered is shown in Figure 2. In this figure, each circle represents a distinct point in an assumed (realistic) mission profile. Obviously, such a history involves highly difficult aspects for all equivalent damage theories. While Figure 2 is specifically for a disk, it is hard to imagine that vanes or combustor liners would involve less complicated design points. A review of one vane analysis showed that the state of multiaxial stresses is not constant over a cross section. Most frequently, the state of stress was best chartacterized as equal-biaxial compression. Since the principal loading in vanes is thermally induced stresses, the equal biaxial state of stress is analogous to a hot spot in a large body.

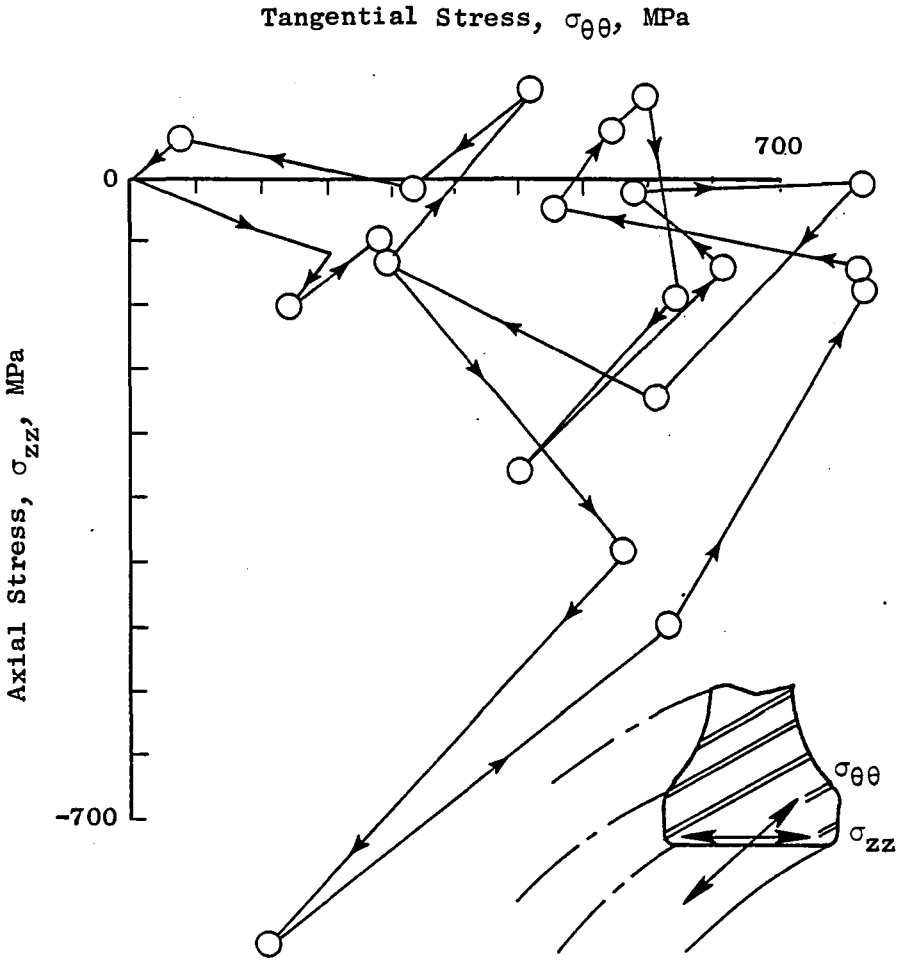

Figure 2. Example of the Complex States of Stress That Can Evolve During a Simulated Mission in a Disk Bore.

One final aspect needs to be mentioned before discussing the developed criteria. In the current approach, there is no presupposition of a damage mechanism as being correct. There are two main reasons for this (both of which were discussed in the previous section):

1. There is a general lack of agreement of what constitutes a good mechanical measure of damage at high homologous temperatures.

2. Aircraft engine nickel-base alloys are inherently stronger and less ductile than the material generally used to develop the above-mentioned theories. In fact, it is sometimes found that lower homologous temperature damage mesures (e.g., mean stress as in Reference 31) can be used in specific instances to explain effects such as hold time in these alloys.

Consequently, it was the intent to include an examination of proposed micromechanisms in AGTE alloys to aid in criteria selection. However, as discussed in Section 3.1, no consensus could be found.

With these ideas in mind, selected criteria, to which all theories could be subjected, will be presented. These criteria, more or less, are identical in intent to the criteria shown in Figure 3. The individual items have been expanded and/or coalesced into a set of 10 criteria, and assigned a numerical score to aid in quantifying the selection process. Since assigning such a score is fraught with difficulty, theories with "close" numerical ratings would be viewed as equivalent in overall effectiveness. The 10 selected criteria are listed in Table I and discussed individually below.

1. Evaluation of the theoretical basis of a method is very important for establishing limitations and extrapolation ability. However, given the lack of consensus on damage mechanisms, this criterion cannot be weighted too heavily. It was decided to score zero for a purely empirical approach, and 10 for a theoretical basis. However, to aid in the evaluation of the applicability of such a theoretical basis, it was decided to include a brief review of proposed micromechanisms as criterion Item 10, below.

2. Each theory should be evaluated on its correlative ability on a scale from zero to 20. Evaluation considered both published data and the results from Item 9. Layering tendencies were considered to be important.

3. Ten points should be given to an approach if it is not unduly sensitive to loading parameters and if the coefficients required to implement the theory are readily determined and not too sensitive to the data set upon which it is based (are they unique?). The comment "unduly sensitive to loading parameters" is admittedly subjective and would be used only if the method is obviously sensitive.

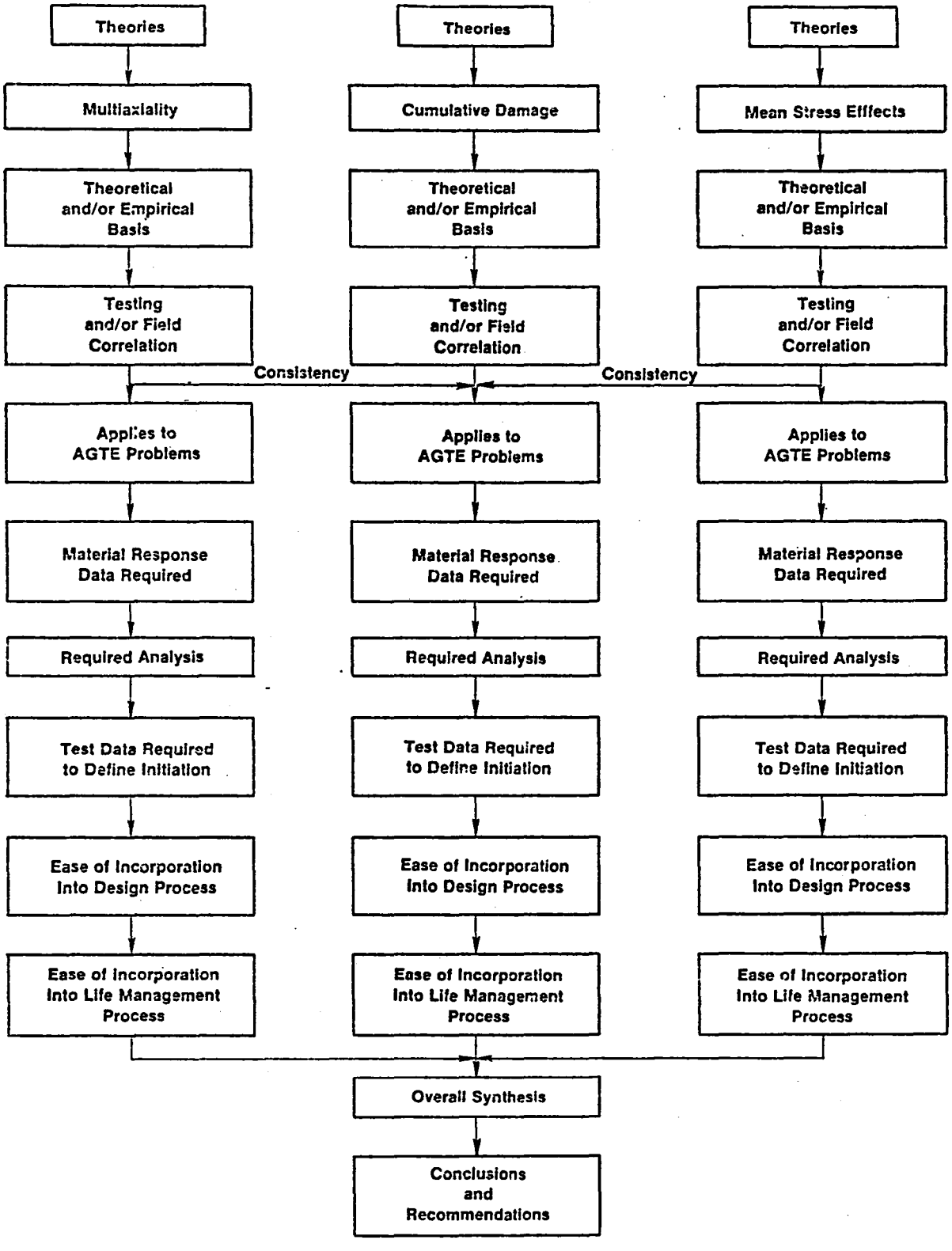

Figure 3. Criteria Diagram.

Table I. Criteria.

Criterion (Weight)	Comments/Considerations
1. Empirical/Theoretical Basis (10)	Zero if empirical, 10 if a theoretical basis
2. Correlative Ability (20)	• Within material scatter • No layering
3. Sensitivity (10)	Judge sensitivity of coefficients to data base or to loading parameter
4. Consistency Check (10)	Is a particular theory of one effect consistent with those for the other effects?
5. Applicability of Engine Problems (25)	σ_2/σ_1 = Principal stress ratio M = Multiaxial, MS = Mean stress, CD = Cumulative damage
a. Blades, Vanes, and Combustor Liners 1. Mean stress ratchett (MS) 2. Superimposed LCF and HCF (MS, CD) 3. All A-ratios are possible (MS, CD) 4. Various sequence effects (CD) (Thermal stress problem) 5. Variable temperature (MS, CD) 6. Various σ_2/σ_1 ratios (M) 7. Anisotropic materials (e.g., Mono, DS) (All)	b. Disks 1. Fully nonproportional multiaxial (all) 2. Potential mean stress decay (MS) 3. Mainly positive A-ratios (MS) 4. Basically two-step process (commercial only) (CD) 5. Variable temperature (CD) -Not as important as in blades and vanes 6. Predominately elastic strain range (All)

Table I. Criteria. (Concluded)

Criterion (Weight)	Comments/Considerations
6. Data Requirements (10)	• Response data (1) • Baseline testing (8) • Presentation format (Design Handbook) (1)
7. Incorporation Into Design (5)	• Elastic analyses
8. Incorporation Into Life Management Process (10)	• Nonlinear analyses
9. Data Evaluation (0)	• Impact on criteria 2 • Mean stress data (Inconel 718) • Hold time, strain rate, and TMF data (René 80, Inconel 718) • Variable temperature/sequence (Inconel 718)
10. Comparison of Expected and Theoretical Micromechanisms (0)	• Impact on criteria 1 • Final evaluation • Recommended research
Total Possible Score = 100 points.	

4. Any theory of mean stress (for example) must be consistent with potentially viable theories of multiaxiality and cumulative damage. If a given theory is mutually consistent with other theories of other effects, it should get 10 points.

5. In this criterion, we assess the applicability of the theory to aircraft gas turbine engine problems. This criterion is further subdivided depending upon the component and type of theory as shown in Table I, 5a and 5b. Twenty-five points were assigned since this criterion represents a major aspect of this research. Each item in the list for each theory type will be weighted equally for a combined possible score of 25. Several items listed in 5a and b may need some explanation. Items 5a(1) and 5b(2) refer to creep-related changes in mean stress that can continuously change as a function of cycles. Because of such potentially continuous changes, it may not be possible to establish a representative cycle, (e.g., at half life as is standard in test data reduction) to use in the damage analysis. Thus an acceptable mean stress theory would have to model this type of behavior. Item 5b(5) suggests that the variation in temperature in a disk may not be as critical as it is in blades and vanes. This is because the range in homologous temperatures may be small enough such that the mechanism of inelastic flow may not change. If the mechanisms change, then interactive effects could occur which would not, in general, be modeled by using isothermal data.

6. The practical significance of the amount and type of data required to implement a theory is an obvious criterion in terms of implied type of analysis and associated testing costs. We have considered three ramifications of data requirements: response data, amount of baseline testing, and handbook data representation. Of these, amount of baseline testing represents the prime emphasis since it is the most costly item. Also, from some perspectives, the more the test requirements, the more likely the theory is empirically based (obviously, this is not always the case). The other two items (each of which are assigned 1 point) actually refer to requirements with respect to the state of the art. Since how requirements on response data and handbook formats are perceived is the result of tradition and engineering practice, it is felt that theories with unusual requirements in these respects should not be penalized too harshly. If excessive data requirements are needed in this regard, then it will impact the amount of baseline testing.

7. If the method is easy to incorporate into the design process, it should receive 5 points. We have not given this criterion a high weighting because the design process is still based predominately on elastic analyses which may restrict the potential utility of some advanced damage theories. Such theories are thought to depend upon relatively accurate assessment of mean and multiaxial stresses (for example) which are best depicted through inelastic analysis methods. Thus we consider the logical introduction of such theories should be in the life management process (LMP) which is more likely to pursue advanced analysis concepts.

8. As discussed in 7 above, if the method can be easily accommodated in LMP, it gets 10 points.

9. As a concurrent activity, proposed theories were evaluated against baseline data sets. Mean stress data on Inconel 718 were available within the General Electric Company for a variety of A-ratios. In addition, the viability of analyzing strain rate René 80 fatigue data on the basis of mean stress criteria was assessed. Such approaches have been used successfully in the past, but are dependent upon the interpretation of damage. Available hold time Inconel 718 data were analyzed to assess trends of short time data in the long time (design) life range. Also, cumulative damage experimental studies have been performed on Inconel 718 incorporating both isothermal and variable temperatures (using one change in temperature after a block of cycles at another temperature) tests. No multiaxial data were analyzed during this investigation.

10. As mentioned above, proposed mechanisms were evaluated and shown to be inconclusive. In other cases, such an evaluation might be more fruitful.

With respect to recommended further research, Item 5a(7), anisotropic materials, and Items 5a(5) and 5b(5), variable temperature, are areas of required further research. Although approaches are available for analyzing thermal-mechanical fatigue, it is felt that much more work is needed in this area of research. In addition, failure criteria for monocrystal and directional solidified materials should be an active area of research for many years.

5.0 THEORY EVALUATION SUMMARY - SIMPLE CYCLES

This section is intended to present a brief synopsis of the work presented in Appendices B, C, and D on cumulative damage, mean stress, and multiaxiality, respectively. Each appendix presents the results of the literature review on each equivalent damage topic. In Appendix B, some cumulative damage theories are compared with a set of isothermal, strain-controlled, Inconel 718 two-step test data where two levels of strain range were applied in either a high/low or low/high sequence. In Appendix C, four different low cycle fatigue, mean stress theories are compared to an extensive set of isothermal, strain-controlled, Inconel 718 data which was tested under several different R-ratios where $\varepsilon_{min.}$ and $\varepsilon_{max.}$ are the minimum and maximum strain levels in a strain-controlled fatigue test, respectively. Thus this section should be viewed as a summary of the preferred techniques discussed in the appendices and as revealed through comparisons with data collected under isothermal conditions; the data comparisons are also presented in the appendices. Note that, ideally, any all-inclusive theory should simplify to the isothermal, simple case. Thus such simple comparisons could be viewed as yielding the proper formulation that should be found on simplification. In Section 6.0, these simple theories are compared to more complicated situations involving hold times, strain rates, and varying temperature.

5.1 CUMULATIVE DAMAGE

As discussed in Appendix B, there are four generic cumulative damage theories:

- Those based on crack growth concepts
- Those which combine the crack initiation and propagation phases of life
- The methods which consider damage accumulation to be nonlinear and stress level dependent (i.e. damage curve approaches)
- Endurance limit reduction models.

The results of two review papers were used to discuss several proposed methods up to about 1970. These theories generally were heavily empirical and appeared to offer little to the goals of the current study. Similiarly, a detailed review of more recent theories suggested that no theory enjoys a clear advantage over any other in terms of its theoretical background or in terms of its general acceptance in the technical community.

However, it was shown in Appendix B that the current double linear damage rule (DLDR) due to Manson and Halford best described the sequence effect of a series of simple thermal Inconel 718 two-step tests. This theory was based on

a damage curve approach and for two-step loading was analogous to the combined initiation-propagation theories. In this form, it was easy to apply and hence would be useful in design studies. The theory of cumulative damage which separated initiation and propagation phases as the explanation of loading sequence effects was generally appealing, and the acceptance of the DLDR would, hopefully, allow for further development. It appears that such initiation/propagation models need to consider the effects of small flaws. This is currently an active area of research.

The DLDR technique is fully specified by calculating the cycles to failure of various portions of a loading spectrum and, as such, is compatible with any general creep-fatigue damage parameter or other equivalent damage criteria. Nevertheless, it must be realized that three different versions of the DLDR have been suggested, and at least one study (Reference 47) has proposed an experimental technique for improving the assumed universal constants to account for material dependent variations. Thus it appears that in accepting one DLDR method it must be recognized as an empirical technique which could be improved by additional experimental evaluation. Finally, it is shown in Appendix E and discussed in Section 6.0 that temperature variations in two-step tests seem to confound such techniques. Further work will be required before general acceptance is gained for AGTE application.

5.2 MEAN STRESS THEORIES

Four low cycle fatigue, mean stress theories were reviewed extensively in Appendix C, and compared, in Appendices C and E, to data sets of Inconel 718 including various combinations of alternating and mean strain. The theories were:

- Equivalent strain approach (ε_{eq})
- Leis parameter (P_L)
- Manson-Halford modification of Morrow's method (MMHM)
- Theory of Cruse and Meyer (CM).

These theories were selected over theories based on mean plastic strain or purely high cycle fatigue criteria (e.g., nonlinear Goodman diagrams). The mean stress theories involve combined measures of strain range and either mean or maximum stress and are best suited for representing low cycle fatigue, mean stress effects. These effects can occur in strain-controlled fatigue critical regions of components where the strain range is predominately elastic. Due to the high relative strength and low ductility of typical AGTE alloys, such theories would be most appropriate for the design life of hot path components. The mean plastic strain theories are viewed as best representing inelastic-strain ratchetting problems. Furthermore, except for the Manson-Halford theory, these theories do not model pure mean stress (ultimate tensile or creep-rupture) failures as $R \to 1$. Hence, for vibration problems (a major consideration in blade design), the HCF approaches or data are still required when these LCF theories are implemented.

As shown in Appendix C, of these four theories, the equivalent strain and the Leis parameter methods were the best in data consolidation. The equivalent strain involves the determination of one fitting parameter, m, and appeared to be the best overall approach if the appropriate mean stress data were available to determine the constant m. Using the data available for Inconel 718, m was found to follow an Arrhenius plot over a temperature range of 21° to 566° C; there was very limited data at the lowest temperature, however. This plot considered all the Inconel 718 data from Appendices C and E. Conversely, the Leis method involved no such fitting parameter and appeared to be the best predictive technique of the approaches considered.

In Section 6.0 and Appendix E, these approaches are considered again in the light of various strain rate René 80 fatigue data at 980° C. The problems of hold times and thermal-mechanical cycling are introduced and discussed in the context of mean stress parameters. In that section, we also consider the problem of heat-to-heat variability in the mean stress response and the subsequent effect on the predictability of various R-ratio data.

5.3 MULTIAXIALITY

Two types of generic theories are found in the multiaxial literature: those involving scalar equivalence quantities (e.g., effective stress or strain or octahedral plane quantities) and those involving maximum shear stress (or strain) and the associated stress (or strain) normal to the plane of maximum shear. Of the two general groups, the shear strain theories appear to be of a more fundamental character since they include a definition of the expected plane of failure. In response to this criticism, recent theories utilizing equivalence quantities have been developed to incorporate a concept of direction on a octahedral shear plane; these theories are largely untested and do not necessarily incorporate the physical plane of cracking. Conversely, the fundamental creep and creep-rupture work of Leckie, Hayhurst, et al. (References 48, 49, and 50) has demonstrated the utility of generalized equivalence quantities in that research area. In any case, sufficient work has been done to provide several practical approaches for implementation of the equivalence quantity theories. The utility of the triaxiality factor (which incorporates a measure of hydrostatic stresses) as demonstrated by Mowbray (Reference 51) and Manson and Halford (References 52 and 53) appears to be a concept of practical significance in modifying uniaxial, plastic strain-life relationships. Similiarly, the Sines relationship (References 54 and 55) may be another practical approach of incorporating multiaxial mean stress effects into the elastic strain-life line. As shown in Appendix D, this method is compatible with the MMHM. Perhaps the generalization of the uniaxial mean stress equivalent strain approach discussed in Section 5.2 and Appendix B to a multiaxial form as presented by Walker (Reference 56) may offer another viable multiaxial mean stress approach.

The acceptance of any material-independent method (e.g., effective stress) overlooks the fact that no single parameter enjoys universal acceptance; rather, the most appropriate approach is probably material dependent. This was shown

in Appendix D through a discussion of the lack of acceptance of the triaxiality factor. In the older literature, this neglect was often supported by the fact that the ratio of endurance limits in bending and torsion was material dependent. Nevertheless, all predictive, multiaxial criteria predict that this ratio is constant (the constant value depends upon the theory) and is not material dependent. Noting that there is a true lack of multiaxial data for AGTE alloys, it would appear that experimental verification of any proposed criterion is in order for these alloys. Furthermore, the stress state in hot path components is usually characterized as equal biaxial; it would appear that positive stress ratios should be used in such an experimental investigation. This is particularly true since at least one current theory (that of Brown and Miller, Reference 57) specifically predicts different criterion for positive and negative principal stress ratios.

It is noted that this section has not mentioned the problems associated with nonproportional cycling discussed in Appendix D. Such problems are not considered to be of current practical interest in typical AGTE since, generally, insufficient information is available to quantify the extent of nonproportional loading (Figure 2 being a notable exception). It is anticipated that nonproportional loadings will occur in AGTE due to the combined mechanical and thermal loadings; individually, these loads would not normally produce the same principal stress ratios. In purely thermally loaded structures (which almost is the case for vanes and combustor linears), the extent of nonproportional loading is less clear.

6.0 THEORY EVALUATION SUMMARY - COMPLEX CONDITIONS

Section 5.0 briefly reviewed the results of the comparisons of the three equivalent damage concepts for relatively simple conditions which were detailed in Appendices B, C, and D. For application to hot path components of AGTE, these equivalent damage concepts must be shown to have utility under rather severe conditions of time-dependent inelastic flow and variable temperatures. This section is an attempt to examine some of the preferred approaches to combinations of these more complicated conditions and summarizes the discussion in Appendices A and E. Section 6.1 examines the ability of two of the more promising mean stress theories to correlate isothermal LCF data. This section also summarizes the results of a sensitivity study on the impact of mean stress variations on calculated lives. Section 6.2 presents the results of some two-step tests in which both temperature and load are changed; two mean stress parameters are used in this study. Since the two temperatures employed in these tests were modest, 343° and 566° C, the amount of time-dependent behavior is limited. Time dependence was not explicitly considered in the two-step tests, but subsequent work involving higher temperatures does attempt to include this dependence. Following this discussion, the section concludes with a brief discussion of the truly critical problem, the thermal mechanical fatigue problem.

6.1 MEAN STRESS THEORIES

It has long been appreciated that the mean stress plays a role in the determination of low cycle fatigue life. The reason for this can be seen in an examination of the cyclic constitutive behavior (Appendix A). The results of the cyclic property portion of the program conclusively demonstrated how the increasing value of R_ϵ increased the mean stress at low strains. For the same strain range, this increased the maximum stress in the cycle and generally produced shorter lives. It should also be remembered that from a mechanistic viewpoint different materials will react differently to the presence of high maximum stress. In this case, the Inconel 718 material used to generate these data was not particularly defect sensitive. It would be expected that defect sensitive materials would be much more adversely affected by the high maximum stress in the cycle as it would promote early crack initiation. Despite being defect insensitive, the current results demonstrate that pure range quantities are unable to adequately correlate fatigue data under a range of R_ϵ conditions.

In Appendix C, several mean stress theories were reviewed and two were selected for the subsequent data analyses. These two parameters were:

1. Equivalent Strain
2. Leis Parameter

These two parameters were about equal in their ability to correlate the LCF data. The Leis parameter is somewhat easier to use since equivalent strain contains a numerical constant that must be determined by a best fit to the test data.

Constant amplitude LCF data were generated at two temperatures and four values of R_ε. Both parameters gave equivalent fits to the data at both temperatures. The results gave no preference to either method except for the necessity to determine the numerical constant in the equivalent strain approach. In addition to the elevated temperature tests, some very limited data for a single R_ε were generated at room temperature. The three values of the constant fit a straight line on an Arrenhius or reciprocal temperature plot; it will be interesting to see if further data supports this preliminary finding.

One of the problems discerned in Appendix A was the amount of scatter in the mean stress data. This arises from two sources. One of these is the normal material property variation. The second is related to this but reflects the low level of plastic strain in the test region. Thus very small changes in plastic strain can introduce significant variations in mean stress. In an effort to discover whether the mean stress parameters would be so sensitive to this variation that they would be useless for life prediction, bounds were fitted to the mean stress data and ranges of the two parameters computed. Correlations were made between the range of predicted and observed LCF life for both parameters. It was found that the range of predicted lives lay within a factor of ± 2 of the observed lives for almost all data points for both parameters. The results of this study showed it is important that, at low to moderate strain ranges, the mean stress be accounted for in predicting LCF life. At the same time, the study showed that the parameters are not so sensitive to variability in mean stress that they are useless as predictors of LCF life.

6.2 TWO-STEP TESTS WITH CHANGING TEMPERATURE

In addition to the standard two-load level cumulative damage tests, a number of experiments were conducted in which the temperature was also changed during the second part of the test. In all the experiments, the specimens were cycled at 566° C for various percentages of life. The temperature was then lowered to 343° C and the specimen cycled to failure. The load was raised, lowered, or held constant to yield various life combinations. In some of the tests, the R_ε ratio was kept the same in both sections of the test while in others it was not.

All the results were evaluated on the basis of a linear cumulative damage model. The range parameter (i.e., total strain range) was evaluated on the basis of cycles to failure while the two mean stress parameters employed cycles to crack initiation. For the range parameter, both sets of R_ε data clustered around the unit damage line. For the mean stress parameters, both the equivalent strain and Leis parameters gave an equally good fit to the data in which the strain ratio was maintained constant. While this data set was

limited, all the values were about 15% to 20% conservative. There was a slightly larger data set for the variable R_ε data, and the results are more difficult to analyze. First, most of the data gave a damage summation that was in the range $0.6 \leq$ damage ≤ 1.4. Since the temperature was lowered, the concept of a high-low sequence can have a different interpretation here, but the tests in which the high load occurred first gave the shortest lives. Based on cycles to failure (or initiation), virtually all of these tests would be interpreted as a high-low sequence (i.e., $N_1 < N_2$). All of the damage sums based on the Leis parameter were less than unity while two of the three damage sums were less than unity when the equivalent strain was used. For both the constant and increasing load tests, the majority of data had a damage sum greater than unity. Generally, the equivalent strain was more conservative than the Leis parameter. There is a fair amount of scatter in the data, so considerable additional work is needed in this area. Since the two mean stress parameters were able to correlate the baseline data, this suggests that it is not the mean stress parameters themselves that are at fault, but rather, the cumulative damage model that requires the additional work.

6.3 INFLUENCE OF TIME DEPENDENCE ON MEAN STRESS EFFECTS

All of the preceding mean stress and cumulative damage work assumed that the process was time independent. Subsequent work examined the effect of strain rate and cycle shape on mean stress effects. Two situations were examined. One effort evaluated the combined role of mean stress, strain rate, and tension/compression hold times in Inconel 718 at moderate temperatures. The Ostergren damage model was employed to analyze a wide variety of data; the majority of data were found to fall within a factor of ± 2 of the perfect correlation line. These analyses were used to demonstrate the potential effect of combined hold times and mean stress changes at elevated temperatures in the long life regime where little data are available.

At much higher temperatures, 980° C, René 80 data were used to examine another time-dependent model, Coffin's frequency modified model. This model required that a number of parameters be determined from the data; these constants were determined using several approaches and the implications of these different methods were analyzed. The Coffin model was compared to the Ostergren model and to the other mean stress theories; while the frequency modified model did an adequate job, the Ostergren model provided a comparable correlation. The mean stress theories did not do nearly as well, with the Leis parameter having almost twice the relative error of the other techniques. Moreover, simple strain range gave the best fit of all the data. Since the Leis parameter did a good job in analyzing the lower temperature Inconel 718 data while strain range was unable to correlate baseline data, this makes it clear that the most viable method of analyzing fatigue data will depend on the material as well as the temperature and other test parameters.

6.4 APPLICATION OF THE THEORIES TO THERMAL-MECHANICAL PROBLEM

Data that were used in all the comparisons for the mean stress theories were obtained under isothermal conditions. To be applicable to many hot section components in gas turbines, the theories must be capable of analyzing structures which undergo simultaneous variations in temperature and load, i.e., thermal-mechanical fatigue. These cycles can be relatively simple, for example, in phase with maximum/minimum load and temperature occurring together, out of phase with maximum load at the time of minimum temperature, or the cycle can be any imaginable combination. Many hot path components, e.g., turbine blades, tend to operate in the out-of-phase mode. Several sets of isothermal data were examined using the Smith-Watson-Topper model and reasonable agreement with the data was found. However, the model required a number of assumptions for application to thermal-mechanical fatigue. For instance, since the specimen is undergoing a temperature cycle, what are appropriate values of temperature dependent material parameters? Moreover, many hot path components are coated for environmental protection; these bimaterial components have to be considered as a unit since frequently, cracking originates in the coating. Presently, it is still unclear what isothermal conditions can be used to bound the thermal-mechanical problem. It is clear that a great deal of work needs to be done before isothermally based damage concepts and models can be applied to thermal-mechanical problems.

7.0 DISCUSSION AND RECOMMENDATIONS

The adoption of a particular set of equivalent damage methods for application to AGTE must consider several factors beyond those developed for lower homologous temperatures as discussed repeatedly herein. Those factors which appear to be of particular importance are the time dependence of the inelastic strain and other time dependent effects, such as oxidation, the lack of consensus of the most applicable phenomenological damage parameter for such applications, and the combined variation of load (or stress or strain) and temperature (e.g., TMF). These factors and the impact they were found to have on the individual equivalent damage concepts are discussed in the ensuing sections.

7.1 MEAN STRESS

As mentioned in Section 3.0, there is no consensus of what micromechanisms or phenomenological measures best represent damage in elevated temperature applications of AGTE alloys. Of the three equivalent damage measures discussed, this lack of a physical basis most directly impacted the mean stress theories and their application to hot section components. As shown in Appendix C, mean stress theories can be effective (and are required) in data consolidation when the temperature and/or test control conditions result in benign time-dependent effects.

However, the elevated temperature mean stress cases analyzed in Appendix E and Section 6.0 demonstrated the need to introduce elevated temperature damage concepts into the mean stress formulation. In this appendix, it was shown that Ostergren's damage function was effective in correlating elevated temperature Inconel 718 hold time and strain-rate data. This approach was used to illustrate the potential effects of mean stress during constant strain tension hold times at elevated temperatures where stress relaxation would occur. It has demonstrated analytically that such tension stress relaxation could result in a beneficial effect on fatigue life if the strain range was low enough such that increased plastic flow would not occur during the stress reversal. This effect requires a consistent damage parameter, and should be experimentally verified. In addition, the analysis of the strain-rate Rene' 80 data at 980° C illustrated the problems associated with using low temperature mean stress measures at temperatures in the creep regime. The Ostergren approach which does include a measure of elevated temperature damage (through the frequency term, ν) was superior to two of the three time-independent mean stress approaches to which it was compared. The equivalent strain approach in this case degenerated to just strain range ($m = 1$ was indicated by the data analysis) and was found to be the best method of correlating the data. In other words, a simple polynominal curve fit of total strain versus cycles to crack initiation was the best method. While there is some reluctance to say that this result means that time-dependent effects are unimportant in the failure process for this alloy at 980° C, it clearly shows the problems associated with determining the best damage parameter and the best measure of mean stress equivalent damage.

Appendix E showed that the mean stress developed in a thermal-mechanical fatigue cycle depends upon the phasing between the temperature and

mechanical strain. Since this relationship is out-of-phase in most AGTE applications, the mean stress will be positive (as in Figures E-24 and E-25) and the maximum stress will occur at the lowest temperature of the TMF cycle. Combining this stress level and some measure of strain (as suggested by several mean stress models) to predict the TMF life resulted in uncertainty since the isothermal data were not collapsed into one curve (e.g., Figure E-26 where the curves depend on the temperature of the data). The previous discussion indicated the need to develop the best isothermal parameter in order to correctly identify the most consistent mean stress model. Note though that different mechanisms can be active in different temperature regimes which suggests that different damage parameters would be required for the various temperature regimes. In considering damage parameters for TMF applications, more than one mechanism and potentially synergistic effects which could require consideration of more than one parameter or, perhaps, the development of a single unique parameter for TMF applications might be contemplated.

It is clear that the present state of the art prevents a definite recommendation of a single best mean stress parameter. However, certain comments can be made. First, it must be recognized that any such parameter will depend upon the material and the application. In most of this work, the best parameters for AGTE alloys appeared to be those that utilized the product of a stress measure and a strain measure. The specific parameter selected for an application should reflect this consideration; and, in addition, it should also reflect the nature of the elevated temperature damage. In this regard, it was not our intention to indicate a preference for the Ostergren approach; it was a convenient vehicle for examining combined models of elevated temperature damage and mean stress. Other measures of damage have been proposed as discussed in Section 3.2. Both Ostergren and Leis have proposed methods which are similar in concept to strain-range partitioning but which still maintain a measure of mean stress. With this idea in mind, the general product form is suggested,

$$D = f_1 (\sigma_a, \sigma_m)\, g_1 (\Delta\varepsilon,\ \Delta\varepsilon_p,\ \Delta\varepsilon_c,\ \Delta\varepsilon_{pc},\ \ldots\nu) \qquad (1)$$

as perhaps the most definitive mean stress parameter form that could be recommended for elevated temperature applications at this time. While Equation 1 does not present a specific functional relationship, it would appear that such a general form should be considered until experimental results can be used to place further restrictions on the functional form. The type of experiments that might be performed should reflect the application, and these are briefly considered next.

As noted in Appendix E, most isothermal hold time and slow frequency tests are conducted in the low life regime where, normally, there is more inelastic strain than that in gas turbine components. Therefore, some extrapolation method is relied on to predict the life in the design regime. It would be useful to conduct some experiments in the longer life regime, perhaps as suggested in Figure 4. In this figure, stress-strain path OFAC is thought to represent a typical path which would occur at a stress-concentrated region of a hot path component. Path AC is thought to represent the actual time-dependent path wherein neither stress nor strain is held constant as is done

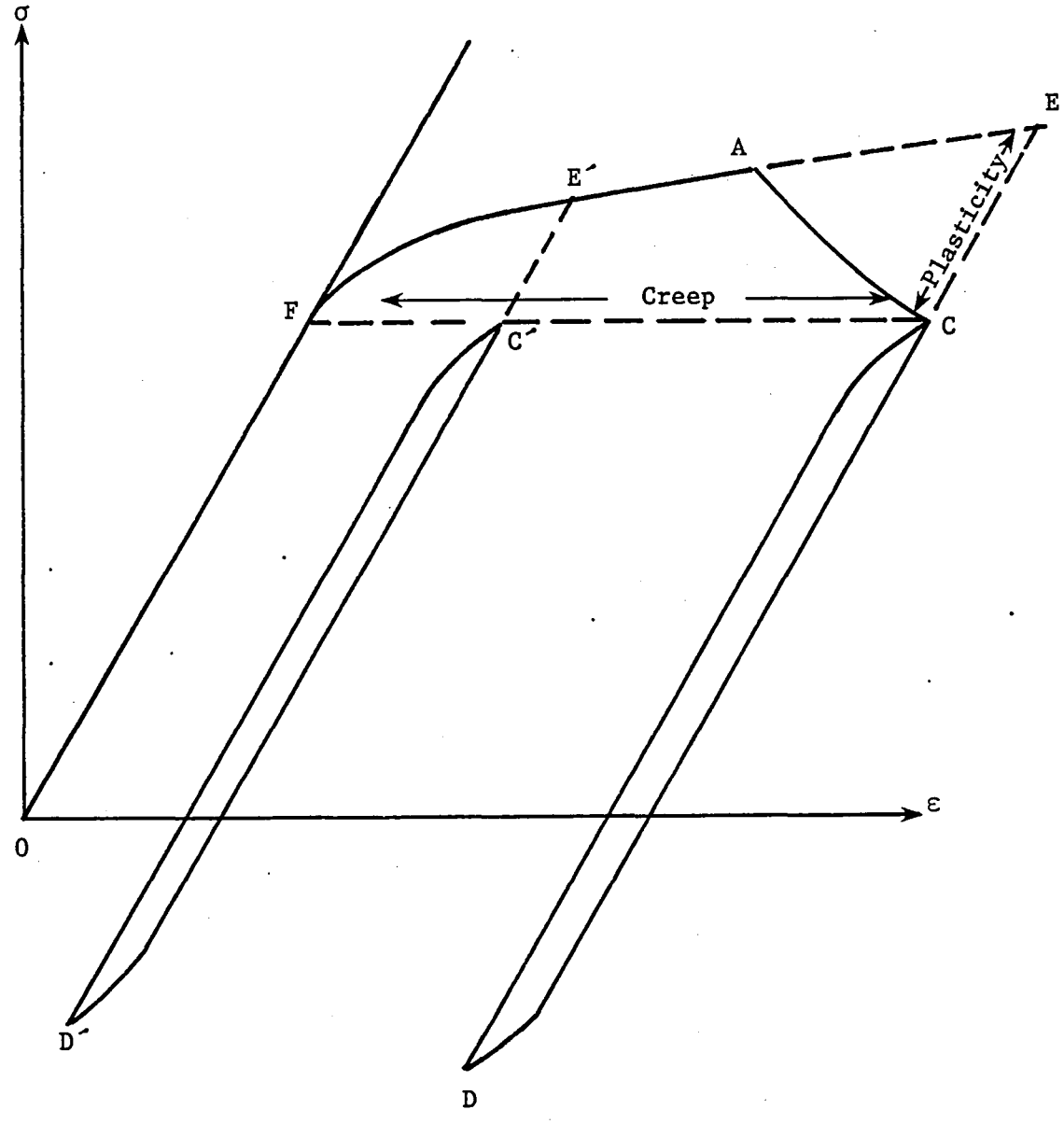

Figure 4. Comparative Tests in the Long-Life Region.

in typical experimental idealizations. Actually, several intermediate cycles would occur during the path from A to C, but these have been deleted for clarity. Point C is thought to represent the final steady-state response point of the critical structural element. The cycle CDC then represents the steady-state cycle. At this point, at least two other paths could be used to reach Point C. Path OFAEC represents a rapid loading and unloading (from E to C). Following such an excursion, various tests could be conducted on different test specimens (i.e., using various frequencies). If tests of this sort were compared with tests conducted under the full path OFACD, it might be concluded which parameters best correlate the observed life rankings. Alternatively, the creep path OFC could be followed which would probably involve substantially more time and creep strain to arrive at Point C. Tests could then be conducted in a similar fashion as the plasticity path OFAEC; and, again, the results could be compared to the others and consistency checks made on the proposed damage parameter. Obviously, several variations could be made such as the path OFE'C'D' wherein the loop C'D' could be controlled to be nearly the same as CD (since the loops are considered to be basically elastic). Such experiments could also be performed with initially compressive loadings to yield an overall comparison of tensile and compressive mean stresses. Or, being realistic, all tests might be run with such compressive loadings since hot path components are normally initially loaded in compression in the fatigue critical regions.

Regardless of the findings of such tests, the need still exists to verify the selected damage parameter in TMF. To insure consistency, the phase relationship between temperature and strain should be varied in different tests to produce different levels of mean stress. By controlling other pertinent variables (e.g., temperature range and strain range), the influence of mean stress should become known. The goal of such tests would be to provide the best damage parameters and approach for linking isothermal and TMF test results. As a practical matter, the use of high temperature, isothermal mean stress criteria should be more conservative than simple range quantity criteria (e.g., $\Delta\varepsilon$) when applied to out-of-phase TMF cycles. This is because of the high tensile mean stress that develops in such cycles due to the higher strength at lower temperatures. In in-phase TMF cycles, it is less clear whether or not a mean stress criteria would be more conservative; it would depend upon the magnitude of the mean (or maximum) stress compared to those in the high temperature data set.

One other practical matter must be raised in this regard. The use of any mean stress parameter requires accurate, constitutive equations and inelastic stress analysis methods. Generally, such techniques are not employed in standard design analysis. The mean stress effects detailed in Appendix A (e.g., the hump-shaped, complete stress-strain curve) lie outside the capabilities of most plasticity theories which do not consider cycle-to-cycle changes in mean stress and cyclic softening. Approximations to these effects can be made; but, again, they are outside the practice of typical design engineers. Thus the sensitivity of such mean stress approaches to the capabilities of the stress analysis codes is a real consideration that must be made in adopting a mean stress parameter. Analysis of the Leis and equivalent strain parameters in

Appendix E shows that it is not too sensitive in this regard. Also, the comparative plot of four mean stress methods in Appendix C suggests that most of these methods should show a similar sensitivity for Inconel 718. This could well change if another material had been used in generating such comparisons.

Finally, the adoption of any such approach will require more testing to insure adequacy and develop the statistics of the method. This is particularly true if it is found that general TMF experiments are required to check the validity of a given approach on a new alloy. Design handbook formats would have to be changed to reflect the new approach.

7.2 CUMULATIVE DAMAGE

As shown in Appendix B and discussed in Section 5.1, use of the DLDR as suggested by Manson and Halford for design practice has been adopted. This is based on several considerations. First, the consensus is that the normally observed sequence effect in fatigue is a consequence of the formation, growth, and linkup of microcracks and the final propagation of the macrocrack to failure. This philosophy is consistent with the general philosophy of the DLDR although it is not explicit in the later version of the DLDR. Thus the adoption of the DLDR approach can be viewed in a more general sense as an acceptance of a general physical concept; the details of the application of the DLDR still require more work. Second, the method worked best on our set of two-step Inconel 718 data. As shown by Adams (Reference 47), test techiques can be used to improve the predictive capability of the method. The method is easily applied, and could be used in its most general form by programming it into a digital computer. It is also potentially consistent with any damage parameter, etc., since only the cycles to failure for a given cycle type is required input.

Such an endorsement must be countered by the experimental findings presented in Section 6.2. In that section, it was shown that for a set of two-step test data (where temperature was changed in the second block of loading) that would be viewed classically as high/low tests, results behaved as low/high. In analyses of these data, both the Leis parameter and the equivalent strain parameter will be used to take out any consideration of differences in mean stress that developed during the tests. It was shown in Appendices C and E that both of these mean stress techniques were effective in data consolidation for Inconel 718; so by using these parameters, the sequence effect should have been predictable since only the cycles to failure in the two steps are required to apply the DLDR. Since the predictions went in the wrong direction compared to the test results, this suggests that synergistic effects are occurring which lie outside the formulation of the present DLDR and the mean stress parameters. It should be noted that some of these tests were conducted so that the calculated isothermal lives in both steps were equal. Such a test is designated an equal life test and it is suggested that such experiments may have general potential in helping to understand synergistic effects in TMF as is now discussed.

Recall that in the discussion of TMF in Section 7.1 it was indicated that interactive effects between different damage mechanisms at different temperatures of a TMF experiment could occur. Such considerations suggest, in turn, that only through TMF testing could it be hoped to develop an improved approach for predicting the low cycle fatigue of some AGTE components. To this end, the equal life test is believed to have potential utility. Consider two temperatures T_l and T_h such that $T_l < T_h$. It is assumed that isothermal fatigue data for T_l can be accurately predicted by some damage parameter P_l. Also, consider the case where the damage mechanisms at the two temperatures are different such that some other damage parameter, P_h, is required to accurately describe the isothermal data at temperature T_h. For instance, P_l might be the equivalent strain parameter whereas P_h might be the Ostergren damage function (or P_h might simply be an indicator of a method such as strain-range partitioning or frequency modified fatigue life). The specifics are not relevant to this discussion. Such parameters might be displayed in a plot such as Figure 5. Next, consider a two-step test where temperature is also changed in the second block. Such a test could be run as suggested in Figure 5 where the life in both blocks of loading would be the same, i.e., N_{il}. Several possibilities could occur as shown in Figure 6. First, since the calculated life in both blocks should be the same, rules such as the DLDR would predict the linear Palmgren-Miner's law. Consider the case where the high temperature is applied first, followed by the lower temperature block. Since it has been suggested that time exposures at high temperatures can have a detrimental effect on low temperature ductility (e.g., References 58 and 59), a detrimental effect might be expected compared to the linear rule. Conversely, the results given in Appendix E showed a beneficial effect compared to either the linear law or the DLDR. It should be possible to continue by mixing the two block types several times in one test but still maintaining the equal-life philosophy. If constructed properly, in the limit, such a mixing procedure would lead to a complete TMF experiment.

Ultimately, what would come of such a test series would be a consistent damage methodology. Several alternatives in damage concepts would have to be considered including cumulative damage, the damage parameter(s) and perhaps generalized concepts of cycle counting (e.g., rain flow counting). In composing the makeup of this methodology, it would be desirable to maintain the isothermal parameters as reference points. That is, by carefully constructing the cumulative damage law and the concepts of cycle counting, it should be possible to maintain the isothermal damage parameters as a special case of the more generalized concepts. In all of this, though, it would be crucial to perform metallographic analyses in order to have a consistent framework of the damage parameters and the associated damage philosophies.

Finally, after all comparisons, it was found that the DLDR was conservative. This indicates that it could be applied in design analyses to predict the effect of minor cycles and of different cycles (cold day versus hot day starts, short haul versus long missions, etc.). Generally, it might not be expected to be conservative in the temperature variations as discussed above in the case of embrittlement. Such considerations would require TMF experiments to add confidence in the life predictions.

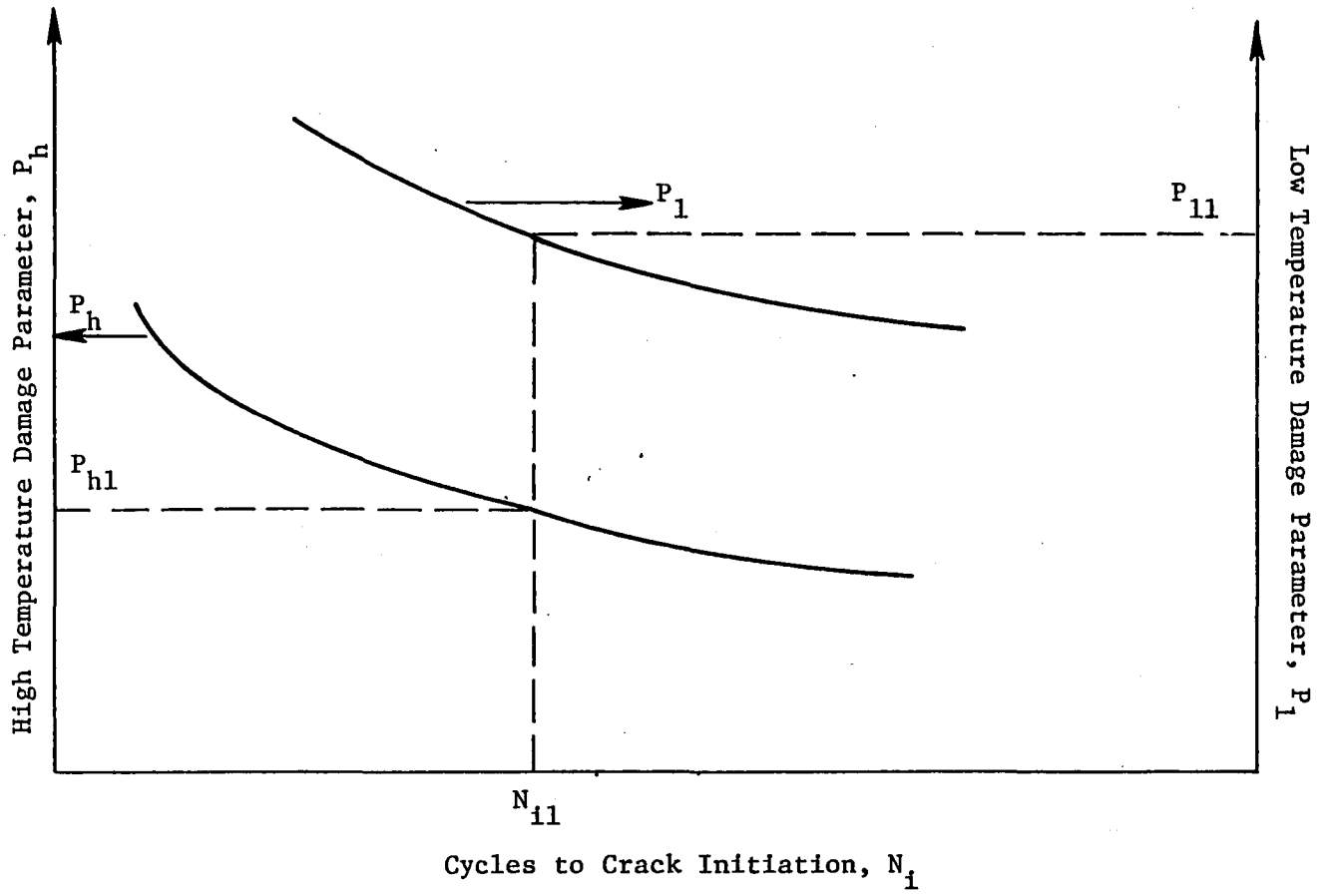

Figure 5. Generalized Equal-Life Test.

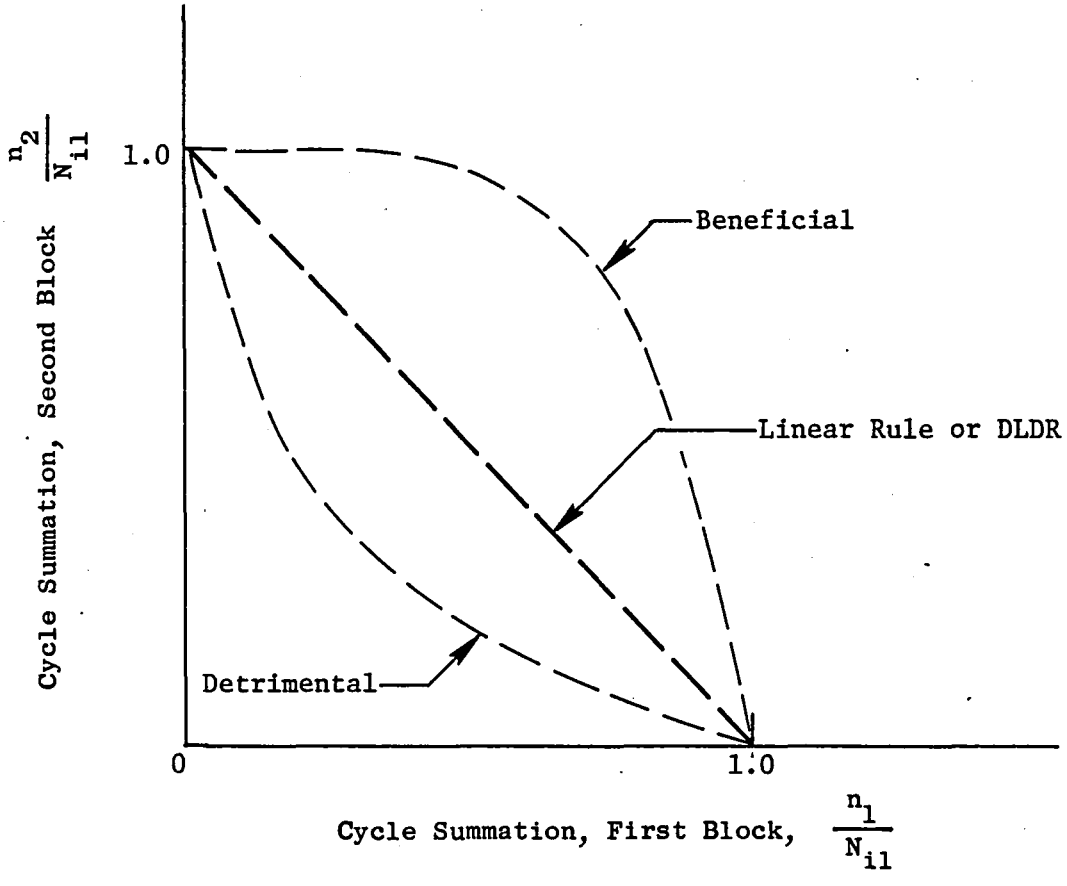

Figure 6. Potential Results of Equal-Life Tests.

7.3 MULTIAXIALITY

All of the considerations noted above are true in the case of multiaxial relationships, and the uncertainties would be expected to multiply in a theoretical sense. However, certain specific suggestions can be made which should generally improve industry use of multiaxial equivalence relationships as mentioned in Section 5.3. Based on the results of the literature survey, recommendations will be made for the use of scalar invariant quantities. As noted in Section 5.3, nonproportional loading is not considered to be a crucial issue; nevertheless, if multiaxial relationships are applied to nonproportional loading problems, the user should exercise care as noted in Appendix D.

As shown schematically in Figure 7, all equivalent multiaxial invariant quantities should be calculated on the basis of ranges of the stress and strain components. The relationships to be developed are for a generalized Coffin-Manson formulation

$$\frac{\Delta\epsilon}{2} = \epsilon'_f (2Nf)^{-\alpha} + \frac{\sigma'_f}{E} (2N_f)^{-\beta} \tag{2}$$

where ϵ'_f, α, σ'_f, E, and β have their usual meaning. As shown in Appendix D under certain restrictions, the following relationships are true

$$\Delta\epsilon_e = \frac{\Delta\sigma_e}{E^*} + \Delta\epsilon_e^P \tag{3}$$

where

$$\Delta\sigma_e = \sqrt{\frac{3}{2} \Delta S_{ij} S_{ij}}, \tag{4}$$

$$\Delta\epsilon_e = \sqrt{\frac{2}{3} \Delta e_{ij} \Delta e_{ij}}, \tag{5}$$

$$\Delta\epsilon_e^P = \sqrt{\frac{2}{3} \Delta\epsilon_{ij}^P \Delta\epsilon_{ij}^P}, \tag{6}$$

$$E^* = \frac{3E}{2(1+\mu)}, \tag{7}$$

$$S_{ij} = \sigma_{ij} - \frac{1}{3} \sigma_{kk} \delta_{ij}, \tag{8}$$

$$e_{ij} = \epsilon_{ij} - \frac{1}{3} \epsilon_{kk} \delta_{ij}, \tag{9}$$

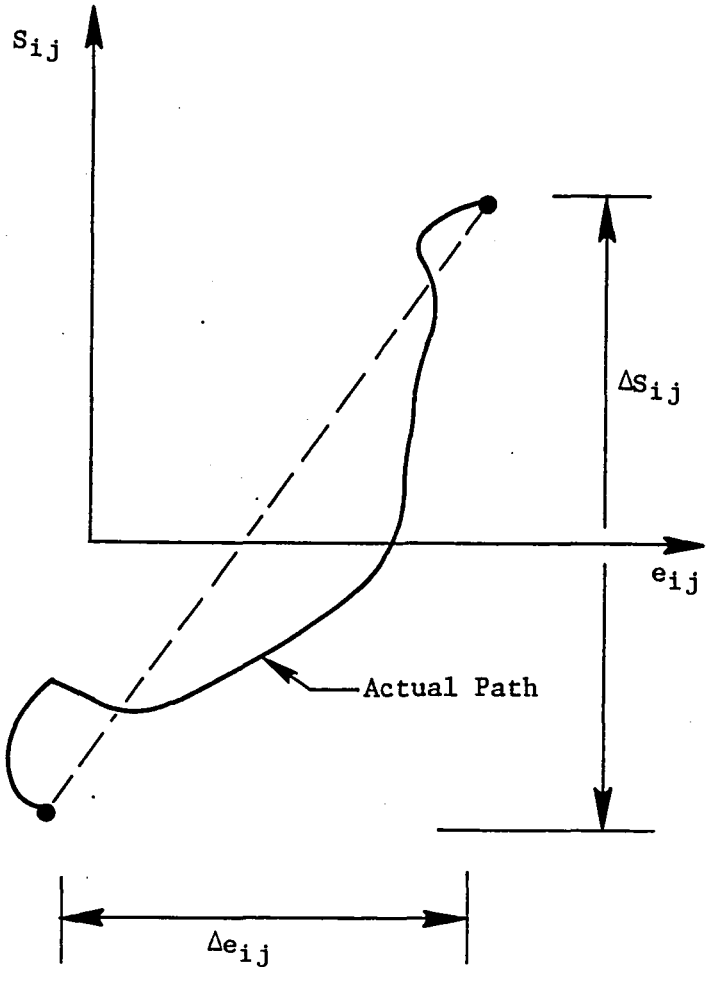

Figure 7. Schematic of the Quantities to be Used in the Multiaxial Relationships.

σ_{ij} are stress tensor components, ε_{ij} are the strain tensor, ε^{P}_{ij} are the plastic strain (or inelastic strain) components, and the Δ symbol refers to changes over a loading cycle as shown in Figure 7.

Based on the identity in Equation 3, one could write,

$$\Delta\varepsilon^{P}_{e} = \varepsilon'_{f}(2N_f)^{-\alpha} \tag{10}$$

$$\frac{\Delta\sigma_e}{E^*} = \frac{\sigma'_f}{E^*}(2N_f)^{-\beta} \quad . \tag{11}$$

This would represent the procedures if normal invariant quantities were used. For a more complex situation, the triaxiality factor, TF, suggested in the work of Mowbray and Manson and Halford is a practical and meaningful modification to Equation 10. This factor, as discussed in Appendix D, is a method of including the first invariant of the stress tensor into Equation 10. The triaxiality factor is defined by

$$TF = \frac{\sigma_1 + \sigma_2 + \sigma_3}{\frac{1}{\sqrt{2}}\sqrt{(\sigma_1 - \sigma_2)^2 + (\sigma_1 - \sigma_3)^2 + (\sigma_2 - \sigma_3)^2}} \tag{12}$$

where the σ_i are the principal stresses. Different functions of TF were suggested in the two cited papers, and it appears that the one by Manson and Halford would be more conservative in the case of equal biaxial stressing which seems to be the most important in thermal stress problems of AGTE components. This consideration modifies Equation 10 to give

$$\Delta\varepsilon^{P}_{e} = \frac{\varepsilon'_f}{f_2(TF)}(2N_f)^{-\alpha} \tag{13}$$

where f_2 (TF) would be selected from either of the two works. In the case of Manson and Halford, f_2 = MF, where MF is defined by equation 15, Appendix D. The complete relationship would then become,

$$\frac{\Delta\varepsilon_e}{2} = \frac{\varepsilon'_f}{f_2(TF)}(2N_f)^{-\alpha} + \frac{\sigma'_f}{E^*}(2N_f)^{-\beta} \tag{14}$$

Modification of the strength term σ'_f/E^* could be contemplated based on the old, multiaxial fatigue literature which showed the endurance limit relationship in tension and torsion was material dependent. However, no specific recommendation is offered since it is sometimes found in the literature that the equivalent stress formulation is adequate, and insufficient multiaxial data on AGTE alloys was found.

One other factor should be considered; that of mean stresses. An easy and consistent formulation is readily available in both the MMHM mean stress approach and the Sines multiaxial relationship. This would modify the elastic portion of the Coffin-Manson (Equation 2) (the plastic curve modification is not considered attractive for reasons discussed in Appendix C):

$$\frac{\Delta\sigma_e}{E^*} = \left(\frac{\sigma'_f - k^* I_{\underset{\sim}{\sigma}_{Static}}}{E^*} \right) (2N_f)^{-\beta} \qquad (15)$$

where

$$I_{\underset{\sim}{\sigma}_{Static}} = \sigma_{1m} + \sigma_{2m} + \sigma_{3m},$$

k^* would be the multiaxial counterpart to k in the MMHM (they differ only by using E^*), and σ_{im} are the mean values of the principal stress cycles. Restricting the formulation to proportional loading cases reduces the ambiguity in interpretation of $I_{\underset{\sim}{\sigma}_{Static}}$.

However, considering the difficulties in application with the MMHM method, further research is recommended into multiaxial equivalent relationships of the uniaxial product form given in Equation 1. As discussed in Appendix D, Leis recommended and verified in certain cases a multiaxial equivalent to his parameter, and Walker suggested one for essentially the equivalent strain approach (which was demonstrated on a limited basis). Two factors are crucial in the successful development of such a relationship. First, some consideration of the function f_2 (TF) should be included. Second, there is a question as to what measure of maximum stress (or strain) to use. Leis suggests the maximum value of equivalent stress (care, of course, must be taken to ensure consistency with the signs of the principal stresses) while Walker uses a measure of the hydrostatic strain, arguing consistency with Sines criterion (see Appendix D for his formulation). This question can only be resolved by a careful study of multiaxial data.

Finally, it is noted that there is a true lack of multiaxial data on AGTE alloys. Often multiaxial data show that the equal biaxial case is the most detrimental in low cycle fatigue [that is also reflected in the f_2 (TF) function]. As discussed in the appendix, all functions such as f_2 (TF) are material dependent, and as such, should be verified on each alloy of interest in a given application. Thus it is recommended that equal biaxial tests be conducted to both justify the f_2 (TF) function and to investigate the most appropriate mean stress formulation.

8.0 CONCLUSIONS

The following conclusions are suggested by this research:

1. The equivalent strain relationship is the best mean stress criteria for low homologous temperatures and AGTE alloys if the appropriate isothermal data are available. The Leis technique appears to be the best predictive mean stress parameter when data are not available to determine the exponent in the equivalent strain technique.

2. The best formulation of a mean stress criterion depends upon the damage mechanisms which are modeled by the elevated temperature damage parameter. The parameters considered in this report indicate that the product of a stress measure (e.g., maximum stress) times a strain measure seems to work best for this class of alloys. Mathematical formulations which used only the numerical value of the mean stress were found to be less effective.

3. A full verification fo mean stress theories will not be complete until application has been made to thermal mechanical fatigue. In AGTE hot gas path components, the mean stresses are generally tensile and occur at the lower temperatures of the cycle. Mean stress theories must be able to account for these severe conditions.

4. Isothermal mean stress theories singled out for examination herein should be verified in the longer life (design) regime. Most experimental results are obtained in the shorter cycle life range where more inelastic strain is present. A specific series of experiments was described.

5. The double linear damage rule is the best isothermal cumulative damage technique currently available. However, as presently used, the technique is overly conservative when used in predicting a series of two-step tests where a temperature change was introduced into the second block of loading.

6. A test series was described for developing a consistent damage methodology. These tests used a so-called equal life technique to aid in the formulation of uniaxial equivalent damage criteria, and involved changing temperature during the experiments.

7. A multiaxial equivalence criterion was developed based on a literature review. The criteria deemed important were the use of a triaxality factor function and a consistent mean stress formulation.

8. A need exists for multiaxial test data on aircraft engine industry alloys. These experiments should concentrate on positive biaxial stress ratios, and should study the effect of mean stress. In general, multiaxial relationships for elevated temperature applications

will remain an open research area for quite awhile. Current research should concentrate on lower temperature phenomena which would suggest criteria at elevated temperatures. Uniaxial damage considerations at elevated temperatures appear complicated enough for the present.

REFERENCES

1. Floreen, S. and Kane, R.H., Fatigue of Engineering Materials and Structures, 2, 1980, p. 401.

2. Shahinian, P. and Sadananda, K., J. of Engineering Materials and Technology, Trans. ASME, 101, 1979, p. 224.

3. Mills, W.J. and James, L.A., ASME Paper No. 78-WA/PVP-3.

4. Domas, P.A., General Electric Company, unpublished research.

5. Cook, T.S., "Effect of Frequency on Fatigue Crack Growth in a Nickel-Base Superalloy," to be published.

6. Runkle, J. and Pelloux, R., ASTM STP675, 1979, p. 501.

7. Scarlin, R., IFC 4, 2, 1977, p. 849.

8. Gell, M. and Leverant, G.R., Fatigue at Elevated Temperatures, ASTM STP520, 1973, p. 37.

9. Swanson, J. and Marcus, H., Met. Trans., 9A, 1978, p. 291.

10. Duquette, D. and Gell, M., Met. Trans., 3, 1971, p. 1325.

11. Sidey, D. and Coffin, L., ASTM STP675, 1979, p. 528.

12. Woodford, D., Met. Trans., 12A, 1981, p. 299.

13. Scarlin, R., ASTM STP675, 1979, p. 396.

14. Lawless, B., Antolovich, S., Bathias, C., and Boursier, B., "The Effect of Microstructure on the FCP and Overload Behavior of Waspalloy at Room Temperature," submitted for publication.

15. Mills, W.J. and James, L.A., Fatigue of Engineering Materials and Structures, 3, 1980, p. 159.

16. Sadananda, K. and Shahinian, P., Met. Trans. A, 8A, 1977, p. 439.

17. Floreen, S., Met. Trans. A, 6A, 1975, p. 1741.

18. Cowles, B.A., Sims, D.L., Warren, J.R., and Miner, R.V., J. of Engineering Materials and Tech., Trans. ASME, 102, 1980, p. 356.

19. Kikuchi, M., Shiozawa, K. and Weertman, J.R., "Void Nucleation in Astroloy: Theory and Experiments," Acta Met., in press.

20. "Characterization of Low Cycle High Temperature Fatigue by Strain Range Partitioning Method," Advisory Group for Aerospace Research and Development Conference Proceedings No. 243, AGARD-CP-243, April 1978.

21. Manson, S.S., "The Challenge to Unify Treatment of High Temperature Fatigue - A Partisan Proposal Based on Strainrange Partitioning," Fatigue at Elevated Temperatures, ASTM STP520, ASTM, 1973, pp. 744-782.

22. Hirschberg, M.H. and Halford, G.R., "Strainrange Partitioning - A Tool for Characterizing High-Temperature Low-Cycle Fatigue," NASA TMX-71691, April 1975.

23. Coffin, L.F., Jr., Carden, A.E., Manson, S.S., Severud, L.K., and Greenstreet, W.L., "Time-Dependent Fatigue of Structural Alloys - A General Assessment (1975)," ORNL Report 5073, Oak Ridge National Laboratory, January 1977.

24. Coffin, L.F., Jr., "Fatigue at High Temperature," Fatigue at Elevated Temperatures, ASTM STP520, ASTM, 1973, pp. 5-34.

25. Coffin, L.F., Jr., "A Note on Low-Cycle Fatigue Laws," Report No. 70-C-309, General Electric Co., Schenectady, N.Y., September 1970.

26. Coffin, L.F., Jr., "The Effect of Vacuum on the High-Temperature, LCF Behavior of Structural Materials," Proc. Int. Conference on Fatigue: Chemistry, Mechanics, and Microstructure, 1972, pp. 590-600.

27. Coffin, L.F., Jr., "Fatigue at High Temperature - Prediction and Interpretation," James Clayton Memorial Lecture, Proc. Inst. Mach, Eng. (London), 1974, pp. 188, 109.

28. Coles, A. and Skinner, D., "Assessment of Thermal Fatigue Resistance of High Temperature Alloys," J. Roy. Aeronaut. Soc., 69. 343, 1965.

29. Ashby, M.F., "A Final Report on Deformation-Mechanism Maps," Acta Metal., 20, July 1972, pp. 887-897.

30. Coffin, L.F., "The Concept of Frequency Separation in Life Prediction for Time-Dependent Fatigue," ASME-MPC Symposium on Creep-Fatigue Interaction, 1976, pp. 349-363.

31. Ostergren, W.J., "Correlation of Hold Time Effects in Elevated Temperature Low Cycle Fatigue Using a Frequency Modified Damage Function," 1976 ASME-MPC Symposium on Creep-Fatigue Interaction, December 1976, pp. 179-202.

32. Majumdar, S. and Maiya, P.S., "A Damage Equation for Creep-Fatigue Interaction," 1976 ASME-MPC Symposium on Creep-Fatigue Interaction, December 1976, pp. 323-335.

33. Mowbray, D.F., "Derivation of a Low-Cycle Fatigue Relationship Employing the J-Integral Approach to Crack Growth," Cracks and Fracture, ASTM STP-601, 1976, pp. 33-46.

34. Kaisand, L.R. and Mowbray, D.F., "Relationships Between Low-Cycle Fatigue and Fatigue Crack Growth Rate Properties," J. of Testing and Evaluation, 7, 5, 1979, pp. 270-280.

35. Chaboche, J.L., Policella, H., and Kacymasek, H., "Application of the SRP Method and Creep-Fatigue Damage Approach to the LCHTF Prediction of IN100 Alloy," AGARD-CP-243, Characterization of Low-Cycle High Temperature Fatigue by the Strain Range Partitioning Method, August 1978, pp. 4-1 to 4-20.

36. Chaboche, J.L., "Thermodynamic and Phenomenological Description of Cyclic Viscoplasticity with Damage," European Space Agency Technical Translation, ESA-TT-548, May 1979.

37. F. Erdogan, "Stress Distribution in Bonded Dissimilar Materials with Cracks," J. of Applied Mech., Trans. ASME, 87, 1965, p. 403.

38. Cook, T.S., "Flaws in Wedges," Ph.D. Dissertation, Lehigh University, 1971.

39. Cook, T.S. and Tracey, D.M., "Stress Distribution in a Cracked Bimaterial Plate," Fracture, 3, 1977, pp. 1055-1057.

40. Tracey, D.M. and Cook, T.S., "Analysis of Power-Type Singularities Using Finite Elements," Int. J. for Num. Methods in Engng., 11, 1977, pp. 1225-1233.

41. Erdogan, F., Gupta, G.D., and Cook, T.S., Methods of Analysis and Solutions of Crack Problems, Ed. G.C. Sih, Noordhoff International Publishing, The Netherlands, 1973, pp. 368-425.

42. Strangman, T.E. and Hopkins, S.W., "Thermal Fatigue of Coated Superalloys," Ceramic Bulletin, 55, 1976, p. 304.

43. Leverant, G.R., Strangman, T.E., and Langer, B.S., "Parameters Controlling the Thermal Fatigue Properties of Conventionally Cast and Directionally Solidified Turbine Alloys," Superalloys: Metallurgy and Manufacture, 3rd Int. Symposium, Seven Springs, PA, 1977, p. 285.

44. Gemma, A.E. and Phillips, J.S., "The Application of Fracture Mechanics to Life Prediction of Cooling Hole Configurations in Thermal-Mechanical Fatigue," Engng. Frc. Mech., 9, 1977, p. 25.

45. Rau, C.A., Jr., Gemma, A.E., and Leverant, G.R., "Thermal-Mechanical Crack Propagation in Nickel and Cobalt Base Superalloys Under Various Strain-Temperature Cycles," Fatigue at Elevated Temperatures, ASTM STP-520, 1973, p. 166.

46. Menon, M.N., "Life Prediction Techniques for Analyzing Creep-Fatigue Interaction in Advanced Nickel-Base Superalloys," AFML-TR-76-172, November 1976.

47. Adams, J.H., "Nonlinear Damage Cumulation in Solution Treated and Aged Titanium, 6Al-4V," Paper 81-GT-106, ASME J. of Engineering Power.

48. Hayhurst, D.R., "Creep Rupture Under Multi-Axial States of Stress," Journal of the Mechanics and Physics of Solids, Vol. 20, No. 6, December 1972, pp. 381-390.

49. Leckie, F.A. and Hayhurst, D.R., "Creep Rupture of Structures," Proc. Royal Society Lond., A, 340, 1974, pp. 323-347.

50. Hayhurst, D.R., Trampczynski, W.A., and Leckie, F.A.," Creep-Rupture Under Non-Proportional Loading," Acta Metallurgica, Vol. 28, 1980, pp. 1171-1183.

51. Mowbray, D.F., "A Hydrostatic Stress-Sensitive Relationship for Fatigue Under Biaxial Stress Conditions," Journal of Testing and Evaluation, JTEVA, Vol. 8, No. 1, January 1980, pp. 3-8.

52. Manson, S.S. and Halford, G.R., "Treatment of Multiaxial Creep-Fatigue by Strainrange Partitioning," MPC-3, 1976 ASME-MPC Symposium on Creep-Fatigue Interaction, ASME, 1976.

53. Manson, S.S. and Halford, G.R., "Discussion to Multiaxial Low-Cycle Fatigue of Type 304 Stainless Steel," by J.J. Blass and S.Y. Zamrik, Journal of Engineering Materials and Technology, Vol. 99, Series H, No. 3, July 1977, pp. 283-285.

54. Sines, G., "Failure of Materials Under Combined Repeated Stresses with Superimposed Static Stresses," NACA TN 3495, National Advisory Committee for Aeronautics, November 1955.

55. Sines, G. and Ohgi, G., "Fatigue Criteria Under Combined Stresses or Strains," Journal of Engineering Materials and Technology, Trans. ASME, Vol. 103, No. 2, April 1981, pp. 82-90.

56. Walker, K., "The Effect of Stress Ratio During Crack Propagation and Fatigue for 2024-T3 and 7075-T6 Aluminum," Effects of Environment and Complex Load History on Fatigue Life, ASTM STP462, ASTM, 1970, pp. 1-14.

57. Brown, M.W. and Miller, K.J., "A Theory for Fatigue Failure Under Multiaxial Stress-Strain Conditions," The Institution of Mechanical Engineer Proceedings, 1973, Vol. 187, 65173, pp. 745-755.

58. Antolovich, S.D., Domas, P., and Strudel, J.L., "Low Cycle Fatigue of René 80 as Affected by Prior Exposure," Met. Trans., Vol. 104, December 1979, pp. 1859-1868.

59. Woodford, D.A., "Environmental Damage of a Cast Nickel-Base Superalloy," General Electric Company, Schenectady, New York, Report No. 80 CRD 160, July 1980.

APPENDIX A - CYCLIC DEFORMATION CHARACTERISTICS OF INCONEL 718

In its simplest definition, a cyclic stress-strain curve represents material load-deformation behavior after a given number of load applications. The deformation response can be either transitory or stable, but the latter is usually specified for consistency. The resulting stress-strain test represents an effort to characterize and understand the deformation behavior of a material as it undergoes repeated loadings. In particular, a comparison of the cyclic stress-strain curve (CSSC) to the initial monotonic curve defines the cyclic hardening/softening characteristics of the material that are fundamental properties of the material. These data are very useful; but when cyclic material properties are used in a component life analysis, the situation becomes more complex. Here, it is helpful to have a cyclic curve that reflects the actual state of stress in the component, that is, not only the stress range but also including any mean stress. Such a cyclic curve has been termed the complete cyclic stress-strain curve by Cook (Reference 1) and is defined by the locus of tips of the load-displacement hysteresis loops. Because the maximum (or tip) stress, σ_T, in the loop is the sum of the alternating and mean stress, it can be written as

$$\sigma_T = \sigma_A + \sigma_M. \tag{1}$$

The complete CSSC describes both the cyclic hardening/softening and the mean stress relaxation, thereby giving a total picture of material cyclic behavior. Since the mean stress plays a key role in the damage accrual process, an understanding of cyclic behavior is basic in equivalent damage considerations. For this reason, this appendix includes considerable detail on the cyclic behavior of Inconel 718.

Testing Procedures

According to the initial definition of the cyclic curve given above, a specimen would be cycled until its deformation behavior stabilized and then the specimen would be tensile tested. Figure A-1 shows the result of such a test in which a specimen was cycled to half its estimated life, $N_f/2$, and then monotonically pulled to failure. The comparison of the initial and half-life monotonic curves demonstrates the amount of cyclic softening undergone by forged Inconel 718 at this temperature, 343° C. The third curve shown in the figure is termed the stable cyclic curve and was obtained from the alternating stress-alternating strain hysteresis loop taken just prior to the tensile test. The agreement between this cyclic curve and the half-life monotonic curve indicates that the loop amplitude method is an acceptable technique to obtain the CSSC. In fact, the techniques based on the hysteresis loops have come to be most frequently used as they do not require the destruction of the specimen.

There have been a number of techniques suggested to obtain the cyclic curves from the hysteresis loops (Reference 2), but the two most common

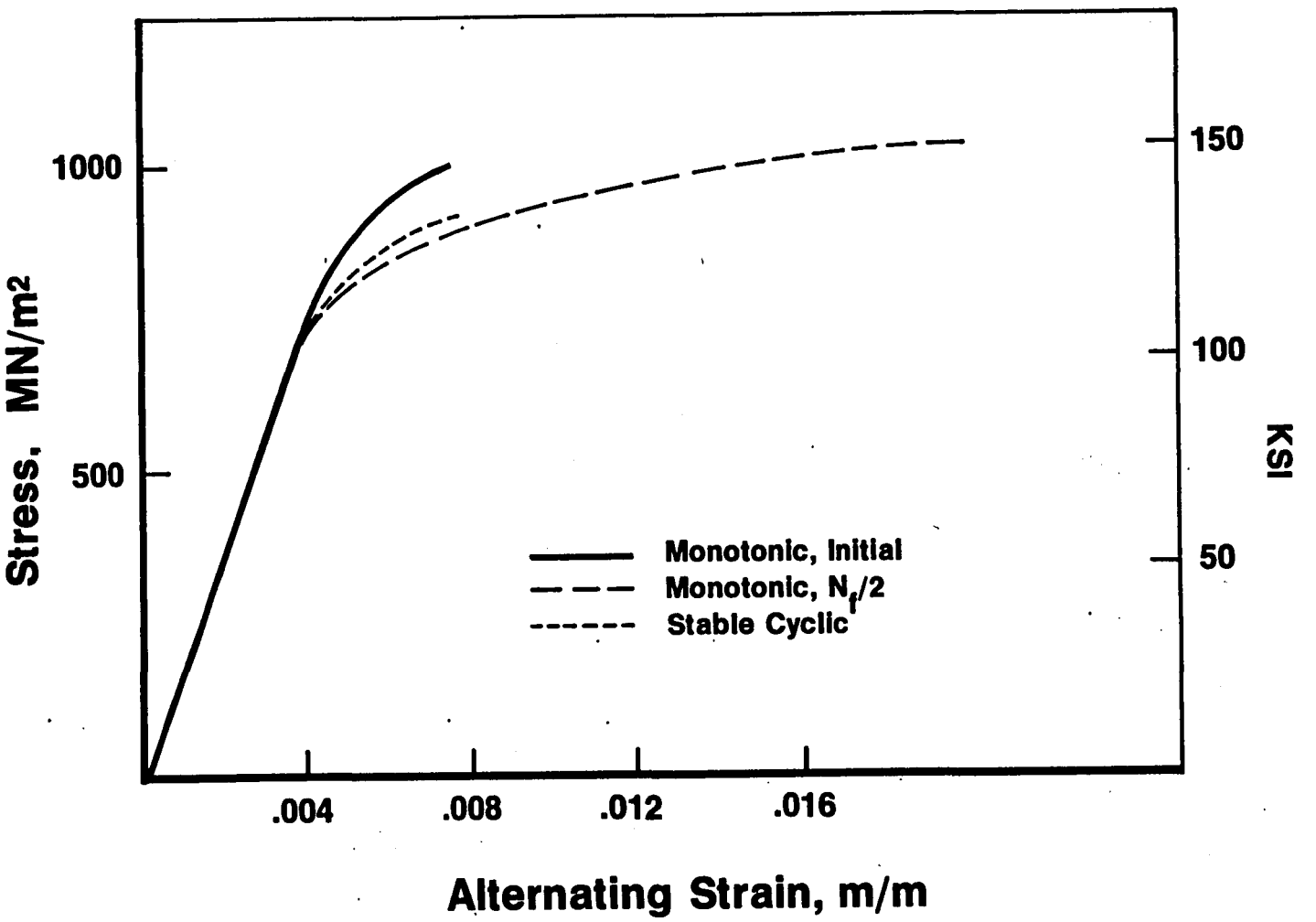

Figure A-1. Comparison of Monotonic and Cyclic Stress-Strain Curves for Inconel 718, R_ε = -1, 343° C.

methods plot either the alternating stress against alternating strain or the maximum stress against maximum strain of the hysteresis loops, σ_T versus ε_T. The bulk of cyclic stress-strain testing has been done under $R_\varepsilon = -1$ conditions; and here, the two definitions yield the same curve. In general, however, the presence of a mean stress in the hystersis loop makes it important to distinguish between the CSSC defined by the loop tips and loop amplitude. For $R_\varepsilon = -1$, the mean stress is zero and, as given in Equation 1, both definitions yield the same CSSC. For other strain ratios with nonzero mean stress, the two definitions produce different cyclic curves. The cyclic curve describes the cyclic softening of the material for all strain ratios. The complete CSSC, defined by the loop tips, includes the mean stress and describes the relaxation and the softening of the material.

It is also necessary to distinguish the two curves for experimental considerations. Testing in the $R_\varepsilon = -1$ condition is advantageous; because, if the test is conducted in the incremental amplitude method of Figure A-2a, the entire CSSC up to $\varepsilon_{max.}$ can be obtained from a single test. This results, Figure A-3a, from the hysteresis loops being nested and centered about the origin. When a constant amplitude test (Figure A-2b) is conducted at $R_\varepsilon = -1$, the hysteresis loop at a given strain range is exactly the same as the loop obtained at the range in the incremental amplitude test. This is not the case, Figure A-3b, for $R_\varepsilon = 0$ tests which produce a mean stress. Moreover, the fact that each hysteresis loop no longer has the same R_ε means that only 1 point on the cyclic curve can be obtained for a given strain range. Figure A-3b shows what this means for $R_\varepsilon = 0$ by pointing out that the hysteresis loop for a constant amplitude test lies outside the envelope for loops generated by the incremental amplitude test even though $\varepsilon_1 < \varepsilon_2$. Obviously, the point in cyclic space corresponding to $2\varepsilon_1$ cannot be obtained from the incremental test at a range of $2\varepsilon_2$.

Mean Stress Effects - Complete Versus Cyclic Amplitude Curves

Figure A-4 shows the difference between the cyclic and complete cyclic curves at 538° C for several values of R_ε for material taken from a single heat of Inconel 718. For small strain ranges, the hysteresis loops contain a mean stress; this produces the humped shape of the complete CSSC. As the strain range increases, sufficient plastic strains are accumulated to allow the mean stress to relax. The material also cyclically softens which contributes to the decrease in maximum stress.

Figures A-5 and A-6 show the same curves with data from two additional heats of $R_\varepsilon = 0$ tests added. These two heats, B and C, show good agreement with the previous cyclic amplitude curve but the maximum stress values lie somewhat below the values from heat A. From relation (1), the variance between heats A, B, and C must be the behavior of the mean stress. Figure A-7 gives the mean stress as a function of strain range for all three heats. There is a linear relation between the mean stress and the strain range for strains less than 1.2% and positive R_ε; for larger strain range, the mean stress approaches zero almost asymptotically. Note that for $R_\varepsilon = -1$, the mean stress is approximately zero for all strain ranges.

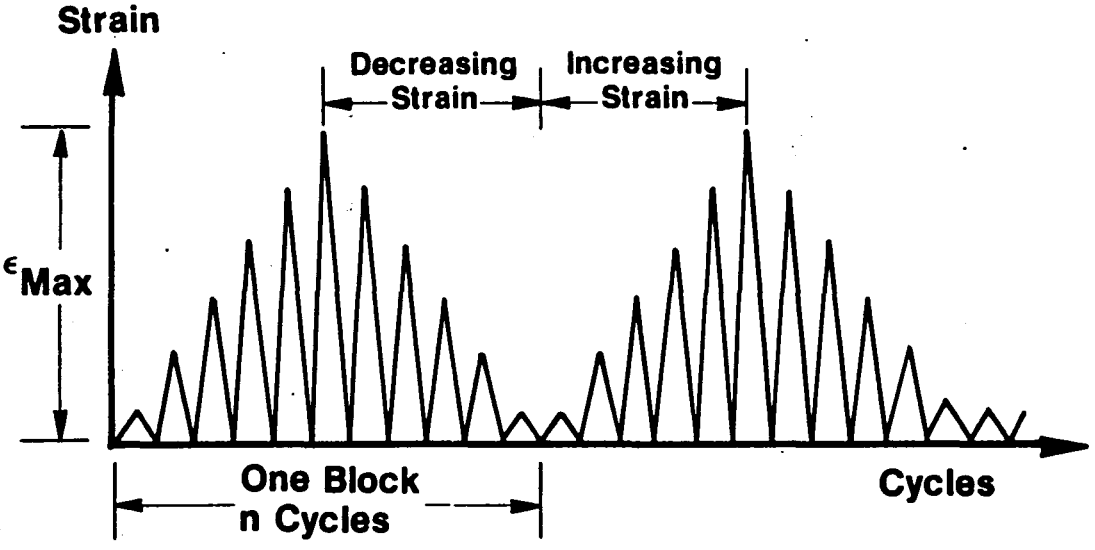

(a) Incremental Strain Amplitude

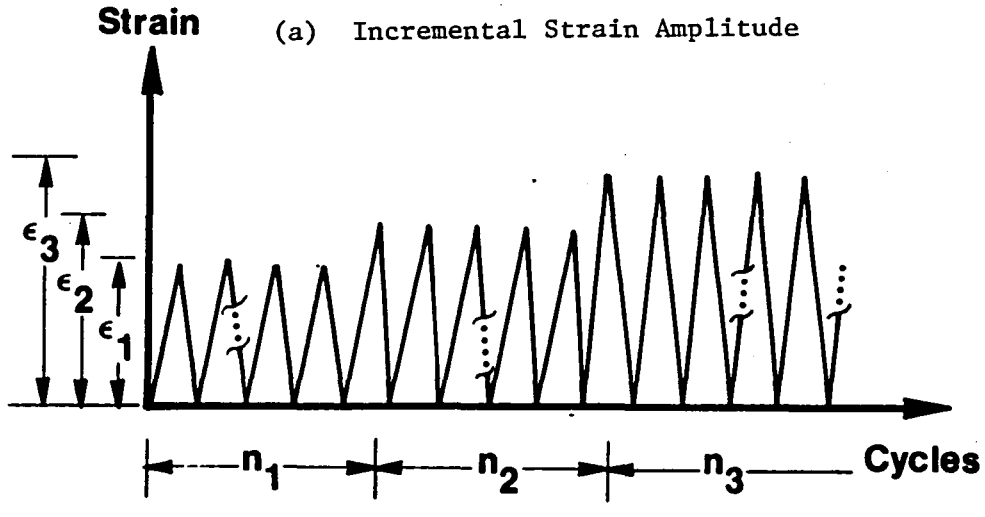

(b) Constant Strain Amplitude Block Sequence

Figure A-2. Strain Cycle Waveforms Used to Obtain Cyclic Stress-Strain Curves.

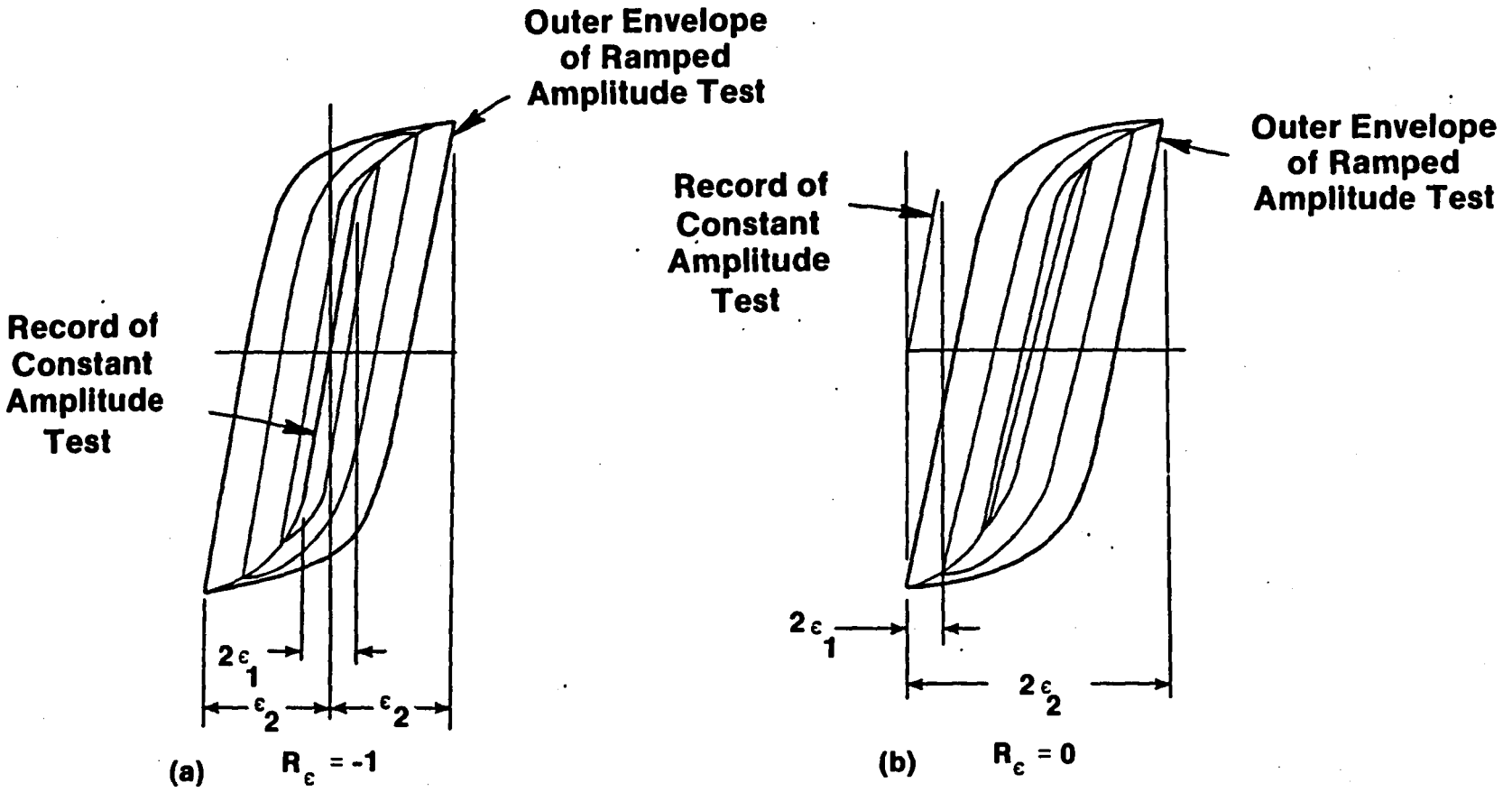

Figure A-3. Comparison of Stress-Strain Records Obtained for Constant Amplitude and Incremental Amplitude Waveforms.

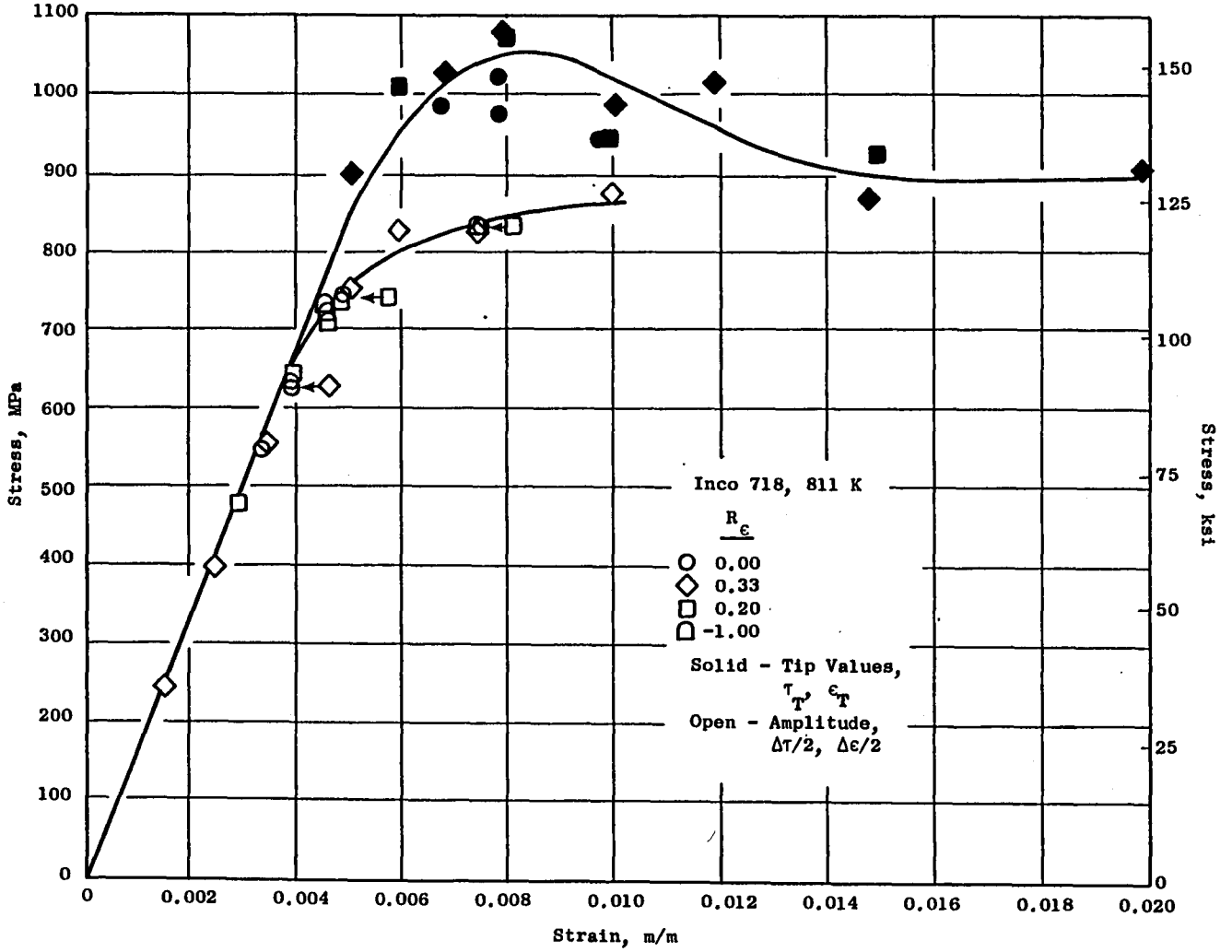

Figure A-4. Effect of Strain Ratio, R_ε, on the Stable Cyclic and Complete Cyclic Stress-Strain Curves at 538° C.

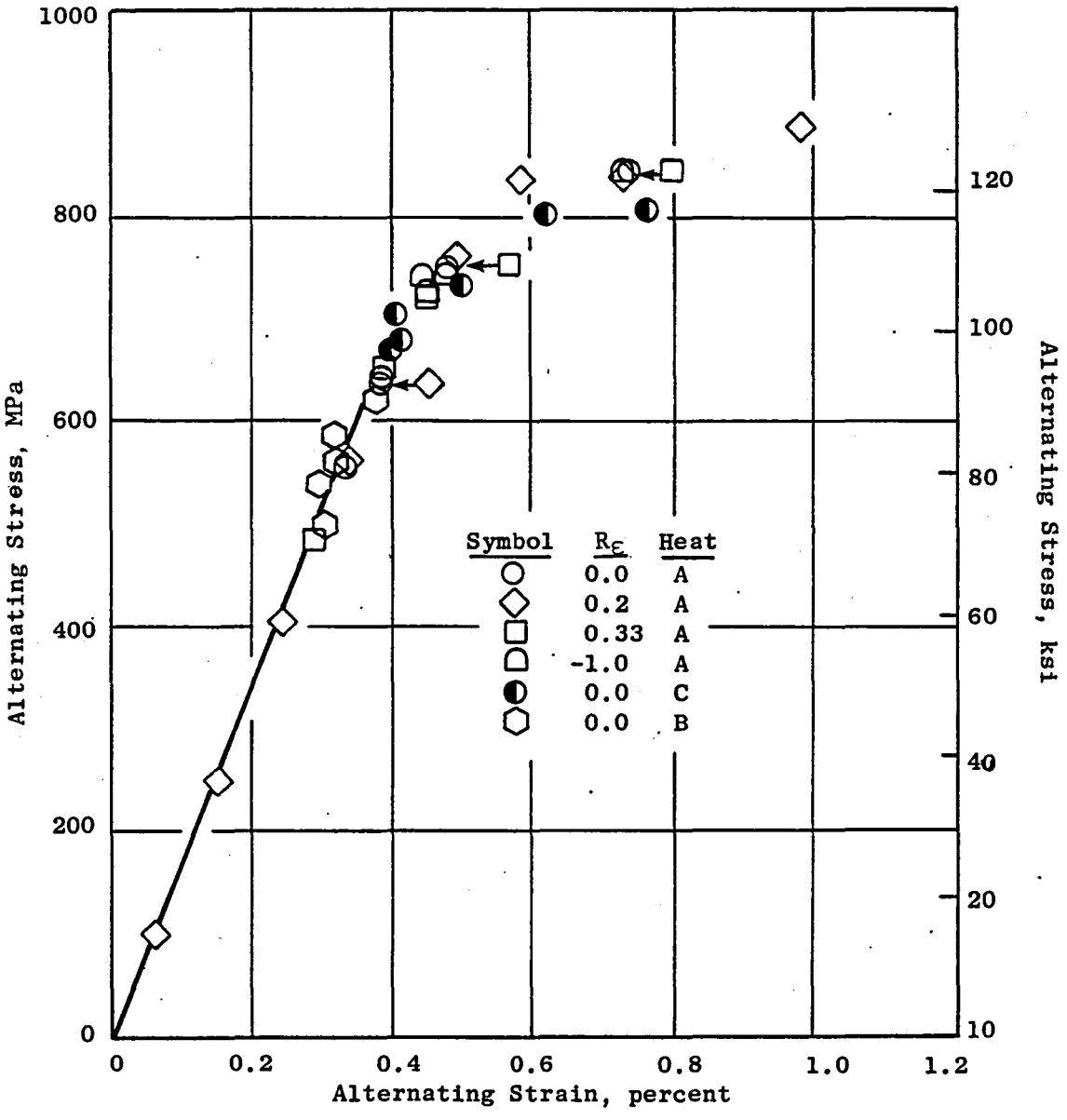

Figure A-5. Alternating Stress Versus Alternating Strain for Inconel 718 at 538° C with R_ϵ as a Parameter.

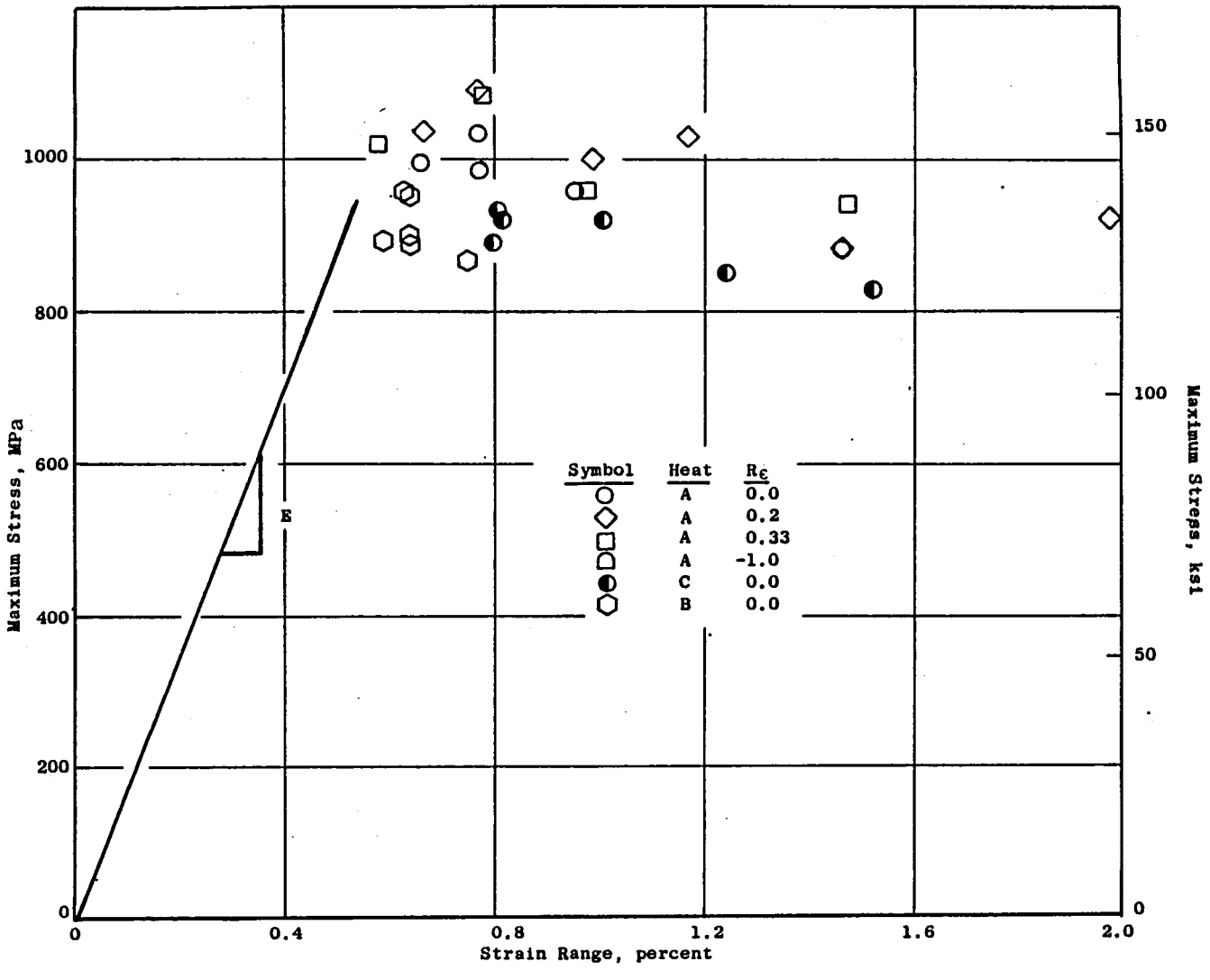

Figure A-6. Complete Cyclic Stress-Strain Curve; i.e., The Maximum Stress Versus Strain Range for Inconel 718 at 538° C.

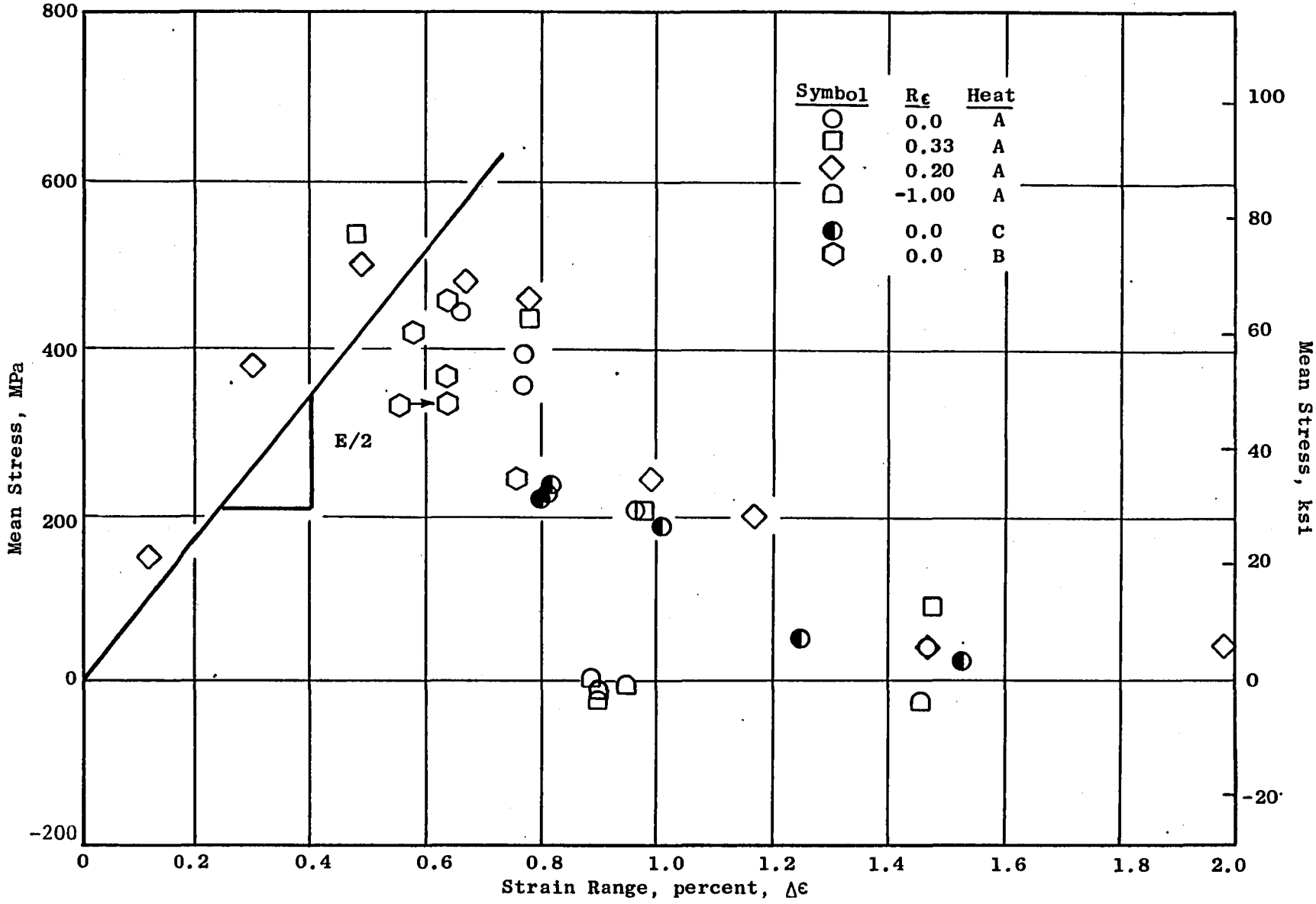

Figure A-7. Mean Stress as a Function of Total Strain Range, 538° C.

Figure A-5 indicates that the cyclic curve is independent of R_ε, but it is unclear whether or not the complete curve is also independent of the strain ratio. To answer this question, some further experiments were conducted at 566° C at several values of R_ε. Figure A-8 shows the cyclic amplitude curves and again demonstrates the independence of this curve on R_ε. The variation in stress at 0.75% strain results from the experimental technique and the inhomogeneous properties of the forging used to obtain the specimens (Reference 3). Figure A-9 plots the mean stress as a function of strain range and indicates a layering of mean stress values as a function of R_ε. Linear fits were made to the data between the elastic line and the strain range 1.1%. When these values were added to the alternating stress from Figure A-8, the complete cyclic curve results, Figure A-10. This curve demonstrates that over the small strain ranges, the complete CSSC does depend on R_ε; but at larger strain, the curve loses this dependence as the mean stress approaches zero. The increase in mean stress over the small strain range is a function of the strain hardening of the initial monotonic curve. That is,

$$\varepsilon_{max.} = \frac{\Delta\varepsilon}{1-R_\varepsilon}$$

and so the higher the value of R_ε, the larger the maximum strain and stress in the hysteresis loop.

Cyclic Softening

It has been pointed out that the humped shape of the complete CSSC results from relaxation of the mean stress and from the cyclic softening of the material. Figure A-1 shows that, even at 343° C, forged Inconel 718 softens considerably throughout its life. The relative roles of relaxation and softening become clearer if the individual stress components of Equation 1 are plotted. Figure A-11 shows this variation for a single specimen cycled at four strain ranges in the constant amplitude block loading sequences of Figure A-2b. The plot shows both softening, as measured by the alternating stress, and relaxation, as gaged by the mean stress, continue throughout the life of the specimen (Reference 4). The actual changes are small but they are, nevertheless, real and can cause problems if half-life values of specimens with very different lives are compared. (This is one of the reasons for the scatter at 0.75% strain in Figure A-6 as discussed in Reference 3.)

Figure A-12 presents another view of cyclic softening. The plastic strain range for two specimens with two values of R_ε is plotted as a function of cycles. The figure shows a small but significant increase in plastic strain over the life of the specimen.

History Dependence of the Cyclic Behavior

The cyclic behavior of a given specimen is the result of the processing history of the material, as well as the particular experimental program. In

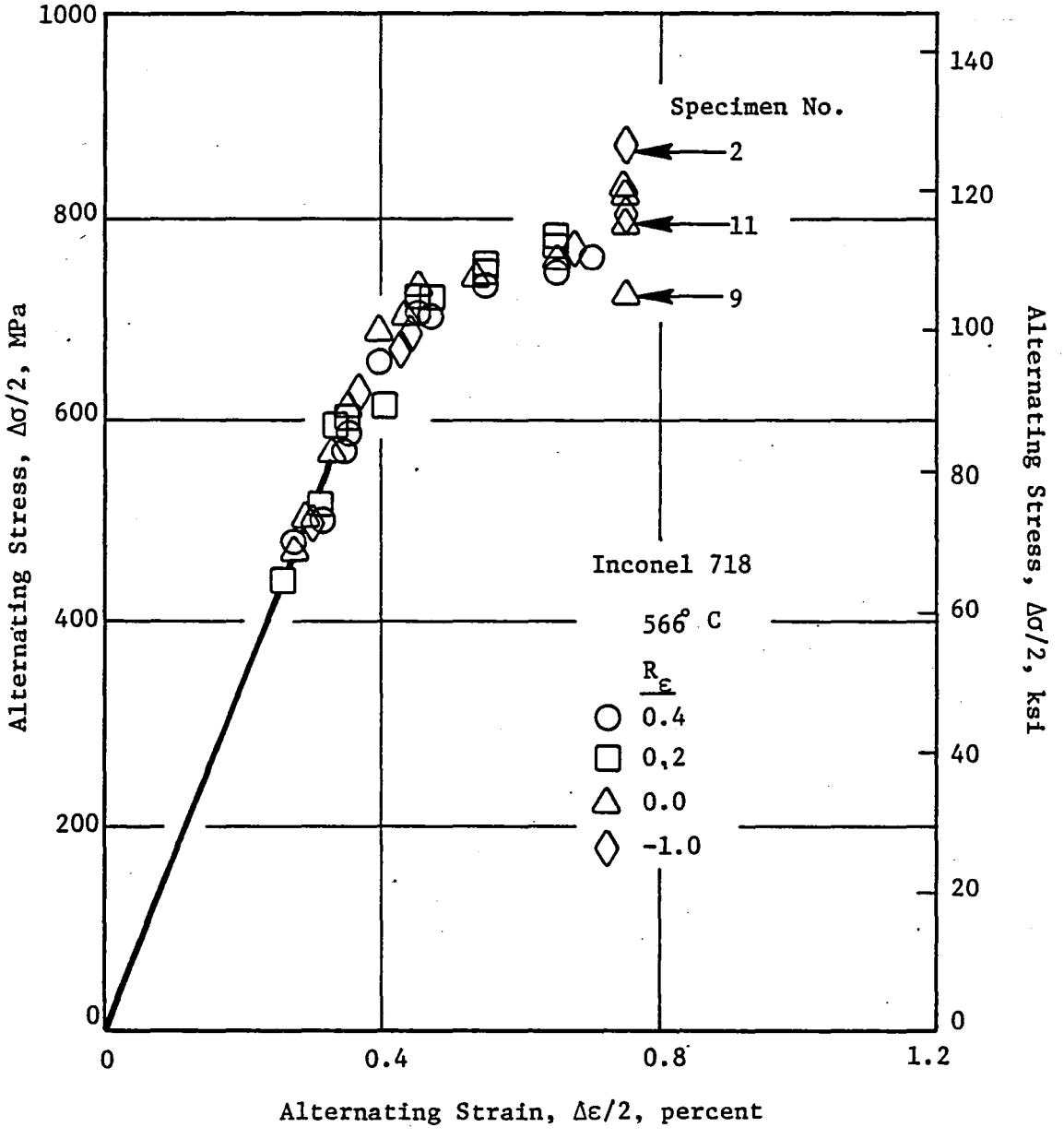

Figure A-8. Alternating Stress-Strain Behavior of Inconel 718, 566° C.

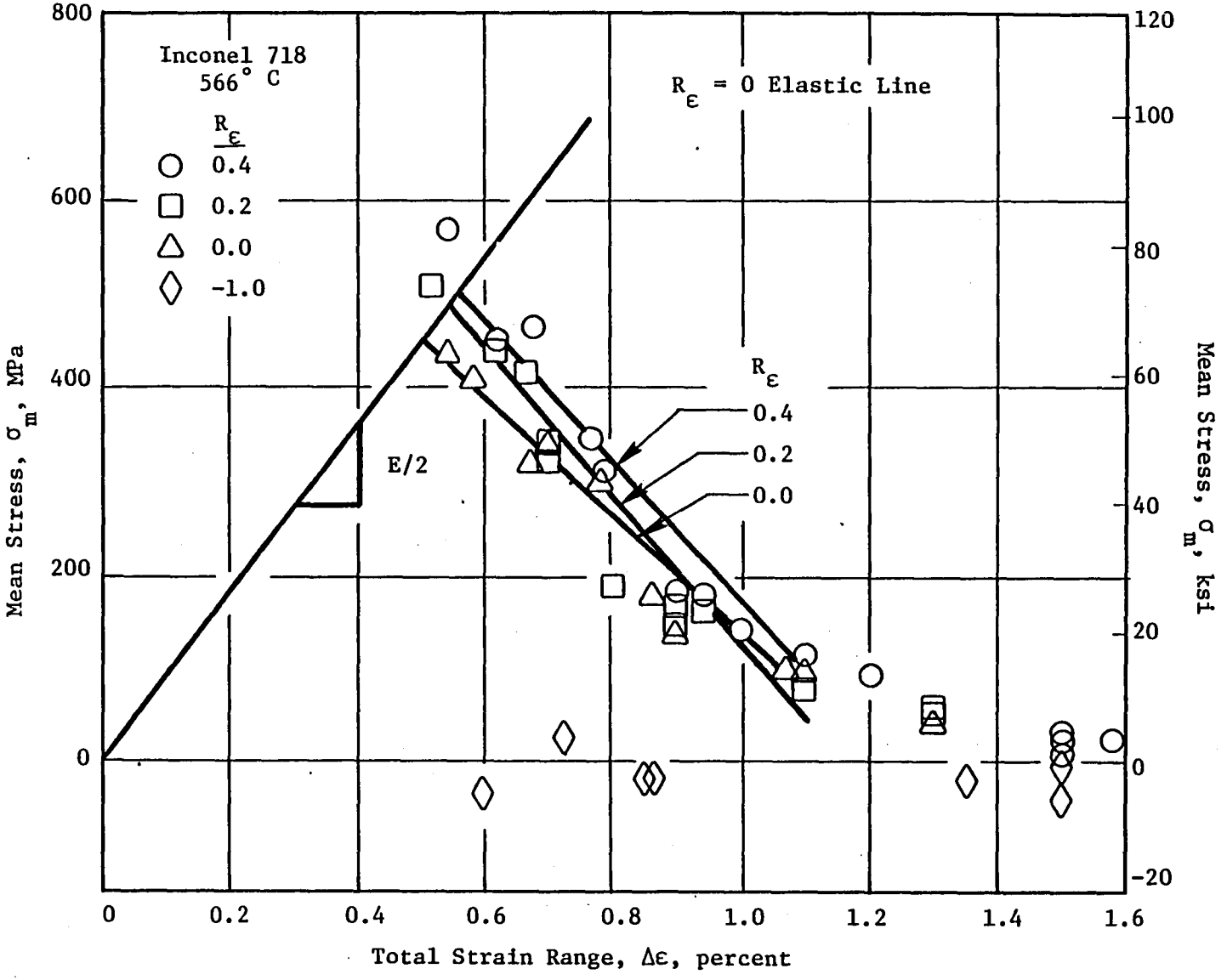

Figure A-9. Development of Mean Stress as a Function of Strain Range, Inconel 718, 566° C.

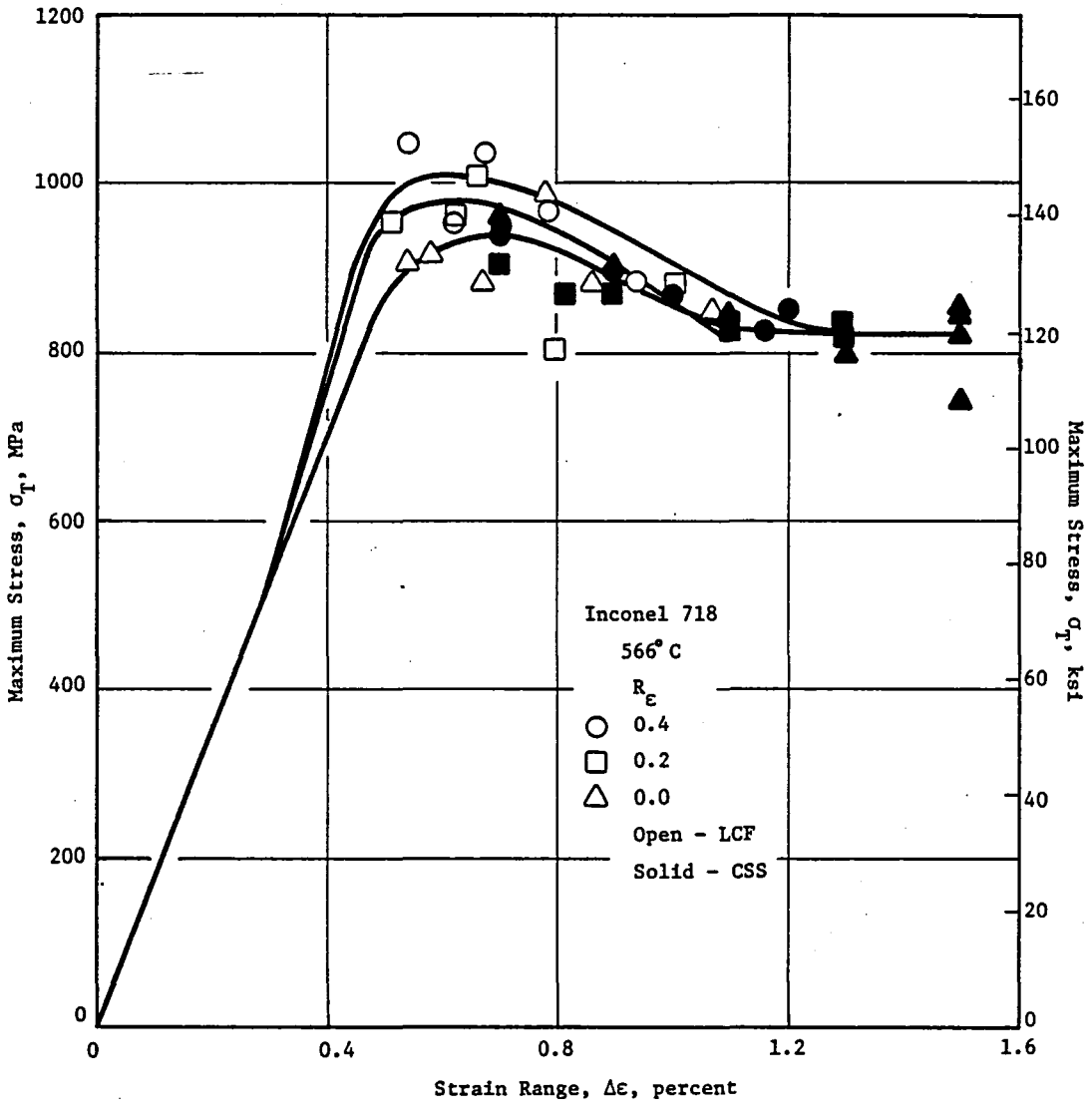

Figure A-10. Complete Cyclic Stress-Strain Curve for Inconel 718, 566° C.

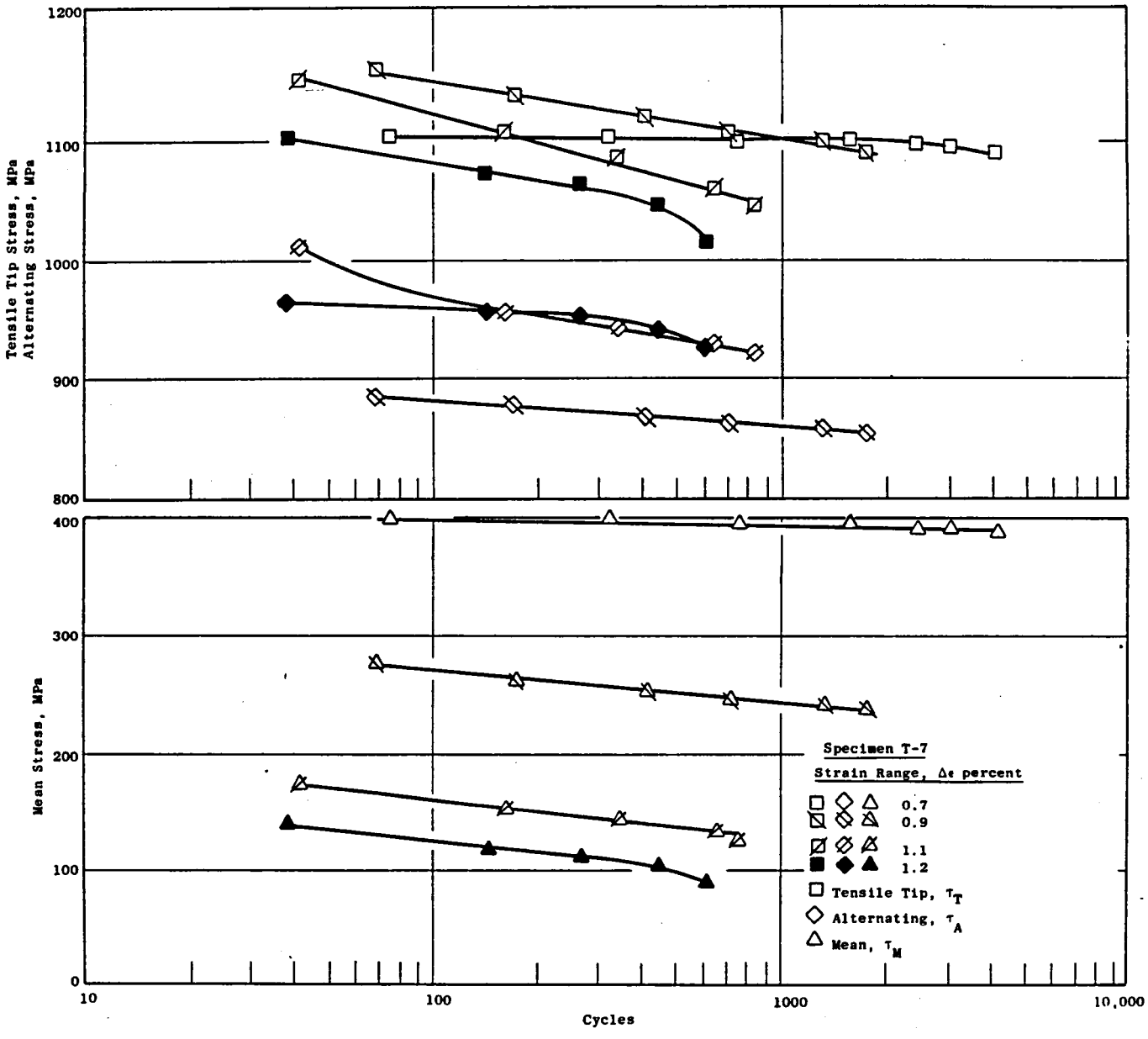

Figure A-11. Variation in Tip, Alternating, and Mean Stress as a Function of Cycles and Strain Range, R_ε = 0, 21° C.

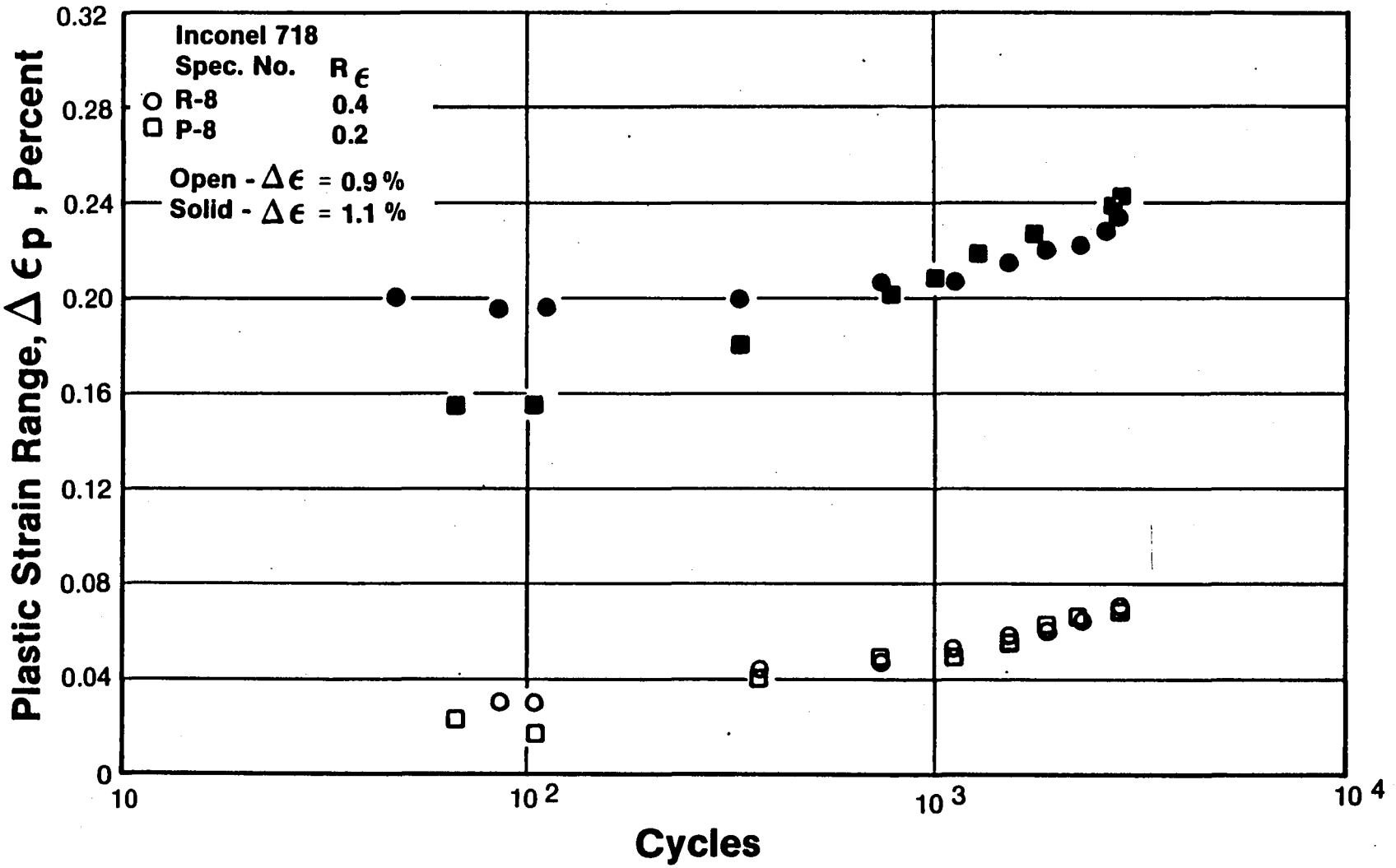

Figure A-12. Development of Plastic Strain in Two Specimens with Different Loading Histories.

light of this, Figure A-12 presents some interesting data on the development of plastic strain during cycling. First of all, a comparison of the portion of the monotonic curves obtained during initial loading of the two specimens showed that specimen R-8 was about 8% weaker than P-8, indicating that the specimens came from quite different areas of the forging. Then, while both specimens underwent incremental strain histories of 150 blocks, the maximum strains were somewhat different, namely

	R_ε	$\Delta\varepsilon$, %
P-8	0.2	0.7,0.9,1.1,1.3
R-8	0.4	0.7,0.9,1.0,1.1,1.2

At the lowest strain level, 0.7% , the plastic strains are very small so these are not plotted. At $\Delta\varepsilon$ = 0.9%, P-8 initially shows less plastic strain as it is stronger, but the difference between R-8 and P-8 rapidly disappears as the specimens are cycled. At the higher strain range, 1.1%, the behavior is similar but for a slightly different reason. Since P-8 was stepped from 0.9% to 1.1%, it has a lower level of plastic strain at the start. Specimen R-8 was raised from 0.9% to 1.0% and then to 1.1%; thus when R-8 began cycling at 1.1%, it already had a much higher level of deformation due to its accumulation of plastic strain at 1.0%. However, the difference in plastic behavior between the two specimens rapidly disappears and the plastic ranges are the same by the end of the cycle block. For these levels of plastic strain, this demonstrates the homogenizing effect of the cycling. At higher levels of strain, this effect is demonstrated by Specimen 9, in Figure A-8, which was much lower than the rest of the specimens at the alternating strain of 0.75%. The initial monotonic curve for Specimen 9 lies midway between P-8 and R-8, but it appears to cyclically soften more than either of these specimens. However, if it is noted that Specimen 9 has longer life and the maximum stress in Figure A-10 raised by 55 MPa, the value lies only slightly below the other stress values in the figure. It appears that the plastic strain was not as effective in "homogenizing" the material in this specimen as much as in R-8 and P-8 but the difference is fairly small. This indicates that the microstructure will not generally be a complicating factor in cyclic constitutive tests and behavior.

APPENDIX A - REFERENCES

1. Cook, T.S., "Cyclic Stress-Strain Behavior of Inconel 718," Mechanical Testing for Deformation Model Development, ASTM STP765, 1982, pp. 269-283.

2. Landgraf, R.W., Morrow, J. Dean, and Endo, T., Journal of Materials, Vol. 1, No. 4, March 1969, pp. 176-188.

3. Cook, T.S., "The Effect of R_ε on Cyclic Stress-Strain Behavior of Inconel 718," submitted for publication.

4. Cook, T.S., "Stress-Strain Behavior of Inconel 718 During Low Cycle Fatigue," J. of Engineering Materials and Technology, Trans. ASME, 104, 3, July 1982, pp. 186-191.

APPENDIX B - CUMULATIVE DAMAGE THEORIES

In this appendix, some cumulative damage theories are described. The first section is essentially an interpretive summary of two earlier cumulative damage review reports (References 1 and 2). The first section is followed by several others where other theories (different than those reviewed in References 1 and 2) are discussed and compared where appropriate to an Inconel 718 data set of two-step loadings. It was found that in more recent cumulative damage theories which might be applicable to hot path component design, each theory contains elements of the general nonlinear damage problem; however, none of the theories encompassed all aspects of the problem. Elements considered to be important included sequence effects (high/low, low/high, etc.) in fatigue and creep rupture, and creep fatigue damage cumulation including differences between tension and compression stresses.

Alternatively, one could consider the creep fatigue problem separately from sequence cumulative damage thereby assuming that the problem of cumulative damage is independent of what actually comprises damage. In essence, this is what would be assumed if many of the theories were applied to a creep fatigue problem, since damage is often expressed in terms of only the cycles to failure and the number of applied cycles for a given loading profile. Whether such a separation can accurately be made remains a question for further research. More generally, what is being addressed in these comments is the problem of assessing "equivalent damage" concepts when a universally accepted definition for damage in elevated temperature thermal-mechanical applications of nickel-base superalloys is nonexistent.

Reviews of Kaehele and O'Neill

About every 10 years, a detailed review is conducted on cumulative damage theories (at least since 1963). The two reviews that are used here are due to Kaehele (Reference 1) in 1963 and O'Neill (Reference 2) in 1970. Kaehele reviews the theories of Valluri, Grover, Corten-Dolan, Freudenthal-Heller, Palmgren-Miner (the linear damage rule), and Shanley. O'Neill discusses the approaches suggested by Machlin, Shanley, Valluri, Palmgren-Miner, Marco-Starkey, Grover, Corten-Dolan, Schranton-Crandall, Swanson, Henry, Manson-Nachtigall-Freche, Gatts, Bluhm, Trobe, Freudenthal-Heller, Kirkby-Edwards and Poppleton. While both reviews are for airframe applications, their conclusions appear relevant for the current study. In this regard, the terse words of O'Neill perhaps best illustrate the state of affairs as of, at least, 1970;

> "Since the linear rule, popularly, if inaccurately, referred to as Miner's Rule, became widely known twenty-five years ago, its deficiencies have inspired numerous modifications and alternative theories; perhaps the most appropriate comment on these efforts is that the linear rule is still the only cumulative damage theory in general use."

and,

"....most of them [the reviewed theories], indeed, are largely empirical with very little theoretical basis."

These comments echo Kaehele's earlier statement,

"In conclusion, no radical 'breakthroughs' appear in the area of cumulative-fatigue-damage evaluation in aircraft structures, either in physical understanding or in theoretical techniques."

With this scenario, a detailed review was not performed of the above-noted earlier theories; instead, an attempt was made to abstract the pertinent concepts involved in various theories by using these two review papers.

At least four recurring themes are found in many cumulative damage theories: (1) crack growth, (2) crack initiation and propagation, (3) damage curve analysis methods, and (4) endurance limit reduction models. In the following paragraphs, these themes are presented as discussed by Kaehele and O'Neill for the various theories.

The concept that cumulative damage can be treated as the growth of pre-existing flaws is a central part of the theories of Valluri, Shanley, and Schranton and Crandall. In general, these theories closely approximate the linear damage rule and deviate from the linear rule only if either the critical crack length or initial crack length is assumed to be stress level dependent. However, the assumption that the critical flaw depends upon stress level (e.g., as in linear elastic fracture mechanics) results in predicting the opposite ordering effects than that observed in fatigue testing. (The order effect results from testing smooth specimens at two different levels of alternating stress, i.e., $\Delta\sigma_1$, are applied first for n_1 cycles which is followed by $\Delta\sigma_2$ until failure. Assuming that the mean stress effect is accounted for, or alternatively negligible, then it is normally found that $M = n_1/N_1 + n_2/N_2 > 1$ if $\Delta\sigma_1 < \Delta\sigma_2$ and $M < 1$ if $\Delta\sigma_2 < \Delta\sigma_1$. In the above, N_1 and N_2 are the cycles to failure corresponding to the stress ranges $\Delta\sigma_1$ and $\Delta\sigma_2$, respectively, being applied alone for the total lifetime; and n_2 is the number of cycles applied during the application of $\Delta\sigma_2$ in the two-step history.) Indeed, if one assumes the Paris law of crack growth,

$$\frac{da}{dN} = A\,[\Delta K]^m \qquad (1)$$

for such two-step loadings; then, the results show that variations from Miner's Rule are obtained as a result of the differences in critical flaw size of the two different stress levels. The small resulting variation from Miner's Rule is opposite that observed in fatigue testing with respect to the sequence of loading effect noted above. In this context, it is also noted that the crack

growth retardation phenomenon that is often observed after a reduction in stress level in a crack-growth test is also diametrically opposed to the sequence effect in fatigue testing.

If the initial crack size is defined as the crack size at the transition from multiple microcracks to a growing single dominant crack, then the notion that the initial crack size is stress level-dependent appears peculiar. Support for this idea comes from Miller and Zachariah (Reference 3) who combine initiation and Stage I propagation and from one of Shanley's theories; both models consider the initial flaw length to decrease with the applied stress level. Certainly from the view of conventional linear elastic fracture mechanics, the threshold relationship

$$\Delta K \alpha \Delta\sigma \sqrt{\pi a}$$

implies that the crack size at which Stage II propagation commences decreases as the stress rises. This is not the model of Miller and Zachariah. They argue that under high stress, the material will form more and larger slip bands; large numbers of microcracks form and grow in these bands. When one of the cracks becomes dominant, it will be relatively large because of the extent of damage in the slip bands. It may be that such an approach is, in fact, an attempt to model the complex process of microcrack initiation and linkup. As pointed out by a recent National Materials Advisory Board report (Reference 4), the process of microcrack initiation and linkup has received little attention from a modeling point of view. In terms of these two theories, which treat the initial crack size as being stress level dependent, it appears that the multiple initiation and linkup process is being combined into a single dominant crack theory.

The concept that damage is comprised of two different phases denoted as initiation and propagation is attributed by Kaehele and O'Neill to Langer and Grover. If a_i denotes the percentage of total life, N_i, consumed in crack initiation at stress range $\Delta\sigma_i$, then the initiation cumulative damage rule is written as

$$\sum \frac{n_i}{a_i N_i} = 1$$

and, subsequently, during the propagation phase

$$\sum \frac{n_i}{(1-a_i)N_i} = 1.$$

It is easily shown that if a_i is constant for all $\Delta\sigma_i$ the linear damage rule results. That the a_i is assumed to be a function of stress level is consistent with the concept that the higher percentage of life is composed of propagation in low cycle fatigue and that initiation comprises the higher life percentage in high cycle fatigue. The evolution of the Langer-Grover theory seems to have currently resulted in the approach of Reference 3, and the double

linear damage rule (Reference 5). In the DLDR, the breakdown of total life into two separate phases is accomplished by the establishment of a so-called "kneepoint" of an otherwise continuous curve. The continuous curve is the result of normalizing an empirical crack length equation for smooth specimens which is a function of cycles to failure and universal constants. The resulting two-phase equations do not, therefore, actually represent initiation and propagation lifetimes. This is by design as the authors state that their earlier work with the initiation and propagation concept resulted in physical inconsistencies. Despite this empirical background, our comparison of the DLDR with some two-step Inconel 718 data shows a reasonable correlation as will be discussed later.

Another theme present in several methods is that which can be called damage curves. The basis of the DLDR is an example of such an approach, and as is shown by Kaehele, several of the previously mentioned methods can be cast into this format. Figure B-1 illustrates the idea. In Figure B-1a, the curve is for a stress-independent theory, while Figure B-1b is for a stress-dependent theory. If interactions are not included in a given theory, then the damage curve in Figure B-1a can be expressed as

$$D = f\,[\Sigma(n_i/N_i)].$$

However, this expression results in the Palmgren-Miner Rule at failure. For the stress-dependent theory, Figure B-1b, a sequence effect is predicted. Two theories of this type are given by Marco and Starkey and by Corten and Dolan. In the Marco-Starkey theory, damage is defined as

$$D = \left(\frac{n}{N}\right)^x$$

where the exponent x is dependent upon stress level. The original Corten-Dolan theory can also be cast into this form; however, in subsequent work, the exponent was considered to be constant, and the sequence effect was modeled through an interaction term (called the damage-nuclei number). This latter interaction term gave rise to the idea of developing an effective S-N curve which is based upon experimental data; total life is then to be assessed using the Palmgren-Miner Rule in conjunction with the fictitious curve. The idea of a fictitious curve is also developed in the Freudenthal-Heller theory. In both cases, the effective curve is based on test results involving loadings that approximate that of the structure. In neither case is damage cumulation viewed in an incremental fashion; the effective curve is simply used with the linear rule. The idea of using effective curves that change as a function of loading history is embedded in the Manson, Nachtigall and Freche theory (as reviewed by O'Neill) and the later theory due to Hashin, et al. (References 6 and 7). These two theories are related as shown later.

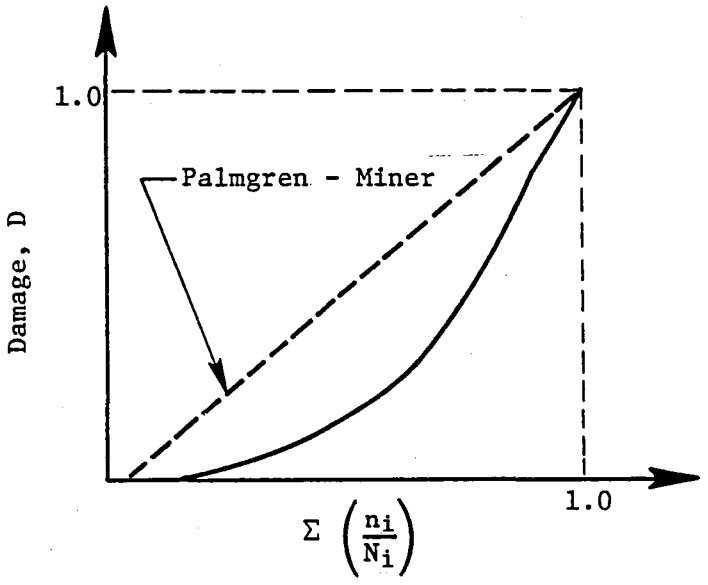

(a) Stress Independent Theories - After Kaehele

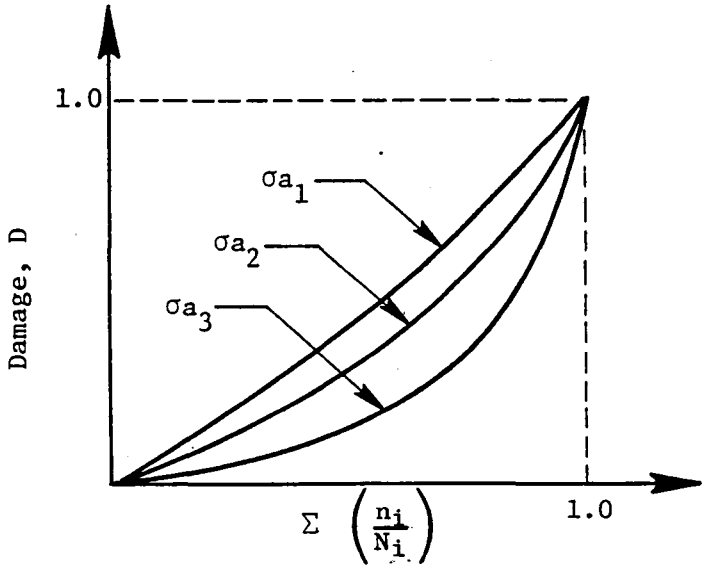

(b) Stress Dependent Theories - After Kaehele - For the Observed Sequence Effect $\sigma a_1 > \sigma a_2 > \sigma a_3$

Figure B-1. Damage Curve Concept.

The final theme that is found in cumulative damage theories is that damage is related to a reduction in endurance limit as a function of stress history. This concept is found in the theories of Henry; Gatts; Manson, Nachtigall and Freche; Bluhm; and a theory developed by Dubuc, et al. (Reference 8) which will be reviewed later in this appendix. These theories are somewhat problematical (with the exception of the Manson, et al. theory) for the current application since they rely heavily on the concept of an endurance limit. Generally, such an endurance limit is either not useful for elevated temperature applications involving major and minor cycle legs since the components are designed for finite lifetimes, or an endurance limit is not exhibited in high cycle fatigue testing at high temperatures due to, at least, time-dependent phenomena. Regardless of the absolute existence of such a stress level, the concept could be useful if a fictitious or, better, "realistic" level is demonstrated consistently and good correlations are achieved. For these reasons, we have reviewed the method of Dubuc, et al.

As is previously mentioned, the methods of Manson, et al. and Hashin, et al. (References 6 and 7) are found to have strong similarities. In fact, mathematically, the two methods are shown to be mirror images of each other. To understand these approaches, consider Figure B-2 where it is assumed that the original S-N curve can be formulated as $f(S) = A\ N^{-\alpha}$ where $f(S)$ is some function of stress, S; A and α are constants; and N is the cycles to failure. Furthermore, it is assumed that a stress of magnitude, S_1, is applied for n_1 cycles [$n_1 < N(S_1)$]. The function $f(S)$ could be any function and, therefore, might be capable of modeling any S-N curve shape. The rules that are developed by the two methods apply for any such functional stress dependence; Hashin, et al. developed the method for log linear and semilog linear dependence, while Manson, et al. apparently considered only log-linear dependence.

After the application of n_1 cycles of stress level S_1, the approach of Hashin, et al. is to assume that a life-used curve can be developed which passes through the point $[f(S_1), n_1]$; the remaining life for any other stress level is assessed as the difference between the new curve and the old curve. Writing the new curve as

$$f(S) = A^1 N^{-\beta} \qquad (2)$$

the three possibilities that result are detailed in Figures B-2a, b, and c:

1. $\alpha = \beta$, which yields to Palmgren-Miner Rule, Figure B-2a.

2. $\beta > \alpha$, which yields a rule with the reverse sequence effect when compared to fatigue test results, Figure B-2b.

3. $\alpha > \beta$, which yields a method with comparable sequence effect to that observed in fatigue testing, Figure B-2c.

Since Approach 3 is the most appropriate method, it is examined in what follows. For a two-step history, the result of method 3 is

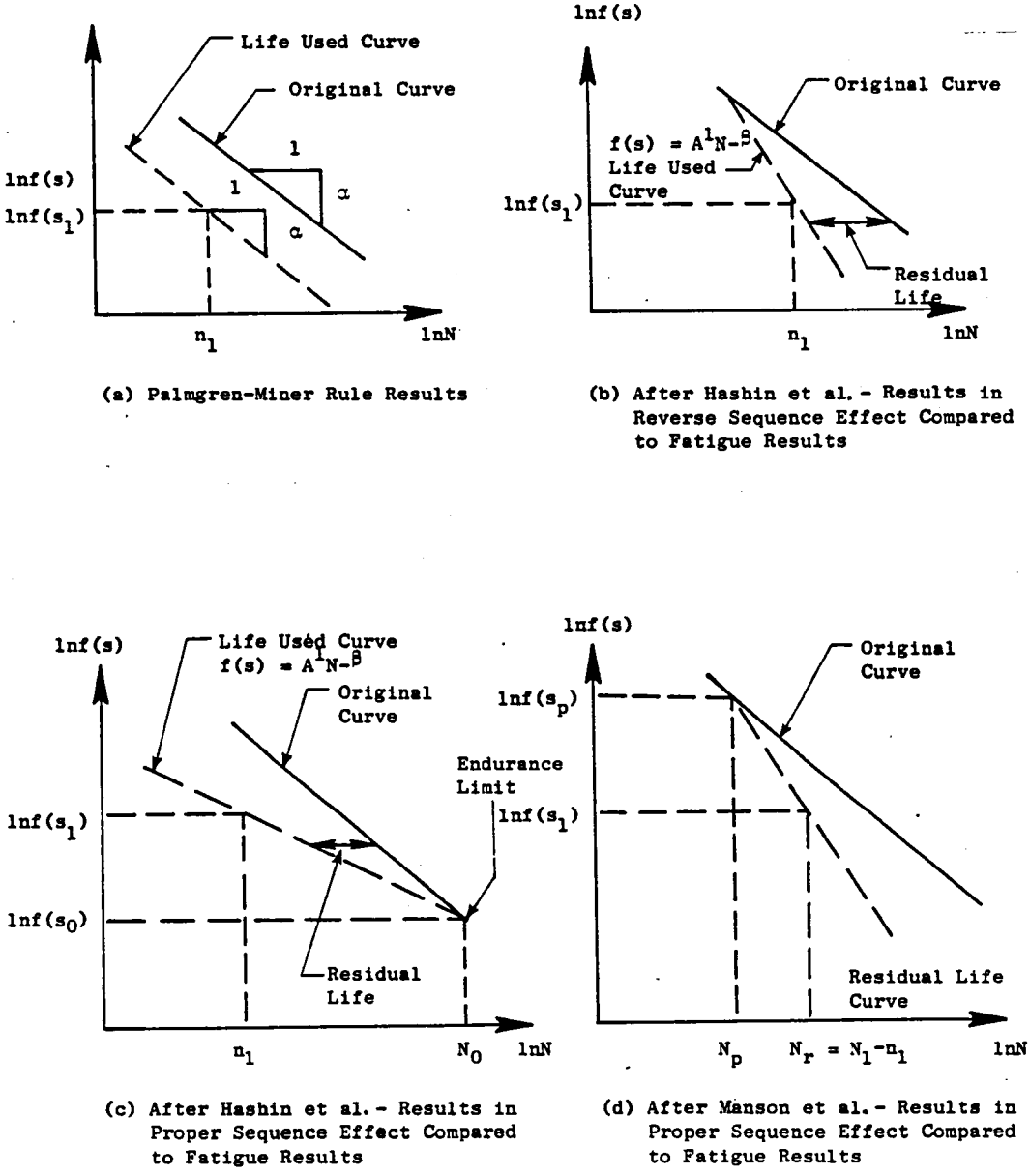

Figure B-2. Comparison of the Approaches of Hashin, et al. and Manson, et al.

$$\beta_2 = \frac{n_2}{N_2} = 1-\beta_1^{\ln(N_o/N_2)/\ln(N_o/N_1)} \quad (3)$$

where $\beta_1 = n_1/N_1$ and N_o is the break point of Figure B-2c.

The approach of Manson, et al. determines the new curve differently. The form of the curve is assumed to remain the same, but the curve rotates about the point $[f(S_p), N_p]$ that is shown in Figure B-2d. The new-rotated curve is also assumed to pass through the point $[f(S_1), N_r]$ where N_r is the residual life at stress S_1 [i.e., $N_r = N_1 - n_1$, $N_1 = (A/f(S_1))^{1/\alpha}$]. For a two-step loading history, this method yields,

$$\beta_2 = (1-\beta_1)^{\ln(N_2/N_p)/\ln(N_1/N_p)} \quad (4)$$

Equation 4 can be inverted for direct comparison with Equation 3,

$$\beta_1 = 1-\beta_2^{\ln(N_1/N_p)/\ln(N_2/N_p)} \quad (5)$$

Comparing Equations 3 and 5, it is seen that the forms are identical, and that the exponents depend upon the relative magnitude of N_1 and N_2 to the point of rotation for the new curve (Figures B-2c and d). The results of the two methods are mirror images in that if the ratios of cycles are identical (such that the exponents are the same) then the relationship between β_1 and β_2 is reversed as is expressed by Equations 3 and 5. The identical cycle ratios between the two methods require that the proximity of the N_i to either N_o or N_p be the same. Since N_o is on the order of 10^7 cycles while $N_p \sim 10^3$ cycles, the predicted relationship between β_1 and β_2 is the same as the N_i approaches N_o for the Hashin method and as the N_i approaches Np for the Manson, et al. method. All of the above discussion is summarized in Figure B-3.

The question remains, which, if either, of the two methods is correct. The comments in Reference 9 by Manson seem to be appropriate here. In Reference 9, Manson, an author of the previously mentioned DLDR, points to discrepancies between the method of Equation 4 and an older version of the DLDR through data comparisons. He shows that the DLDR predicts not only a rotation tendency but also a translation of the residual life curves (e.g., Figure B-2d). The data also tend to show a similar tendency of rotation and translation. Thus the method of Equation 4 appears overly simplified. However, with respect to the method of Hashin, et al., it appears:

1. The construction of the residual curves is incorrect since the rotation of the data is basically as shown in Figure B-2d

2. Actual comparisons would have to be made to confirm this suspicion.

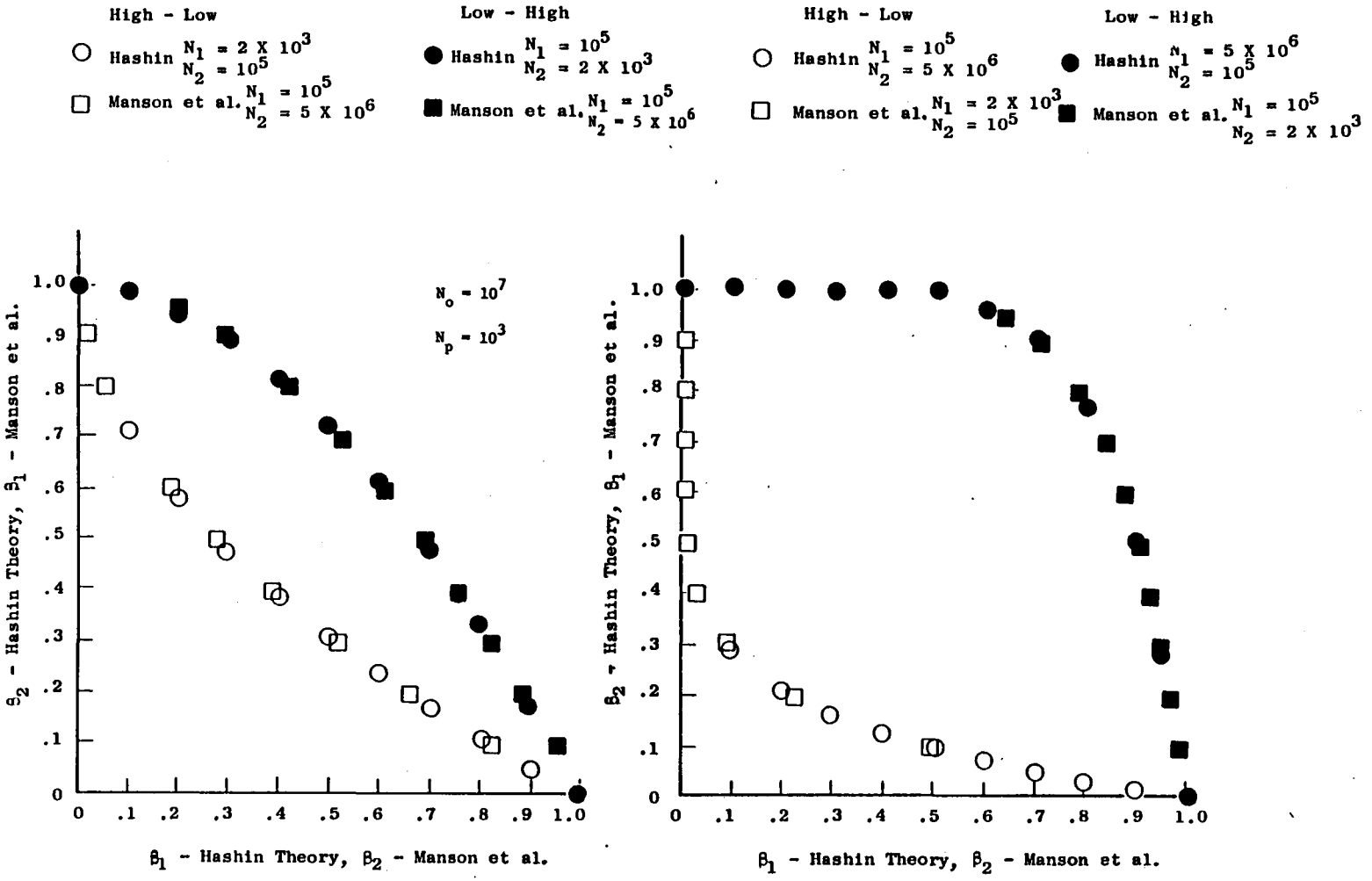

Figure B-3. Comparison of the Methods of Hashin, et al. and Manson, et al.

Finally, it is noted that both methods are insensitive to the actual selection of N_o and N_p. In addition, as reviewed by O'Neill, the method of Manson, et al. also contains a model for the reduction of endurance limit. This is not detailed in Reference 2 so we have not included it in this comparisons.

Ecole Polytechnique Approaches

The approaches suggested by Bui-Quoc, Biron, Dubuc, and colleagues for cumulative damage fatigue are given in References 8 and 10 to 15; Reference 16 suggests an approach for cumulative damage in creep rupture testing. Their first method is detailed in Reference 8 with References 12, 14 and 15 giving extensions to the basic approach. In References 10 and 11, these authors change from the previous approach of Reference 8 to a method that is patterned after an earlier version of the double linear damage rule which is given in Reference 17. The approach of Reference 8 develops separate methods for stress- and strain-controlled experimental data. In Reference 10, it is apparent that the sequence effect in strain control is greater than could be predicted by the earlier method; and, therefore, the DLDR approach-based model is developed. As will be shown, the strain-controlled sequence effect in Inconel 718 appears to be larger than is predictable by either of these methods.

Here, only the strain-controlled theory of Dubuc, et al. (Reference 8) is considered since the theory is compared to strain-controlled data. It is noted that the theory is considered by the authors to be a unifying approach since elements from the methods of Shanley, Valluri and Gatts are inherent parts of their theory. The stress control theory is developed first in this paper, and the strain control theory follows by analogy. Here, we will outline the important features. Since the theory is developed first for stress control, a strain parameter, λ, is defined which translates the shape of an $\Delta\varepsilon$-N curve to that of an S-N curve:

$$\lambda = 1 + \ln (\varepsilon/\varepsilon_o) \tag{6}$$

where ε is the total strain amplitude, $\varepsilon_o = \sigma_e/E$, σ_e is the endurance stress amplitude, and E is Young's modulus. Based on the concept of Gatts, it is assumed that

$$\lambda e = (\lambda_s/\lambda_f)^m \tag{7}$$

where,

λe = instantaneous endurance strain parameter = $1 + \ln (\varepsilon'_o/\varepsilon_o)$
λ_s = instantaneous ductility parameter = $1 + \ln (\varepsilon'_f/\varepsilon_o)$
λ_f = original ductility parameter = $1 + \ln [(1-R)\varepsilon_f/\varepsilon_o)]$
m = an empirical constant
ε'_o = instantaneous endurance strain
ε'_f = instantaneous ductility
ε_f = true fracture strain (presumably, $\varepsilon_f = -\ln (1-RA)$ where RA is the reduction in area).

(The theory due to Gatts actually assumes that the strength and endurance limit stresses are linearly related. Gatts' assumption appears consistent with the concepts of linear elastic fracture mechanics in that the ratio of endurance stress to failure stress would equal the ratio of the threshold stress intensity level to the critical stress itensity level.)

Then assuming damage is related to the rate of change in endurance limit per cycle, and based on assumptions taken from the above mentioned theories, it is found that,

$$\frac{d\lambda e}{dn} = -\frac{1}{K}\left(\frac{\lambda-\lambda'}{\lambda}\right)^{b}(\lambda-\lambda_e)^2 \tag{8}$$

where λ is the maximum strain parameter $[1 + \ln(\varepsilon_{max.}/\varepsilon_o)]$; λ' is the minimum strain parameter $[1 + \ln(\varepsilon_{min.}/\varepsilon_o)]$; n is cycles; and K and b are constants. Defining failure as

$$\lambda_{ef} = (\lambda/\lambda_f)^m$$

the total life, N, is found to be given by the equation,

$$N = \frac{K_\varepsilon}{(1-R)}\lambda^{-c}\left[\frac{1}{\lambda-1} - \frac{1}{\lambda - (\lambda/\lambda_f)^m}\right] \tag{9}$$

where c is a constant that is found to depend upon the R-ratio, and K_ε is a constant which is related to K in Equation 8. Empirical relationships are derived for determining the endurance limit strain and the value of c for R = -1 from tensile properties. For use with other R values, the Gerber relation is used to develop an expression for the endurance limit strain as a function of R. Similarly, an empirical relationship for the R dependence of the exponent is given. It is noted that one of these empirical relations is subsequently changed in Reference 15.

Based on the Gerber equation, the following expression is developed for the relationship between the R-dependent endurance strain, ε_o, and the corresponding strain at R = -1, ε_o^* :

$$\frac{\varepsilon_o}{\varepsilon_o^*} = \frac{\Delta\varepsilon_o}{\Delta\varepsilon_o^*} \equiv \xi(R) = \frac{\gamma_u^*}{2}\frac{(1-R)}{(1+R)}\left[-\gamma_u^*\frac{(1-R)}{(1+R)} + \sqrt{4+\left[\gamma_u^*\frac{(1-R)}{(1+R)}\right]^2}\right] \tag{10}$$

where $\gamma_u^* = \sigma_u/(E\varepsilon_o^*)$. For later reference, the relationship between R dependent exponent c is given by,

$$\frac{c}{c^*} = \left\{\left[1 + \ln\frac{2\xi(R)}{1-R}\right]\left[\frac{\ln(\varepsilon_f/\varepsilon_o^*)}{\ln(\varepsilon_f/\varepsilon_o)}\right]\right\}^{1/6} \tag{11}$$

(c^* is the value of c for R = -1), and the empirical relationship between the strain range at 10^5 cycles (ε_s^*) and the endurance strain is given as,

$$\frac{\varepsilon_o^*}{\varepsilon_s^*} = 0.6 \tag{12}$$

To predict the sequence effect, the theory assumes

$$\frac{dD}{dn} = -\mu \frac{d\lambda_e}{dn} \tag{13}$$

where D is damage, n is cycles, and μ is a constant. Substituting Equation 8 into Equation 13, and normalizing the value of D at failure to be unity, D is given as

$$D = \frac{\beta\,(\lambda-1)}{\beta(\lambda-1) + (1-\beta)\,[\lambda - (\lambda/\lambda_f)^m]}, \tag{14}$$

where β is the cycle ratio n/N. A consistent damage curve analysis is then used (this is a stress-dependent theory in Kaehele's nomenclature, Reference 1) to define damage cumulation. For a two-step history, the predicted sequence effect is given as,

$$\beta_2 = \frac{n_2}{N_2} = 1 - \frac{D_1\,[\lambda_2 - (\lambda_2/\lambda_{f2})^m]}{(\lambda_2 - 1) + D_1\,[1-(\lambda_2/\lambda_{f2})^m]} \tag{15}$$

where D_1 is the amount of damage that is predicted by Equation 14 for conditions of β_1, λ_1, and λ_{f1}. For future reference, it is noted that Equations 14 and 15 can be combined to yield,

$$F\left[\left(\frac{\lambda_1}{\lambda_{f1}}\right)^m - \lambda_1\right] - \left[\left(\frac{\lambda_2}{\lambda_{f2}}\right)^m - \lambda_2\right] = 0 \tag{16}$$

where,

$$F = \frac{(1-\beta_1)\,(1-\beta_2)}{\beta_1\,\beta_2}\,\frac{(\lambda_2 - 1)}{(\lambda_1 - 1)}$$

To evaluate this theory requires an estimate of the endurance limit strain, ε_o, since it is required in the basic definition of λ (Equation 6), and since the basic sequence data to be evaluated are Inconel 718 data

at 566° C, ε_o is estimated from strain-controlled continuous cycling baseline data at 566° C. Figure B-4 shows a comparison of the fit of Equation 9 to a general curve fit which was developed by General Electric. This curve fit is based on data for the same material at several temperatures (including 566° C) and strain levels. To establish the value of ε_o (and ε_o^*), several attempts were made using Equations 10 and 12, all of which yielded values that appeared too high. In these estimates, use was made of an empirical relationship given in Reference 8 which is $\varepsilon_o^* = 0.36\sigma_u/E$. (In Reference 15, this estimated value is further expressed as a function of temperature and melting point temperature which in the present case resulted in only a 7% change in the value otherwise calculated.) Finally, it was assumed that Equation 12 was correct when the actual value of ε_s was used. This gave the value of ε_o which was used to develop the curve in Figure B-4. The curve fit of Equation 9 was obtained by using this value of ε_o and rearranging the equation such that linear regression could be used. In these calculations, m was assumed to be eight as is used in all of the reviewed references. It was noted that this c value was predicted by the empirical relations in Reference 15, but K_ε was not.

With the value of ε_o thus obtained, predictions of the sequence effect were made using Equations 14 and 15 and compared to actual data as shown in Figure B-5. It was demonstrated that the predicted sequence effect by this method was much less than was observed experimentally. The outer dotted line in Figure B-5 was developed by optimizing the value of m such that the differences between the predictions and the data were minimized. This optimization was accomplished by iteratively solving for the value of m which would satisfy Equation 16 for each of the sequence data points. A reasonably consistent value of m was found for all the data using this technique; the average value was $\bar{m} = -0.94$. Even though this negative value of m is physically meaningless, in terms of Equations 14 and 15, it gave good predictions of the data as shown in Figure B-5. The authors in Reference 8 specify that m should be greater than unity, but suggest that a value different than eight might be required for high strength steels.

One other aspect of this analysis needs to be mentioned. In the analysis, R was assumed to be a constant value of zero, which was not exactly true in the experimental work. Since the R-ratio changed when the strain range was changed in these tests, it is possible that β_2 in Figure B-5 might be incorrectly calculated since the cycles to failure would conceivably be less due to the change in R-ratio. The high/low sequence involved the biggest change such that a second strain range was applied with R being on the average 0.4; in the low/high sequence, the second R value was 0.13. In Appendix A, some general observations are given on the stress strain behavior of Inconel 718 as a function of R-ratio.

To approximate the influence of R-ratio, Equations 9 to 11 were used to calculate the predicted cycles to failure for each R-ratio. These calculations showed that the Dubuc, et al. method would predict that the cycles to failure for the second strain range in the high/low sequence would change by 23%; for the second block of the low/high sequence, the cycles to failure would change by 8%. The data points in Figure B-5 were then changed to reflect

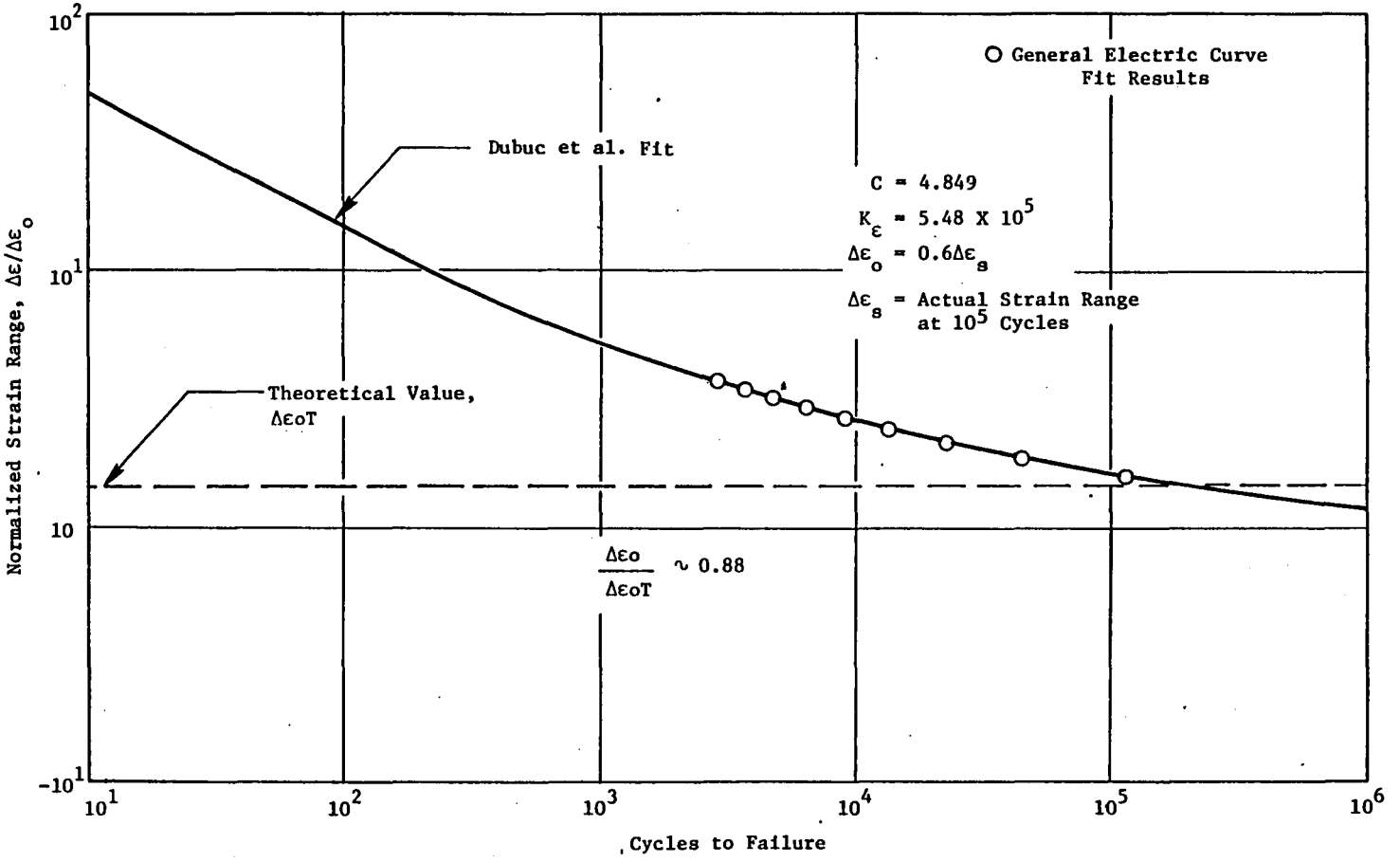

Figure B-4. Estimated Strain-Life Behavior for Inconel 718, 566° C (1050° F), R = 0.

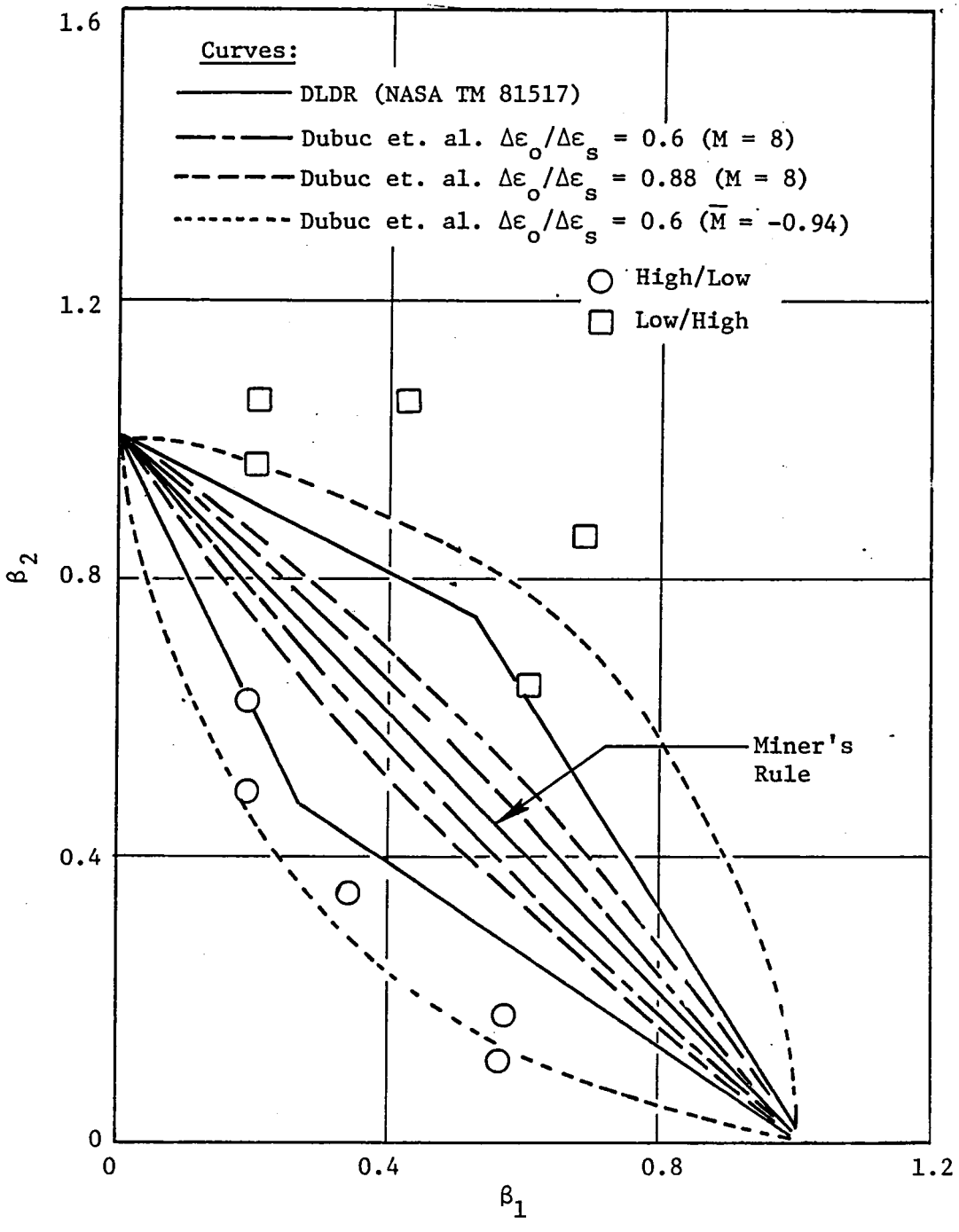

Figure B-5. Sequence Test Results Versus Theories, Inconel 718, 566° C (1050° F).

this difference as is shown in Figure B-6. Recalculation of the predicted sequence using Equations 14 and 15 showed that the predicted lines in Figure B-5 did not change materially when account was made of the R-ratio effect. Thus it appeared that although the data changed relative location the theory still underpredicted the sequence effect.

DLDR Techniques

References 5, 10, 11 and 17 develop DLDR techniques for cumulative damage fatigue. These methods were used to predict the sequence effect for Inconel 718 as is shown in Figure B-7. As shown, all methods tend to underpredict the observed effect, although the prediction of the method of Reference 5 was the best.

With respect to the DLDR, it is noted that the Reference 18 demonstrates an experimental-based approach for developing the exponent in the DLDR (Reference 5). That is, damage in Reference 5 was assumed to be given by

$$D \propto \left(\frac{n_1}{N_1}\right)^{\frac{2}{3} N_1^{0.4}}$$

whereas in Reference 18,

$$D = \left(\frac{n_1}{N_1}\right)^{\alpha}$$

where α is expressed as a polynomial in (log N). Comparisons of predictions of the two approaches with complex block-loaded specimens show that the experimental-based approach gives better results. Thus, while evaluation of the method of Reference 5 has shown it to be the best for the Inconel 718 data, there is concern in concluding that it will always correlate as well as is demonstrated. However, as a prediction scheme for these data, it is the best that has been found.

Ostergren and Krempl Approach

In Reference 19, a method is presented for representing the creep fatigue damage in metals; however, the approach cannot predict a sequence effect. Thus from the point of view of equivalent damage measures, this method does not appear to be of interest to this study. However, the intent of the paper is to elevate life prediction methodology from the status of art to be compatible to that of stress analysis which is viewed as a "mathematical discipline". In

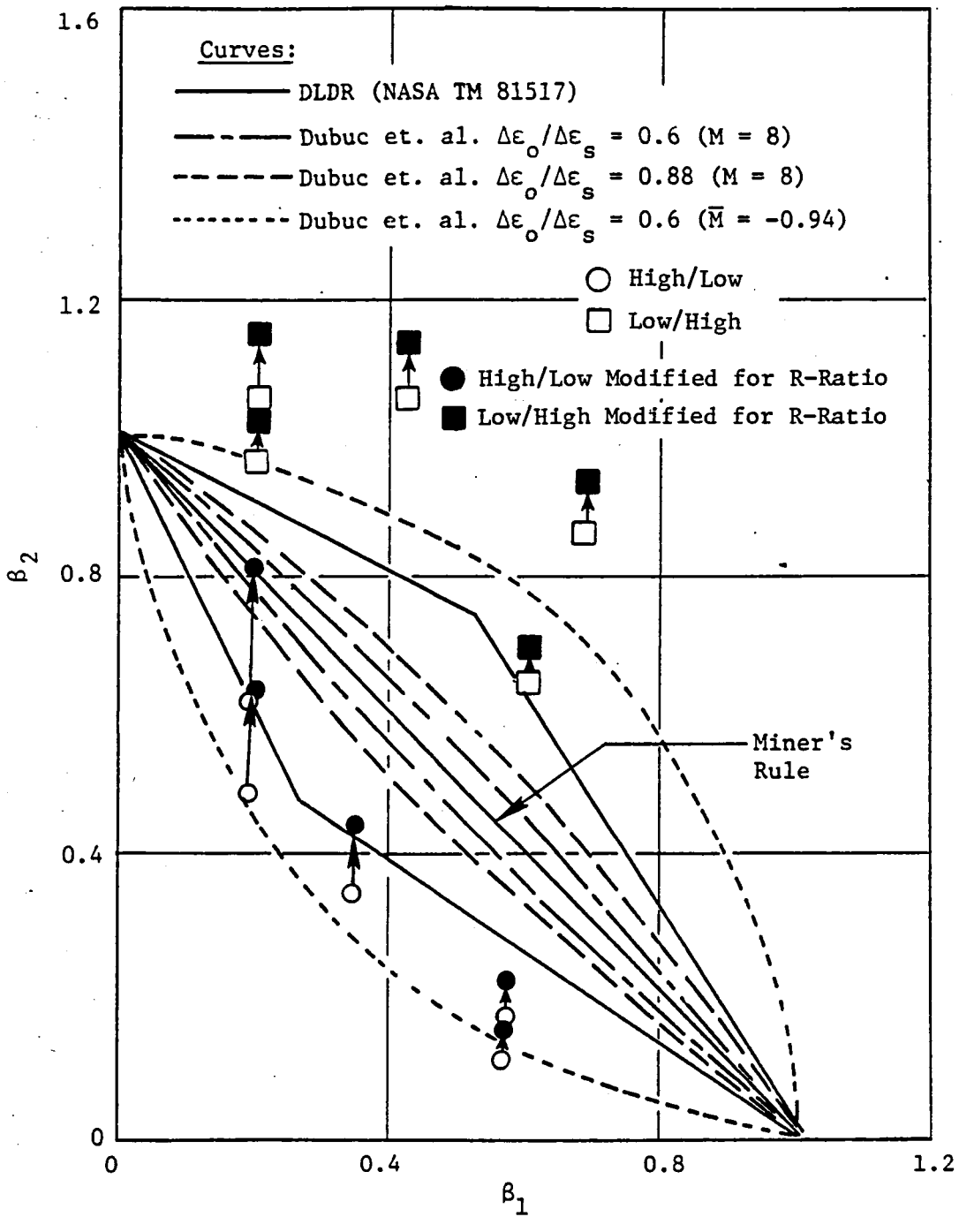

Figure B-6. Sequence Test Results Versus Theories, Inconel 718, 566° C (1050° F), Adjusting for R-Ratio.

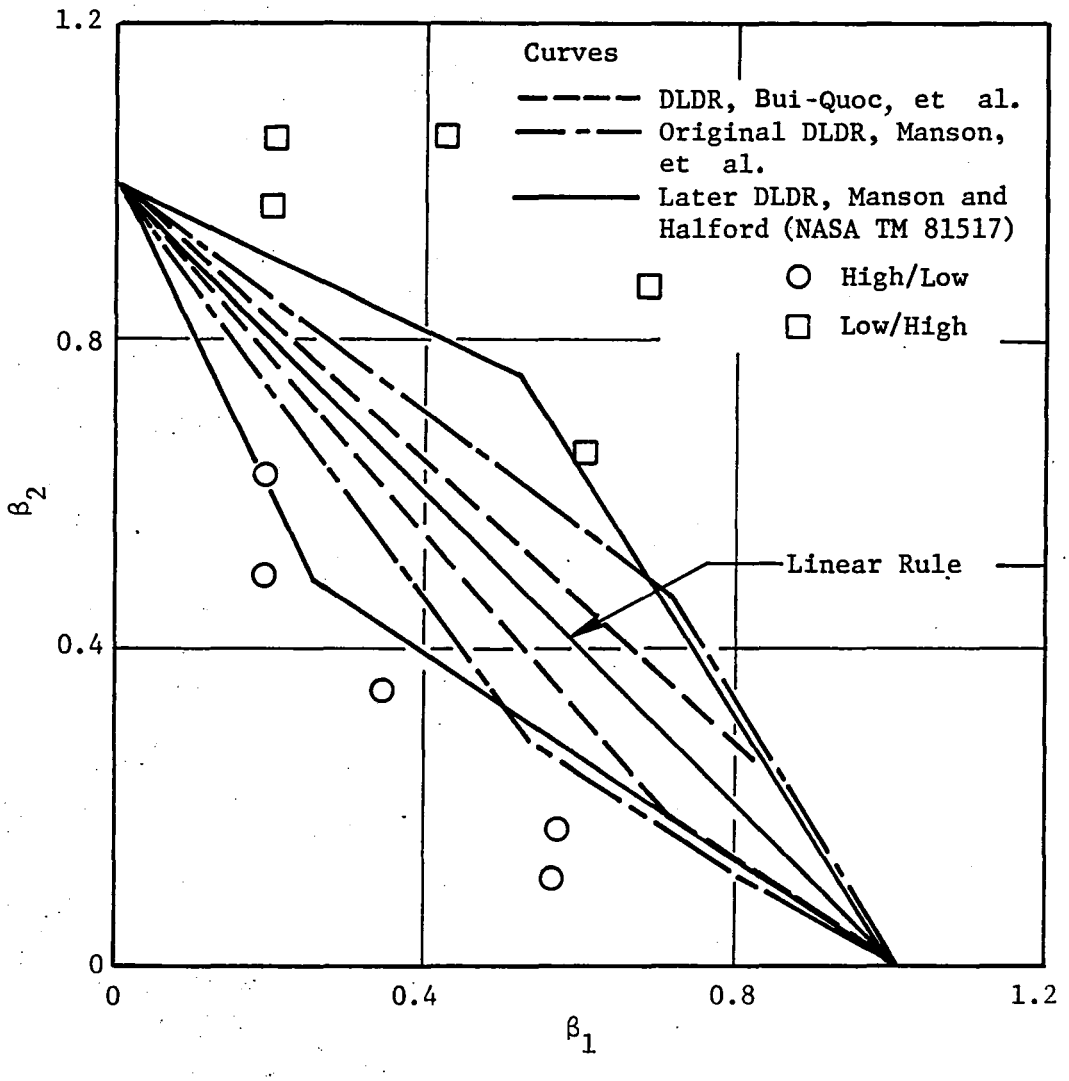

Figure B-7. Sequence Test Results Versus Theories, Inconel 718, 566° C, Three DLDR Theories.

so doing, these authors have investigated some forms of differential equations which might be useful for damage analysis; the specific form that is evaluated in detail cannot predict a sequence effect. It is shown that the assumption

$$\frac{dD}{dt} = g\,(D)\; f\left[\phi, \frac{d\phi}{dt}\right] \tag{17}$$

where g and f are functions, ϕ is the controlled variable (e.g., either stress or strain), and t is time, will not predict a sequence effect. The authors develop interesting conditions on Equation 17 and present correlations for time-dependent effects for Type 304 stainless steel and cast Inconel 738 by assuming a specific functional form for f and specific forcing functions. For the present purposes, showing that equations of the form of Equation 17 cannot predict a sequence effect is a useful result.

Sequence Effects in Creep Rupture

The sequence effect in creep rupture is generally found to be the opposite to that found in fatigue. Consider the application of a stress, σ_i, for a time period t_i; in what follows, the time to rupture is denoted by t_{ri}. Then, using Robinson's rule for a multiple stress history,

$$T = \Sigma\, t_i/t_{ri} = 1,$$

it is normally found (References 16, 20, and 21) for two-step loadings that $T > 1$ if $\sigma_1 > \sigma_2$, and $T < 1$ if $\sigma_1 < \sigma_2$; models for this effect are found in these three references. The model in Reference 16 is developed along the lines of the fatigue theory of Bui-Quoc, et al., except that the rate of damage accumulation is related to the rate of decrease in creep rupture strength. The model in Reference 20 is an experimentally-derived theory which uses the concept of remaining life curves. These latter curves are developed by experiments.

In Reference 21, Chaboche describes a stress-dependent theory; this theory is a perturbation of Kachanov's relation given by

$$\frac{dD}{dt} = \left\{\frac{|\sigma|}{A\,[1-D]}\right\}^{r} \tag{18}$$

where r and A are temperature-dependent constants. Note that Equation 18 is of the same form as Equation 17, and hence Equation 18 does not predict a sequence effect. Chaboche modified Equation 18 by writing

$$\frac{dD}{dt} = \left(\frac{|\sigma|}{A}\right)^{r} (1-D)^{-K\,(\sigma)} \tag{19}$$

where K (σ) is a stress-dependent exponent. Integrating Equation 19 and applying the condition $t = t_r$ at $D = 1$, it is found that

$$t_r = \frac{1}{[K(\sigma) + 1]} \left(\frac{|\sigma|}{A}\right)^{-r} \quad . \tag{20}$$

Damage can be written as

$$D = 1 - [1 - t/t_r]^{1/[K(\sigma)+1.]} \tag{20a}$$

Equation 20a can be curve fit to stress-dependent damage curves which can be derived based on tertiary creep measurements. This gives K (σ) through Equation 20a, and Equation 20 can be used to generate the other constants. The tertiary creep-derived damage curves can be expressed as

$$D = 1 - \left(\frac{\dot{\varepsilon}_c^o}{\dot{\varepsilon}_c}\right)^{1/(N+1)} \tag{21}$$

where $\dot{\varepsilon}_c$ is the creep rate, and $\dot{\varepsilon}_c^o$ and N are from Norton's creep law of secondary creep, $\dot{\varepsilon}_c^o = (\sigma_o/\lambda)^N$. The development of Equation 21 according to Chaboche depends upon the interpretation of damage as the linkup and growth of microcracks. His development uses an effective stress (called S) concept whereby the actual stress, σ_o, is replaced by

$$S = \frac{\sigma_o}{1-D} \quad . \tag{22}$$

Then, Norton's creep law is written as

$$\dot{\varepsilon}_c = \left(\frac{1}{1-D}\right) \left[\frac{\sigma_o}{\lambda\,(1-D)}\right]^N \tag{23}$$

where the extra (1-D) term on the right-hand side apparently results from assuming that the inelastic strain rate is derivable from a potential function. Rearranging Equation 23 gives Equation 21. As is mentioned by Chaboche, Equation 22 should be limited by some theoretical cohesive stress level, which would mean that, theoretically, the value of D at failure, D_f, would be stress level dependent and $D_f < 1$. The assumption that $D_f = 1$ is said to introduce only small errors. Finally, in Reference 21, the approach of Equations 19 through 23 was applied to a set of IN-100 data.

All of the above approaches assume damage accumulates at the same rate in tension and compression. However, Lemaitre and Plumtree (Reference 22) express the rate of damage accumulation in creep rupture in basically the same form as Equation 18,

$$\frac{dD}{dt} = \left\{\frac{|\sigma|}{A\pm\ [1-D]}\right\}^{r} [1-D]^{-q} \qquad (24)$$

where A± is a constant that depends upon whether or not the stress is tensile or compressive. No examples are given where differences exist in tensile and compressive behavior. It can be shown that Equation 24 still results in the linear time fraction rule; only the time to rupture becomes a function of loading direction in applying Equation 24.

Combined Rupture and Fatigue Methods

The methods of Lemaitre and Plumtree, and Chaboche combine the previous creep-rupture damage methods with fatigue damage. In these methods, fatigue and rupture are numerically treated as the same scalar quantity as is the effective stress of Equation 22. The approach of Lemaitre and Plumtree does not predict a sequence effect. In the Chaboche method, the stress dependent exponent, K (σ), in Equation 20a is treated as a constant as it is stated that the sequence effect in stress rupture is small. The fatigue sequence effect is maintained in his theory. Both methods treat creep-fatigue interactions, but neither method treats the case where damage accumulation is different in tension and compression.

Since the method of Lemaitre and Plumtree (Reference 22) does not predict a sequence effect, it is not reviewed here in detail. In their approach, damage is measured through changes in the dependent variable in the strain-controlled fatigue test (by analogy with Equation 21, the change in stress is used). Therefore, damage is directly measured (and the damage-life fraction law is calculated) through the decrease in stress throughout the test. In one of their cases (Alloy 800), the stress response is stable up to about half life, after which a steady decrease in stress is measured. Hence an incubation cycle count (designated as N^*) is hypothesized such that creep-fatigue interaction would not occur until this cycle count is exceeded. Thus, if a creep rupture test is conducted after an application of n cycles, no interaction between the prior cycling and the rupture test would be expected if $n<N^*$. Interactions are expected if $n>N^*$. The creep rupture damage equation is calibrated by using Equation 21 in this case. Creep rupture damage is then considered to accumulate continuously, such that creep fatigue interactions would be predicted to occur whenever creep is applied first and followed by cycling. Therefore, in this case, the creep fatigue interaction diagram is highly nonlinear as is schematically shown in Figure B-8.

In the case of continuous cycling experiments, "fast" and "slow" cyclic frequencies were used to calibrate two different damage functions by using the stress decay as a function of cycles. For future comparisons, these damage functions can be written in the form of the cycle ratio as,

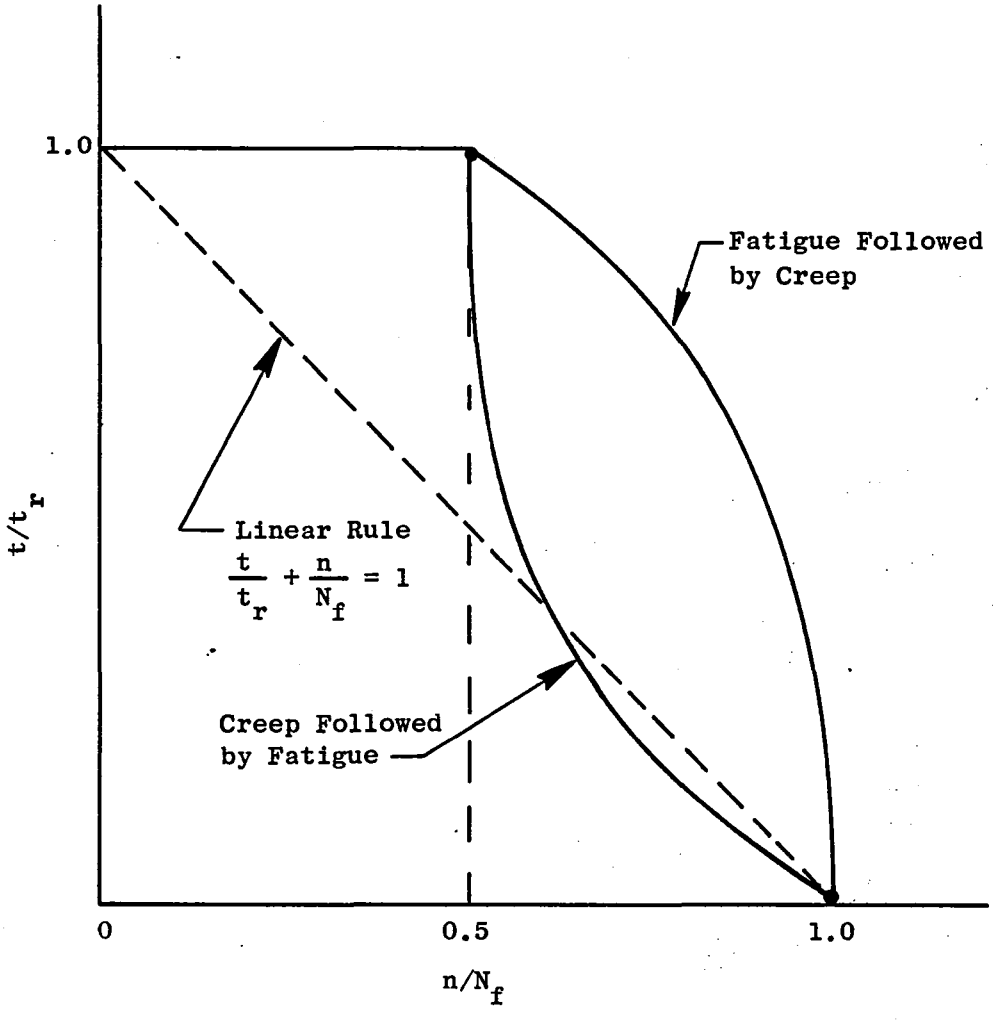

Figure B-8. Schematic of the Results for Alloy 800.

$$D = 1 - \left[1 - \frac{n}{N_f}\right]^{\frac{1}{P+1}} \tag{25}$$

where the exponent depends upon whether the cycling is fast enough to be considered pure fatigue or slow enough to induce intergranular cracking.

Since Chaboche's approach includes a fatigue sequence effect, it is compared to the Inconel 718 data at 566° C. Damage accumulation in fatigue is given by the expression.

$$\frac{dD}{dN} = \left[1 - (1-D)^{\beta+1}\right]^{\alpha} \left[\frac{\sigma_{max.} - \sigma_m}{M\,(1-D)}\right]^{\beta} \tag{26}$$

where

$$\alpha = 1-a\left(\frac{\sigma_{max.} - \sigma^*_e(\sigma_m)}{\sigma_u - \sigma_{max.}}\right) \tag{27}$$

$$\sigma^*_e = \sigma_e + \left(\frac{1-b\sigma_e}{\sigma_u}\right)\sigma_m \tag{28}$$

$$M = M_o\left(1 - \frac{b\sigma_m}{\sigma_u}\right)$$

where a, M_o, and β are temperature-dependent coefficients; $\sigma_{max.}$ is the maximum stress; σ_m is the mean stress; σ_e is the fatigue limit under R = -1 stress cycling; σ_u is the ultimate stress; and b is a temperature independent constant. Integrating Equation 26, and assuming $N = N_f$ at D = 1, one has

$$N_f = \frac{1}{(\beta+1)\,(1-\alpha)}\left(\frac{\sigma_{max.} - \sigma_m}{M}\right)^{-\beta} \tag{29}$$

Damage, D, can then be expressed as

$$D = 1 - \left[1 - \left(\frac{n}{N_f}\right)^{(1/1-\alpha)}\right]^{1/(\beta+1)} \tag{30}$$

Comparing Equations 30 and 25, it is seen that the sequence effect is introduced through the stress dependent function α, Equation 27. Using Equation 30, it is found for two-step loadings that

$$\beta_2 = 1-\beta_1\left(\frac{1-\alpha_2}{1-\alpha_1}\right)$$

or using Equation 27,

$$\beta_2 = 1-\beta_1^P, \tag{31}$$

where

$$P = \left(\frac{\sigma_u - \sigma_{max.1}}{\sigma_u - \sigma_{max.2}}\right)\left(\frac{\sigma_{max.2} - \sigma^*_{e\ 2}}{\sigma_{max.1} - \sigma^*_{e\ 1}}\right),$$

the subscripts refer to the order of loading, and σ^*_e is from Equation 28. It is noted in passing that the reciprocal of P was quoted in Reference 23.

Since the sequence effect is predicted, based on stress only (Equation 31), more details of the experimental stress condition of the two-step Inconel 718 tests were required to apply this approach (see Appendix A for details). These data were taken in strain control, but the mean strain changed upon change in strain range. Given the cyclic softening tendencies of this alloy, the net effect of the change in strain range (in terms of stresses) was that the stabilized maximum stress for both cyclic strain ranges was nearly the same (within 4 ksi); only the mean stress changed appreciably. This was despite the fact that the strain range was changed by 30%.

In addition, it was necessary to assume values of σ_e and b. From the work on the method of Reference 8 (cited earlier in this appendix) σ_e was taken to be $E\epsilon_o$; b was taken to be 0.78 based upon work in Reference 16 on IN-100. Using these assumed values, the steady-state stresses and Equation 31, the predictions in Figure B-9 were made. As shown, the data trends are underpredicted.

Since σ_e and b were estimated, an optimization of these predictions was attempted. Equation 31 was rearranged to the form,

$$\sigma_e\ (1-X) + B\ (\sigma_{m2} - X\ \sigma_{m1}) + X\ \sigma_{max.1} - \sigma_{max.2} = 0 \tag{32}$$

where

$$X \equiv \left(\frac{\sigma_u - \sigma_{max.2}}{\sigma_u - \sigma_{max.1}}\right)\ \frac{\ln\ (1-\beta_2)}{\ln\ \beta_1}$$

and $B = 1-b\sigma_e/\sigma_u$. A linear regression technique was applied to all the data (except those with $\beta_2>1$) and Equation 32. The results showed small variations in the derived coefficients of Equation 32, and the index of correlation was correspondingly low (0.139). The derived value of σ_e was approximately three times the value that was assumed in generating the predictions shown in Figure B-9. In view of the data of Figure B-4, such a value was too high to be of practical use. Other attempts were made in conjunction with Equation 32; all of them resulted in physical inconsistencies.

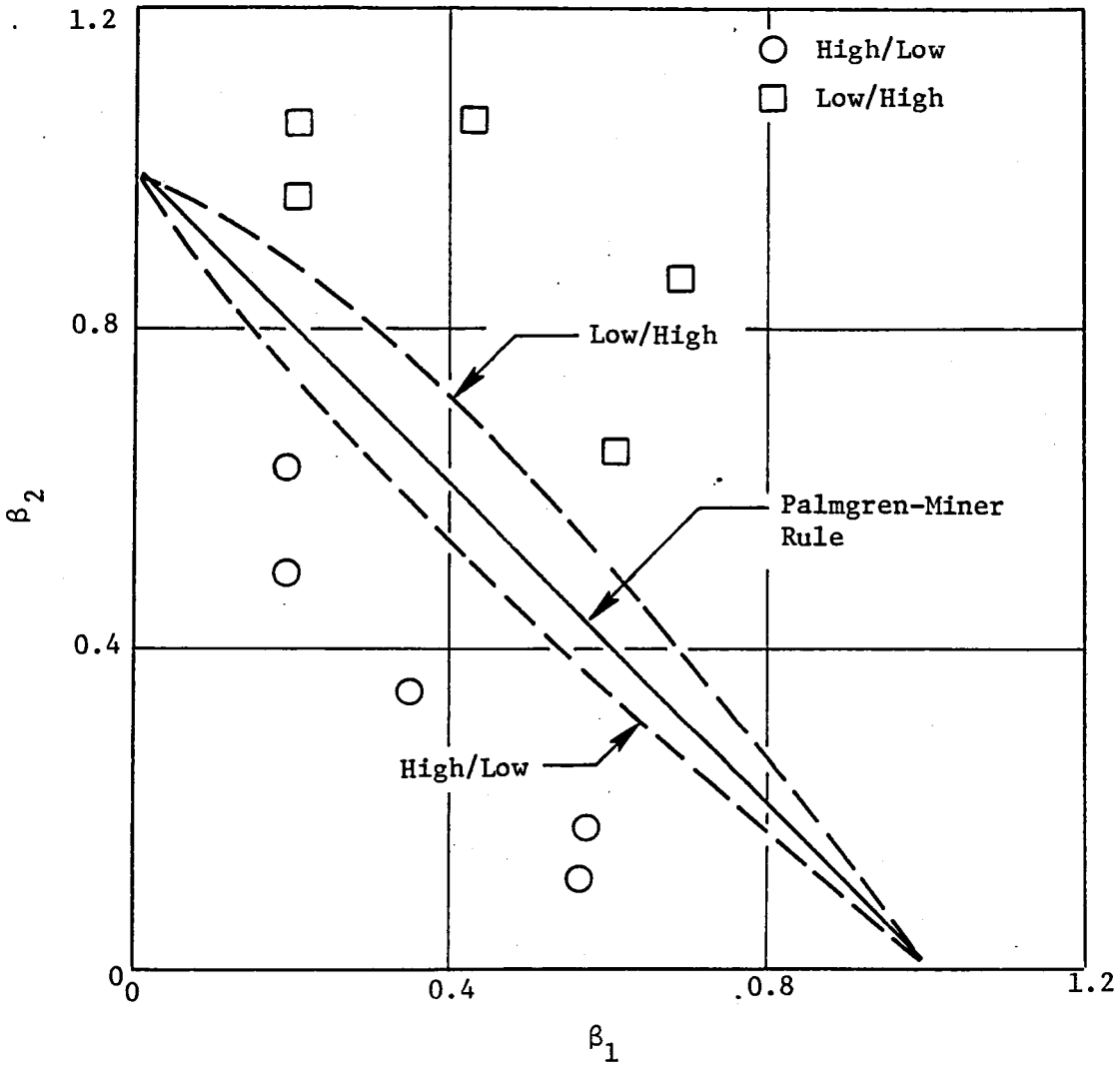

Figure B-9. Chaboche Predictions, Two-Step Sequence Tests, Inconel 718, 566° C.

In Reference 21, this theory was used to correlate some Inconel 718 data at 550° C with good results. These data were apparently collected under load control, and since the theory is stress-based, this may explain the differences in the correlations. It is interesting to note that the mean stress part of this theory is derived from Sines' multiaxial theory (Appendix D), and is similar to the uniaxial theory due to Manson and Halford (Appendix C).

Other Approaches

Various other techniques have been suggested. Plastic hysteresis loop energy criteria were suggested in Reference 13, 24, and 25. Another cumulative damage rule for creep is developed in Reference 26. Reference 27 discusses the effect of mean stresses and strains on cyclic damage summation. In Reference 28, Ibrahim and Miller describe an approach which considers initiation and Stage I crack propagation separately. The initiation flaw, a_i, is assumed to be stress dependent such that a_i increases as the stress level decreases. This is different than the previous approach of Miller and Zachariah; and in Reference 28, it is stated that in Reference 3 some aspects of the method were contradictory.

APPENDIX B - REFERENCES

1. Kaehele, L., "Review and Analysis of Cumulative-Fatigue-Damage Theories," Memorandum RM-36SO-PR, The Rand Corporation, August 1963.

2. O'Neill, M.J., "A Review of Some Cumulative Damage Theories," Report ARL/SM 326, Department of Supply, Australian Defense Scientific Service, Aero. Research Labs., June 1970.

3. Miller, K.J. and Zachariah, K.P., "Cumulative Damage Laws for Fatigue Crack Initiation and Stage I Propagation," Journal of Strain Analysis, Vol. 12, No. 4, 1977, pp. 262-270.

4. National Materials Advisory Board, "Analysis of Life Prediction Methods for Time Dependent Fatigue Crack Initiation in Nickel-Base Superalloys," Publication NMAB-347, National Academy of Sciences, Washington, D.C., 1980.

5. Manson, S.S. and Halford, G.R., "Practical Implementation of the Double Linear Damage Rule and Damage Curve Approach for Treating Cumulative Fatigue Damage," International Journal of Fracture, Vol. 17, 1981, pp. 169-192.

6. Hashin, Z. and Rotem, A., "A Cumulative Damage Theory of Fatigue Failure," Materials Science and Engineering, 34, 1978, pp. 147-160.

7. Hashin, Z. and Laird, C., "Cumulative Damage Under Two Level Cycling: Some Theoretical Predictions of Test Data," Naval Air Systems Command, Office of Naval Research, Contract N00014-78-C-0544, Technical Report No. 3, August 1979.

8. Dubuc, J., Bui-Quoc, T., Bazergui, A., and Biron, A., "Unified Theory of Cumulative Damage in Metal Fatigue," Welding Research Council Bulletin 162, June 1971, pp. 1-20.

9. Manson, S.S., "Interfaces Between Fatigue, Creep, and Fracture," International Journal of Fracture Mechanics, Vol. 2, No. 1, March 1966, pp. 327-363.

10. Bui-Quoc, T. and Biron, A., "Order Effect of Strain Applications in Low-Cycle Cumulative Fatigue at High Temperatures," Paper L 9/2, 4th Int. Conf. SMIRT, August 1977.

11. Bernard-Connolly, M., Biron, A., Bui-Quoc, T., "Low Cycle Cumulative Damage with Two-Strain Repeated Blocks on a Stainless Steel at High Temperature," Paper No. 78-PVP-88, ASME, April 5, 1978.

12. Bui-Quoc, T., "High-Temperature Fatigue-Life Estimation. Extension of a Unified Theory," Exp. Mech., Vol. 15, No. 6, June 1975, pp. 219-225.

13. Bui-Quoc, T., "Cyclic Stress, Strain, and Energy Variations Under Cumulative Damage Tests in Low-Cycle Fatigue," J. of Testing and Evaluation, Vol. 1, No. 1, ASTM, 1973, pp. 58-64.

14. Bui-Quoc, T., Choquet, J.A., and Biron, A., "Cumulative Fatigue Damage on Large Steel Specimens Under Axial Programmed Loading with Nonzero Mean Stress," J. Eng. Mat. and Tech., Vol. 98, July 1976, pp. 249-255.

15. Bui-Quoc, T. and Biron, A., "Effect of Relative Mean Strain in High-Temperature Low-Cycle Fatigue of a Stainless Steel," J. of Press. Vessel Tech., November 1979, pp. 238-242.

16. Bui-Quoc, T., "An Engineering Approach for Cumulative Damage in Metals Under Creep Loading," J. of Eng. Mat. and Tech., October 1979, Vol. 101, pp. 337-343.

17. Manson, S.S., Freche, J.C., and Ensign, C.R. "Application of a Double Linear Damage Rule to Cumulative Fatigue," Fatigue Crack Propagation, ASTM STP 415, Am. Soc. Testing Matls. , 1967, pp. 384-412.

18. Adams, J.H., "Nonlinear Damage Cumulation in Solution Treated and Aged Titanium 6Al-4V," Paper 81-6T-106, ASME, J. of Eng. Power.

19. Ostergren, W.J. and Krempl, E., "A Uniaxial Damage Accumulation Law for Time-Varying Loading Including Creep-Fatigue Interaction," Report No. RPI CS 77-2, Rensselaer Polytechnic Institute, August 1977. See also: Paper 78-PVP-63, ASME, presented at Joint ASME/CSME Pressure Vessels and Piping Conf., Montreal, Canada, June 25-30, 1978, Vol. 101, J. of Press. Vessel Tech., May 1979, pp. 118-124.

20. Woodford, D.A., "Creep Damage and the Remaining Life Concept," J. of Eng. Matls. and Tech., Vol. 101, October 1979, pp. 311-316.

21. Chaboche, J.L., "Thermodynamic and Phenomenological Description of cyclic Viscoplasticity with Damage," European Space Agency Technical Translation, ESA-TT-548, May 1979.

22. Lemaitre, J. and Plumtree, A., "Application of Damage Concepts to Predict Creep-Fatigue Failures," Paper No. 78 PVP-26, ASME.

23. Chaboche, J.L., Policella, H., and Kacymasek, H., "Application of the SRP Method and Creep-Fatigue Damage Approach to the LCHTF Prediction of IN-100 Alloy," AGARD-CP-243, Characterization of Low-Cycle High Temperature Fatigue by the Strain Range Partitioning Method, August 1978, pp. 4-1 to 4-20.

24. Radhakrishnan, V.W., "Cumulative Damage in Low-Cycle Fatigue," Experimental Mechanics, Aug. 1978, pp. 292-296.

25. Obtaya, Y. and Shiratori, E., "Cumulative Damage in Low Cycle Fatigue," Bulletin of the JSME, Vol. 14, No. 71, May 1971, pp. 418-426.

26. Radhakrishnan, V.M., "Cumulative Damage in Creep," Engineering Fracture Mechanics, Vol. 11, 1979, pp. 373-383.

27. Watson, P. and Topper, T.H., "Fatigue-Damage Evaluation for Mild Steel Incorporating Mean Stress and Overload Effects," Experimental Mechanics, Vol. 12, No. 1, January 1972, pp. 11-17.

28. Ibrahim, M.F.E. and Miller, K.H., "Determination of Fatigue Crack Initiation Life, " Fatigue of Engineering Materials and Structures, Vol. 2, 1980, pp. 351-360.

APPENDIX C - ANALYSES OF SOME MEAN STRESS THEORIES

Of the three areas of study covered in this report, the topic of mean stress yielded the fewest number of hits through the literature survey. Generally, two generic theories have been suggested: those involving mean plastic strains (References 1, 2, and 3) and those involving mean or maximum stress (References 4, 5, 6, 7, 8, 9, and 10). Of these two types of theories, the mean or maximum stress theories appear to be the most applicable in the current effort. The mean plastic strain theories are most applicable in the regime where plastic strain dominates, or in case where inelastic strain ratchetting is occurring (e.g., Manson in Reference 11). Due to the strength level of typical alloys that are used in aircraft gas turbine engines, elastic strain ranges are typically larger than the inelastic ones in most design cases; the transition fatigue life (the cyclic life where the elastic and inelastic strain ranges are equal) is normally around 1000 cycles. This means that the design life is normally greater than the transition life, and the mean stress theories are more appropriate.

If mean stress theories are divided into those applicable to the high and low cycle regimes, then this study will concentrate on LCF models. High cycle fatigue theories can be applied to LCF problems by extending the functional form into the LCF regime, but there are several potential problems in doing this. HCF theories are normally based on mean and alternating stress levels; they include no strain measure which is normally deemed important in LCF problems. HCF theories are normally nonlinear in the stress terms which naturally leads to nonlinear techniques for determining the appropriate constants. As shown in Reference 12, one such HCF theory ranked third (out of three theories) for three of four materials and was ranked second for the fourth material when applied in the LCF regime (the other two theories were LCF theories which are evaluated in this appendix). Finally, it is noted that most HCF theories assume that the constant life curves should fair into the ultimate tensile strength at R = 1. At elevated temperatures where time-dependent processes become important, it is probable that the HCF curves would also be time dependent and that these curves should fair into the rupture strength (for a given time to rupture) at R = 1 as suggested by HCF studies in this temperature regime (References 13 and 14).

In this appendix, four current LCF mean stress theories are compared to two sets of Inconel 718 data. In Appendix E, these theories as well as the Ostergren approach (Reference 9) are compared to a set of elevated temperature René 80 data. Before showing the results of these analyses, a brief discussion is given of the analytical techniques employed here and elsewhere in this report.

Regression Models

The bulk of the mean stress models described in this report was fit to data by using standard regression analysis techniques. Consider a set of data with one dependent variable, $\bar{Y}_i$ (i=1, 2, ... n), and a corresponding

single independent variable, x_i (i = 1, 2, 3, ... n) where n is the number of data points in the data set. Assume that these data can be described by an equation of the form,

$$Y = \sum_{j=1}^{m} a_j \, f(x)^{j-1} \tag{1}$$

where a_j are unknown coefficients to be determined and f(x) is some function of the independent variable, x [only two such functions are used in this report: f(x) = x and f(x) = ln(x)]. The coefficients are determined by minimizing an error term,

$$S(\underset{\sim}{a}) = \sum_{i=1}^{n} \left\{ \bar{Y}_i - \sum_{j=1}^{m} a_j \, f(x_i)^{j-1} \right\}^2 , \tag{2}$$

a typical term of which is

$$\frac{\partial S}{\partial a_k} = \sum_{i=1}^{n} \left\{ \left[\bar{Y}_i - \sum_{j=1}^{m} a_j \, f(x_i)^{j-1} \right] f(x_i)^{k-1} \right\} = 0. \tag{3}$$

Expansion of Equation 3 leads to a matrix equation (e.g., see Reference 15) in terms of the a coefficients which is solved in the current study by a technique known as Gauss-elimination. A special purpose computer program was written to aid in the evaluation process. The program handled the numerical manipulation of the data, performed the regression analyses, and printed out comparative and summary information for each of the mean stress theories. In certain cases (when m in Equation 2 was 2 or 3) that are mentioned in various portions of this report, the linear regression was accomplished by using existing programs in a Texas Instrument SR-52 programmable calculator.

For one mean stress theory (Reference 7), it was necessary to perform nonlinear regression due to the particular combination of R-ratios and the form of the theory. Nonlinear regression was performed in the current study by using a preexisting program which was described in Reference 16. In other cases which involved the solution of one nonlinear equation in one unknown, an existing program on the above-mentioned programmable calculator was used.

Two statistical measures were utilized to compare the results of the regression analyses of the various mean stress theories. One, denoted by E, was given by

$$E^2 = \frac{1}{n} \sum_{i=1}^{n} \left(1. - \frac{N^i_{pred}}{N^i_{act}} \right)^2 , \qquad (4)$$

where n was the number of data points, and N^i_{pred} and N^i_{act} are the predicted and actual cycles to failure, respectively. Equation 4 was conceived to be a measure of average error for a given theory and data set. Alternately, this equation has the form of the standard deviation. However, it is often assumed that fatigue data follows a log-normal distribution for which the standard deviation, σ, is as follows:

$$\sigma^2 \propto \frac{1}{n} \sum_{i=1}^{n} \left(\ln N^i_{pred} - \ln N^i_{act} \right)^2 = \frac{1}{n} \sum_{i=1}^{n} \left[\left(\ln \frac{N^i_{pred}}{N^i_{act}} \right) \right]^2 \qquad (5)$$

As it turns out, the first term of a Taylor's series expansion of Equation 5 is given by Equation 4 which indicates that for small errors in a data set the results of the two formulas would be the same. This is illustrated in Figures C-1 and C-2 wherein x is the ratio of N^i_{pred}/N^i_{act}. Figure C-1 shows the close agreement of the two functions about x = 1. Figure C-2 shows the square of the two functions which are the contributions to the summations in Equations 4 and 5. Note that Equation 4 would appear symmetric about x = 1 if semilogarithmic coordinates had been used. Different values of x in Equation 5 contribute the same amount to the value of σ as long as constant factors are involved (e.g., "factors of two", x = 0.5 or x = 2.0). Equation 4 gives the same value for the same percentage difference in data points (e.g., 100% error, x = 0 or x = 2). As shown in Figure C-2, the two functions flip-flop in terms of which is larger as the value of x passes through x = 1. Therefore, comparing the magnitudes of both functions could be potentially useful in judging the skewness of the data. As mentioned above, alternate interpretations can be given to Equation 4, whereas Equation 5 is best thought of as a measure of the standard deviation of a log-normal distribution.

One benefit of a standard deviation calculation is that the degree of improvement of various theories can be directly assessed in terms of the reduction of scatter in a data set (assuming a log-normal distribution). For use in engine design applications, such a minimum life calculation is needed in at least preliminary design and in the life management process until better "pedigree" information can be clearly established from field returned parts. In the latter case, the minimum life would still be used; the pedigree data are used to establish actual scatter and average behavior. For a log-normal distribution, the -3 sigma life, $N_{-3\sigma}$, is related to the average life, $\bar{N}$, by

$$\ln N_{-3\sigma} = \ln \bar{N} - 3\sigma . \qquad (6)$$

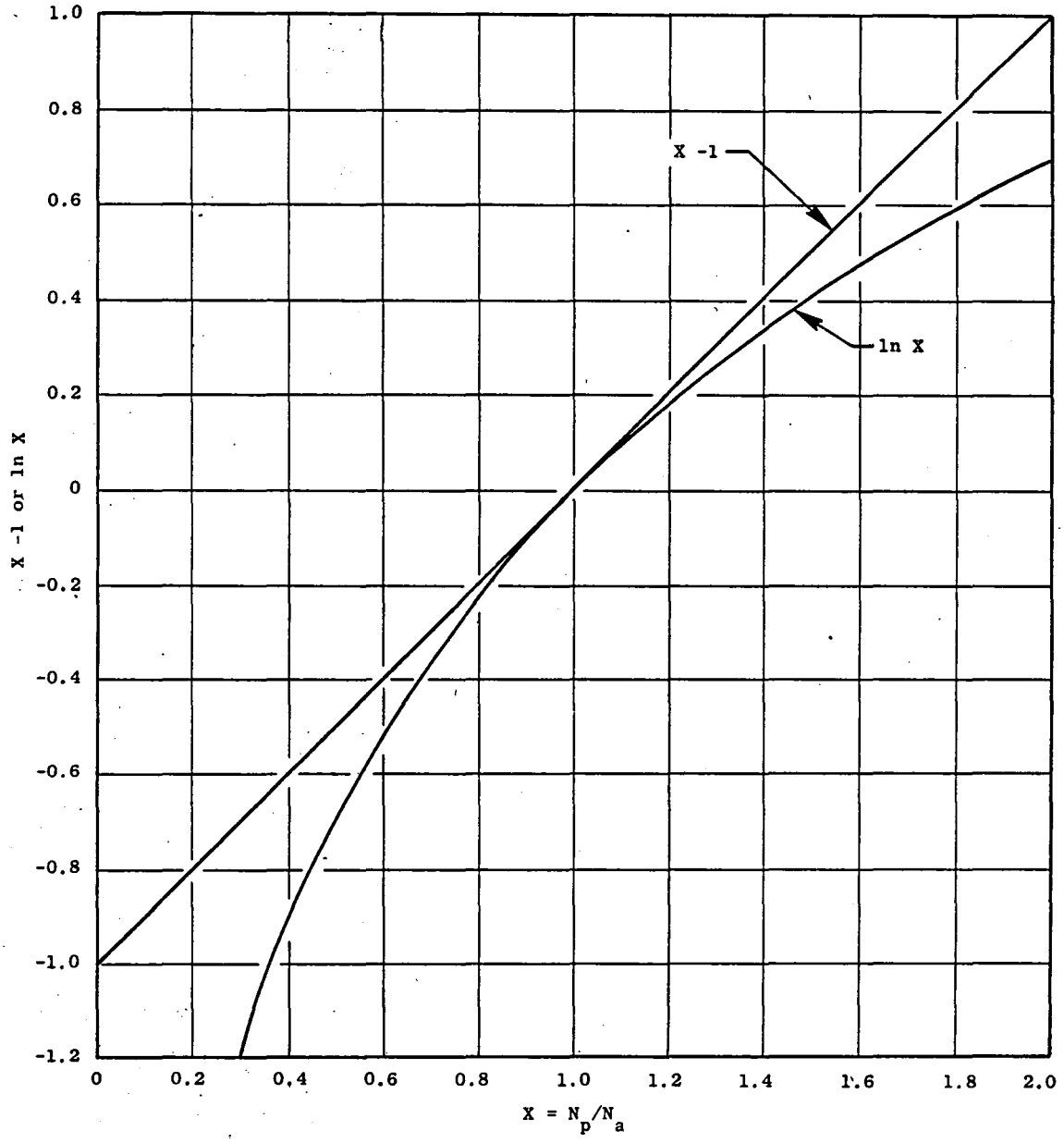

Figure C-1. Comparison of ln X and X -1.

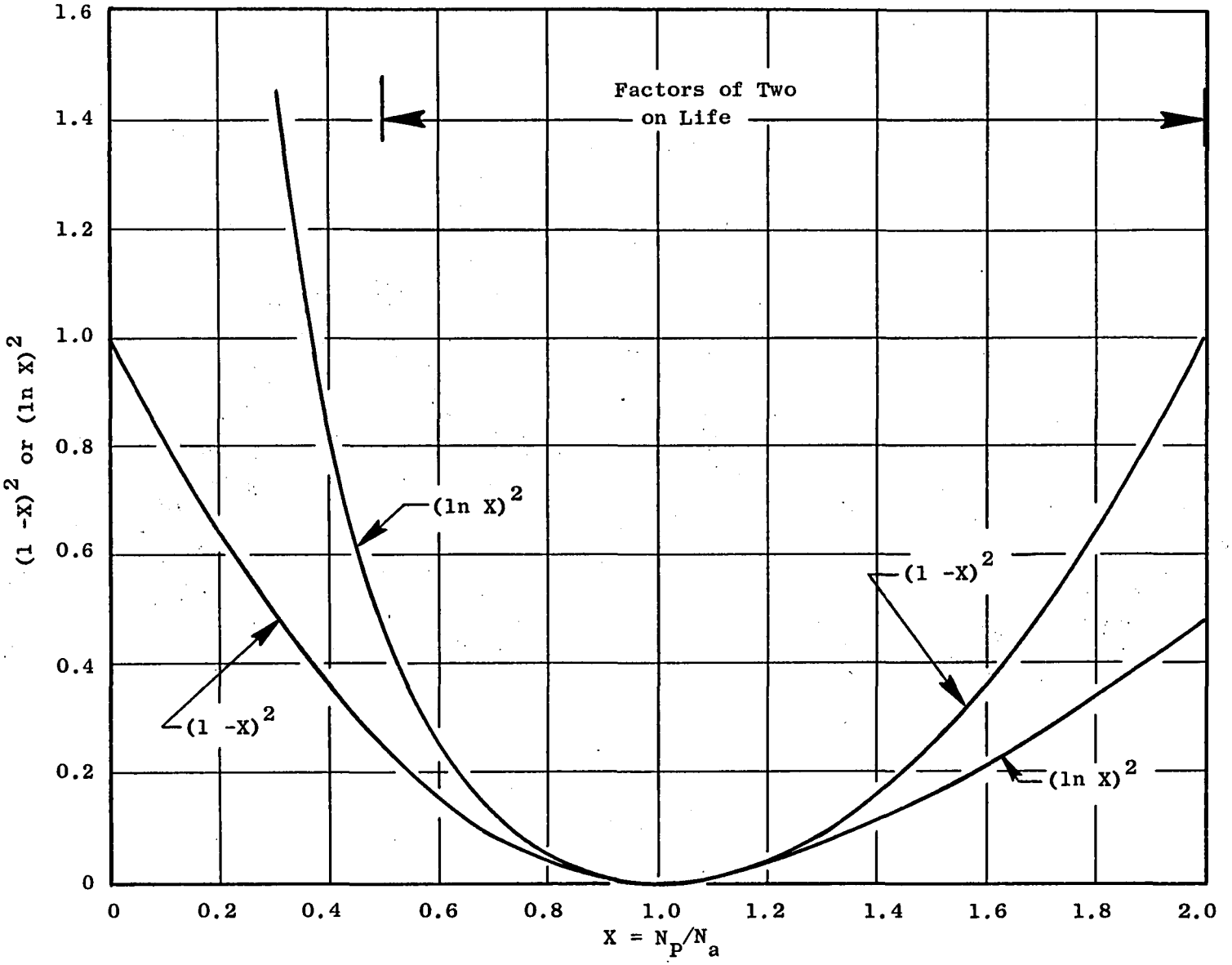

Figure C-2. Comparison of Equations 4 and 5.

Rearranging Equation (6) gives,

$$N_{-3\sigma} = e^{-3\sigma} \bar{N}. \tag{7}$$

In other words, for this simple example, the σ calculation provides a multiplier on the average life.

Analysis Of Some Mean Stress Prediction Techniques

Four different methods of predicting the effect of mean stress are compared in this section: the equivalent strain, ε_{eq}, approach (Reference 4); the Manson and Halford modification of Morrow's method (MMHM) (Reference 7); the approach of Cruse and Meyer (CM) (Reference 6); and Leis' method (Reference 5). A brief description of each approach is given first, followed by a comparison of the correlations based on each method.

The equivalent strain (ε_{eq}) is defined by

$$\varepsilon_{eq} = \left(\frac{\sigma_{max.}}{E}\right)^{1-m} (\Delta\varepsilon)^m \tag{8}$$

where m is an arbitrary correlation parameter which is optimized to correlate the data. Note that if m = 0.5, then

$$\varepsilon_{eq} = \left(\frac{\sigma_{max}\ \Delta\varepsilon}{E}\right)^{1/2}; \tag{9}$$

if m = 0, then

$$\varepsilon_{eq} = \frac{\sigma_{max}}{E}; \tag{10}$$

and if m = 1, then

$$\varepsilon_{eq} = \Delta\varepsilon. \tag{11}$$

Equation 9 is related to the Smith-Watson-Topper parameter (Reference 17); and, therefore, the optimization of m would yield this method if m = 0.5 is indicated by the data analysis. Obviously, as indicated by these equations, the parameter m adds great versatility to the analysis of data for different materials. However, to be most useful, m should not be strongly temperature dependent; at the least, m should follow some reasonable functional form.

The current MMHM is described by the equation,

$$\frac{\Delta\varepsilon}{2} = \left[\frac{\sigma_f' - k_m\sigma_m}{E}\right](2N_f)^b + \left[\left(\frac{\sigma_f' - k_m\sigma_m}{\sigma_f'}\right)^{c/b} K'^{\left(\frac{b-c}{b}\right)}\right]^{\beta} \varepsilon_f' (2N_f)^c \quad (12)$$

where σ_f', b, ε_f', and c are curve fit constants for $R_\varepsilon = -1$; k_m is the constant which describes the mean stress dependence; and σ_m is the mean stress. The exponent β has been added for discussion purposes only, and K' is a parameter which relates to the potential dependence of the transition fatigue life on mean stress (it is assumed to be unity in this study). Note that the first term on the right-hand side corresponds to the elastic strain range, while the second term corresponds to the plastic strain range. If $k_m = 1$ and $\beta = 0$, this is the approach originally suggested by Morrow (Reference 18). If $\beta = 0$, and k_m is introduced, this is the method suggested by Manson (Reference 19); and if $\beta = 1$, it is the Manson-Halford method that is suggested in Reference 7.

The Cruse and Meyer method is given by

$$N_f = A\,\Delta\varepsilon_{t.}^{B}\,10^{C\sigma_m} \quad (13)$$

where A, B and C are regression constants. As pointed out in Reference 12, if $\sigma_m = 0$, then this method suggests that life and total strain range are log-linearly related which is not generally true.

The Leis parameter, P_L, is described by the equation,

$$P_L = E\left(\sigma_{max.} + \frac{\Delta\sigma}{2}\right)\frac{\Delta\varepsilon}{2} \quad . \quad (14)$$

In utilizing Equation 14, no specific relationship is assumed between the parameter and cyclic life; plots of the data with P_L versus life are to be made and the relationship described by curve fits.

These theories were compared to two sets of Inconel 718 data as described below. The first study considered a smaller set of data which was from tests performed at 538° C (1000° F). This study showed some interesting results with respect to predictability and also allowed easier determination of the constants in the MMHM since $R_\varepsilon = -1$ data were included. The subsequent study was made on a more extensive data set enabling more definitive conclusion to be drawn.

An Initial Study on Inconel 718 at 538° C

Three theories were compared to a series of Inconel 718 data. The zero mean stress ($R_\varepsilon = -1$) data were assumed to follow the two-slope Coffin-Manson form,

$$\Delta\varepsilon = A N_f^{-\alpha} + G N_f^{-\gamma} \tag{15}$$

where

$$\Delta\varepsilon_p = A N_f^{-\alpha}, \tag{16}$$

$$\Delta\varepsilon_e = \frac{\Delta\sigma}{E} = G N_f^{-\gamma} \tag{17}$$

and A, α, G and γ are curve fit constants which are related to those in Equation 12. The Leis parameter (Equation 14) can be directly determined by Equations 15 and 17 to be (assuming no mean stresses)

$$P_L = \frac{E^2 G N_f^{-\gamma}}{2}\left(A N_f^{-\alpha} + G N_f^{-\gamma}\right). \tag{18}$$

The Smith-Watson-Topper parameter,

$$P = E\frac{\sigma_{max.}\Delta\varepsilon}{2}, \tag{19}$$

is related to P_L in this case by the relationship $P_L = 2P$. Therefore, once curve fits of $R_\varepsilon = -1$ data are obtained, these two parametric approaches can be used to predict the results at other conditions by calculating the appropriate parameter and solving an equation such as 18. Conversely, the MMHM of Equation 12 is a correlating technique. In terms of Equation 15, Equation 12 can be written as

$$\Delta\varepsilon = A\left[1 - \frac{k}{AE}\right]N_f^{-\alpha} + G\left[1 - \frac{k}{AE}\right]^{c\beta/b} N_f^{-\gamma} \tag{20}$$

where it is assumed that $K' = 1$ and $k = k_m/2^{\alpha-1}$. Both the cases, $\beta = 0$ and $\beta = 1$, are considered.

The strain-controlled Inconel 718 data set consisted of 18 data points with R ratios of -1, 0, 0.2, and 0.33. Of these 18 points, four were stopped at 1.5×10^5 cycles, and four failed at the point of transition from the gage section to the shank section. These latter points were treated in the analyses as premature failures. Five of the data points were for $R_\varepsilon = -1$ (of which one was a runout). The remaining four $R_\varepsilon = -1$ data points were fit to the form of Equation 17 by linear regression. These four data points had small mean stresses which were ignored in the analysis. The plastic strain Equation 16 was determined by fitting all of the 10 results which had not failed in the

transition region or stopped before failure. This was done in accordance with Equation 20 with $\beta = 0$, which suggested that mean stresses would not change the plastic strain-life characteristics. In any event, it was found that only minor changes in the overall fit of Equation 16 resulted when either all 10 points or only the 4 $R_\varepsilon = -1$ points were used. In using Equation 20 with $\beta = 1$, the fit of Equation 16 was determined by using only the 4 $R_\varepsilon = -1$ data points in order to be consistent with the theory.

Using Equation 18, predictions of the data are made and the resulting comparison plots are shown in Figures C-3 and C-4 for the P and P_L approaches, respectively. Note that the Smith-Watson-Topper approach grossly overestimates the mean-stress effect while the Leis parameter, though still conservative, is much more accurate. Comparing Equations 14 and 19, it is seen that both parameters can be written as linear combinations of mean stress and alternating stress, with the Leis parameter more strongly emphasizing the alternating component (by a factor of 2). As such, it appears that this material is not as strongly mean-stress sensitive as is suggested by the P parameter. As another illustration of the mean-stress effect in Inconel 718, note the results shown in Figure C-5, where only strain range is used to predict the cyclic life. As shown, the effect seems to be relatively small, amounting to about a factor of 2 at 10^5 cycles.

The MMHM was analyzed with $\beta = 0$ as follows. The value of k was determined as suggested in the literature by rearranging Equation 20 to the form:

$$k = \frac{E}{\sigma_o} \frac{(AN_f^{-\alpha} + G N_f^{-\gamma} - \Delta\varepsilon)}{N_f^{-\alpha}}$$

As shown in Figure C-6, the values of k so determined exhibited substantial scatter, particularly for the data with low mean stress levels. When only the data with a mean stress level above 90 MPa (13 ksi) were selected (ignoring the data that failed in the transition region), a reasonably constant value of k was found (0.302). The overall correlation is shown in Figure C-7. As the figure shows, a good correlation is obtained; and, consistent with expectations, the variation in k at low mean stress does not have a significant effect on the correlation.

Finally, the MMHM method with $\beta = 1$ was compared with these Inconel 718 data. In Figure C-6, the value of k as a function of mean stress was also plotted. These values of k were determined by iteratively forcing the predicted cycles to failure from Equation 20 to agree with the actual cycles to failure. For low values of mean stress, the life was short and the influence of mean stress was minimal. At longer lives, the mean stress was higher. Note, however, that k was higher for low mean stress, and that k was more strongly dependent upon the method selected for determining its value at smaller mean stresses (i.e., either $\beta = 0$ or 1). In the high mean stress, longer life range, the difference in k determined by either method was reduced. This was because the contribution of the plastic strain range to the total

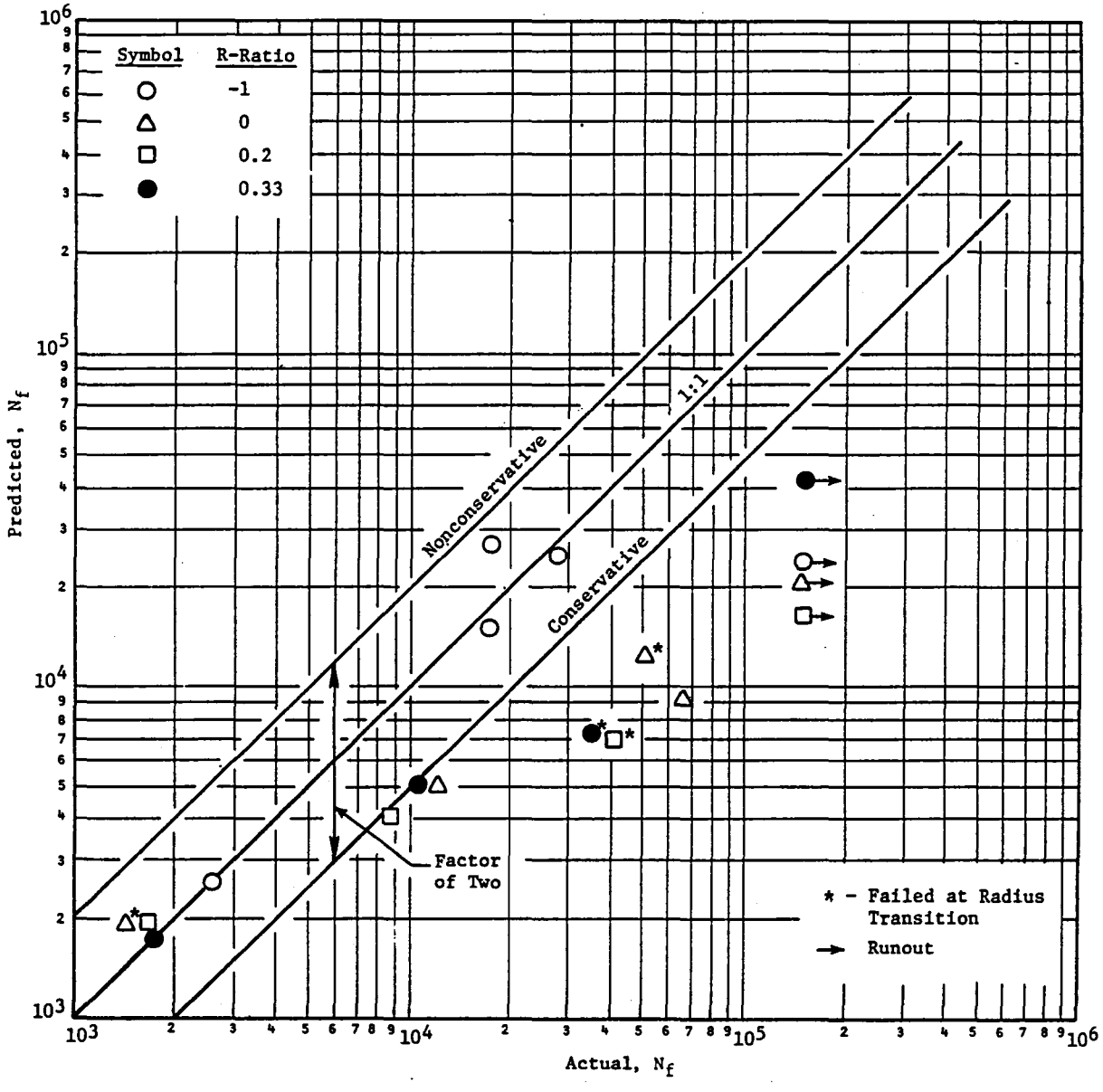

Figure C-3. Inconel 718, 538° C Comparison of Mean Stress Data and Predictions Using the Smith-Watson-Topper Parameter, $P = \sigma_{max} E\Delta\varepsilon/2$.

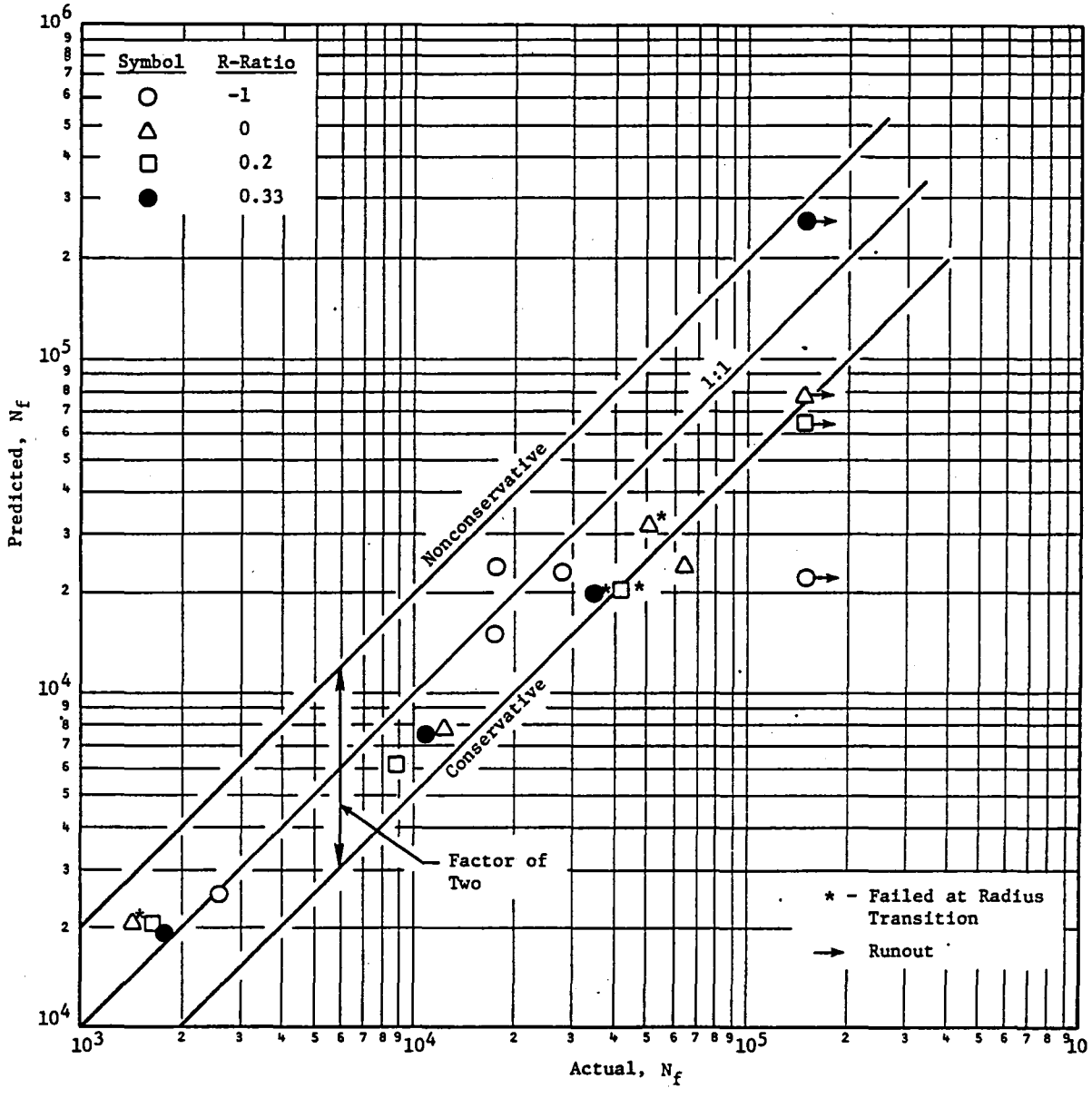

Figure C-4. Inconel 718, 538° C, Comparison of Mean Stress Data and Prediction Using the Leis Parameter, $P_L = (\sigma_{max} + \Delta\sigma/2) E\Delta\epsilon/2$.

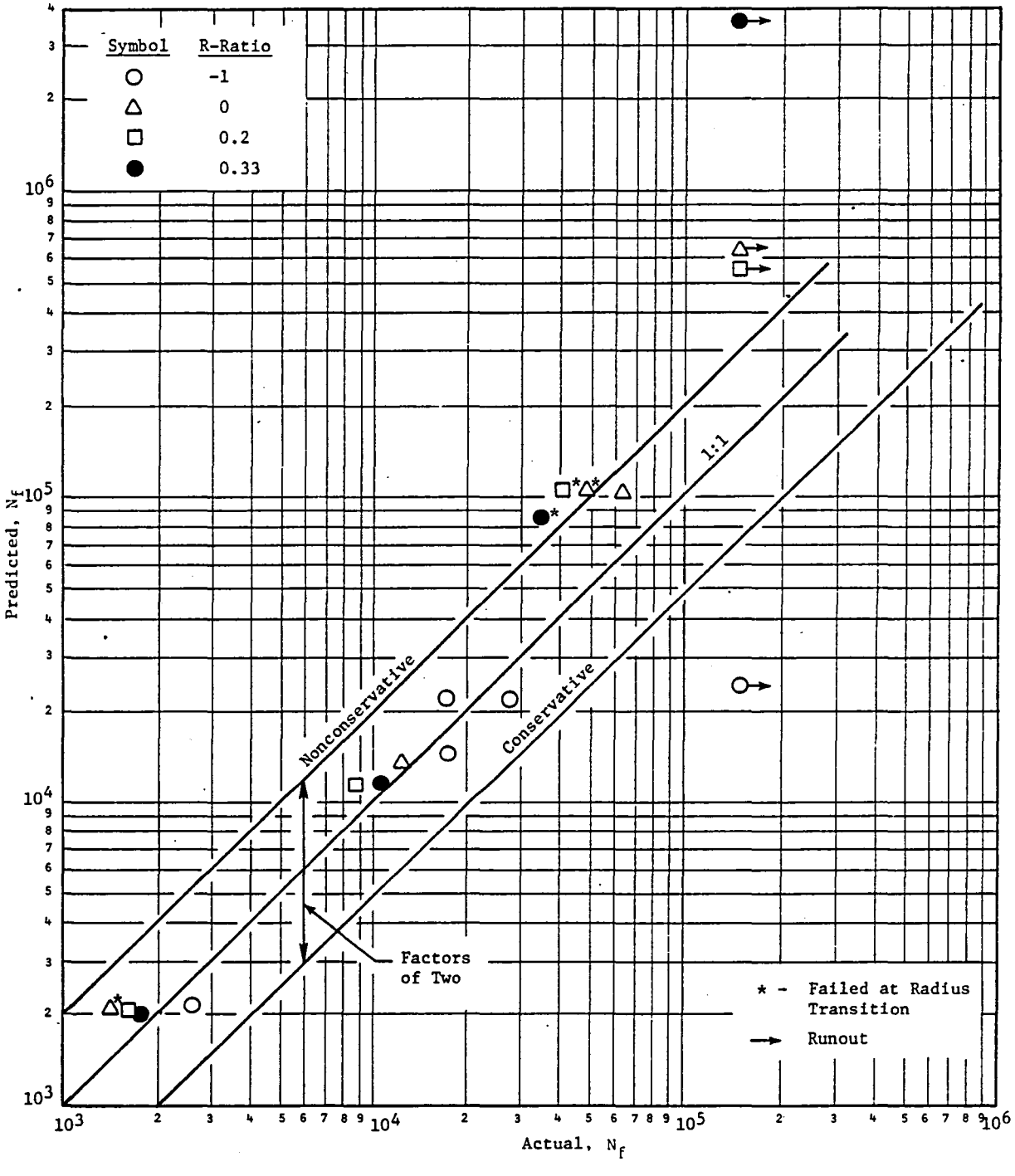

Figure C-5. Inconel 718, 538° C Correction of Mean Stress Data Using Total Strain Range.

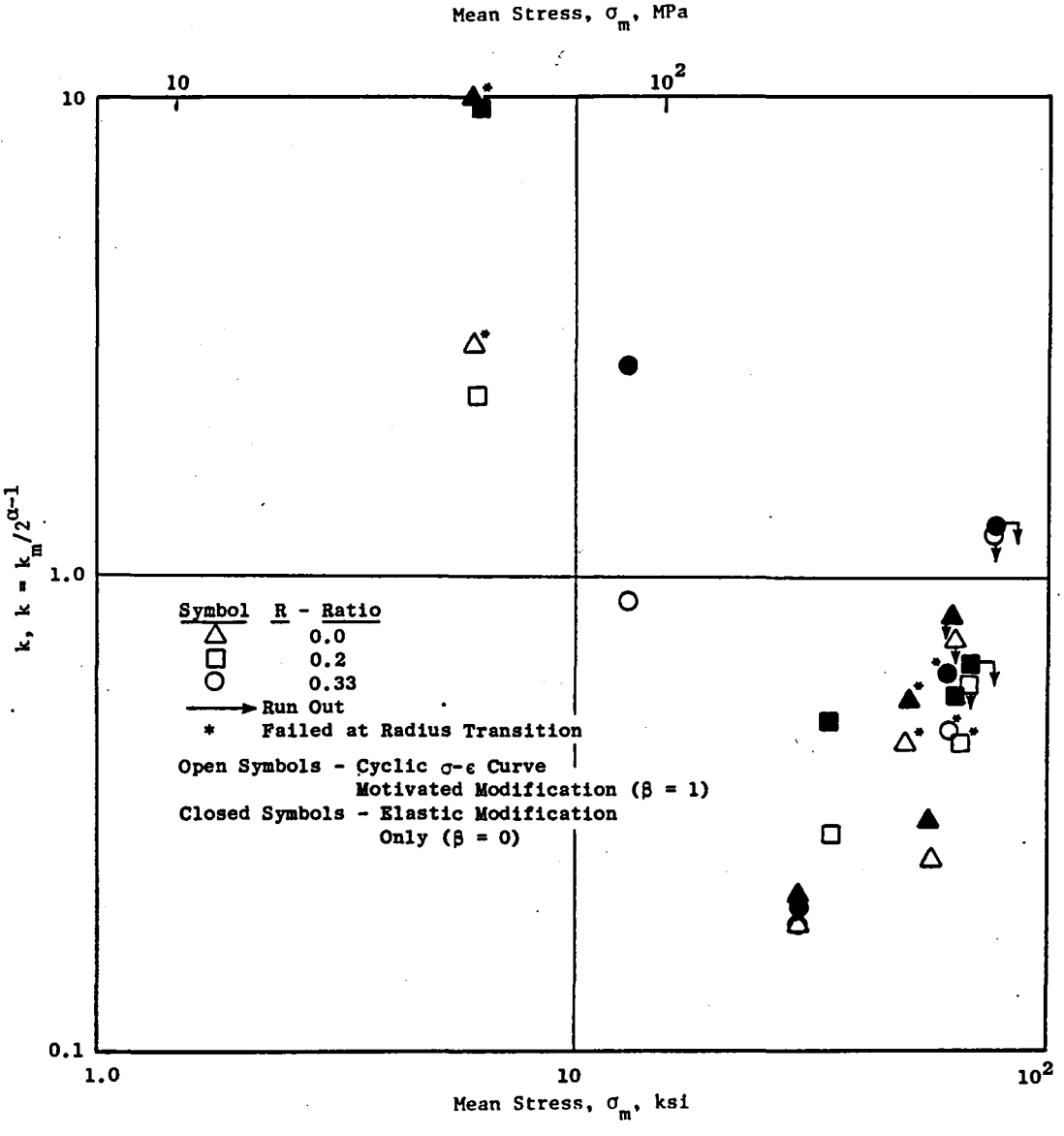

Figure C-6. Variation of k With Mean Stress for Inconel 718 at 538° C.

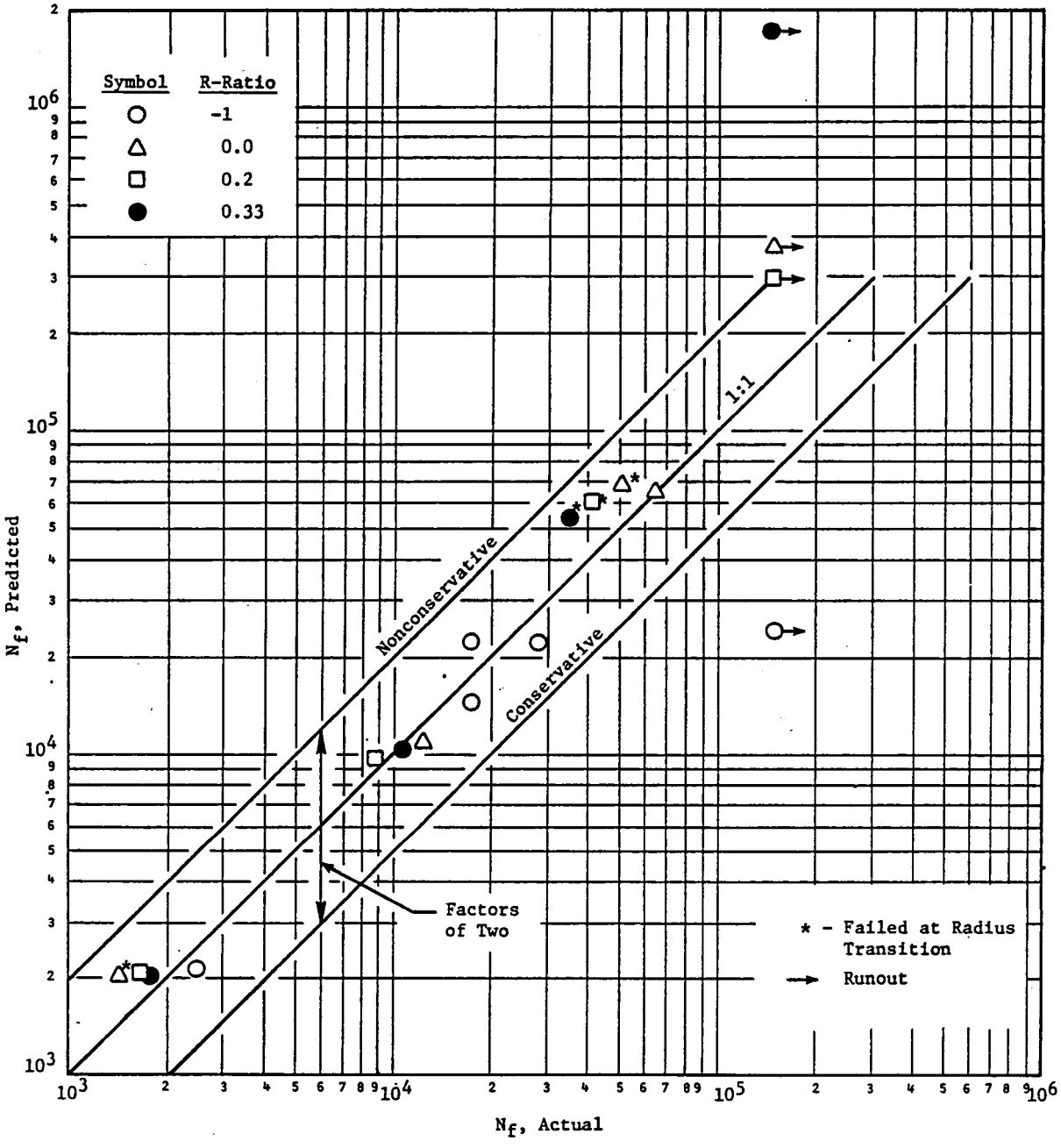

Figure C-7. Inconel 718, 538° C Correlation of Mean Stress Data Using MMHM, k = 0.302, β = 0.

strain range was small (note that the plastic strain range was influenced by the value of β while the elastic strain range was not). Therefore, it appeared that the inclusion of $\beta = 1$ was not necessary, in this case, due to the lack of significant plastic strain range in the long life range.

Figure C-8 shows a comparison of the predicted versus actual lives based on an average value of k obtained for $\sigma_m > 90$ MPa (13 ksi). In this plot, k was 0.226 compared to 0.302 for $\beta = 0$.

Detailed Evaluation of the Mean Stress Effect in Inconel 718

As part of this study, several mean stress theories were compared with an extensive set of strain-controlled Inconel 718 data at two different temperatures - 343° C (650° F) and 510° C (950° F). In total, there were 65 data points which included three different heats of material and three different strain R-ratios. The strain R-ratios varied from -21.0 to 0.0 representing a wide variety of mean stress conditions since both positive and negative mean stresses were included in the data set. A breakdown of data by strain R-ratio, temperature, and heat is given in Table C-I.

Table C-I. Composition of the Inconel 718 Data Set.

Temperature, ° C	Heat No.	Number of Data Points R = 3	R = -21	R = 0.0
343	1	4	9	6
	2	4	4	2
	3	0	4	2
		8	17	10
510	1	0	4	4
	2	4	9	5
	3	0	4	0
		4	17	9

The analyses of these data proceeded as follows. For the Leis method and the ε_{eq} approach, life was assumed to be related to the appropriate parameter by the equation,

$$\ln N_f = \sum_{i=1}^{4} a_i \, x^{i-1} \qquad (21)$$

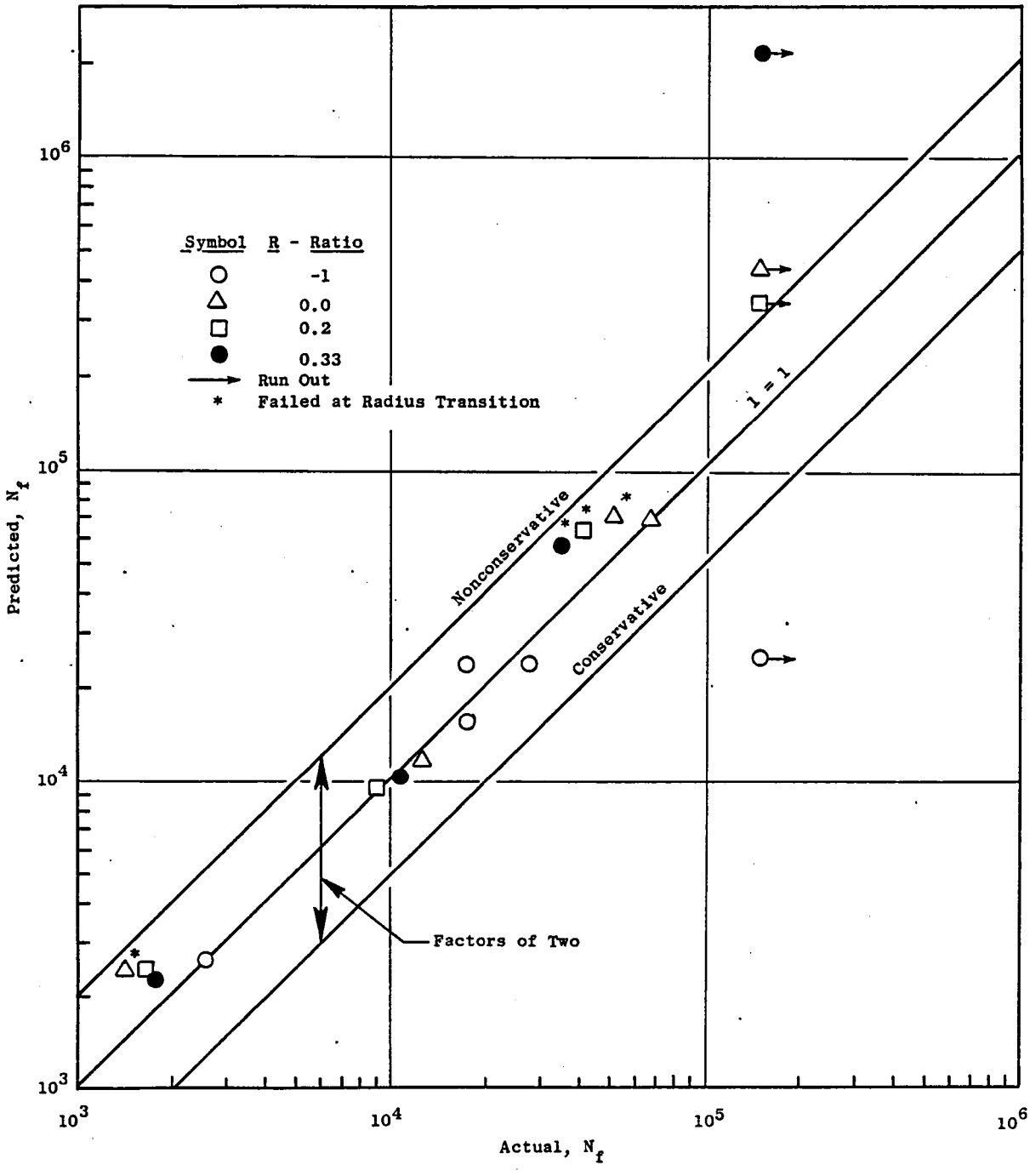

Figure C-8. Comparison of Predicted Versus Actual Inconel 718 at 538° C Based on MMHM With $\beta = 1$ ($k = 0.226$).

where x was either P_L or ε_{eq}, and the a_i were determined by linear regression of the data sets. The CM method was treated directly by first taking the logarithm of both sides of Equation 13 and applying linear regression. In Reference 4, the ε_{eq} approach is described in terms of an explicit relationship with the life; that technique would, it seems, require a nonlinear regression technique, so Equation 21 was adopted. The approach of Equation 21 was used in a similar study in Reference 12.

However, in the current case, the analysis of MMHM required nonlinear regression since there were no $R_\varepsilon = -1$ data. Accordingly, fully nonlinear methods were employed in this study. These methods were (A) the regression was applied to Equation 12; (B) the elastic and plastic strain range portions were regressed separately and added to give the total life prediction, and (C) with $\beta = 0$, the total life relationship was regressed. Method C resulted in a totally unrealistic value for the elastic slope, b. Hence, the results were not reported. In Method B, k_m and b were first determined by the analysis of the elastic lines; and, subsequently, these constants were used in regressing the $\Delta\varepsilon_p$ lines.

The results based on the MMHM are interesting, and are summarized in Table C-II. Life was predicted two ways for each method: (1) using the results of the elastic strain-range life fit only, and (2) based on the total strain life relationship. That is, for either method, A or B, life predictions could be based on either total strain range or elastic strain range. As shown in the table, the error depended upon how the regression was done and which strain (either elastic or total) was used. For example, in Method B where the elastic and plastic strain-life relationships were determined independently, the error was less when the predicted life was based on the elastic strain alone than when the life prediction was based on total strain. The value for the constant k_m, based on Method A at 510° C, was higher than expected, and the associated slopes of the elastic and plastic lines were reversed with the slope on the elastic line being higher. A comparison of three of the predictions at 343° C is given in Figures C-9 through C-11.

A summary of all the results is given in Table C-III, and comparison plots are shown in Figures C-12 through C-17. Figure C-18 shows how m was optimized for the ε_{eq} approach. As shown in Table C-III, the minimum value of m where E was based on crack initiation was temperature dependent. However, as shown in Figure C-18, E was not too sensitive to m over the range from about 0.7 to 0.9 at 510° C. When E was based on the regression of N_f, then m was not temperature dependent. The temperature dependence of m was not resolved in this study. Further evaluation of a limited amount of room temperature data suggested a reciprocal relationship with absolute temperature.

Examination of all of the comparison plots suggests that no method is totally satisfactory since either layering of the R-ratio data is observed or criss-crossing is found. However, as shown in Figures C-19 and C-20, there is a substantial effect of R-ratio, particularly in the range of 10^4 cycles or greater as is expected. In addition, comparing the average error, E, for lives based on total strain (from Figure C-18 with m = 1) to those in Table C-III, it is seen that most of the approaches reduce E compared to total strain

Table C-II. Results of the MMHM Analyses.

Temperature, °C	Method A(1)				Method B(4)			
	$\Delta\varepsilon_t$(2)		$\Delta\varepsilon_e$(3)		$\Delta\varepsilon_e$(3)		$\Delta\varepsilon_t$(2)	
	E	k_m	E	k_m	E	k_m	E	k_m
343	48.74	1.819	259.6	1.819	51.3	0.772	72.7	0.772
510	54.14	354.2	97.1	354.2	76.8	0.528	129.0	0.528

(1) Method A is a total regression of Equation 6 with all constants determined by using $\Delta\varepsilon_t$ as the dependent variable, and σ_m and N_i as independent variables.

(2) E is based on using the total strain range and iteratively solving Equation 6 for the predicted cycles to initiation.

(3) E is based on using the elastic strain range and the first term on the right-hand side of Equation 6 to determine the predicted cycles to initiation.

(4) Method B is to determine the constants of the elastic strain range - N_i portion of Equation 6 by nonlinear regression; the $\Delta\varepsilon_p$-N_i line is then fit using the results of the elastic fit.

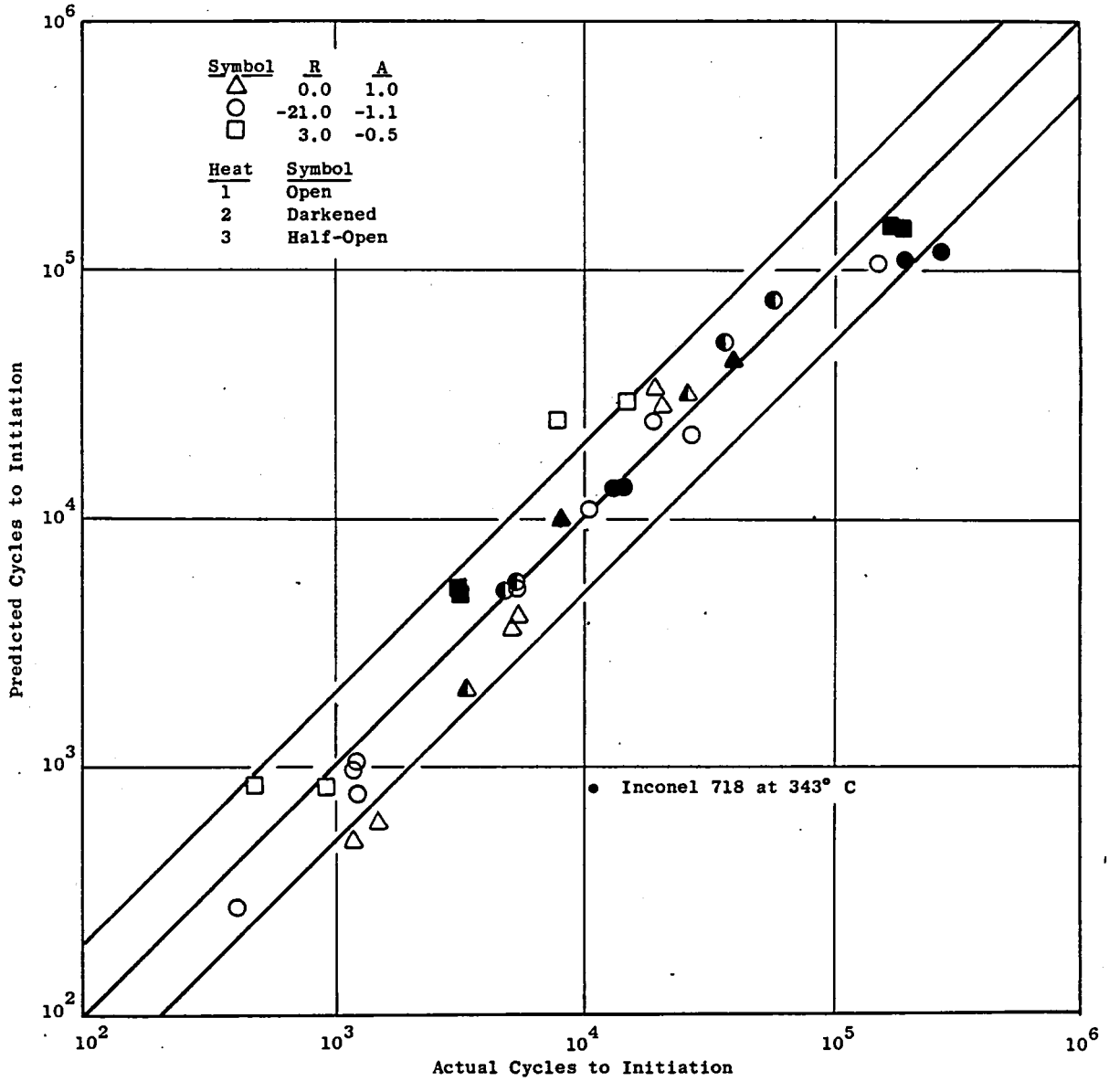

Figure C-9. Predictions By the MMHM - Method A Using Total Strain Range.

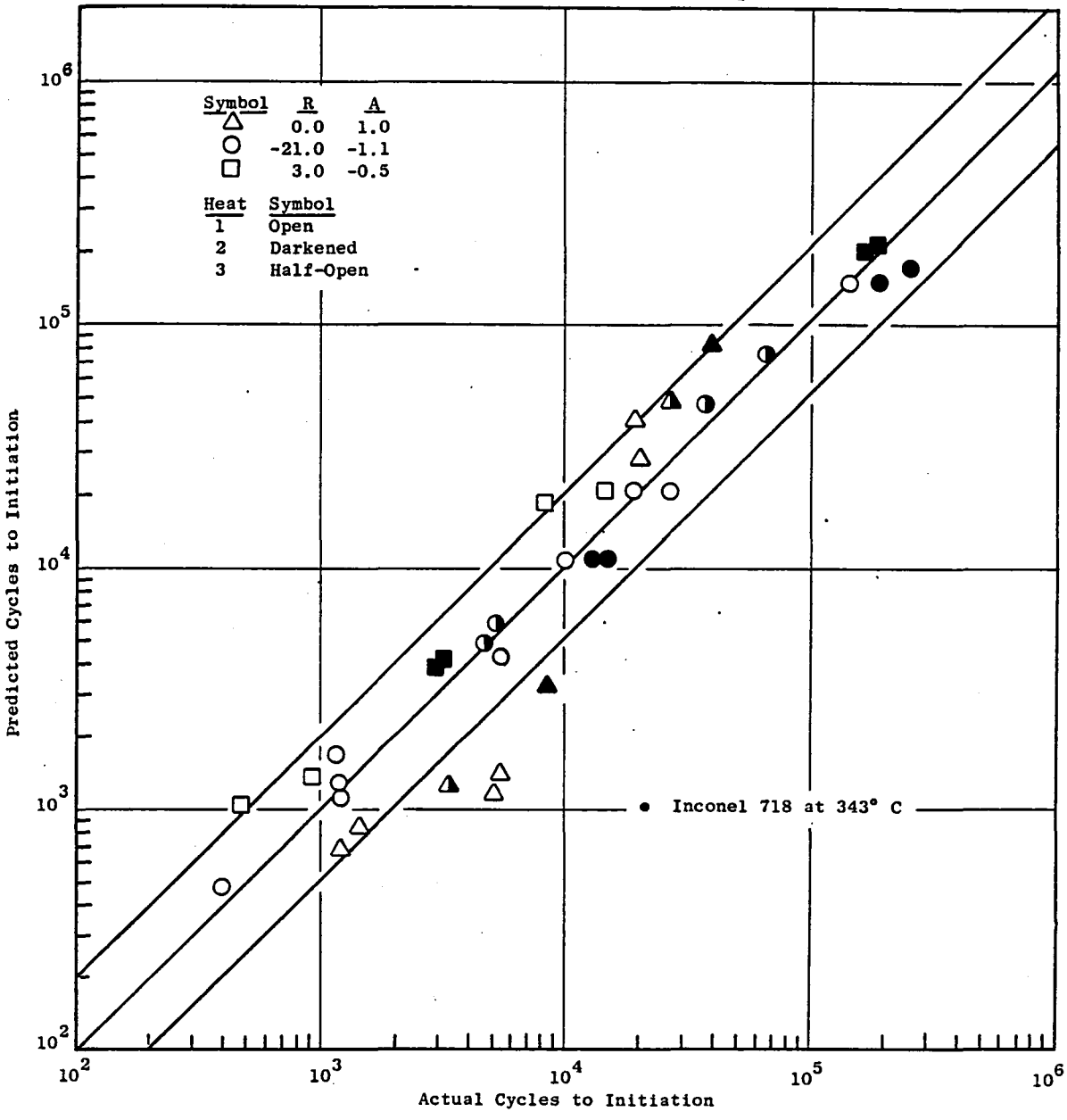

Figure C-10. Predictions By the MMHM - Method B, Based on Elastic Strain Range.

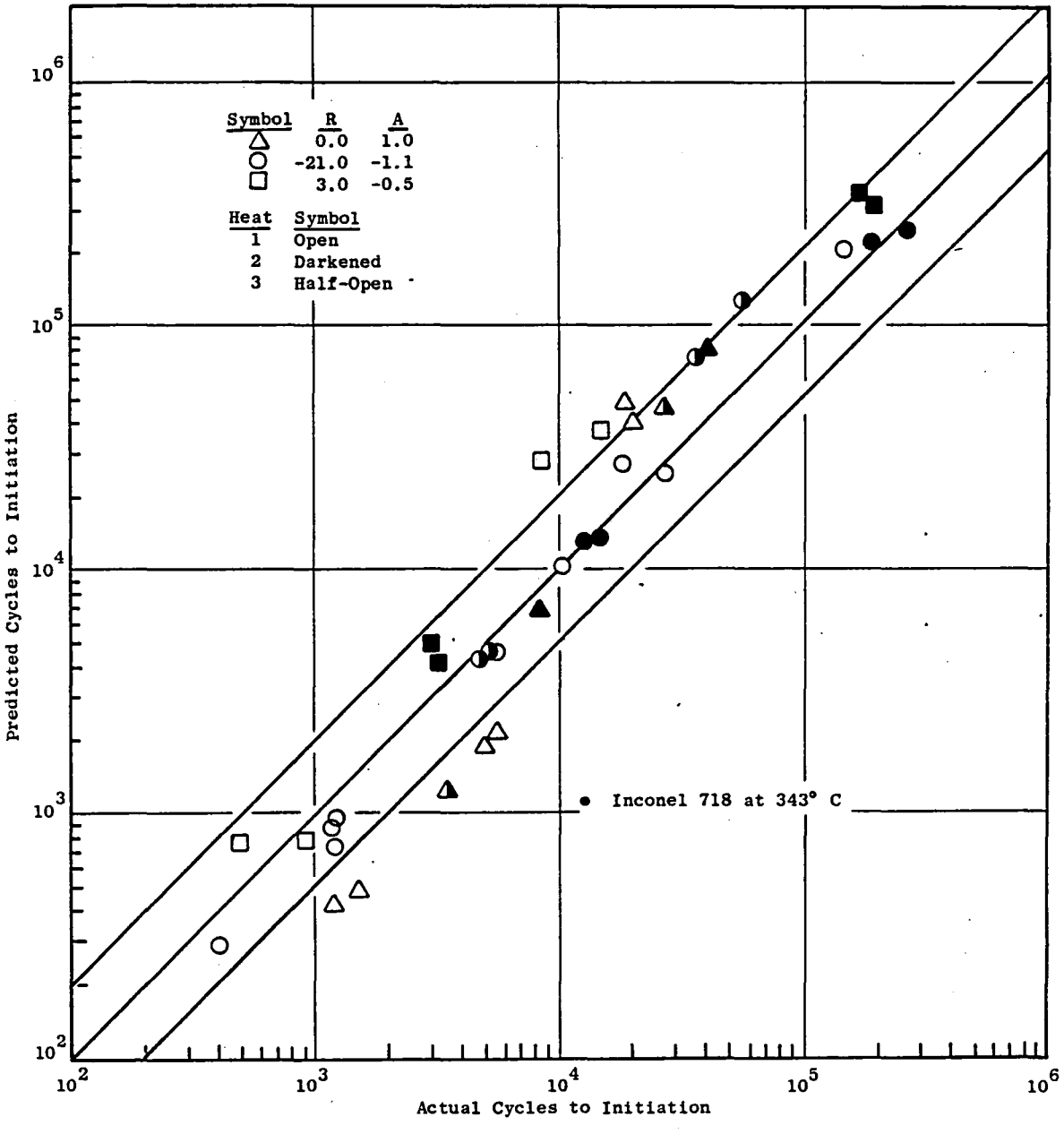

Figure C-11. Predictions By the MMHM - Method B Based on Total Strain Range.

Table C-III. Comparison of All Results for Inconel 718.

Method	Temperature, ° C	E $(N_i)^{(1)}$ $(\sim\sigma)^{(2)}$	m	E$(N_f)^{(1)}$	m
Leis	343	55.1 (0.427)	---	50.3	---
ε_{eq}	343	38.05 (0.318)	0.652	34.89	0.66
CM	343	54.78 (0.448)	---	52.11	---
MMHM(3)	343	48.74 (0.4355)	---	---	---
Leis	510	44.76 (0.467)	---	46.65	---
ε_{eq}	510	45.53 (0.47)	0.8	47.03	0.69
CM	510	53.35 (0.5108)	---	55.46	---
MMHM(3)	510	54.14 (0.545)	---	---	---

(1) $$\%, E^2 = \frac{1}{n} \sum_{i=1}^{n} \left(1. - N^i_{pred}/N^i_{act} \right)^2$$

(2) $$\sigma^2 = \frac{1}{n} \sum_{i=1}^{n} \left[\ln \left(N^i_{pred}/N^i_{act} \right) \right]^2$$

(3) See Table C-II.

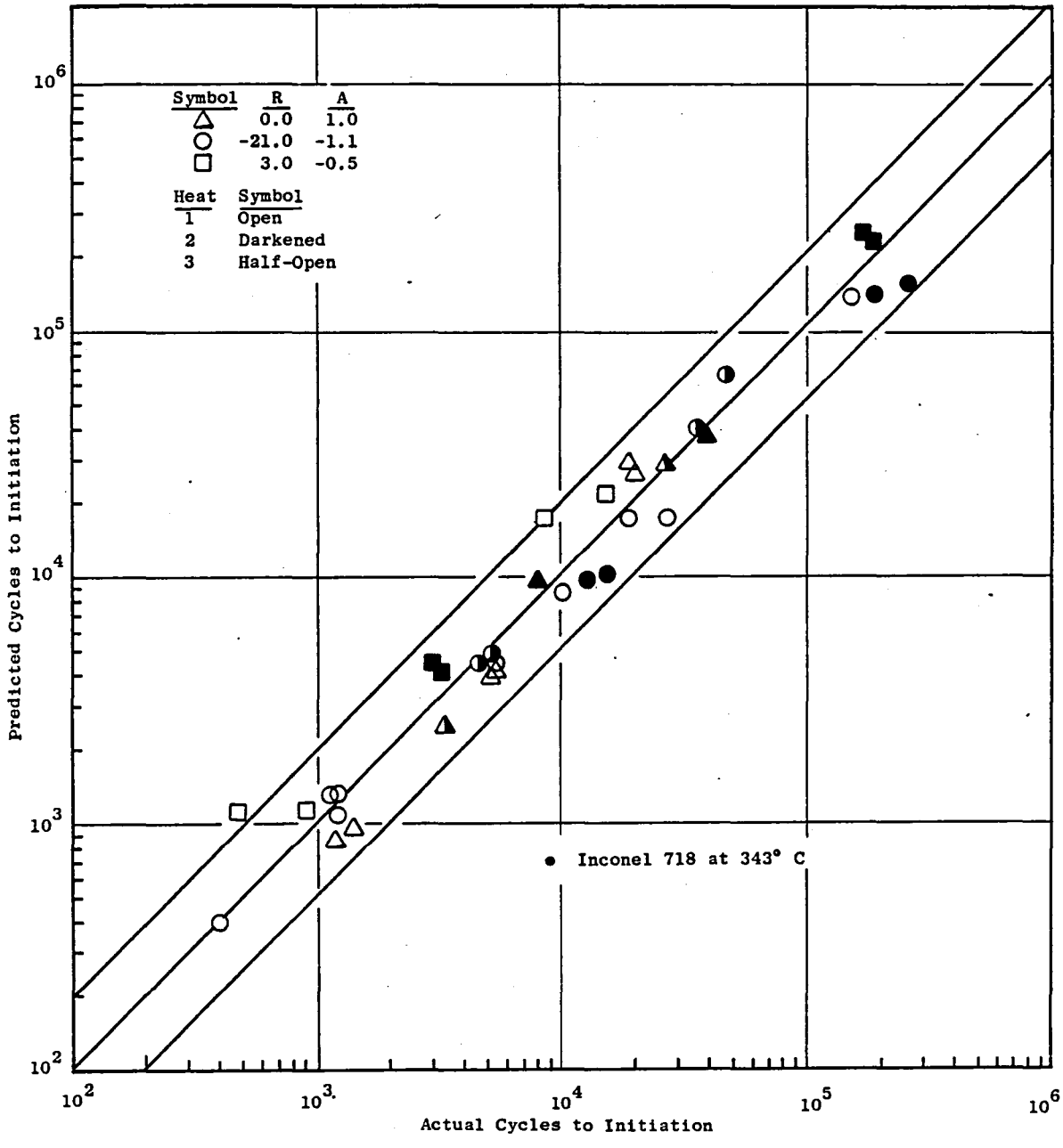

Figure C-12. Predictions Based on ε_{eq}, m = 0.652.

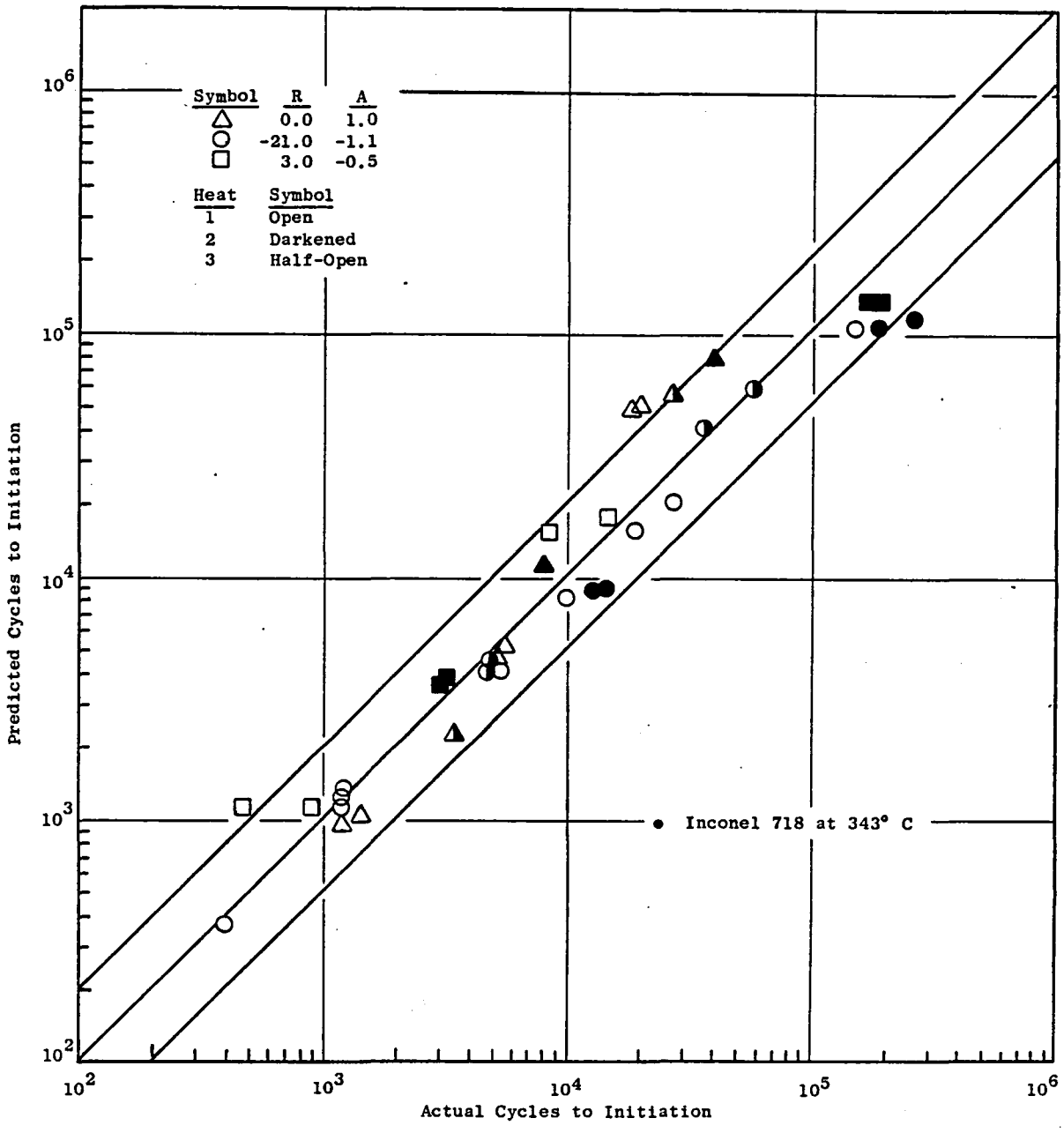

Figure C-13. Predictions Based on Leis Method.

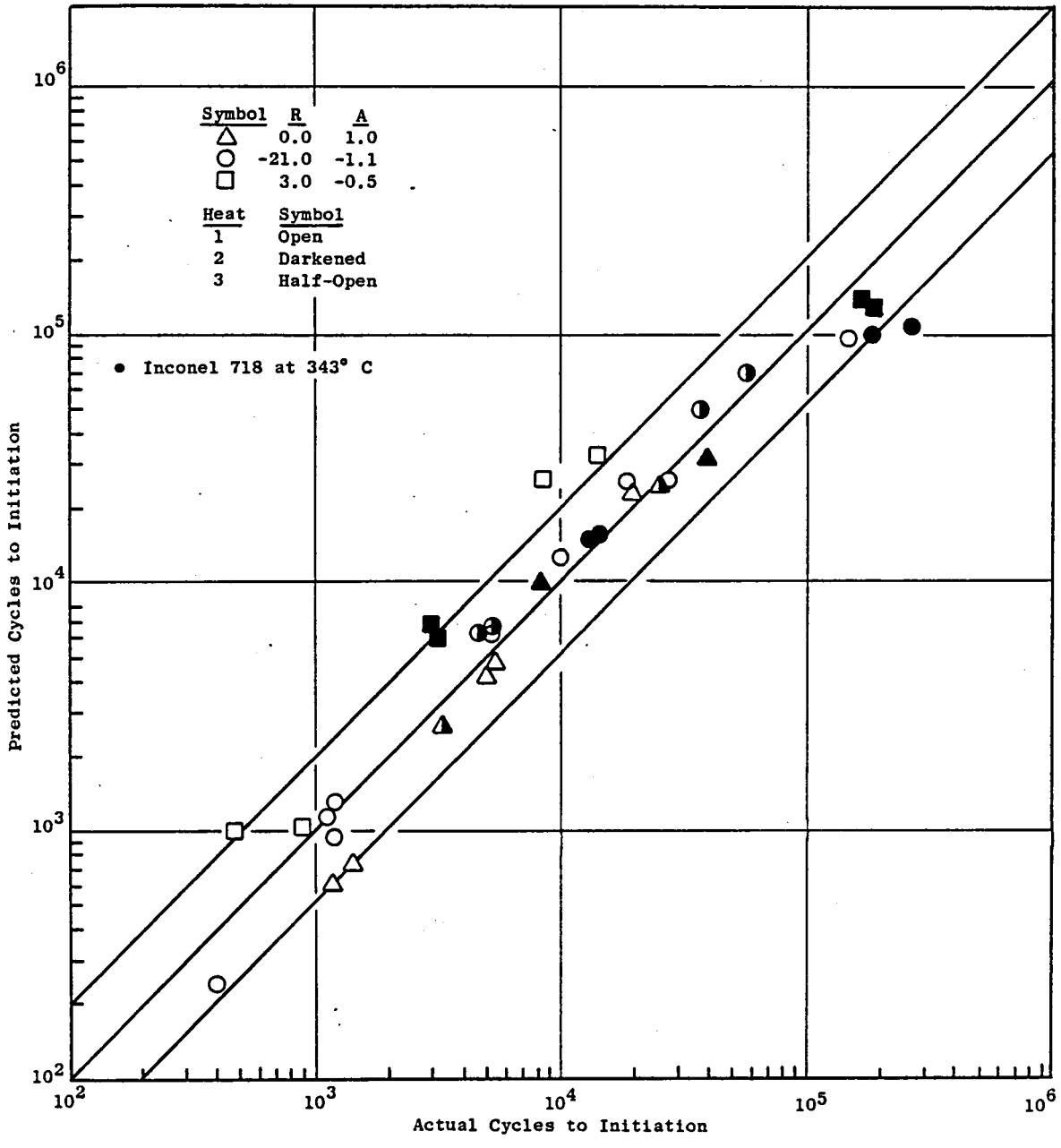

Figure C-14. Predictions Based on the CM Approach.

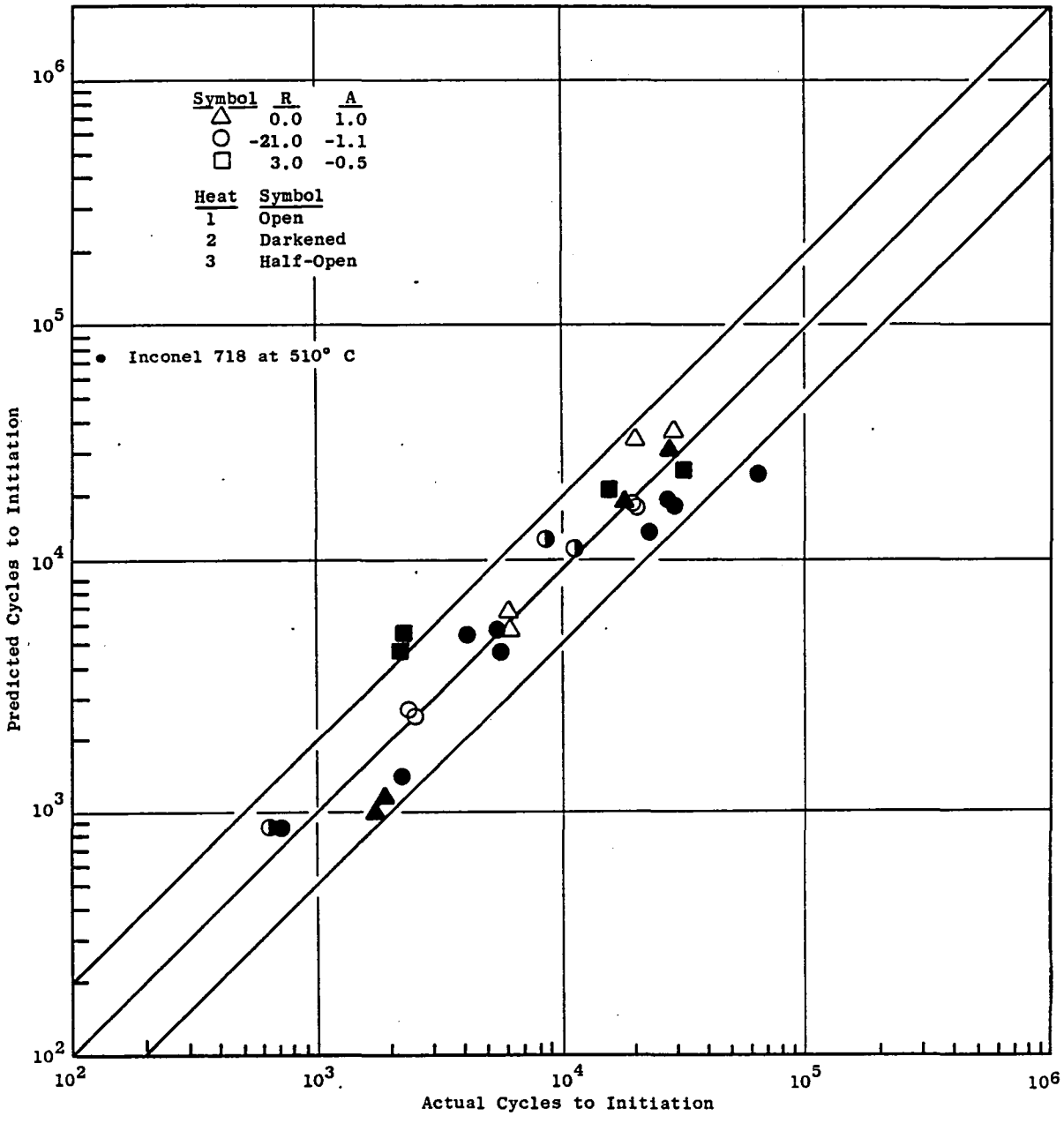

Figure C-15. Predictions Based on the Equivalent Strain Approach.

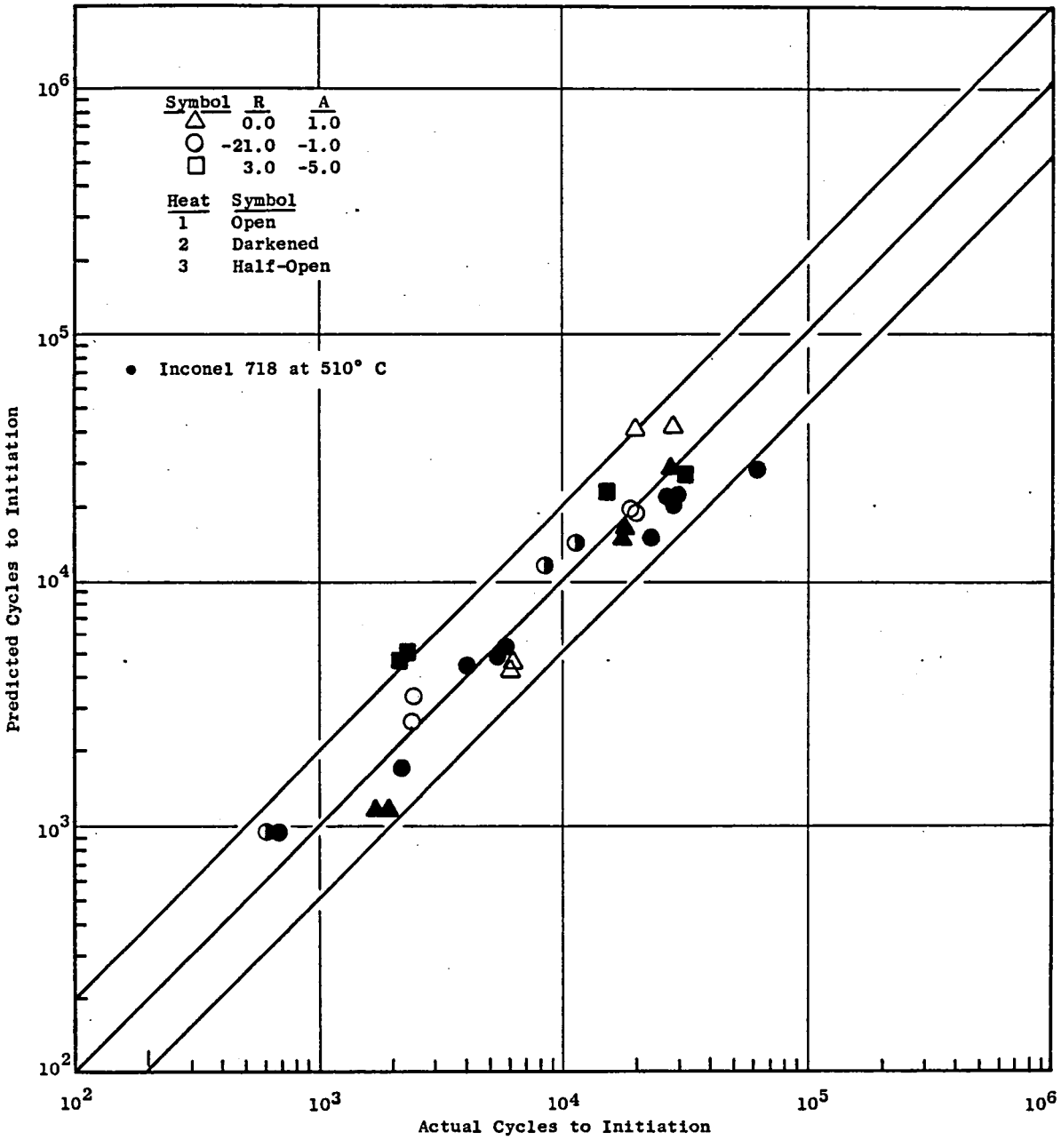

Figure C-16. Predictions Based on the Leis Method.

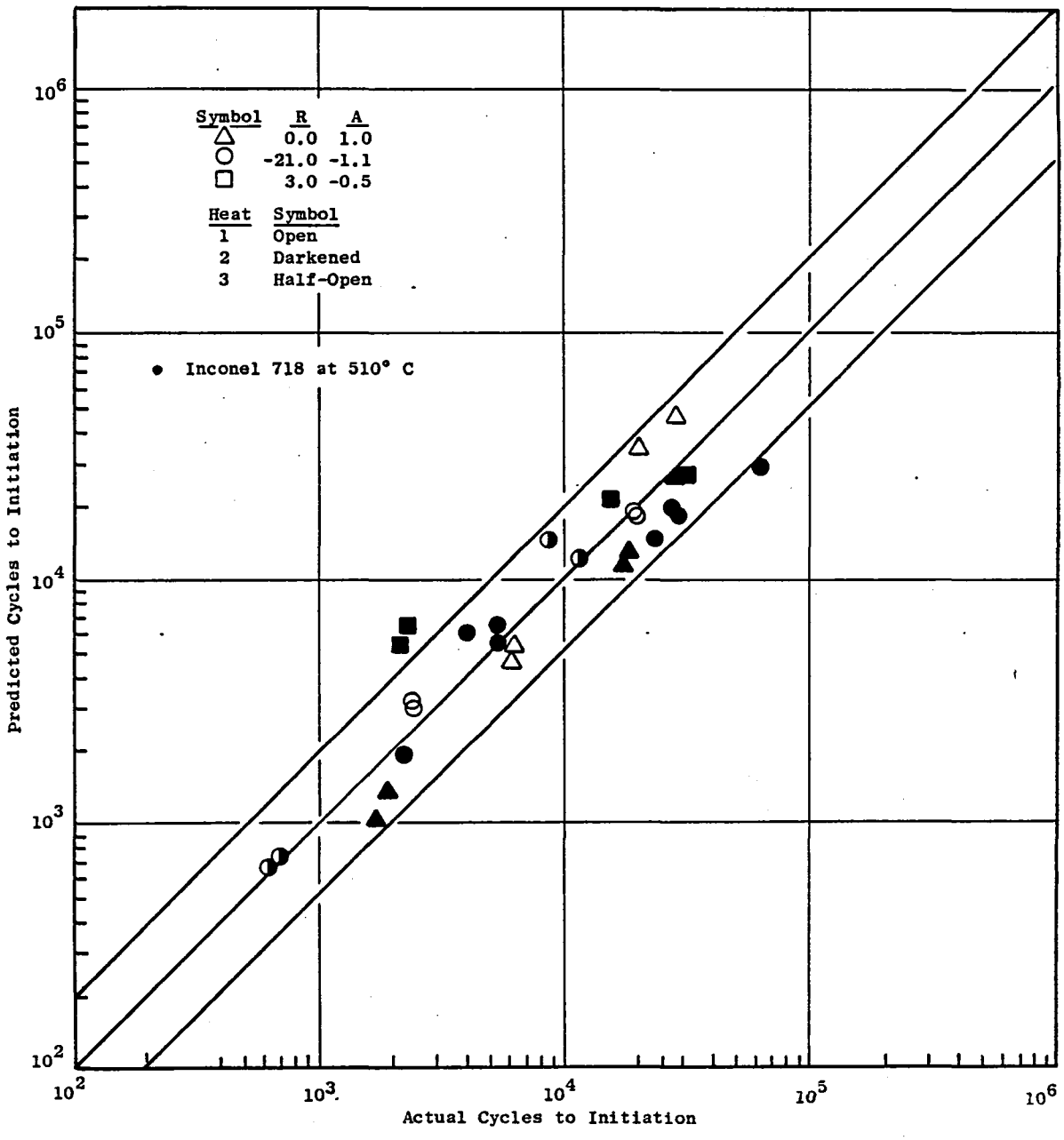

Figure C-17. Predictions Based on the Approach of CM.

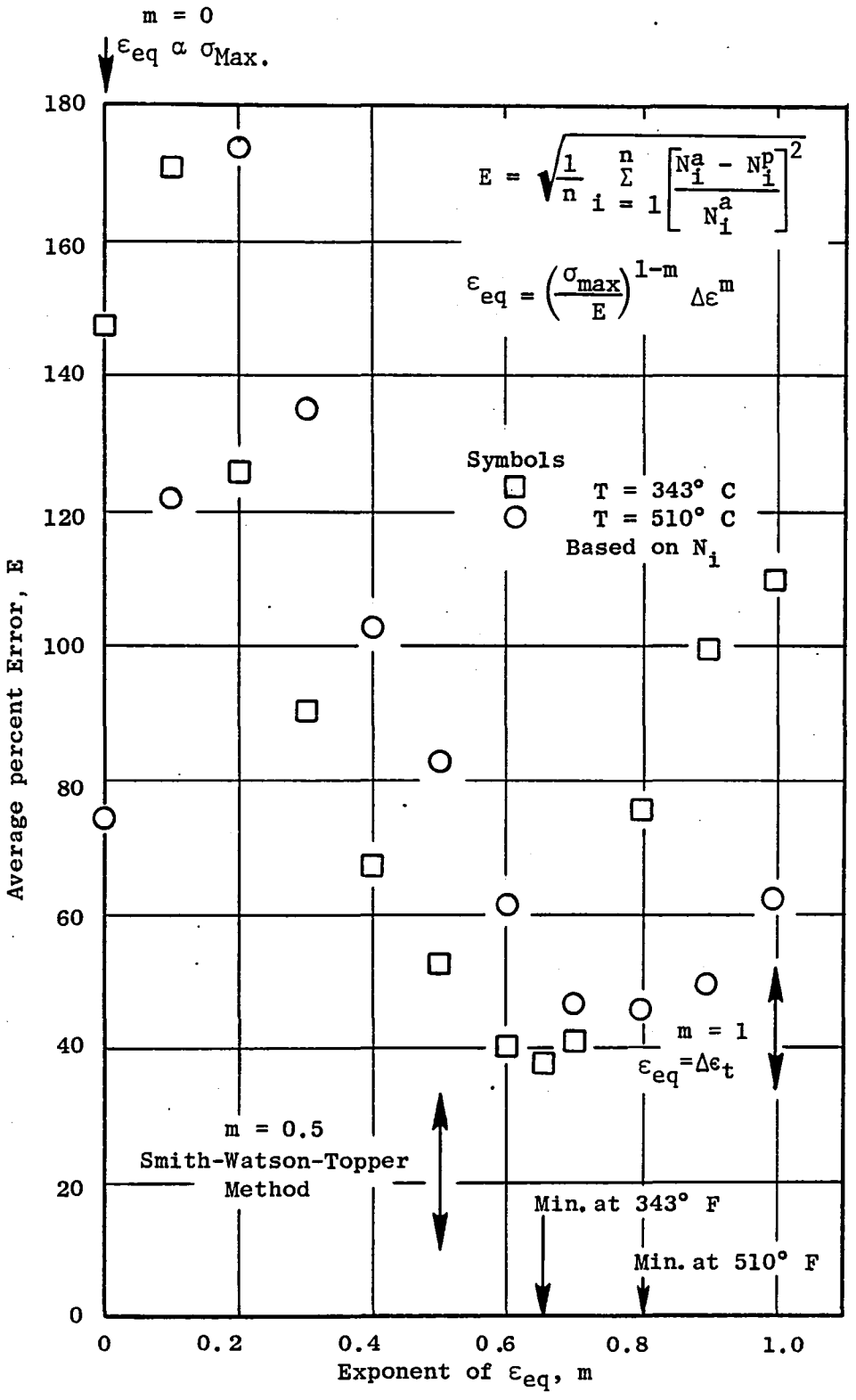

Figure C-18. Optimization of m for the ε_{eq} Approach.

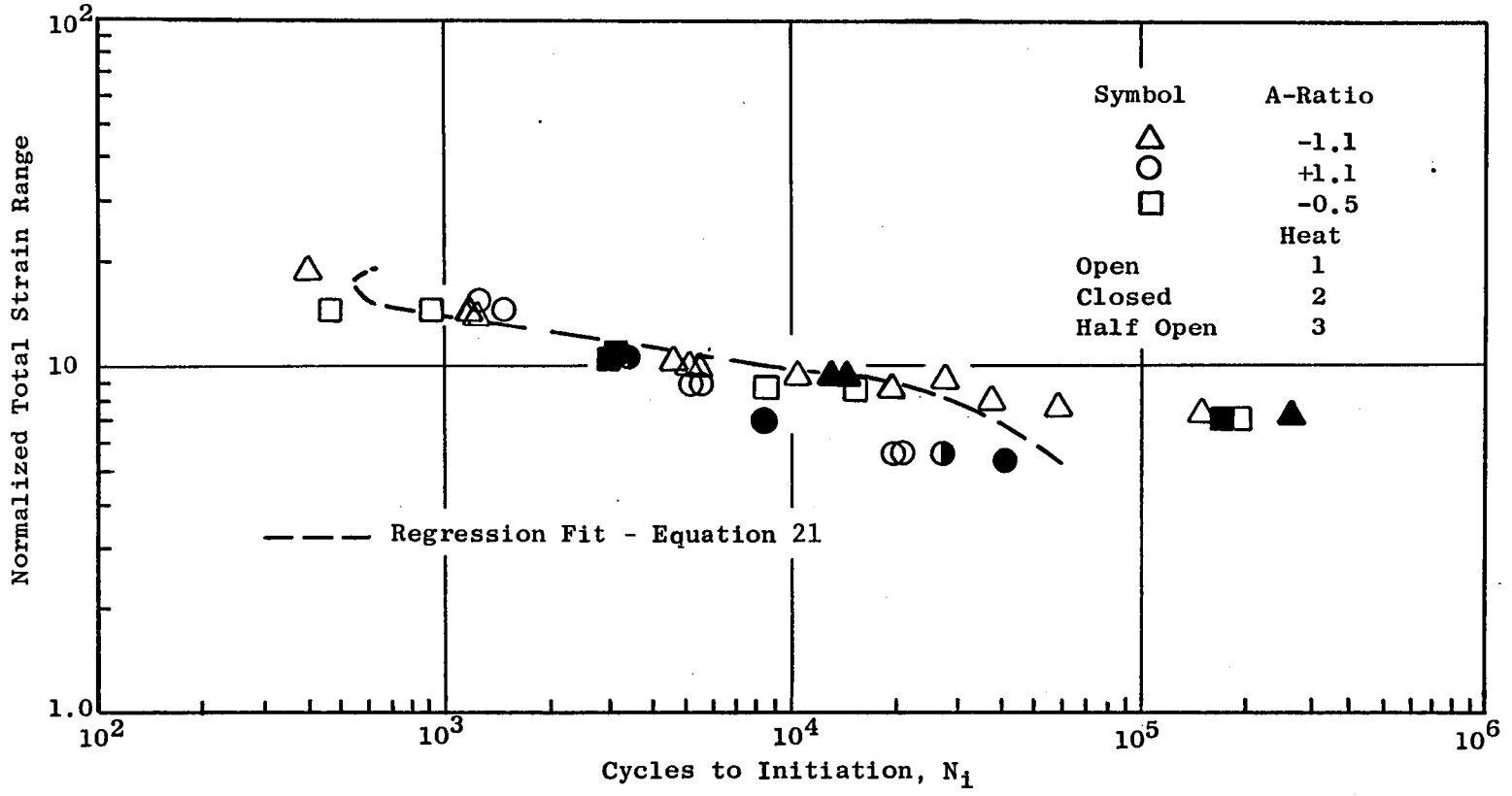

Figure C-19. Inconel 718 at 343° C, Effect of R-Ratio.

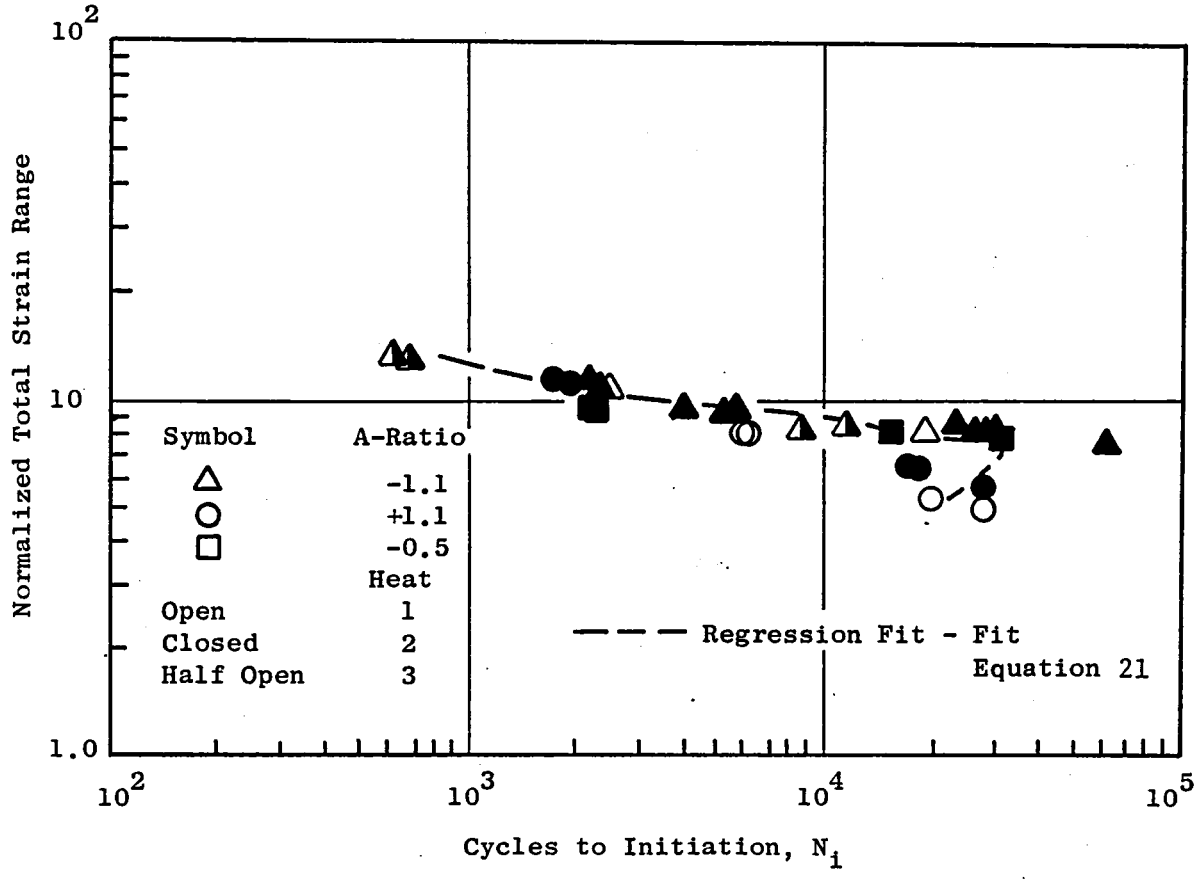

Figure C-20. Inconel 718 at 510° C, Effect of R-Ratio.

predictions, particularly at 343° C. Note that the regression lines using Equation 8, based on total strain, are included on Figures C-18 and C-19, and that the resulting fits are, at the very least, not good for extrapolation. In this respect, recall that the CM approach and the MMHM both specify the strain-life relationships; in the current study, both the Leis and the ε_{eq} are fit with polynomials. The methods which specify the form of the strain-life relationship would yield more reliable extrapolations; however, plots of both the Leis and ε_{eq} methods regression lines at 343° C reveal none of the physically unrealistic trends that are shown in Figures C-19 and C-20 for total strain range. Note that the data at 343° C covers a wider range in life than that at 510° C. This may be the reason for the difficulties observed in fitting the MMHM at 510° C.

Based on Table C-III, it is seen that the ε_{eq} method was superior at 343° C, while the Leis method was best at 510° C. Between the two methods, the Leis requires no fitting parameters, and would appear to be superior for this reason. However, a method similar to the ε_{eq} approach (the Walker-relationship, $\bar{\sigma} = \sigma_{max}\,[1-R]^{b}$) is widely used at the General Electric Company in crack growth analyses; and in that case, it is known that b is strongly material dependent. This implies that the goodness of fit of the Leis parameter for other materials would not be as it is in the present case. In addition, in Reference 12, it was found that the equivalent strain approach was the best of the methods investigated (the Leis method was not evaluated in Reference 12). Considering all of this discussion, the most prudent conclusion is that the ε_{eq} method is the best correlating technique that would be most useful when data are available to determine the m parameter. The Leis parameter could be considered as the best predictive technique to be applied in the absence of sufficient mean stress data.

Recall Equation 7 which shows that the value of the standard deviation, σ, in Table C-III can be used to give a factor which is an indication of minimum life. Considering the Inconel 718 results, the range of this factor is 0.261 for the Cruse and Meyer method to 0.385 for the equivalent strain method at 343° C. At 510° C, the range is smaller, being 0.195 for the MMHM to 0.246 for the Leis method. It would appear that the comparisons can yield useful results for judging the relative value of individual theories. When such theory comparisons yield only small differences, then other criteria must be utilized exclusively in theory selection; these additional considerations are required in other cases depending upon the theory usage, etc. Such considerations are discussed in the main body of this report, and they are an integral part in the process of final theory recommendations.

As a final comparison of these theories consider Figure C-21. This figure was constructed by assuming that all methods agreed at one point in life for R = -1, and that the alternating stress in that case was 690 MPa (100 ksi). The curves were generated using the resulting curve fits at 343° C, and the assumption was made that the strain was elastic. Note that only the MMHM predicts an intercept of the mean stress axis for finite mean stresses, and that all methods predict monotonically increasing alternating stresses with

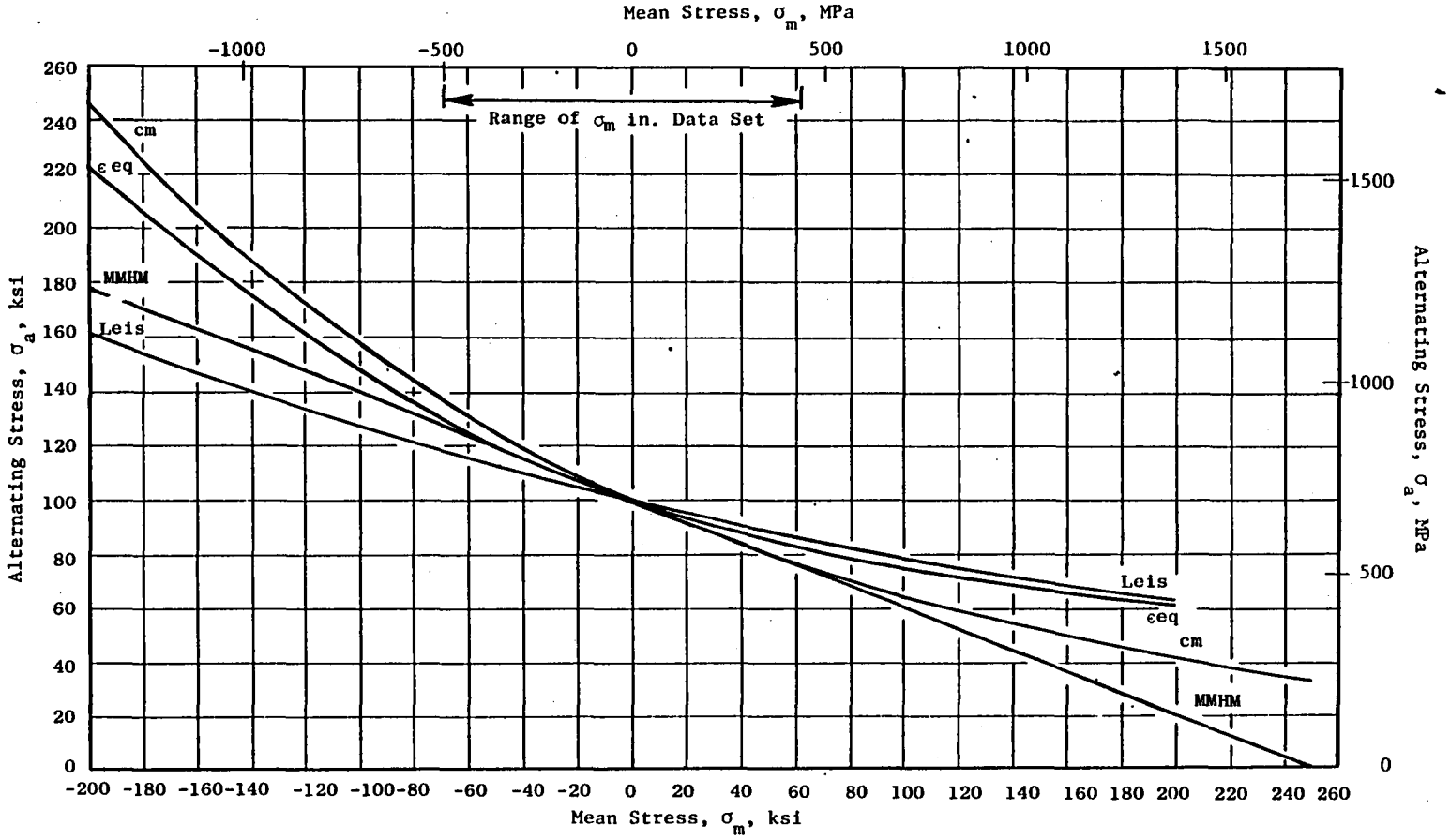

Figure C-21. Predicted Goodman Diagrams Per Each Method, 343° C.

decreasing mean stress. This latter tendency was partially the result of the assumption of elastic strains since the predicted stress ranges for high compressive mean stresses would exceed the elastic limit. No attempt was made to include the effect of yielding on these predictions.

APPENDIX C - REFERENCES

1. Manson, S., Thermal Stress and Low Cycle Fatigue, McGraw-Hill, 1966, pp. 171.

2. Polhemus, J.F., Spaeth, C.E., and Vogel, W.H., "Ductility Exhaustion Model for Prediction of Thermal Fatigue and Creep Interaction," Fatigue at Elevated Temperatures, ASTM STP 520, ASTM, 1973, pp. 625-636.

3. Kikukawa, M., Jono, M., Kawata, T., Song, T., and Himuro, H., "Low-Cycle Fatigue Under Varying Strain Conditions," Bulletin of the JSME, Vol. 20, No. 140, February 1977, pp. 145-152.

4. Rice, R.C., Davies, K.B., Jaske, C.E., Fedderson, C.E., "Consolidation of Fatigue-Crack-Propagation Data for Design Use," NASA CR-2586, October 1975.

5. Leis, B.N., "An Energy-Based Fatigue and Creep-Fatigue Damage Parameter," Trans. ASME, J. of Press. Vessel Technology, Vol. 99, Series J, No. 4., November 1977, pp. 524-533.

6. Cruse, T.A. and Meyer, T.G., "Structural Life Prediction and Analysis Technology," AFAPL-TR-78-106, December 1978.

7. Manson, S.S. and Halford, G.R. "Practical Implementation of the Double Liner Damage Rule and Damage Curve Approach for Treating Cumulative Fatigue Damage, "International Journal of Fracture, Vol. 17, No. 2, 1981, pp. 169-192. (See also Vol. 17, No. 4, 1981, pp. R35-R42.)

8. Bernstein, H.L., "A Stress-Strain-Time Model (SST) for High-Temperature, Low-Cycle Fatigue," Methods for Predicting Material Life in Fatigue, W.J. Ostergren and J.R. Whitehead, eds., ASME, 1979, pp. 89-100.

9. Ostergren, W.J., "Correlation of Hold Time Effects in Elevated Temperature Low Cycle Fatigue Using a Frequency Modified Damage Function," 1976 ASME-MPC Symposium on Creep-Fatigue Interaction, pp. 179-202, December 1976.

10. Sines, G, "Failure of Materials Under Combined Repeated Stresses with Superimposed Static Stresses," NACA TN 3495, National Advisory Committee for Aeronautics, November 1955.

11. Coffin, L.F., Jr., Carden, A.E., Manson, S.S., Severud, L.K., and Greenstreet, W.L., "Time-Dependent Fatigue of Structural Alloys -- A General Assessment (1975)," ORNL Report 5073, Oak Ridge National Laboratory, January 1977.

12. Doner, M., Bain, K.R., and Adams, J.H., "Evaluation of Methods for the Treatment of Mean Stress Effects on Low-Cycle Fatigue," Paper No. 81-GT-122, ASME, J., of Eng. for Power, December 1980.

13. Taira, S., "Lifetimes of Structures Subjected to Varying Load and Temperatures," Creep in Structures, Hoff, N.J., Ed., Academic Press, New York, 1962, pp. 96.

14. Laflen, J.H., "Integrated Creep Rupture Damage in High Cycle Fatigue: A Method of Predicting Goodman Diagram at Elevated Temperatures," M.S. Thesis, University of Cincinnati, 1972.

15. Carnahan, B., Luther, H.A., and Wilkes, J.O., Applied Numerical Methods, John Wiley and Sons, Inc., 1969, pp. 573.

16. Laflen, J.H. and Jaske, C.E., "Cyclic Relaxation Response Under Creep-Fatigue Conditions," Stress Relaxation Testing, ASTM STP 676, A. Fox, Ed., ASTM, 1979, pp. 182-206.

17. Smith, K.N., Watson, P., and Topper, T.H., "A Stress-Strain Function for the Fatigue of Metals," Journal of Materials, JMLSA, Vol. 5, No. 4, December 1970, pp. 767-778.

18. Fatigue Design Handbook, Society of Automotive Engineers, New York, 1968, Chapter 3.2.

19. Walcher, J., Gray, D., and Manson, S.S., "Aspects of Cumulative Fatigue Damage Analysis of Cold and Rotating Structures," AIAA/SAE/ASME 15th Joint Propulsion Conference, Paper No. 79-1190, Las Vegas, June 18-20, 1979.

APPENDIX D - MULTIAXIALITY

Through a review of the current literature on multiaxial fatigue, it was found that the influence of at least two factors remain unresolved with respect to the many popularly used equivalence quantities. These are the effects of superimposed pressure and the effect of nonproportional stress and straining. Before reporting the results of this literature review, it is useful to formally state some of the basic mathematical relationships in multiaxial stress and strain states.

Consider a general multiaxial stress state, $\sigma_{ij}(t)$, which is some function of time, t, and is referred to some fixed coordinate system. At any given time, any such general state of stress (the discussion is actually valid for any symmetric second order tensor) is completely characterized by the solution of the eigenvalue problem,

$$(\sigma_{ij} - \lambda\delta_{ij})\, n_i = 0 \tag{1}$$

where δ_{ij} is Kronecker delta symbol, λ is an eigenvalue, and n_i are the direction cosines of an eigenvector referred to the fixed coordinate system. Equation 1 results in a cubic equation in λ, the solution of which yields the three principal stresses. Back substitution of each of these principal stresses into Equation 1 yields the principal directions. In effect, these principal direction cosines form the components of an orthogonal transformation matrix which rotates the original stress tensor into a diagonal stress tensor. Note that such a state of stress (σ_{ij}) can, in general, be rotated to any other coordinate system which still must be characterized by the same eigenvectors and eigenvalues. This fact leads to the concept of invariants: the stress state is uniquely characterized by these three principal stresses and is independent of rotations of the coordinate system. The so-called invariants of the stress tensor are given by

$$I_\sigma = \sigma_{11} + \sigma_{22} + \sigma_{33} = \sigma_{ii} = \mathrm{tr}(\sigma_{ij}), \tag{2}$$

$$II_\sigma = \frac{1}{2}\left(\sigma_{ij}\sigma_{ji} - \sigma_{ii}\sigma_{jj}\right) = \frac{1}{2}\,\sigma_{ij}\sigma_{ji} - \frac{1}{2}\,I_\sigma^{\,2}, \tag{3}$$

$$III_\sigma = \det \sigma_{ji}, \tag{4}$$

where I_σ, II_σ, and III_σ are the three invariants and det refers to the determinant of a matrix.

The first invariant is directly related to the definition of pressure, p,

$$p = -\frac{1}{3}\ (\sigma_{11} + \sigma_{22} + \sigma_{33}) = -\frac{1}{3}\ tr\ (\sigma_{ij}).$$

Since plastic flow is thought to be independent of superimposed pressure (i.e., the assumption of constant volume or isochoric plastic flow), many plasticity theories are based on the deviatoric stress tensor, S_{ij},

$$S_{ij} = \sigma_{ij} - \frac{1}{3}\ tr\ (\sigma_{\ell m})\ \delta_{ij}$$

$$\equiv \sigma_{ij} + p\ \delta_{ij}.$$

It is easily shown that a uniform increase in the pressure does not influence the deviatoric stress components. As with the stress tensor, three invariants of the deviatoric tensor also exist,

$$I_{\underset{\sim}{S}} \equiv 0,$$

$$II_{\underset{\sim}{S}} = \frac{1}{2}\ S_{ij} S_{ji}, \text{ and}$$

$$III_{\underset{\sim}{S}} = \det\ S_{ij}.$$

The second invariant of the deviatoric stress tensor ($II_{\underset{\sim}{S}}$) is frequently called J_2 and is the basis of the von Mises yield and fracture criteria. It is easily shown that,

$$\sigma_e = \sqrt{3II_{\underset{\sim}{S}}} = \frac{3}{\sqrt{2}}\ \tau_{oct} \qquad (5)$$

$$= \frac{1}{\sqrt{2}}\ \sqrt{(\sigma_1 - \sigma_2)^2 + (\sigma_2 - \sigma_3)^2 + (\sigma_1 - \sigma_3)^2},$$

where σ_e is the effective stress, τ_{oct} is the octahedral shear stress (the maximum shear stress on the octahedral plane), and the σ_i are the principal stresses. It is clear that such equivalence quantities are independent of pressure which is measured by the first invariant of the stress tensor, Equation 2.

In addition to such invariance quantities, it is often suggested that shear stress or strain quantities are those to be used in correlating multiaxial data. Frequently, the stress or strain normal to the plane of shearing is also thought to be important. Mathematically, these quantities are defined by using the normal vector, $\underset{\sim}{n}$, to the plane of interest. The traction vector, $t(\underset{\sim}{n})$, on the plane defined by $\underset{\sim}{n}$ is given as,

$$t_{(\underset{\sim}{n})} = \underset{\sim}{n}\cdot\underset{\sim}{\sigma} = \underset{\sim}{\sigma}\cdot\underset{\sim}{n}$$

whereas the normal stress σ_{nn} to this plane (a scalar) is

$$\sigma_{nn} = \underset{\sim}{n}\cdot\underset{\sim}{\sigma}\cdot\underset{\sim}{n}\,.$$

In this context, it should be noted that the definition of pressure given above is equivalent to the normal stress acting on the octahedral plane with $\underset{\sim}{n} = 1/\sqrt{3}\ (\hat{i} + \hat{j} + \hat{k})$. The maximum shear stress on such a plane is given by

$$\underset{\sim}{\tau}_{max.} = t_{(\underset{\sim}{n})} - (\underset{\sim}{n}\cdot\underset{\sim}{\sigma}\cdot\underset{\sim}{n})\ \underset{\sim}{n}.$$

The shear stress in the direction $\underset{\sim}{s}$ on the plane $\underset{\sim}{n}$ (where $\underset{\sim}{s}$ is some unit vector such that $\underset{\sim}{s}\cdot\underset{\sim}{n} = 0$) is given by

$$\tau = \underset{\sim}{s}\cdot\underset{\sim}{\sigma}\cdot\underset{\sim}{n} = \underset{\sim}{n}\cdot\underset{\sim}{\sigma}\cdot\underset{\sim}{s}.$$

One such unit vector, $\underset{\sim}{s}$, can be selected to yield the magnitude of τ_{max}. While these expressions are written in terms of a stress tensor, identical relationships can be expressed for strain by merely substituting the strain tensor (ε) for the stress tensor. It should be noted that any shear stress (or strain) quantity on any plane and in any direction is independent of superimposed hydrostatic pressure; the normal strain (stress) will always depend on the numerical value of hydrostatic pressure. Note that these relationships are mathematically equivalent to Mohr's circle constructions.

Most multiaxial, experimental work has been undertaken using conditions called proportional (or radial) loading. Under such conditions, the components of the stress tensor change in constant ratio,

$$\sigma_{ij} = R_{ij}f(t)$$

where R_{ij} is a constant tensor and $f(t)$ is some function of time. It is easily shown that the eigenvectors under such conditions are constant and are those of the R_{ij} tensor; the eigenvalues scale with the function $f(t)$. Under the conditions of proportional loading and assuming a J_2 flow theory, an effective strain quantity can be defined which is frequently used in life analyses under multiaxial stressing,

$$\Delta\varepsilon_{et} = \sqrt{\frac{2}{3}\,\Delta e_{ij}\Delta e_{ij}} \qquad (6)$$

where $e_{ij} = \varepsilon_{ij} - 1/3\ \varepsilon_{kk}\delta_{ij}$ are the deviatoric strain tensor components and ε_{ij} are the strain components. The Δ symbol refers to changes over some specific portion of a load cycle. Under the stated assumptions, it can be easily shown that

$$\Delta\varepsilon_{et} = \frac{\Delta\sigma_e}{E^*} + \Delta\varepsilon_e^p \qquad (6a)$$

where

$$E^* = \frac{3E}{2(1+\mu)}\ , \qquad (6b)$$

$$\Delta\sigma_e = \sqrt{\frac{3}{2}\ \Delta S_{ij}\Delta S_{ij}}\ , \qquad (6c)$$

$$\Delta\varepsilon_e^p = \sqrt{\frac{2}{3}\ \Delta\varepsilon_{ij}^p\Delta\varepsilon_{ij}^p}\ , \qquad (6d)$$

μ is Poisson's elastic ratio, E is Young's modulus, and $\Delta\varepsilon_{ij}^p$ are the plastic strain tensor components.

In principal strain coordinates, Equation 6 can be written as

$$\Delta\varepsilon_{et} = \frac{\sqrt{2}}{3}\ \sqrt{[\Delta(\varepsilon_1 - \varepsilon_2)]^2 + [\Delta(\varepsilon_1 - \varepsilon_3)]^2 + [\Delta(\varepsilon_2 - \varepsilon_3)]^2} \qquad (7)$$

where the ε_i are the principal strains. It has been suggested (Reference 1) that Equation 7 can be applied to multiaxial fatigue problems. Note that in this latter equation the ranges in principal strain differences are used, such that the maximum differences in each term are to be choosen from the profile of the entire loading cycle. Conceivably, such an approach would involve tracking the rotation in principal directions as a function of time. In addition, definitions of minor cycles and mean stress can become confused under such general cyclic conditions. Such problems are discussed in References 1 and 2.

A clear distinction between proportional and nonproportional cycling which illustrates this discussion is shown in Figures D-1 and D-2 (Reference 2). Figure D-1 illustrates the variation in direction of the octahedral shear stress on the octahedral plane as a function of the plane stress biaxial stress ratio, $R_{22} = \sigma_2/\sigma_1$. In both figures the principal directions are assumed to remain fixed, and the octahedral shear stress vector, $\underset{\sim}{\tau}_{oct}$ is given as

$$\underset{\sim}{\tau}_{oct} = \underset{\sim}{\sigma}\cdot\underset{\sim}{n} - (\frac{1}{3}\ \sigma_{kk})\underset{\sim}{n} \qquad (8)$$

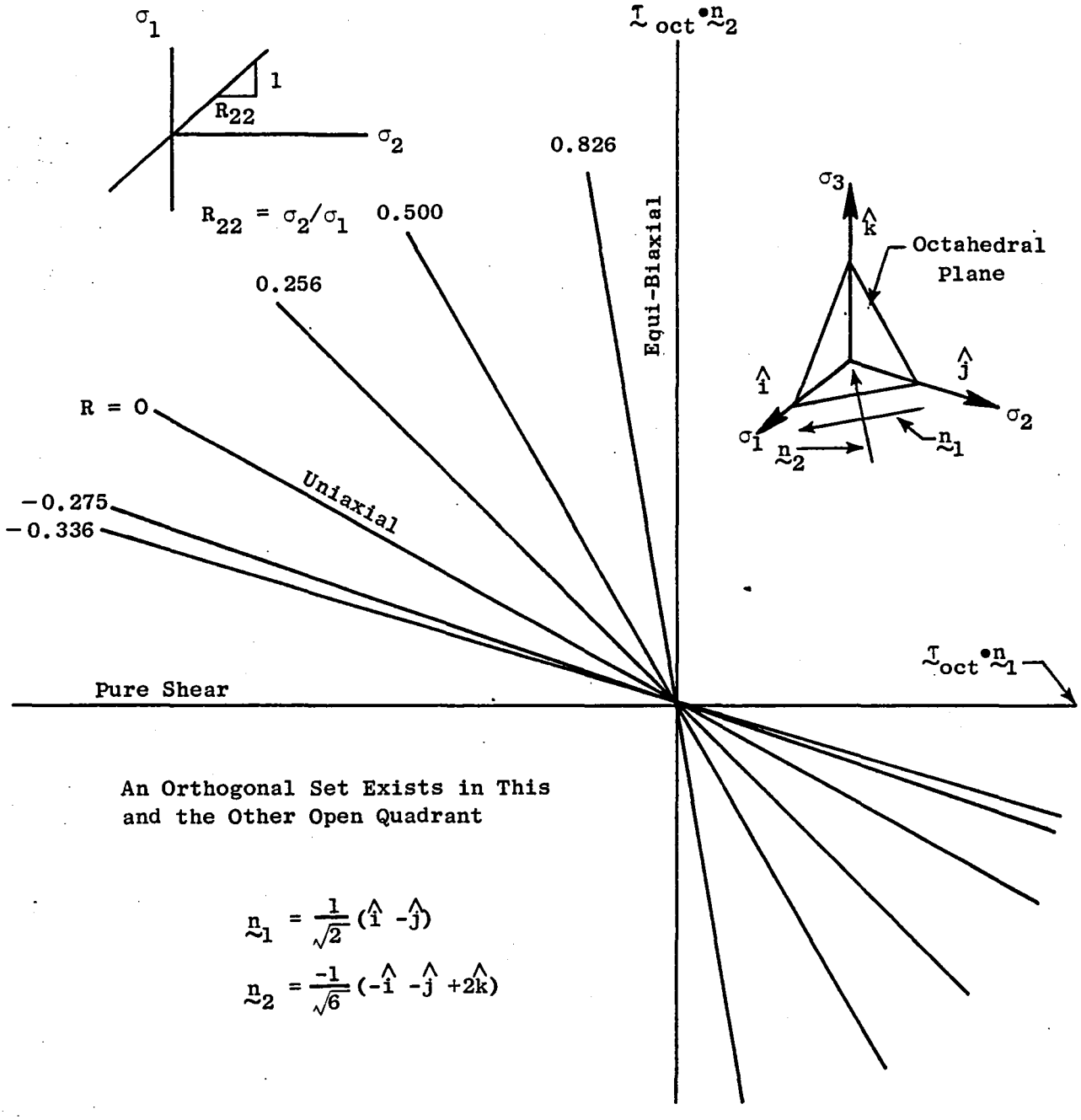

Figure D-1. Variation in the Direction of the Octahedral Shear Stress in a Case of Proportional Loading (After Leis and Laflen).

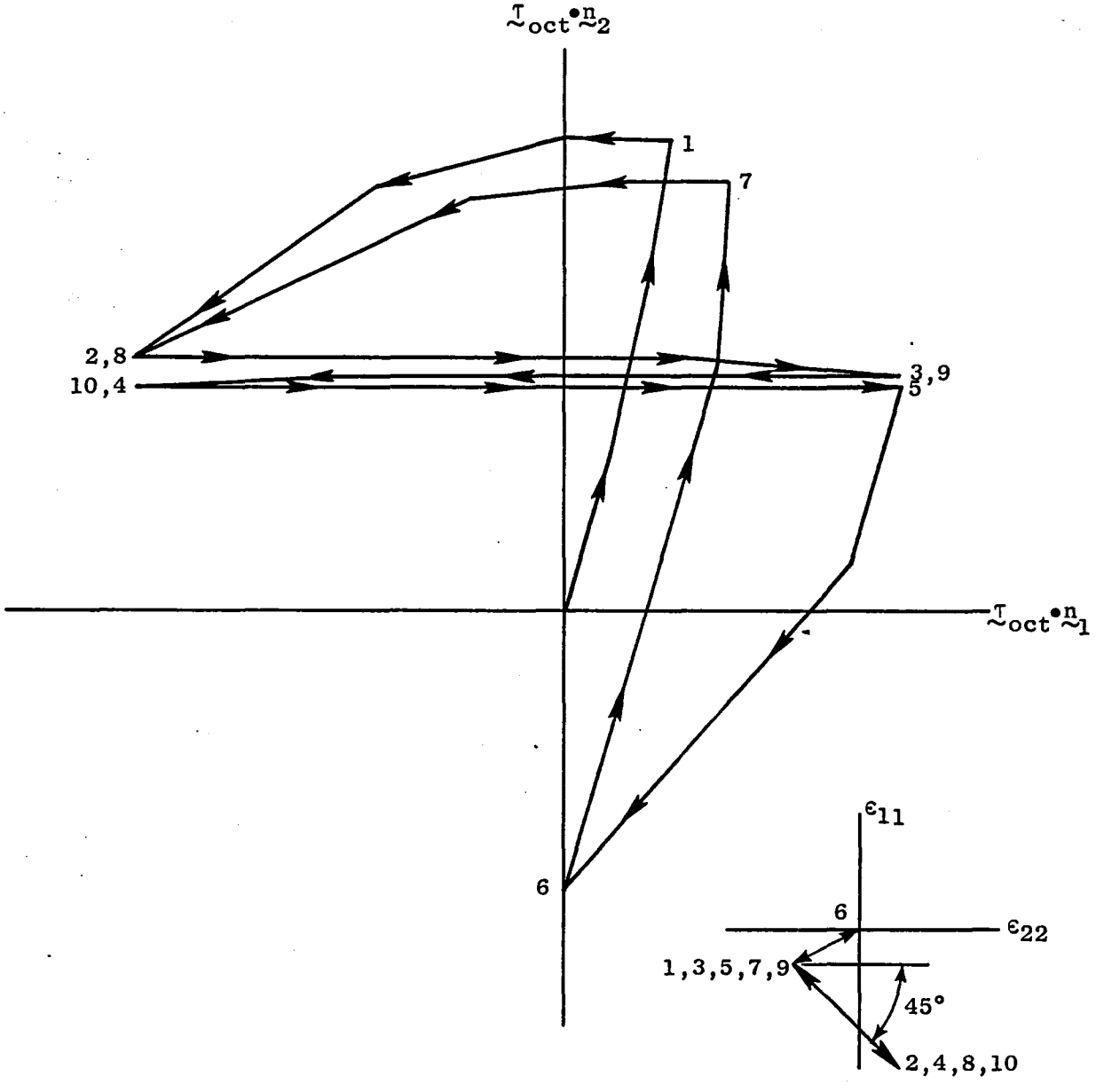

Figure D-2. Variation in the Direction of the Octahedral Shear Stress in a Case of Nonproportional Loading (After Leis and Laflen).

where

$$\underset{\sim}{n} = \frac{1}{\sqrt{3}} (\hat{i} + \hat{j} + \hat{k}).$$

It is easily shown that the magnitude of Equation 8 is given by Equation 5, and is merely the distance from the origin to any point on these figures. Under proportional loading (Figure D-1), it is seen that the direction of $\underset{\sim}{\tau}_{oct}$ is constant as long as the R_{22} ratio is constant; this can also be shown to be the case for the octahedral shear strain. Viewed in this way, it is seen that by using ranges in Equations 6 and 7, the total change along a line is being measured. Conversely, when the loading is nonproportional, there is a variety of points from which the range can be selected (Figure D-2). As shown in this figure, the direction of $\underset{\sim}{\tau}_{oct}$ changes radically during the nonproportional loading path shown in the insert. Note that the magnitude of $\underset{\sim}{\tau}_{oct}$ is still the distance to any given point from the origin. However, the numerical value of Equations 6 and 7 will depend on which points are selected in the evaluation. The selection process is not nearly as obvious as it would be in the proportional case. Clearly, one may need to develop cycle counting concepts such as those used in uniaxial loading (e.g., the rain flow approach) to analyze such nonproportional paths when equivalence quantities are used.

It should also be noted that damage may be smeared over several different slip directions under such loadings due to the change in direction of the octahedral shear stress. But in the case of fixed principal directions, this depends upon how the governing damage parameters are viewed. Since the principal directions are fixed, the plane of the maximum shear stress and strain is constant [but it can be different from the plane of maximum shear stress (or strain) range]. Thus if the plane of maximum shear strain, for example, is viewed as being the appropriate damage parameter, then damage is uniquely defined by one plane in this case. This is not the case for even these parameters when the principal directions change (such as under tension-torsion cycling when there is a phase angle difference between the tension and torsion cycles). Under such conditions of varying principal directions, most authors suggest selecting the plane and direction where their parameter is maximum. However, there is reason to believe that such an approach may still not be adequate (References 3 and 4). One inference of this comes from the constitutive response studies of Lamba (Reference 3) on OHFC copper, where he found additional cyclic hardening occurred under general nonproportional tension-torsion cycling over what could be produced in uniaxial or proportional multiaxial cycling. In this context, these results suggest that the hardening may be due to the loading of additional planes beyond those in the simpler cyclic cases.

With this background in mind, several theories of multiaxial fatigue are reviewed. In addition, the results of the review papers by Krempl (Reference 5) and Garud (Reference 6) are used when appropriate.

Sines Criteria

As a first indication of an early pressure criterion, consider Sines work (Reference 7), which can be written as

$$\sqrt{II_{\underset{\sim}{s}}}\ |_{alt} \leq B - \beta\ I_{\underset{\sim}{\sigma}static} \tag{9}$$

where the subscripts alt and static refer to the alternating and mean values of the stress components and B and β are constants. This criterion is essentially a multiaxial mean stress theory, and is, in fact, the basis of the mean stress effect in Chaboche's work which was reviewed in Appendix B. In particular, note that if uniaxial stresses are used Equation 9 becomes

$$\sigma_a \leq \sqrt{3}\ B - \sqrt{3}\ \beta\ \sigma_m \tag{10}$$

where σ_a and σ_m are the alternating and mean uniaxial stresses, respectively. This theory is intended to be used to model endurance limit fatigue which is the reason for the inequalities in these equations. Note that Equation 9 predicts that mean shear stresses have no effect on the fatigue limit which was verified in Reference 7.

There is an interesting relationship between this criterion and the Manson-Halford modification of Morrow's mean stress method (MMHM) discussed in Appendix C.

Recall from that appendix that the alternating stress is given as

$$\frac{\Delta\sigma}{2} = (\sigma_f' - k_m\ \sigma_m)\ (2N_f)^b$$

which for a given life is given as

$$\frac{\Delta\sigma}{2} = \Delta\sigma_o\ \left(1 - \frac{k_m\ \sigma_m}{\sigma_f'}\right) \tag{11}$$

where $\Delta\sigma_o = \sigma_f'\ (2\ N_f)^b$. Comparing Equations 10 and 11,

$$\sqrt{3}\ B = \Delta\sigma_o,$$

$$\sqrt{3}\ \beta = \frac{k_m\ \Delta\sigma_o}{\sigma_f'}.$$

Since Chaboche's mean stress model is based on the Sines model, it is expected that all three methods should yield nearly the same effects of mean stress.

More recently (Reference 8), Sines and Ohgi have modified Equation 9 so that the relationship between alternating and mean stress is no longer linear,

$$\sqrt{II_{\underset{\sim}{\sigma}}}\,|_{alt} = B - \beta_1 I_{\underset{\sim}{\sigma}}\,|_{static} - \beta_2 (II_{\underset{\sim}{\sigma}}\,|_{static})^{\alpha}$$

where α is a constant to be determined experimentally. For nonproportional, long-life cycling, these authors suggest that Equation 9 be used on the plane of maximum shear stress. In this case, the maximum shear stress is to be used instead of τ_{oct}.

Mowbray's Technique

Another pressure sensitive, biaxial technique has been suggested by Mowbray (Reference 9) wherein the equivalent plastic strain range (Equation 6b) is modified to depend upon the hydrostatic stress,

$$\Delta\varepsilon_e^{p*} = \frac{\Delta\varepsilon_e^p}{1 - m\,\dfrac{\Delta I_{\underset{\sim}{\sigma}}}{3\Delta\sigma_e}} \qquad (12)$$

where $\Delta\varepsilon_e^p$ is given by Equation 6d, $\Delta\sigma_e$ is given by Equation 6c, m ($0 \leq m \leq 1.5$) is an experimentally determined constant, and $\Delta I_{\underset{\sim}{\sigma}}$ is the range in the first invariant of the stress tensor which is given by Equation 2 (the range in the hydrostatic stress). By using Equation 12, assuming that the elastic equivalent strain range is given by

$$\Delta\bar{\varepsilon}_e = \frac{\Delta\sigma_e}{E}\,, \qquad (13)$$

and assuming a log-linear relationship between elastic and plastic strain components and life, it is found that,

$$\frac{\Delta\varepsilon_1}{2} = \frac{\sigma_f'}{E} f(R_{22},\mu)(2N_f)^b + \left(\frac{3}{3-m}\right)\varepsilon_f'\, g(R_{22},m)(2N_f)^c \qquad (14)$$

where

$$f(R_{22},\mu) = \frac{(1 - \mu R_{22})}{(1 - R_{22} + R_{22}^2)^{1/2}}$$

$$g(R_{22},m) = (2-R_{22})\,\frac{\left[3\,(1-R_{22}+R_{22}^2)^{1/2} - m\,(1+R_{22})\right]}{6(1 - R_{22} + R_{22}^2)}\,,$$

$R_{22} = \sigma_2/\sigma_1$, and $\Delta\varepsilon_1$ is the total strain range in the maximum principal direction. The functions g and f are consequences of the stated assumptions. This theory assumes proportional loading. Note that the equivalent elastic strain range (Equation 13) is not consistent with the identity given in Equation 6a for proportional loading. This approach was compared to data for various materials including Inconel 718, and m = 0.7 was used in all cases. The procedure was to determine the constants in Equation 14 for $R_{22} = 0$ (uniaxial loading), and to predict the multiaxial lives by using the resulting constants and the functions g and f. Reasonable correlations were found.

Multiaxial Strain-Range Partitioning

While most multiaxial theories are concerned with the ranges of equivalence quantities (or shear strain or stress ranges), in the case of strain-range partitioning, it is also necessary to consider the direction or sense of loading (tension or compression) and order (i.e., hold times); separate damage curves are derived by conducting uniaxial experiments where compression and tension are easily identified. However, considering the positive nature of equivalence quantities (e.g., Equations 5 and 6), a method is required to define the sign of the direction of loading under multiaxial conditions. The method which was developed for this application (Reference 10) was specifically limited to proportional loading cases.

The developed rule can be succinctly stated as follows. Combining both creep and plastic strains (i.e., the total inelastic strain) in the three (fixed) principal directions, Equation 6d (using these values of inelastic strain instead of the changes) can be used to define the effective inelastic strain. The sign of these inelastic strain values is then selected by using the sign of the principal stress in the direction with the maximum stress range. This is the rule as long as the secondary principal stress range is less than about half of the maximum principal stress range. One example where this latter criterion is violated is in torsion since the two principal stresses are equal in magnitude but opposite in sign. In such cases, it is suggested that alternate definitions of the sign be considered and the sign convention which yields the minimum life should be selected.

A further consideration in this technique involved the use of so-called triaxiality factor, TF,

$$TF = \frac{I_\sigma}{\tilde{\sigma}_e}$$

where I_σ is the first invariant of the stress tensor and σ_e is the effective stress.~ Various suggestions are made (References 10 and 11) for using the TF as a modification on the ductility in the plastic strain-life relationship. The concept is similar to that of Mowbray which was shown in Equation 12. In the current approach (Reference 11), the ductility is modified by a multiaxiality factor, MF, which is a function of TF,

$$MF = \frac{1}{2-TF} \ , \ TF \leq 1,$$

$$MF = TF \ , \ TF \geq 1 \ . \qquad (15)$$

MF was used to explain the difference between experimental results in tension (MF = 1) and torsion (MF = 0.5) by multiplying the calculated effective inelastic strain range by MF. Experimentally, the inelastic strain ranges for a given life differed by a factor of two (with torsion being higher) so that good agreement was found by using MF.

General Coffin-Manson Methods

Several papers (References 12, 13, 14, and 15) have reported correlations of multiaxial fatigue using the Coffin-Manson law

$$N_f^{\alpha} \Delta\varepsilon = C$$

where α and/or C are functions of various multiaxial parameters, and $\Delta\varepsilon$ is some strain measure (frequently, maximum principal strain is used). Note that the methods in Mowbray's technique and multiaxial, strain-range partitioning essentially assumed that only C is a function of the state of stress when cast into this equation form. In general, α is found to be also related to some measure of hydrostatic stress or strain.

Work Methods

Garud (References 6 and 16) published a method based on plastic work per cycle, W_c,

$$W_c = \int \sigma_{ij} d\varepsilon_{ij}^{P} \Big|_{\text{cycle}}.$$

The method was linked to an incremental plasticity theory with a modified Mróz-hardening law. Correlations were presented with some nonproportional fatigue data; it was found that the torsion data were consistently higher than the other data for the same life. Hence, a multiplier of a factor of 0.5 was applied to the work calculated from the torsion data to bring it in line with the uniaxial data. Recall that such a factor was indicated by the multiaxiality factor, MF. Note that plastic work is independent of the hydrostatic stress component as long as the plastic strain increments obey the constant volume assumption.

An attempt to use plastic work in proportional biaxial fatigue was presented in Reference 17 by Lefebvre, et al. In that case, the final form was

$$\Delta\bar{\varepsilon}^{P} \Delta\bar{\sigma} = K N_f^{c}$$

where $\Delta\bar{\varepsilon}^p$ and $\Delta\bar{\sigma}$ were effective plastic strain range and stress range, respectively. The functions K and C were dependent on the stress ratio (i.e., σ_1/σ_2) and C also depended upon the number of cycles to failure.

The Leis mean stress parameter which was reviewed in Appendix C is actually the uniaxial form of a multiaxial theory. The theory is developed by an approximate integration of work over one-half of a cycle such that elastic strain energy is included. This gives rise to the use of total strain rather than inelastic strain which results when the integration is over a total cycle. The theory was developed for proportional cycling. In extending this approach to nonproportional cycling with fixed principal directions, a different tactic was used (Reference 2). A critical direction was identified (based on experimental results) on the octahedral shear plane, and work in that direction was considered to be damaging. As shown in Figure D-1, the direction of loading on the octahedral shear plane is dependent on the biaxial stress ratio; therefore, considering one direction as critical results in a natural weighting or factor on proportional fatigue data (depending on the direction of the loading relative to the assigned critical direction) which would be similar to those discussed above (e.g., MF). This approach was used on proportional fatigue data (the same that was used by Lefebvre, et al.) with reasonable success. It was put forth that such an approach could be used in nonproportional loadings (such as that of Figure D-2) by calculating the work in the critical direction on the octahedral shear plane.

This latter approach to nonproportional cycling is similar in concept to one developed independently by Miller, et al. (Reference 18) and Hull (Reference 19). They consider nonproportional cycling in the elastic regime where one principal stress axis is fixed (such as at a traction-free surface). The concept is that, as the principal axes rotate, one particular orientation will be defined where the octahedral shear stress is a maximum when compared to all other orientations of the principal axes. This octahedral plane is then taken as the critical plane, and the direction of the shear stress is considered to be the critical direction (defined as a vector as in Equation 8). Once the critical plane and direction are established, the variation in the shear stress can be computed throughout the total nonproportional load cycle. In Hull's work, the variation in the normal stress on this octahedral plane is also computed and included in the damage analysis. A relationship is then assumed between these two quantities,

$$\tau_{pa} = A - \alpha\,(\sigma_{pm} + R)^m \qquad (16)$$

where τ_{pa} is the amplitude of the shear stress on the critical octahedral plane and in the critical direction; σ_{pm} is the mean of the variation in critical octahedral normal stress; and α, R, and m (m = 1 is assumed) are constants. Equations (9) and (16) would be identical under proportional loading with m = 1.

A key point to be made about these last two approaches is that both attempt to include a concept of direction into otherwise scalar octahedral

equivalence quantity approaches. Note that without such definitions these types of parameters are scalars which are independent of the direction of loading. This has been one key reason that advocates of shear stress or strain parameters have used in discouraging the use of scalar invariant quantities as discussed below.

Shear Strain and Shear Stress Quantities

The direction of macroscopic Stage I crack propagation is often linked with the planes of maximum shear stress (or strain). As such, these equations are often linked as being key parameters in describing multiaxial fatigue data. The early work of Findley, et al. (References 20 to 25) is a key illustration of such approaches. One of Findley's points was to illustrate the problems with strain energy as a viable parameter. In Reference 24, Findley, et al. performed a series of tests on a disk specimen which was loaded such that the elastic strain energy was constant at the center while shear components still alternated at the center (the loading was nonproportional). While the precise location of crack initiation was not located, the results were deemed by Findley, et al. to be sufficiently conclusive to demonstrate that energy was untenable as a multiaxial criteria.

In these papers, Findley considered the influence of anisotropy and mean stress among other factors. His theory [which according to Garud (Reference 6) is nearly the same as that of Stulen and Cummings, and Guest] was that failure would initiate on the plane where a critical combination of alternating shear stress and the maximum normal stress to this plane existed,

$$\tau_{c\theta\ A} = f - k\,\sigma_{\theta m} \tag{17}$$

where f and k are constants (for a given cyclic life); and $\tau_{c\theta\ A}$ and $\sigma_{\theta m}$ are the alternating shear stress and the associated maximum normal stress on a plane at angle θ to the maximum principal stress direction, respectively. One interesting facet of this approach is that the failure plane is not defined as the one with the maximum shear stress; rather, it is defined as the one with the maximum combination of these two stress parameters. The angle (θ) of the critical plane, as it turns out, depends upon the numerical value of the constant k in Equation 17. Findley shows that this theory is consistent with the experimental observation that mean stresses are more detrimental in tension than in torsion (both of which are predicted by Sines' theory).

Another noteworthy contribution was made by Blass and Findley (Reference 25) who studied the influence of the intermediate principal stress. Note that the equivalent stress (Equation 5) involves all three principal stress components, whereas the maximum shear stress, τ_{max},

$$\tau_{max} = \frac{\sigma_1 - \sigma_3}{2}$$

does not (assuming $\sigma_1 > \sigma_2 > \sigma_3$). Using an internal pressure and tension test system, the intermediate principal stress range was varied from $\Delta\sigma_1$ to $\Delta\sigma_3$ on individual specimens which were tested in fatigue. The results showed that the intermediate principal stress had almost negligible effects, indicating the shear stress theory to be the better criterion. These tests as well as the previously mentioned disk tests reflect attempts at experimentally determining the best criterion. It is surprising that these types of tests have not received more attention, nor been repeated.

A recent theory which is developed along similar lines to that of Findley, et al. is given by Brown and Miller (Reference 26) which is expressed in terms of strains rather than stresses. Their theory is succinctly given by the expression

$$\frac{\varepsilon_1 - \varepsilon_3}{2} = f\left[\frac{\varepsilon_1 + \varepsilon_3}{2}\right]$$

where ε_1 and ε_3 are the maximum and minimum principal strains and f is an unspecified function. Physically, $(\varepsilon_1 - \varepsilon_3)/2$ is the maximum shear strain and $(\varepsilon_1 + \varepsilon_3)/2$ is the strain normal to the plane of maximum shear strain. This is different from Findley's work, since here the critical plane is always the plane of maximum shear strain. Although the functional dependence of these two quantities is unspecified, the theory is portrayed by a plot of data on a so-called Γ-plane which is schematically shown in Figure D-3. On the Γ-plane, data of constant cyclic life is connected to determine the failure criteria. The outer boundaries of the Γ-plane depend on the numerical value of Poisson's ratio (i.e., elastic or plastic - in the figure, $\mu = 0.5$ is assumed), and the boundaries change with this value. Two separate cases are envisaged - Case A and Case B in which these two strain components are the governing parameters. Case A denotes multiaxial situations in which the plane of maximum shear strain is considered to lie normal to the surface of a specimen and cracks propagate along the surface. Case B designates conditions where the plane of maximum shear strain lies at an angle to the surface and cracks propagate away from the surface into the interior.

Specific mathematical representations on the Γ-plane have been discussed by Blass and Zamrik (Reference 27) and Blass (Reference 28); separate equations are chosen for Cases A and B. Considerations of the MF factor is specifically discussed in Reference 27. It is shown on a specific data set that for TF $<$ 1 good agreement is found but for TF $\geq$ 1, the predictions are not as good. It is suggested that, in general, these authors would not expect one functional form of TF to be universally applicable. This opinion is restated by Lohr and Ellison (Reference 29). It should be noted that due to the lack of a specific mathematical function in the Γ-plane any possible variation in the effects of pressure can be accommodated. While such an approach offers great versatility, it also requires much testing.

In References 29 and 30, Lohr and Ellison developed a technique similar to that of the Γ-plane (called Γ^* plane), but they also developed a single equation for normalizing the results. The concept is different than the

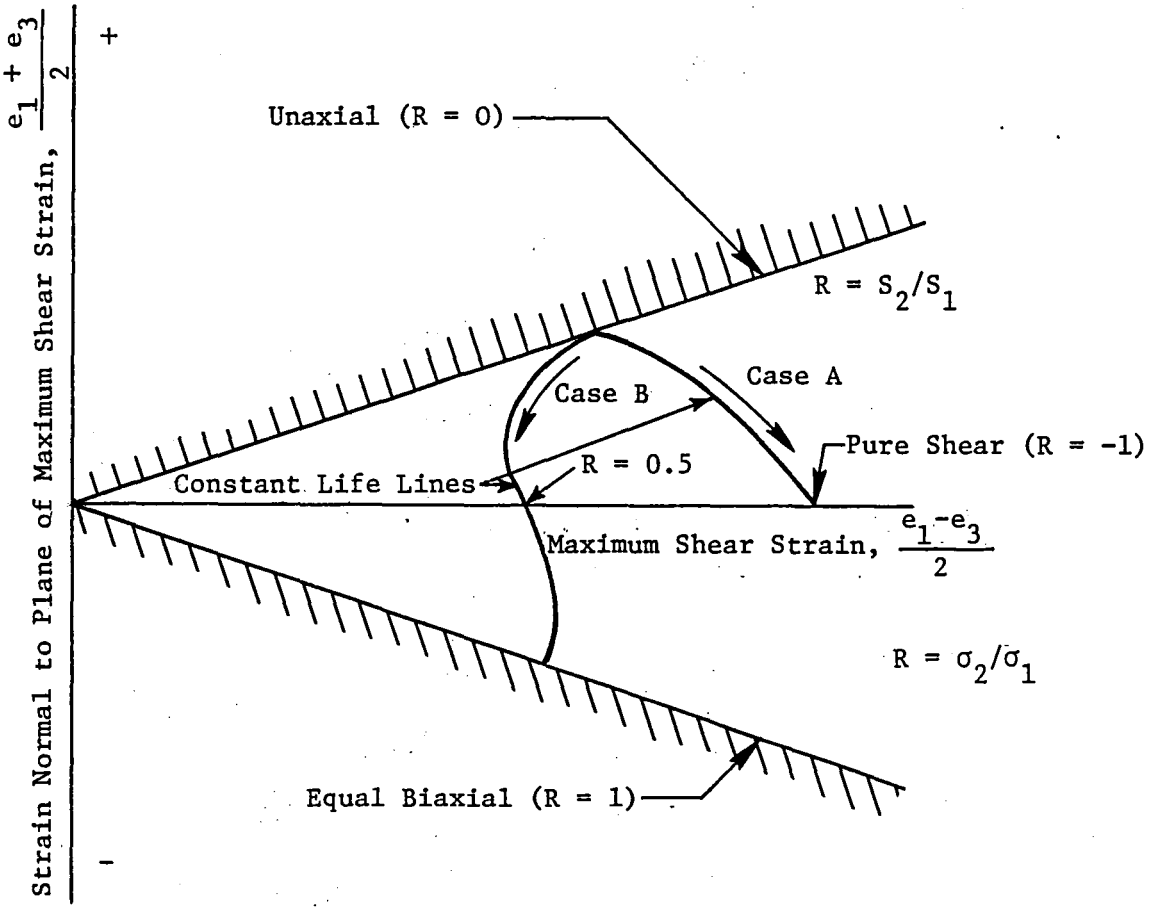

Figure D-3. Schematic Representation of Γ-Plane for Proportional Multiaxial Fatigue Data Where e_1 and e_3 are the Maximum and Minimum Principal Strains, Respectively (After Brown and Miller, Reference D-26).

Γ-plane concept in that a single cracking direction is identified as opposed to two (Cases A and B). The concept is that the crack must grow through the thickness, and that the maximum shear strain (denoted by γ^*) through the thickness is the primary governing parameter. (The free surface is defined by the two principal strains which are controlled, and the thickness is the third direction. Conceivably, in a mixed boundary value problem with pressure boundary conditions, such a definition could lead to uniqueness problems in defining the thickness direction. Note that γ^* is not necessarily the maximum shear strain.) The strain normal to this plane (called ε_n^*) is taken as having a secondary influence. For a given life, it is found that

$$\gamma^* + k\varepsilon_n^* = c$$

where k and c are constants. Plots are made from various experimental studies to show the feasibility of the approach. Good results are obtained.

Kanazawa, Miller, and Brown (Reference 31) studied the out-of-phase, tension-torsion fatigue behavior of a Cr-Mo-V steel and interpreted the results in terms of a Γ-plane analysis. They showed that (on the average) the plane of cracking was the plane of maximum shear strain range which also experienced the maximum range in normal strain (there are two planes of equal maximum shear strain range in such nonproportional loadings, but the range in normal strain on these two planes is different). They showed a correlation at one particular maximum shear strain range for different ratios of torsion and axial strain and various phase angles. The correlation showed that the life was dependent upon the normal strain amplitude within a factor of two on life. Both the maximum shear strain theory and the octahedral shear strain theory were shown to be nonconservative. There are several interacting facets to this type of loading which are instructive to consider. First, under such out-of-phase loading, the normal strain and shear strain on the defined critical plane are not in phase; the authors state that their correlation shows that this phasing is not important. Second, in their tests, the loading was fully reversed on all planes. In more general loading conditions with superimposed mean strains (both torsion and tension), this is no longer the case; and the plane of maximum shear strain is not necessarily the same as the plane of maximum shear strain range (Reference 32). More generally, this points to the need in this type of theory to clearly establish the role of mean and alternating shear and normal strain components. The present authors have seen no systematic study (other than the early work of Findley) which considers the role of mean strain components in this type of theory. Brown and Miller (Reference 26) point this out in their earlier paper and they conjecture that perhaps Findley's theory might be useful. In the context of the paper by Kanazawa, et al., it should be noted that earlier work by Zamrik and Frishmuth (Reference 33) demonstrated a viable correlation of out-of-phase tension-torsion experiments on an aluminum alloy by defining a maximum octahedral shear strain quantity.

Other Approaches

Several other approaches have been suggested in the literature. In this report, there has been little mention of the early work which has been reviewed by Garud (Reference 6); in addition, Garud's review as well as that of Krempl (Reference 34) cites several other experimental and analytical studies of the problems of multiaxial fatigue. Most of these other studies, while noteworthy in their own right, do not appear to introduce significant concepts beyond those mentioned above. One exception is the work of Krempl (Reference 34), Hashin (Reference 35), and Chaboche (Reference 36), who have studied the problem of multiaxial fatigue from the mathematical point of view. These studies involve the use of general functional forms and the concepts of invariants and anisotropy to derive various other specific criteria. Findley (Reference 22) also used such an approach in an earlier paper. Another approach which has bearing on this study is that of Walker (Reference 37); this method develops an approach similar to the uniaxial equivalent stain concept. This concept was discussed in detail in the sections dealing with mean stress effects. Walker suggested the relation

$$\bar{\varepsilon}_v = \Delta\gamma_o^{\,m}\, \varepsilon_T^{\,1-m}$$

where $\Delta\gamma_o$ is the range of the octahedral shear strain, m is an empirical constant, ε_T is related to the volumetric strain by

$$\varepsilon_T = \langle\varepsilon_1\rangle + \langle\varepsilon_2\rangle + \langle\varepsilon_3\rangle,$$

ε_i are the principal strains, and $\langle X\rangle = X$ if $X>0$, and $\langle X\rangle = 0$ if $X\leq 0$. The volumetric strain was selected due to its relationship with the hydrostatic stress which was successfully employed by Sines. Limited correlations of the multiaxial form were shown.

Two other generic study areas involve multiaxial creep rupture and cumulative damage as discussed below.

Multiaxial Creep Rupture

In a series of excellent theoretical and experimental papers, Leckie, Hayhurst, et al. (e.g., References 4, 38, 39, and 40) developed approaches for handling creep rupture problems. For constant states of stress, Hayhurst (Reference 38) developed a general effective stress term,

$$\sigma_{eq} = \alpha\sigma_{mp} + \beta I_{\tilde{\sigma}} + \gamma\,(3II_{\tilde{s}})^{1/2}$$

where α, β, and γ are constants (with the constraint that $\alpha + \beta + \gamma = 1$); σ_{mp} is the maximum principal stress; and I_{σ} and II_s are the stress tensor invariants previously described. Several effective stress theories are contained

within this expression. Two alloys which exhibit the extremes of the expected behavior are copper and aluminum. For copper, it is found that $\alpha = 0.848$, $\beta = 0.064$, and $\gamma = 0.088$. In other words, the material nearly follows a maximum stress criterion. For aluminum, it is found that $\alpha = 0$, $\beta = 0.09$, and $\gamma = 0.91$, nearly an octahedral or effective stress criterion.

In Reference 39, experimental creep rupture results from tests on various specimen configurations of these two materials were compared with analytical predictions. The creep strain behavior was characterized by a Kachanov-type damage parameter which depended on the governing stress dependence (i.e., maximum stress or effective stress). An approximate approach was developed for predicting the rupture life for restricted classes of stress analysis problems, and limitations were discussed relative to the material type and numerical stress analysis requirements. In References 4 and 40, methods for predicting the deformation behavior under nonproportional loading were presented. Of interest to the current study, the damage rate of the two types of materials (copper and aluminum) is given different interpretations. Since aluminum is governed by an effective stress criteria, damage is assumed to occur equally on all planes (i.e., it is isotropic). In the case of copper, this is not the case; and under nonproportional loading, the damage is different and dependent on the plane of maximum loading. If the principal axes rotate, life is shown to increase relative to proportional loading experiments. The experiments on copper actually indicate little interaction through such a rotation and the lifetime is seen to double in this case. In aluminum under nonproportional loading with constant effective stress, it is found that rupture life is constant relative to proportional loading. Thus the need for discerning the type of failure criteria for a given material is clearly indicated.

Multiaxial Cumulative Damage Studies

Four papers were briefly reviewed wherein cumulative fatigue tests under multiaxial stresses were conducted (References 41 to 44). In general, the results of these tests follow those of uniaxial testing: high loading followed by lower loading results in a cycle summation less than unity, and the reverse was true for low loading followed by a higher loading. Blatherwick and Viste (Reference 41) tested mild steel at one principal stress ratio. Using the octahedral shear stress theory, the results were correlated with Henry's theory of cumulative damage. Mattavi (Reference 42) performed tests on SAE 4340 steel by rotating disc specimens; an iterative stress-strain analysis was described for determining the state of stress. He uses a linear cumulative theory which accounts for shifts in the mean strain and concludes that this approach is viable (although as noted by Krempl, Reference 5, the cycle summation varies between 0.52 and 3.06). McDiarmid (Reference 43) performed a large series of tests on an aluminum alloy; most of the tests involved fixed principal stresses (four values were used) although some tests involved changing the principal stress ratio. Blocks of cycles were applied at each condition. He concludes by stating that no well-known uniaxial interaction could correlate his experimental results. He referenced his earlier PhD thesis wherein a stress-dependent theory was developed which might be applicable

(also see Garud, Reference 6). Zamrik and Bilir (Reference 44) reported experimental results on 304 stainless steel at three temperatures and three ratios of uniaxial and torsion strains in the low cycle fatigue range. These results consistently showed the classical failure of the Miner-Palmgren rule for all test conditions. The results were mainly for "high/low" sequences, but limited results were given for "low/high" loadings. Most of the tests indicated a maximum of 30% deviation from the linear summation rule.

After this report was written, the International Symposium on Biaxial/multiaxial Fatigue was held in San Francisco, December 15-17, 1982. Echoing much that has been reported here, three points stood out at the meeting.

1. There are a number of multiaxial fatigue theories available. What is needed is a wide range of data to evaluate these theories. The experiments to supply these data are very difficult to perform, particularly at elevated temperature.

2. There is a wide range of failure modes in multiaxial fatigue. This means that all investigators must report the details of the damage from initiation to final failure. Planes and orientation of damage are vital information.

3. Different materials accumulate damage in separate modes under different loading environments. These damage modes may or may not interact, thereby leading to failure theories which are material dependent.

The meeting demonstrated that there is a great deal of work remaining to be done. Much of the required work is experimental in nature, requiring great skill and ingenuity on the investigator's part. The failure theories can then be sorted out and appropriate ranges of applicability and materials determined.

APPENDIX D - REFERENCES

1. Manson, S.S., Thermal Stress and Low Cycle Fatigue, McGraw-Hill, 1966.

2. Leis, B.N. and Laflen, J.H., "An Energy-Based Damage Postulate for Damage Assessment of Cyclic Nonproportional Loadings with Fixed Principal Directions," MPC-8, Ductility and Toughness Considerations in Elevated Temperature Service, ASME, 1978, pp. 371-389.

3. Lamba, H.S., "Nonproportional Cyclic Plasticity," T&AM Report No. 413, Department of Theoretical and Applied Mechanics, University of Illinois, Urbana, Illinois.

4. Trampczynski, W.A., Hayhurst, D.R., and Leckie, F.A., "Creep Rupture of Copper and Aluminum Under Non-Proportional Loading," to appear in the Journal of Mechanics and Physics of Solids, 1982.

5. Krempl, E., "The Influence of State of Stress on Low-Cycle Fatigue of Structural Materials," ASTM STP 549, American Society for Testing and Materials, 1974.

6. Garud, Y.S., "Multiaxial Fatigue: A Survey of the State of the Art," Journal of Testing and Evaluation, JTEVA, Vol. 9, No. 3, May 1981, pp. 165-178.

7. Sines, G., "Failure of Materials Under Combined Repeated Stresses with Superimposed Static Stresses," NACA TN 3495, National Advisory Committee for Aeronautics, November 1955.

8. Sines, G. and Ohgi, G., "Fatigue Criteria Under Combined Stresses or Strains," Journal of Engineering Materials and Technology, Trans. ASME, Vol. 103, No. 2, April 1981, pp. 82-90.

9. Mowbray, D.F., " A Hydrostatic Stress-Sensitive Relationship for Fatigue Under Biaxial Stress Conditions," Journal of Testing and Evaluation, JTEVA, Vol. 8, No. 1, January 1980, pp. 3-8.

10. Manson, S.S. and Halford, G. R., "Treatment of Multiaxial Creep-Fatigue by Strainrange Partitioning," MPC-3, 1976 ASME-MPC Symposium on Creep-Fatigue Interaction, ASME, 1976. pp. 299-322.

11. Manson, S.S. and Halford, G.R., "Discussion to Multiaxial Low-Cycle Fatigue of Type 304 Stainless Steel," by J.J. Blass and S.Y. Zamrik, Journal of Engineering Materials and Technology, Vol. 99, Series H, No. 3, July 1977, pp. 283-285.

12. Liberting, G.Z., "Short-Life Fatigue Under Combined Stresses," Journal of Strain Analysis, Vol. 2, 1967, pp. 91-95.

13. Havard, D.G. and Topper, T.H., "Biaxial Fatigue of 1018 Mild Steel at Low Endurance," Proc. First Int. Conf. on Pressure Tech., Paper II-99, ASME, 1969, pp. 1267-1277.

14. Pascoe, K.J. and deVilliers, J.W.R., "Low-Cycle Fatigue of Steels Under Biaxial Straining," Journal of Strain Analysis, Vol. 2, pp. 117-126.

15. Parson, M.W. and Pascoe, K.J., "Low-Cycle Fatigue Under Biaxial Stress," The Institution of Mechanical Engineers, Proceedings 1974, Vol. 188, 61/74, pp. 647-651.

16. Garud, Y.S., "A New Approach to the Evaluation of Fatigue Under Multiaxial Loadings," Journal of Engineering Materials and Technology, Vol. 103, No. 2, April 1981, pp. 118-125.

17. Lefebvre, D., Neale, K.W., and Ellyin, F., "A Criterion for Low-Cycle Fatigue Failure Under Biaxial States of Stress," Journal of Engineering Materials and Technology, Vol. 103, No. 1., January 1981, pp. 1-6.

18. Miller, W.R., Ohji, K., Marin, J., "Rotating Principal Stress Axes in High-Cycle Fatigue," Journal of Basic Engineering, Trans. of the ASME, Vol. 89, Series D, No. 1, March 1967, pp. 76-80.

19. Hull, W.C., "A Rational Theory of Failure for Combined Stress High-Cycle Fatigue," Proceedings of the ASME Design Engineering Technology Conference, ASME, New York, 1972, pp. 179-195.

20. Findley, W.N., "Combined-Stress Fatigue of 76S-T61 Aluminum Alloy with Superimposed Mean Stresses and Corrections for Yielding," NACA TN 2924, National Advisory Committee for Aeronautics, May 1953.

21. Findley, W.N., Coleman, J.J., and Hanley, B.C., "Theory for Combined Bending and Torsion Fatigue with Data for SAE 4340 Steel," Proceedings of the International Conf. on Fatigue of Metals, ASME, 1956, pp. 150-157.

22. Findley, W.N., "Fatigue of Metals Under Combinations of Stresses," Trans. of the ASME, Vol. 79, Aug. 1957, pp. 1337-1348.

23. Findley, W.N., "A Theory of Mean Stress on Fatigue of Metals Under Combined Torsion and Axial Loading or Bending," Journal of Engineering for Industry, Trans. ASME, November 1959, pp. 301-306.

24. Findley, W.N., Mathus, P.N., Szczepanski, E., and Temel, A.O., "Energy Versus Stress Theories for Combined Stress - A Fatigue Experiment Using a Rotating Disk," Journal of Basic Engineering, Series D, Trans. of ASME, Vol. 83, No. 1, March 1961, pp. 10-14.

25. Blass, J.J. and Findley, W.N., "The Influence of the Intermediate Principal Stress on Fatigue Under Triaxial Stresses," Materials Research and Standards, ASTM, Vol. 7, No. 6, June 1967, pp. 254-261.

26. Brown, M.W. and Miller, K.J., "A Theory for Fatigue Failure Under Multiaxial Stress-Strain Conditions," The Institution of Mechanical Engineers, Proceedings 1973, Volume 187, 65173, pp. 745-755.

27. Blass, J.J. and Zamrik, S.Y., "Author's Closure to Discussion by S.S. Manson and G.R. Halford on Multiaxial Low-Cycle Fatigue of Type 304 Stainless Steel," Journal of Engineering Materials and Technology, Vol. 99, Series H, No. 3, July 1977, pp. 285-286.

28. Blass, J.J., "Multiaxial Creep and Fatigue Damage Summation for Type 304 Steel," Oak Ridge National Laboratory, ORNL/RM-6438, March 1979.

29. Lohr, R.D. and Ellison, E.G., "A Simple Theory for Low Cycle Multiaxial Fatigue," Fatigue of Eng. Materials and Structures," Vol. 3, 1980, pp. 1-17.

30. Lohr, R.D. and Ellison, E.G., "Biaxial High Strain Fatigue Testing of 1Cv-Mo-V Steel," Fatigue of Eng. Structures, Vol. 3, 1980, pp. 19-37.

31. Kanazawa, K., Miller, K.J., and Brown, M.W., "Low-Cycle Fatigue Under Out-of-Phase Loading Conditions," Journal of Engineering Materials and Technology, Vol. 99, Series H, No. 3, July 1977, pp. 222-228.

32. Leis, B.N. and Laflen, J.H., "Problems in Damage Analysis Under Nonproportional Cycling," Journal of Engineering Materials and Technology, Vol. 102, January 1980, pp. 127-134.

33. Zamrik, S.Y. and Frishmuth, R.E., "The Effects of Out-of-Phase Biaxial-Strain Cycling on Low Cycle Fatigue," Experimental Mechanics, May 1973, pp. 204-208.

34. Krempl, E., "Multiaxial Fatigue. Present and Future Methods of Correlation," North Atlantic Treaty Organization Advisory Group for Aerospace Research and Development, AGARD-CP-155, pp. 5-1 to 5-12.

35. Hashin, Z., "Fatigue Failure Criteria for Combined Cyclic Stress," Department of Materials Science and Engineering, University of Pennsylvania, Contract N00014-78-C-0544 to Naval Air Systems Command Office of Naval Research, Technical Report No. 2, March 1979.

36. Chaboche, J.L., "The Concept of Effective Stress Applied to Elasticity and to Viscoplasticity in the Presence of Anisotropic Damage," Royal Aircraft Establishment, Library Translation 2039, February 1980.

37. Walker, K., "An Effective Strain Concept for Crack Propagation and Fatigue Life with Specific Applications to Biaxial Stress Fatigue," Proceedings of the Air Force Conference on Fatigue and Fracture, AFFDL-TR-70-144, Wright-Patterson Air Force Base, Dayton, Ohio, September 1970, pp. 225-233.

38. Hayhurst, D.R., "Creep Rupture Under Multi-Axial States of Stress," Journal of the Mechanics and Physics of Solids, Vol. 20, No. 6, December 1972, pp. 381-390.

39. Leckie, F.A. and Hayhurst, D.R., "Creep Rupture of Structures," Proc. Royal Society Lond., A, 340, 1974, pp. 323-347.

40. Hayhurst, D.R., Trampczynski, W.A., and Leckie, F.A.," Creep-Rupture Under Non-Proportional Loading," Acta Metallurgica, Vol. 28, 1980, pp. 1171-1183.

41. Blatherwick, A.A. and Viste, N.D., "Fatigue Damage During Two-Level Biaxial-Stress Tests," Wright-Patterson Air Force Base, Dayton, Ohio, February 1967.

42. Mattavi, J.L., "Low-Cycle Fatigue Behavior Under Biaxial Strain Distribution," ASME Paper No. 68-WA/Met-8.

43. McDiarmid, D.L., "Cumulative Damage in Fatigue Under Multiaxial Stress Conditions," The Institution of Mechanical Engineers, Proceedings 1974, Vol. 188, 40/74, pp. 423-430.

44. Zamrik, S.Y. and Bilir, O.G., "Analysis of Biaxial-Fatigue Damage at Elevated Temperatures," Experimental Mechanics, 1975, pp. 373-379.

APPENDIX E - ELEVATED TEMPERATURE TESTING AND ANALYSIS OF INCONEL 718 AND RENE 80

The majority of cumulative damage studies that have been carried out have dealt with a sequence of load levels at a single temperature. While many structures do undergo all their fatigue cycles at a single temperature, hot path components of aircraft gas turbine engines do not. In addition, one approach to verification of life computations is to machine specimens from field-exposed hardware and perform laboratory tests on the specimens. Since these specimens can rarely be tested at conditions identical to their engine exposure, the laboratory cycles become the second phase of a two-step cumulative damage test in which the load and temperature are changed. It is clear, therefore, that an important generalization of damage accumulation models would include not only load sequences but also temperature sequences. When such complexities are introduced, however, the concept of a damage accumulation model becomes more difficult to define. This is because models which are sufficiently general to describe complex elevated temperature behavior, including load and temperature holds and changes, inherently contain damage accumulation concepts. Damage accumulation then becomes a matter of different blocks of cycles or different missions. In the present case, the attempt was made to primarily examine damage accumulation during cycle-dependent behavior through a series of two-step tests involving both load and temperature tests.

Baseline Data

Prior to carrying out the multiple condition experiments, it was necessary to generate reference data at a number of temperatures and strain ratios. The specimens used in this experimental program were all removed from Inconel 718, ring-rolled forgings. The material is comparable to that reported in the detailed R-ratio studies in Appendix C; however, the material is from a different heat and was analyzed separately in order to be totally compatible with the other test results reported in this appendix. The specimens were all smooth round bars, 5.1 mm in diameter, and were tested in longitudinal strain control, Both cyclic stress-strain and low cycle fatigue tests were conducted; the results of the cyclic constitutive behavior program have been discussed in Appendix A. The low cycle fatigue tests were all carried out at a frequency of 20 cpm and at constant amplitude. Three temperatures, 21°, 343°, and 566° C and four values of R_ε, 0.4, 0.2, 0.0 and -1.0, were examined. However, only the 343° and 566° C data will be discussed in this appendix.

Correlation of Mean Stress Theories with LCF Life

During the planning of the two-step experimental program, it was clear that a series of constant amplitude tests at a single value of R_ε would be inadequate for the purposes of this study. When strain control, two-step

tests are conducted, the mean stress in the specimen will be different during each step of the experiment. This is obvious from a reconsideration of the influence of the mean stress on the complete cyclic stress-strain curve shown in Figures A-4 through A-9 of Appendix A. This work showed that over the small strain range $0.6 < \Delta\varepsilon \lesssim 1.2\%$ the influence of R_ε is to raise the mean stress, leading to the expectation of an influence of R_ε on the LCF life. The baseline tests were carried out at a variety of strain ratios to allow an examination of the effect of mean stress on the cyclic life. If this effect was found to be important, then it would be necessary to involve the mean stress theories discussed in Appendix C in the data analysis process and ultimately, in the cumulative damage model.

The first set of baseline data was obtained at 566° C (1050° F), with tests conducted at four R_ε: 0.4, 0.2, 0.0, and -1.0. The results of this testing are shown in Figures E-1 through E-6. Figure E-1 plots the alternating pseudostress, $E\Delta\varepsilon/2$, against cycles to failure, while the second figure, Figure E-2, shows the cycles to failure as a function of effective alternating stress, $\bar{\sigma}_a$, (Reference 1).

$$\bar{\sigma}_a = \sigma_a \left(1 - \sigma_{min.}/\sigma_{max.}\right)^{m-1}$$

where σ_a is the alternating stress, m is an empirical exponent, and $\sigma_{min.}$ and $\sigma_{max.}$ are the minimun and maximum stresses, respectively.

Figure E-1 shows that at high stress levels alternating psuedostress is fairly effective in correlating the data. There does not seem to be any consistent layering of the data over the range of N_f, although $R_\varepsilon = -1.0$ values seem to be longer lived at low stress. In particular, the one runout point at 503.3 MPa (73 ksi) has a much longer life than lower stressed specimens at other values of R_ε.

Figure E-2 shows life values in terms of the effective alternating stress. The pseudostress concept is based entirely on strain range, but the effective alternating stress attempts to adjust the stress range to account for the maximum stress in the cycle. The stress values are taken from the test records and thus reflect the amount of yielding occuring in the actual strain-controlled cycle. The values used are taken at half life and represent approximately stable values (Reference 2). Figure E-2 shows that the effective stress does a better job of correlating the data than does the pseudostress; the runout point now is at the lower stress and there is no data layering. The one disturbing feature of this parameter is the shallow slope of the resulting correlation. The shallowness yields large changes in predicted life for small changes in alternating stress, limiting parameter usefulness as a predictive tool.

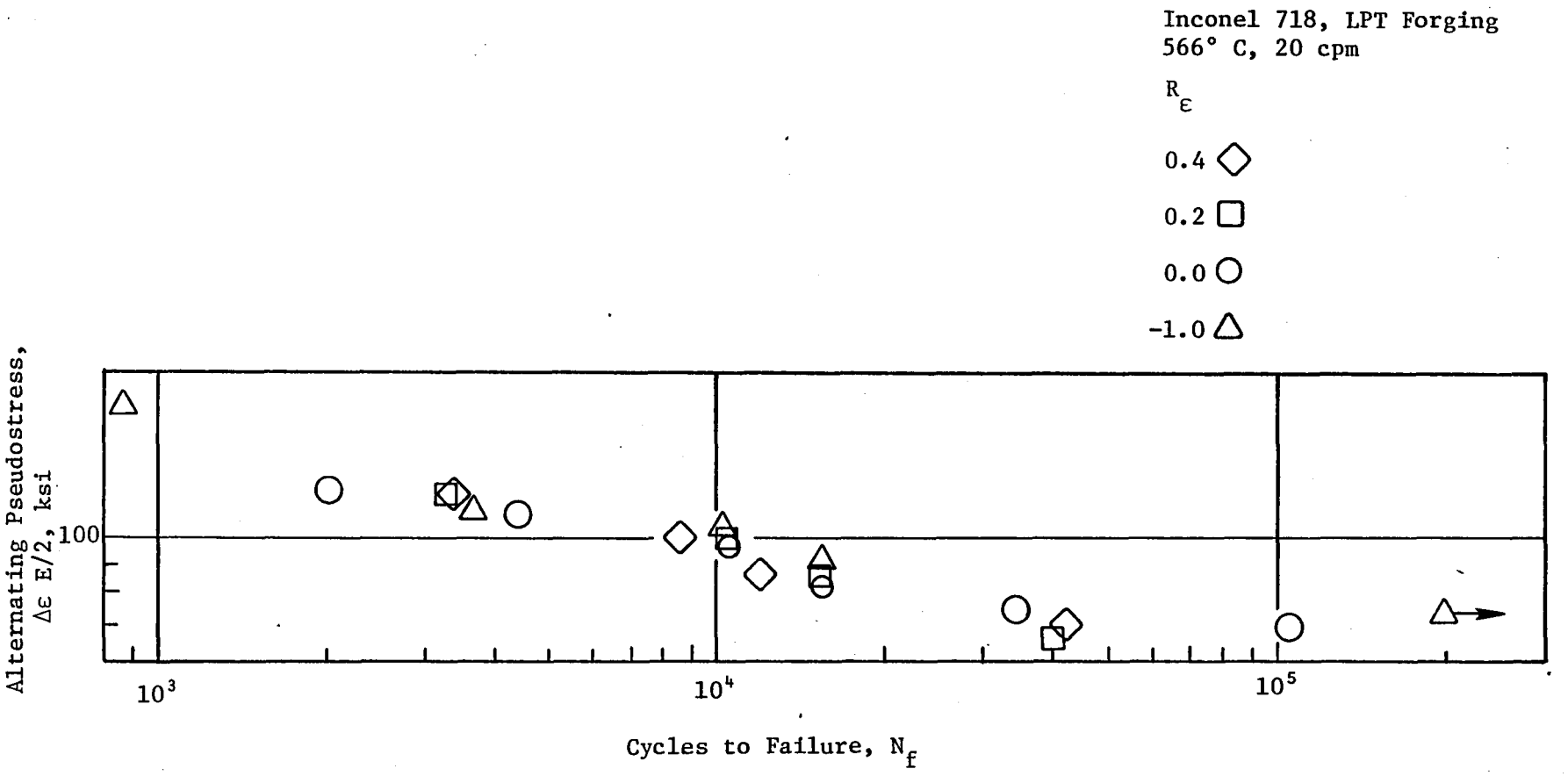

Figure E-1. Baseline Data at 566° C Based on Pseudostress.

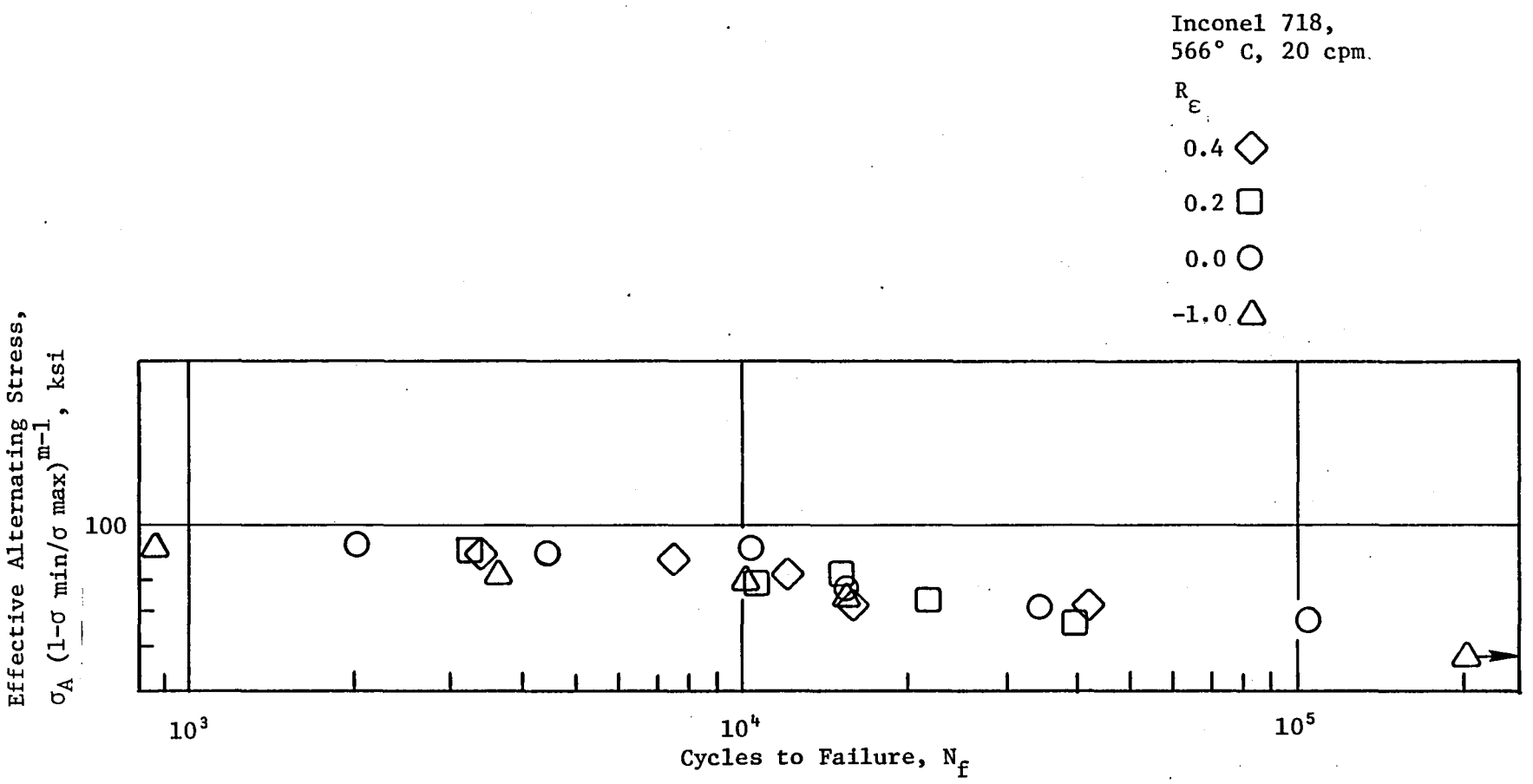

Figure E-2. Baseline Data at 566° C Based on an Effective Stress Concept, m = 0.7.

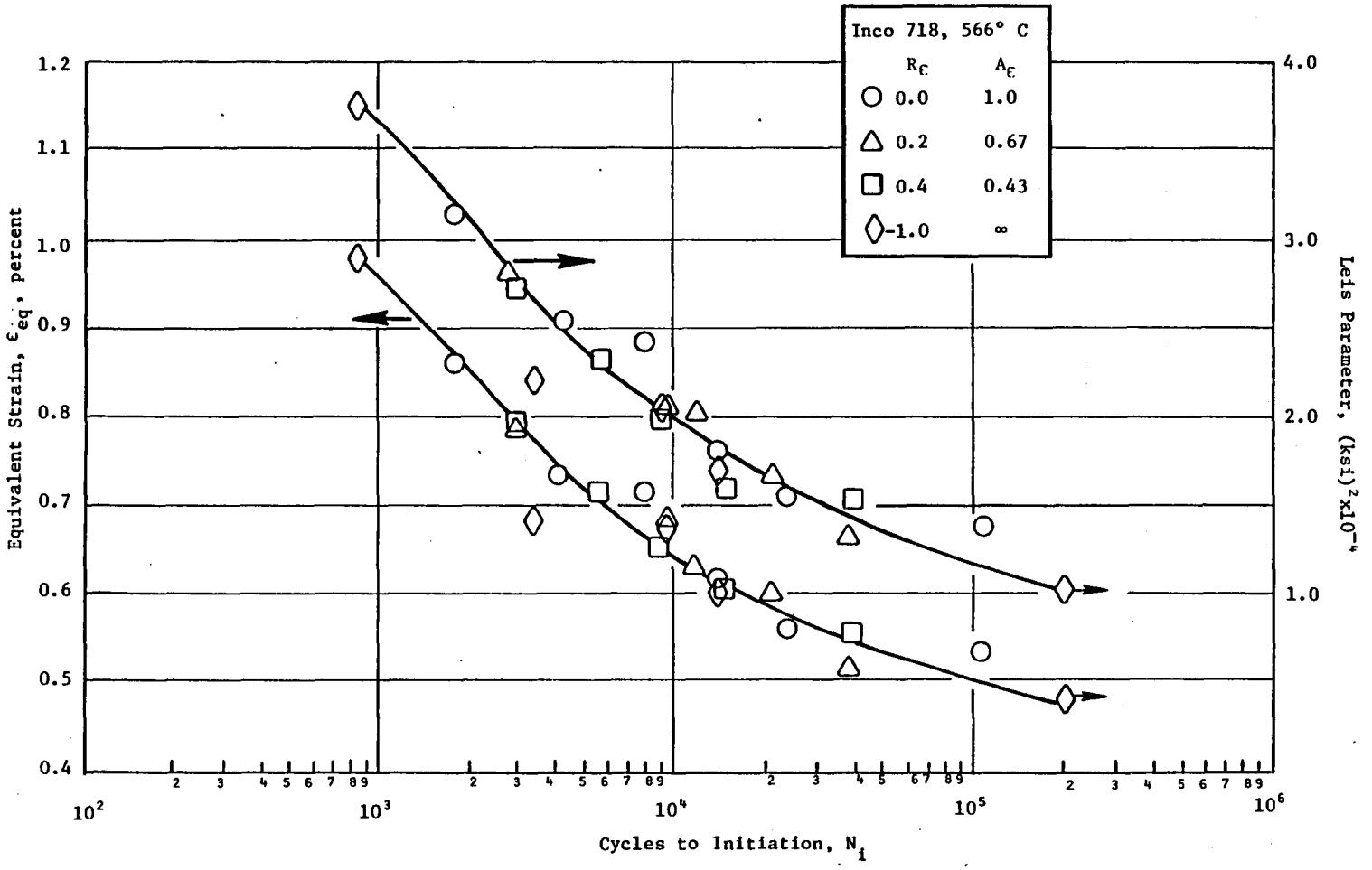

Figure E-3. Baseline Data at 566° C Analyzed by the Equivalent Strain and Leis Parameter Methods.

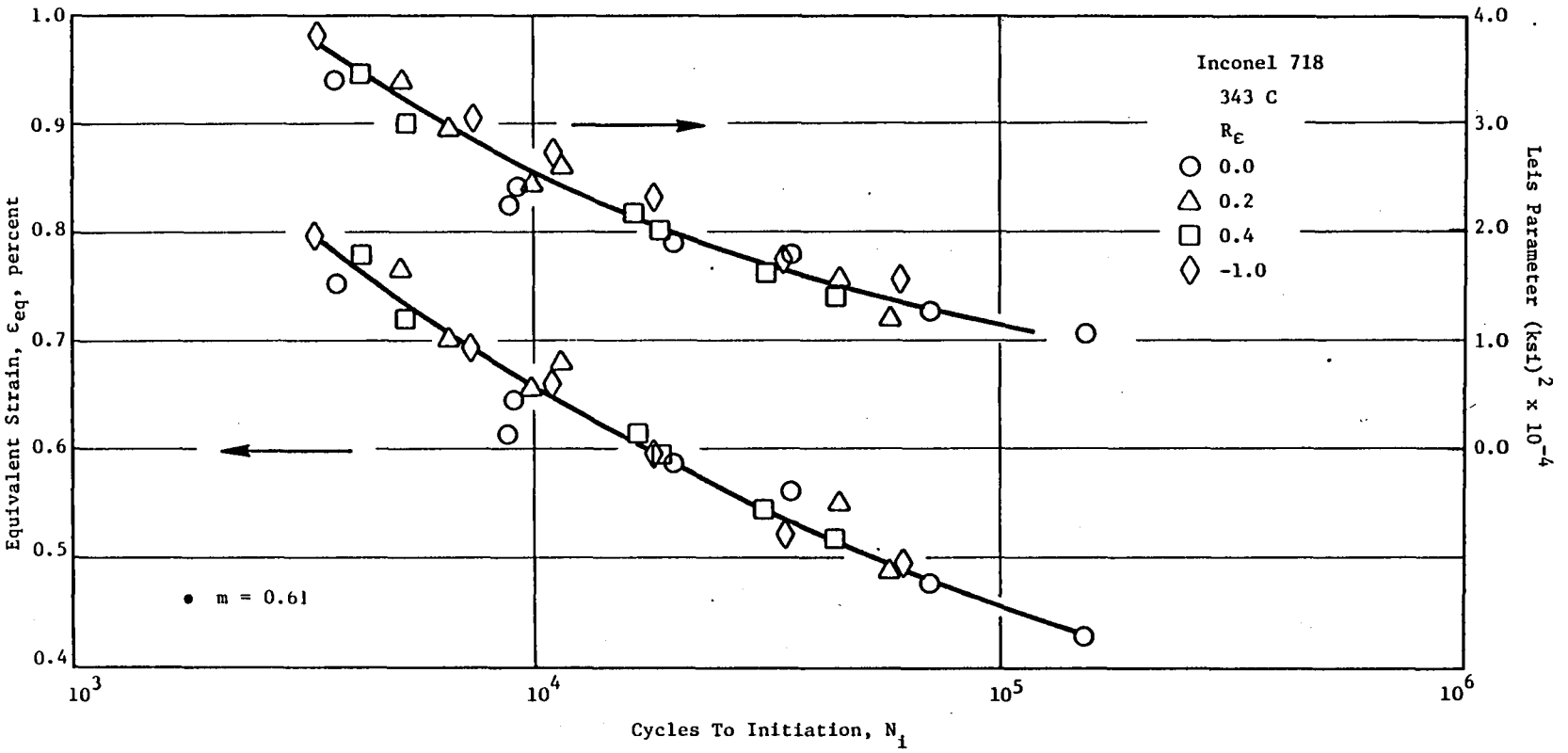

Figure E-4. Baseline Data at 343° C Analyzed by the Equivalent Strain and the Leis Parameter Methods.

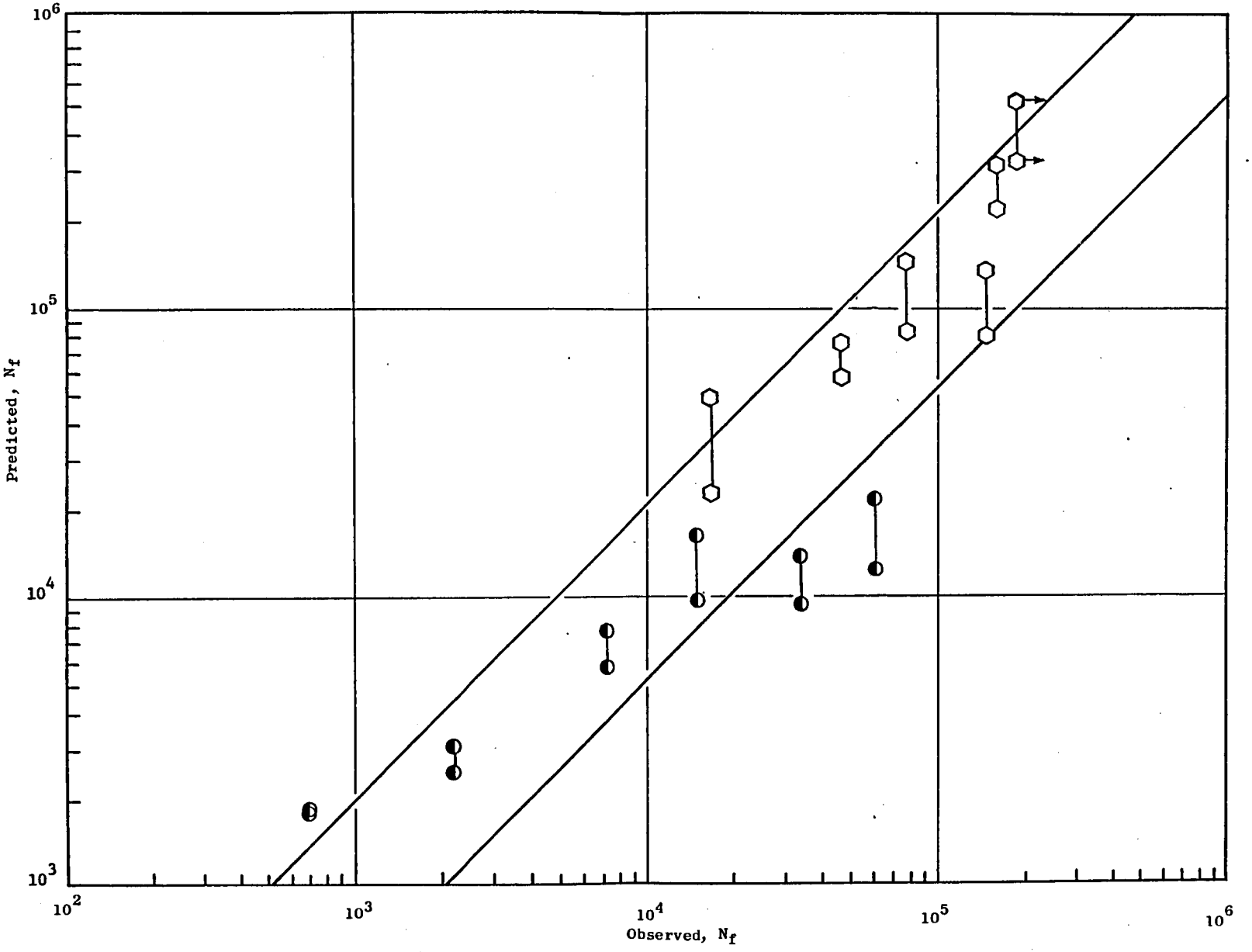

Figure E-5. Variation in Predicted Life Based on Leis Parameter Produced by Variations in Mean Stress.

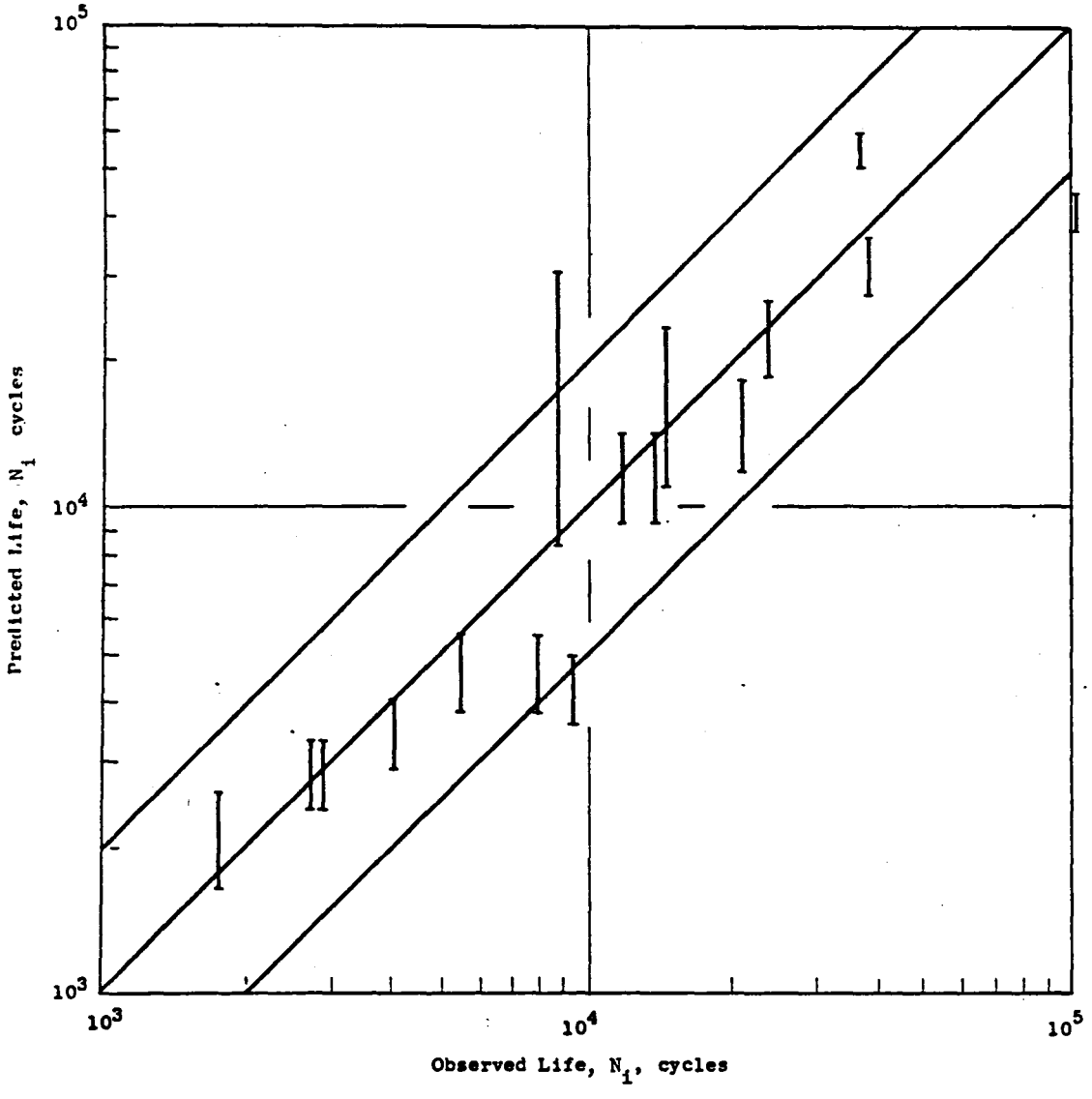

Figure E-6a. Effect of Mean Stress on Life Prediction Using Leis Parameter, Inconel 718, 566° C, R_ϵ - 0.0, 0.2, 0.4.

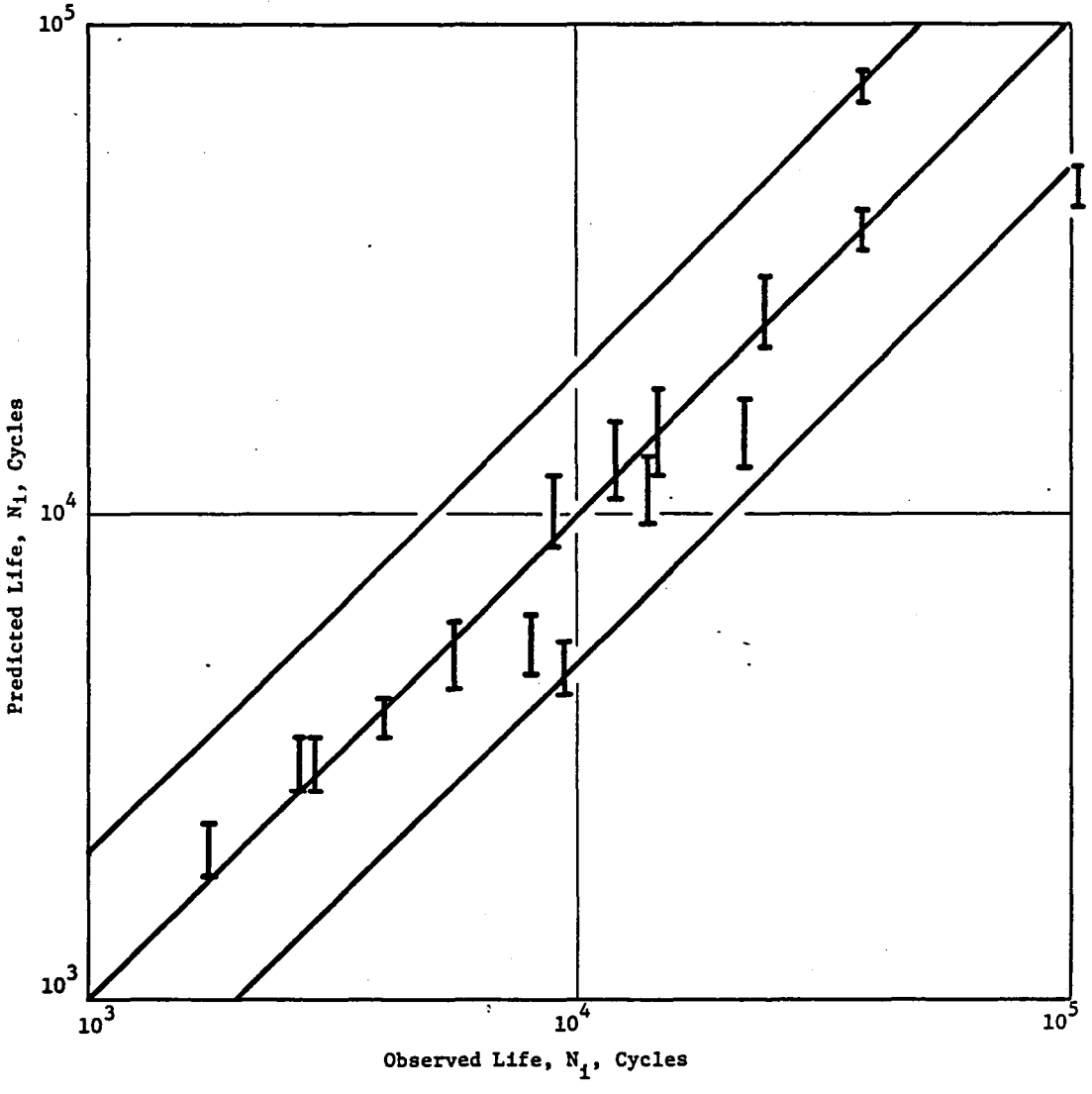

Figure E-6b. Effect of Mean Stress on Life Prediction Using ε_{eq}, Inconel 718, 566° C.

Figure E-3 shows the life correlation in terms of two parameters, equivalent strain and the Leis parameter which were discussed extensively in Appendix C; note that here the life is expressed in terms of cycles to crack initiation rather than cycles to failure. Repeating the definitions given in Appendix C, the parameters are given by:

$$\text{Equivalent Strain, } \epsilon_{eq} = \left(\frac{\sigma_{max.}}{E}\right)^{1-m} \Delta\epsilon^{m}$$

$$\text{Leis Parameter, } P_L = (\sigma_{max.} + \Delta\sigma/2)E(\Delta\epsilon/2)$$

By utilizing the maximum stress in the cycle, the two parameters account for the extent of plasticity in the cycle. Both correlate all the data, except for one $R_\epsilon = -1$ point, rather well. The data sets were fitted with third order polynomials with an error of 34.4% and 33.4% for the equivalent strain and Leis parameters, respectively (the error is defined in Appendix C). A value of 0.72 was used for m; this value was obtained by minimizing the error for the equivalent strain approach.

The second temperature selected for the test program was 343° C. The same four values of R_ϵ were used to obtain baseline data. The results are presented in Figure E-4 as cycles to initiation in terms of the equivalent strain and the Leis parameter. Both curves are third order polynomial fits. In the equivalent strain relation, m = 0.61. The error for the two curve fits is 23.0% and 20.8% for the Leis and equivalent strain parameters, respectively. The correlation is, therefore, slightly better than at 566° C. One interesting point is the tendency of the zero and -1 data to layer above and below the curve for the Leis parameter. The other two values of R_ϵ do not seem to follow any pattern; moreover, this is the only parameter in which such layering was noted.

Influence of Mean Stress Variability on Predicted Lives

The analysis of the LCF data at 343° and 566° C demonstrates that it is important to account for the influence of the mean stress on the LCF lives. This conclusion verifies the results of Appendix C. At the same time, there was a concern that the variation in mean stress observed in individual specimens, for example Figures A-7 and A-9, would lead to an unacceptable level of scatter in the predicted lives when mean stress parameters are used. This concern was examined by fitting bounds to the mean stress data, determining the range of the mean stress and the resulting range of lives predicted by the mean stress parameters, comparing the range of prediced lives with the observed lives. To be completely consistent, each set of data for each value of R_ϵ should have been examined separately. However, because of the relatively modest amount of data available in each set, this was only possible in one of the two data sets.

Figure A-7 of Appendix A shows the variation in mean stress as a function of strain range for several values of R_ε at 538° C. Upper and lower bounds to the $R_\varepsilon = 0$ data were fitted and these approximately coincided with the Heat A and Heats B and C data, respectively. These values were then added to the alternating stress-strain curve of Figure A-5 to obtain an upper and lower range for the maximum stress that can be used in the advanced life parameters. While all of the mean stress parameters could have been evaluated, only two were selected to illustrate the point of mean stress sensitivity. The Leis parameter and equivalent strains were selected as being typical and having promising potential for life prediction.

Figure E-5 shows the correlation of predicted versus observed lives for Heats B and C based on the Leis parameter. Since the mean stresses in these two heats essentially formed the lower bound of the data, this value of P_L yields the upper bound in the predicted life range. The upper bound mean stress gives a higher maximum stress and P_L and lowers the predicted life. The plot shows that at high strain levels where the mean stress has undergone significant relaxation the predicted lives are not particularly sensitive to the mean stress level. However, as the lives transition from low cycle fatigue to high cycle fatigue at approximately 10^4 cycles, the shifts become more pronounced. This is, of course, the region where there is inherently more variation in mean stress as reflected by the complete cyclic stress-strain curve.

The second set of data examined was cycled at 566° C and was given in Figures E-1 to E-3. This time, because of the limited data for each value of R_ε, it was decided to analyze all the $R_\varepsilon > 0$ as a group. This means that this analysis will reflect the sensitivity to the mean stress due to R_ε rather than material variations as in Figure E-5. Again, an upper and lower bound was fitted to the mean stress data and a range of maximum stresses obtained. Figure E-6 gives the range of predicted lives versus observed lives for the three values of R_ε. Figure E-6a uses the Leis parameter while E-6b employs equivalent strain. The result indicates excellent agreement between predicted and observed lives. The result also demonstrates that the range of predicted lives generally still lies within a factor of two with the perfect correlation line; the equivalent strain gives a slightly better correlation. In other words, it is important to take the mean stress into account in predicting elevated temperature lives, but once the mean stress is included, the predicted life is not overly sensitive to the value of the mean stress used. This is an important conclusion when considering heat-to-heat variations between design handbook data and the actual component material. If the parameters were overly sensitive to mean stress variation from heat-to-heat, little confidence in their application would exist.

Analysis of Two-Step Cumulative Damage Tests

Once the baseline data had been obtained and the analysis of the mean stress parameters carried out, two-step load/temperature tests were conducted.

In all cases, the tests reported here were run first at 566° C for various percentages of life. The temperature was then lowered to 343° C and the specimen cycled to failure. The load was raised, lowered, or held constant to yield various life combinations. The tests were run in two different methods. In one set of tests, there was no attempt to correct the second test range for the plastic strain level incurred during the first load step. Even though the second test block is run with a strain range of zero to $\epsilon_{max.}$, the presence of the plastic strain from load Step 1 means that there will be a positive mean strain, i.e., $R_\epsilon > 0$. The value of R_ϵ will depend on the range in Step 1 and the larger the strain range, the higher the value of R_ϵ in Step 2.

In the second group of tests, the strain bias was eliminated in the second load block and the strain ratio, R_ϵ, was maintained at zero for both temperatures. This was done by starting the second test block in the compressive direction and reversing the plastic strain before commencing cycling in Block 2.

The results of some of these tests are shown in Figure E-7 in terms of pseudostress and cycles to failure, N_f. The load changes between the two steps were modest, about 69 MPa, but the linear damage rule gives quite a good fit to the data except for 2 points. This is particularly interesting in view of the failure of the pseudostress parameter to correlate the baseline data at 566° C, Figure E-1.

Since pseudostress is purely a range quantity, the same exercise was performed using the equivalent strain and the Leis parameters. The results are shown in Figures E-8 and E-9. Figure E-8 is for the tests in which R_ϵ of zero was maintained in both test blocks. Again, the difference in load between the two levels was modest. The figure shows that the linear damage rule is quite adequate to describe these test results, being approximately 15% conservative. Generally, the results of the two life parameters are similar.

Figure E-9 shows rather a different picture. In these tests, the difference in load between the two blocks was greater, ranging from zero to 400 MPa. This results in a much greater load sequence effect, as well as a large variation in R_ϵ during the second block. It is unclear from this figure whether or not there is a load sequence effect. The three high/low (based on stress) tests (open symbols) give the lowest life total, as would be expected. The three low/high results (solid symbols) are mixed in with the constant load tests (half open symbols) but, generally, yield life fraction totals that are less than the constant load tests. Figure E-9 also shows a somewhat larger variance between the equivalent strain and Leis parameter results than that displayed in Figure E-8.

While the results of the two test series have been separated, this was done for convenience rather than to indicate any fundamental difference between the test techniques used to acquire the data. As Figures E-3 and E-4 show, the two parameters eliminate the effect of R_ϵ and so the two-step test results should be independent of the R_ϵ value during the second step at 343° C. Failure of the parameters to correlate the failure data in this case seems to suggest that a more complex cumulative damage rule is required.

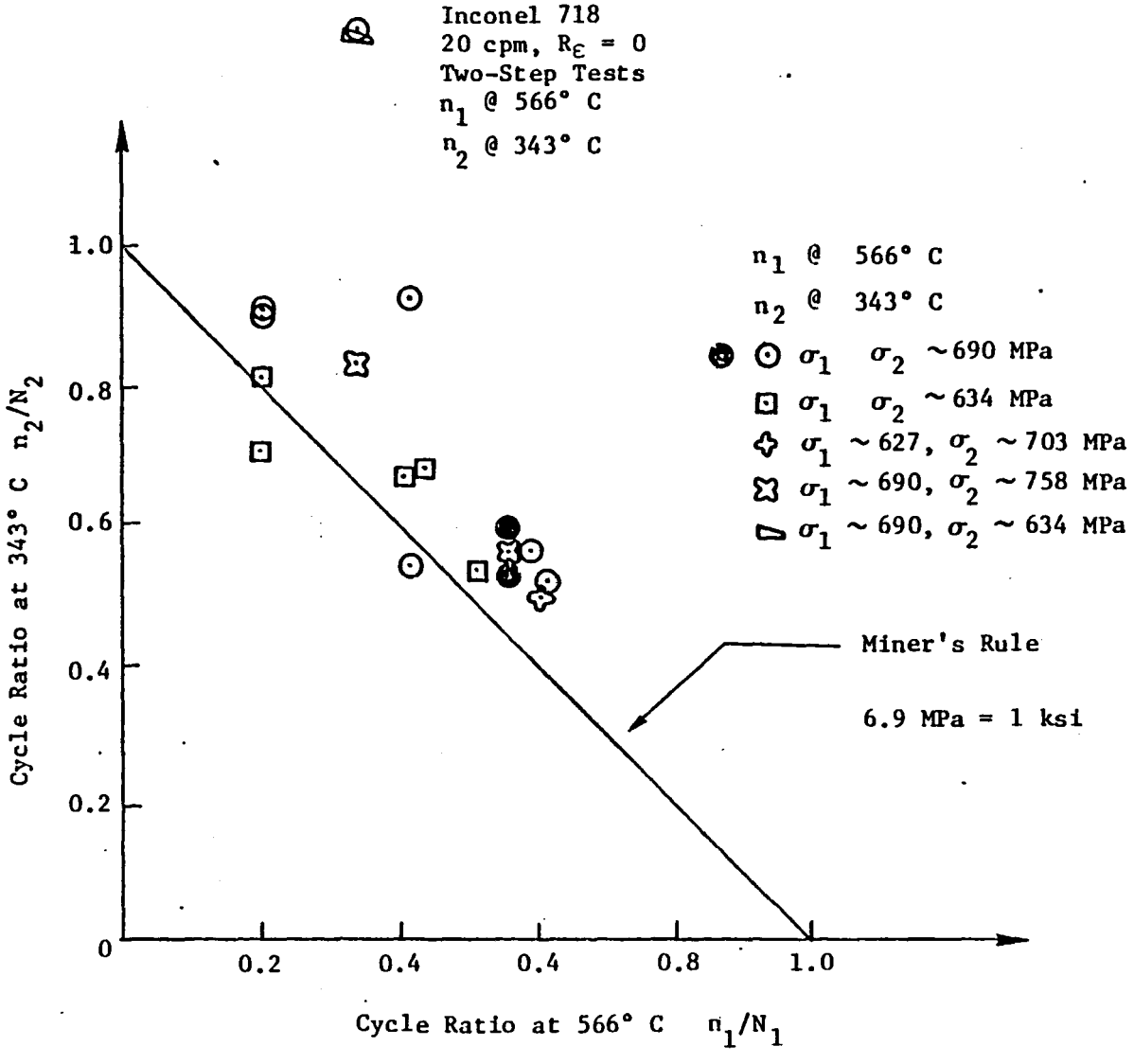

Figure E-7. Results of Two Temperature Tests on Inconel 718 Based on Pseudostress.

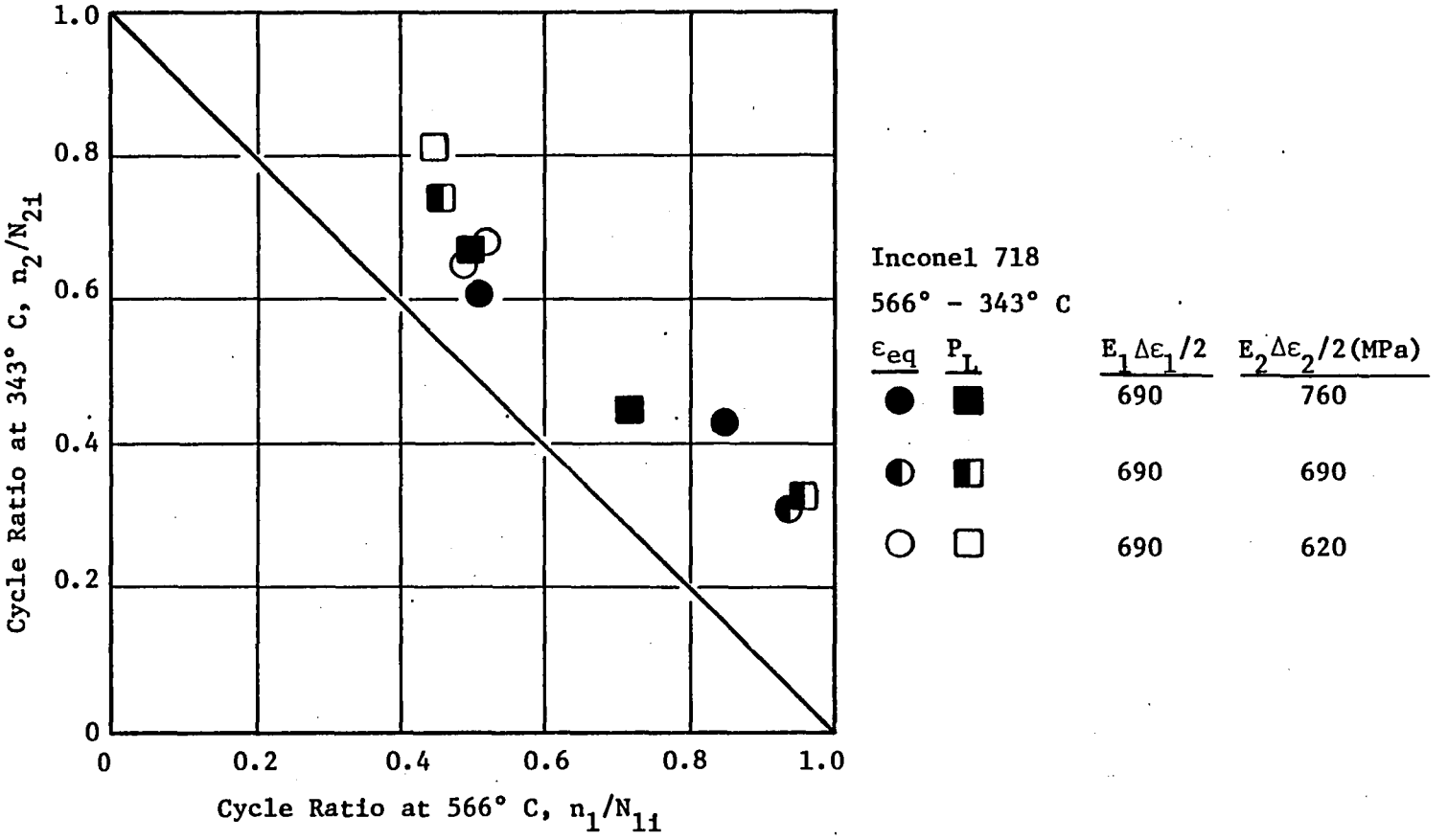

Figure E-8. Results of Two-Step Load Temperature Tests; R_ε = 0 in Both Steps.

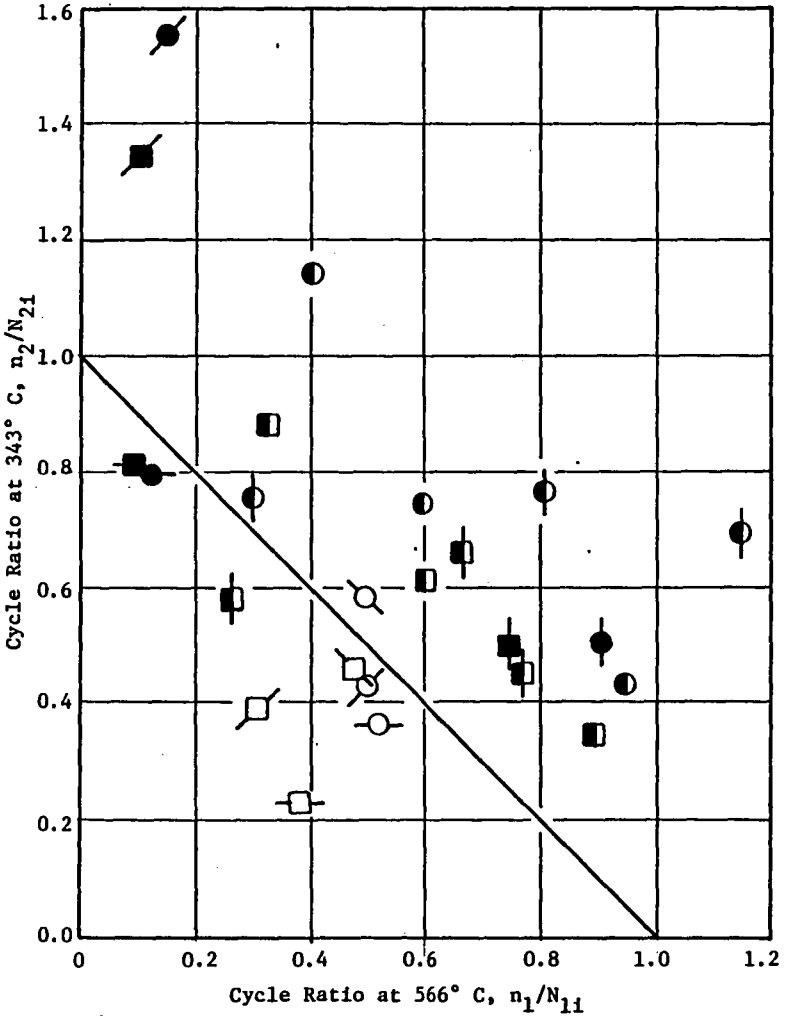

Inconel 718
566° - 343° C

ε_{eq}	P_1	MPa $E_1\Delta\varepsilon_1/2$	$E_2\Delta\varepsilon_2/2$	Approx. Second R_ε
◐	◧	690	690	0.26
◐	◧	620	620	0.22
●	■	620	690	0.23
●	■	550	900	0.11
●	■	550	965	0.09
○	□	965	550	0.55
○	□	900	550	0.47
○	□	830	620	0.43

Figure E-9. Results of Two-Step Load Temperature Tests; R_ε Variable in Second Step.

It must also be remembered that these are time-independent parameters and do not attempt to account for rate effects. While these effects should be minimal at 343° C, they could conceivably be important at 566° C. The correlation ability of the mean stress parameters at this temperature suggests that the effects are either not extensive or else are being accounted for in an empirical manner. Time-dependent effects become increasingly important with increasing temperature and this point will be discussed in the next section.

Initially, it was planned to compare these test results to the predictions of the DLDR which was shown in Appendix B to be the best of the cumulative damage laws through isothermal data comparison. However, it was found that such a formal comparison was not required as the data and the theories went in opposite directions. In the DLDR, a high/low sequence is determined when the cycles to initiation in the first block, N_{1i}, are less than the cycles to initiation in the second block, N_{2i}. In such cases, it is expected that the cycle summation, i.e.,

$$\sum_{j=1}^{2} (n_j/N_{ji})$$

should be less than unity. In virtually all cases and independent of the mean stress parameter that is used, these data would be interpreted as a high/low sequence. This is because $N_{1i} < N_{2i}$, even though in some cases $\Delta\varepsilon_1 < \Delta\varepsilon_2$ (the difference in temperature is enough to cause the cycles to initiation in the two blocks to be interpreted as a high/low sequence). The only two exceptions to this trend are the two data points shown in Figure E-9 where $n_1/N_{1i} < 0.2$. In other cases, $N_{1i} \cong N_{2i}$ for which the DLDR would predict the linear Palmgren-Miner rule. These two data could be interpreted as a low/high sequence when the Leis parameter and equivalent strain approaches are used. In general, the observed sequence effect follows the expected trend for a low/high loading sequence. Thus it appears that the DLDR does not work in this case (though it would be conservative).

In summary, despite the promise shown by the two mean stress parameters in correlating the isothermal results, there remains a great deal of investigating to be done before complex damage accumulation can be predicted. Conversely, the failure of the range parameter to correlate the isothermal data indicates that the excellent damage accrual results obtained using pseudo-stress may be fortuitous. It is also clear that a great deal of damage mechanism studies would be helpful to guide the damage parameter selection process and the cumulative damage modeling efforts.

Combined Effect of Mean Stress and Time

The previous sections on mean stress and cumulative damage have taken the view that the low cycle fatigue process is essentially time independent. This approximation will hold to a greater or lesser extent depending on

the temperature, cycle rate, environment, etc. Two points, strain rate and cycle shape, need to be addressed in connection with mean stress effects. The latter topic will be addressed first as it incorporates both effects.

A brief study was conducted to indicate the potential role of the combined effects of mean stress, strain rate, and tension/compression hold times. These effects were interpreted through the Ostergren damage model (Reference 3) using Inconel 718 data at 538° and 649° C which were available in the literature (References 4 through 6). The data were fitted using linear regression to the form,

$$D = \sigma_t \, \Delta\varepsilon_p = A\nu^b \, N_f{}^c \qquad (1)$$

where σ_t is the tensile stress; $\Delta\varepsilon_p$ is the inelastic strain range; ν is the reciprocal of the cyclic time; N_f is the cycles to failure; and A, b, and c are temperature-dependent coefficients. In References 3 and 5, an effective frequency was defined which depended upon whether the hold time occurred in tension or compression. In the present work, the effective frequency was merely the reciprocal of the total cyclic time. The former definition of frequency was introduced in Reference 3 to account for potential sequence dependent effects; for materials which do not exhibit sequence effects, the total cycle time definition was deemed appropriate. Here, we adopted the simpler definition and demonstrate correlation to within about a factor of 2 (though layering was observed).

Figures E-10 through E-13 present the correlation plots for several forms of Inconel 718 obtained with the Ostergren parameter. The data covers a wide variety of waveforms, strain rates, and hold times. The vast majority of the data fall within a factor of ±2 of the perfect correlation line. The data cover only a limited range of strain ratios, R_ε, so this needs to be explored. However, the excellence of the correlation indicates the Ostergren parameter can be used to express the time dependence in low cycle fatigue.

With such analyses available, it is possible to examine the predicted influence of mean (maximum) stress in two hypothetical regimes. The first regime would be the short, cyclic range where there is substantial plasticity; in this case, the influence of a tensile hold time would tend to lower the tensile stress, but would also tend to increase the inelastic strain level through time-dependent strains. The second regime would be the long life regime wherein there is little cyclic plasticity. In this regime, one might expect that the principal manifestations of the time-dependent strains would be to lower the maximum tensile stress since the reversed plastic strain would be small. After some number of cycles, it might be assumed that the maximum tensile stress would reach a lower steady-state level once the time-dependent strains became negligibly small. In this case, the steady-state cyclic plastic strains might be the same as those without hold times, assuming no interactions.

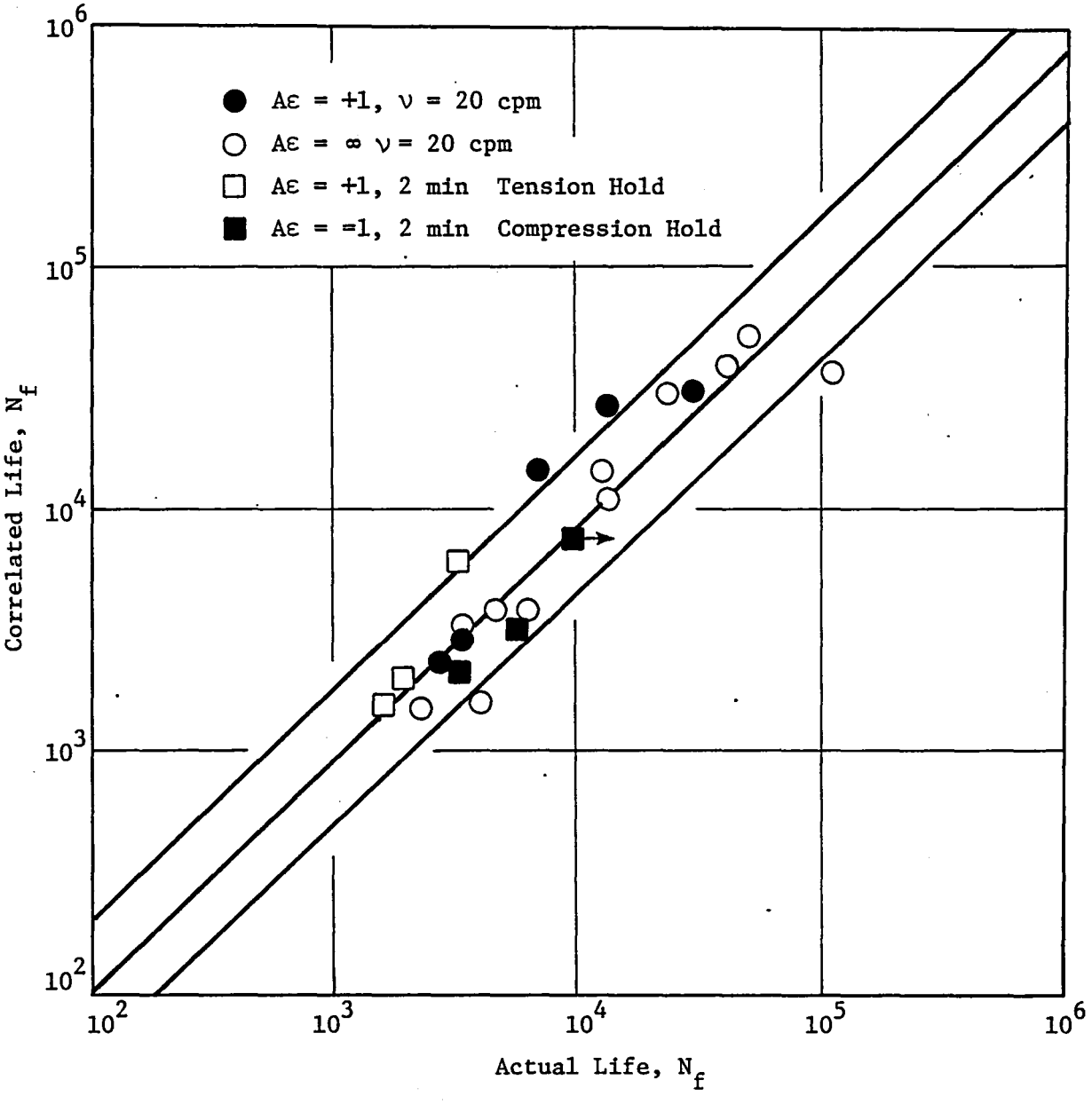

Figure E-10. Cast Inconel 718, 538° C, Reference 5.

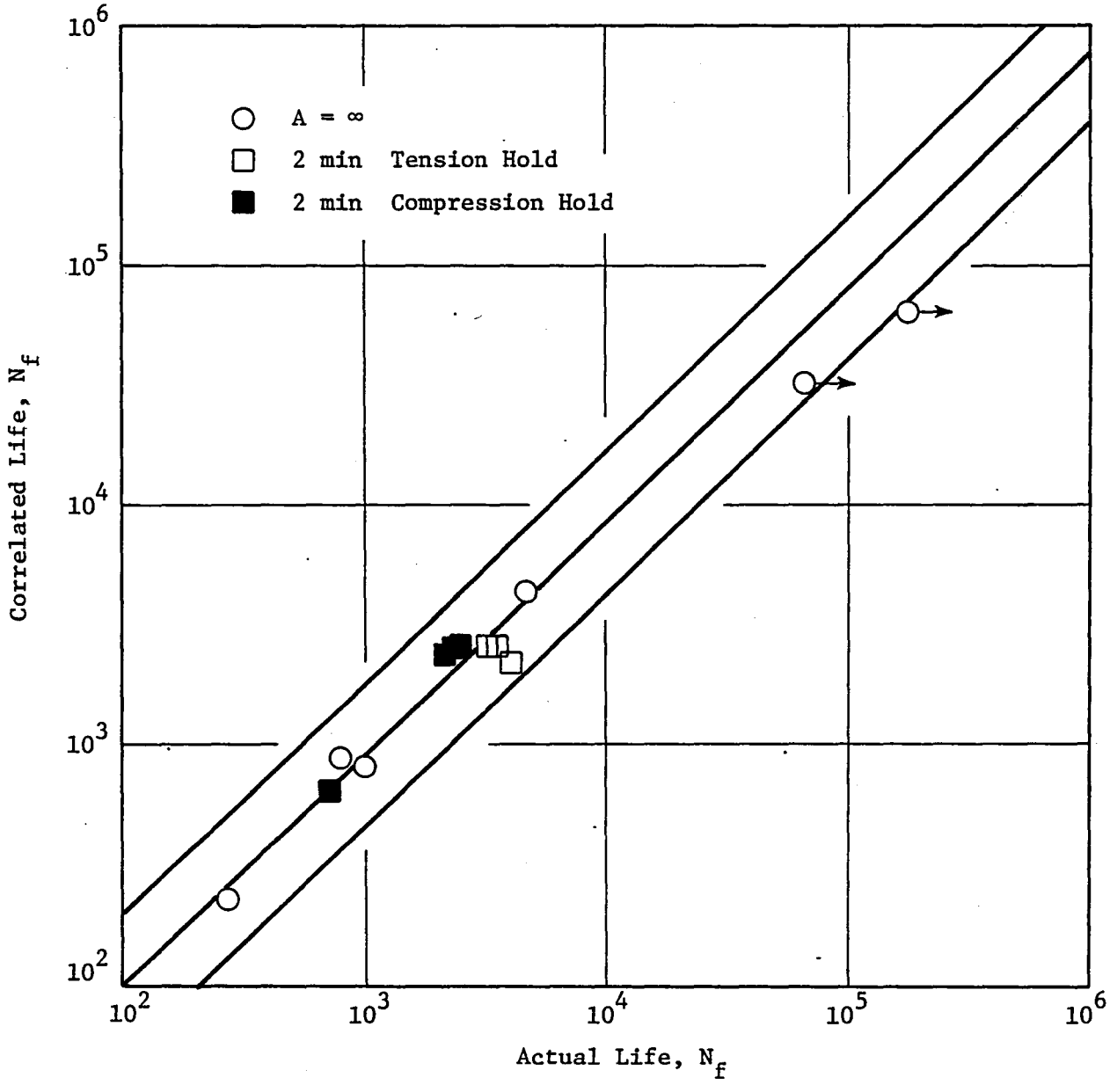

Figure E-11. Wrought Inconel 718, 538° C, Reference 5.

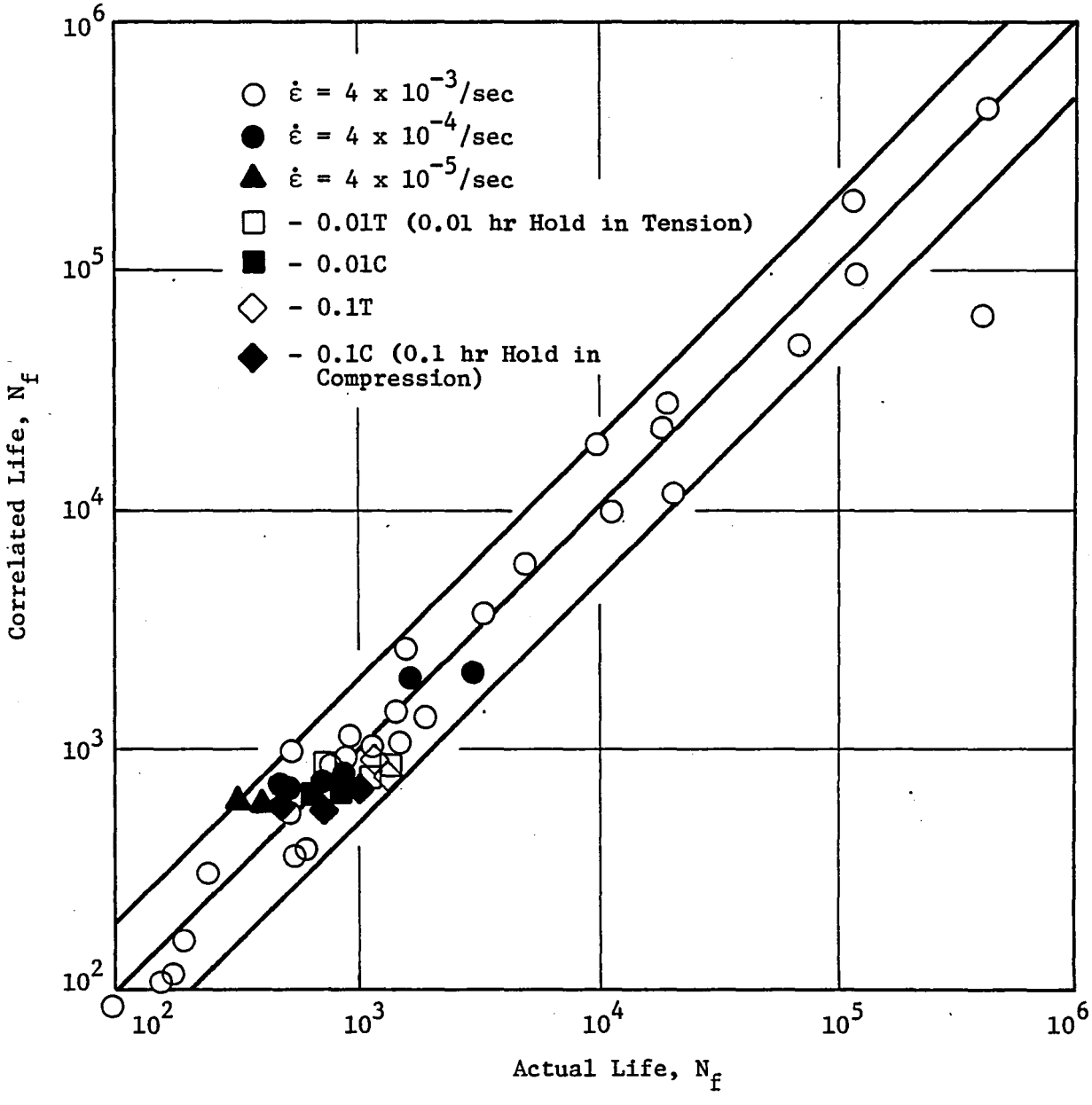

Figure E-12. Inconel 718, 538° C, Reference 4.

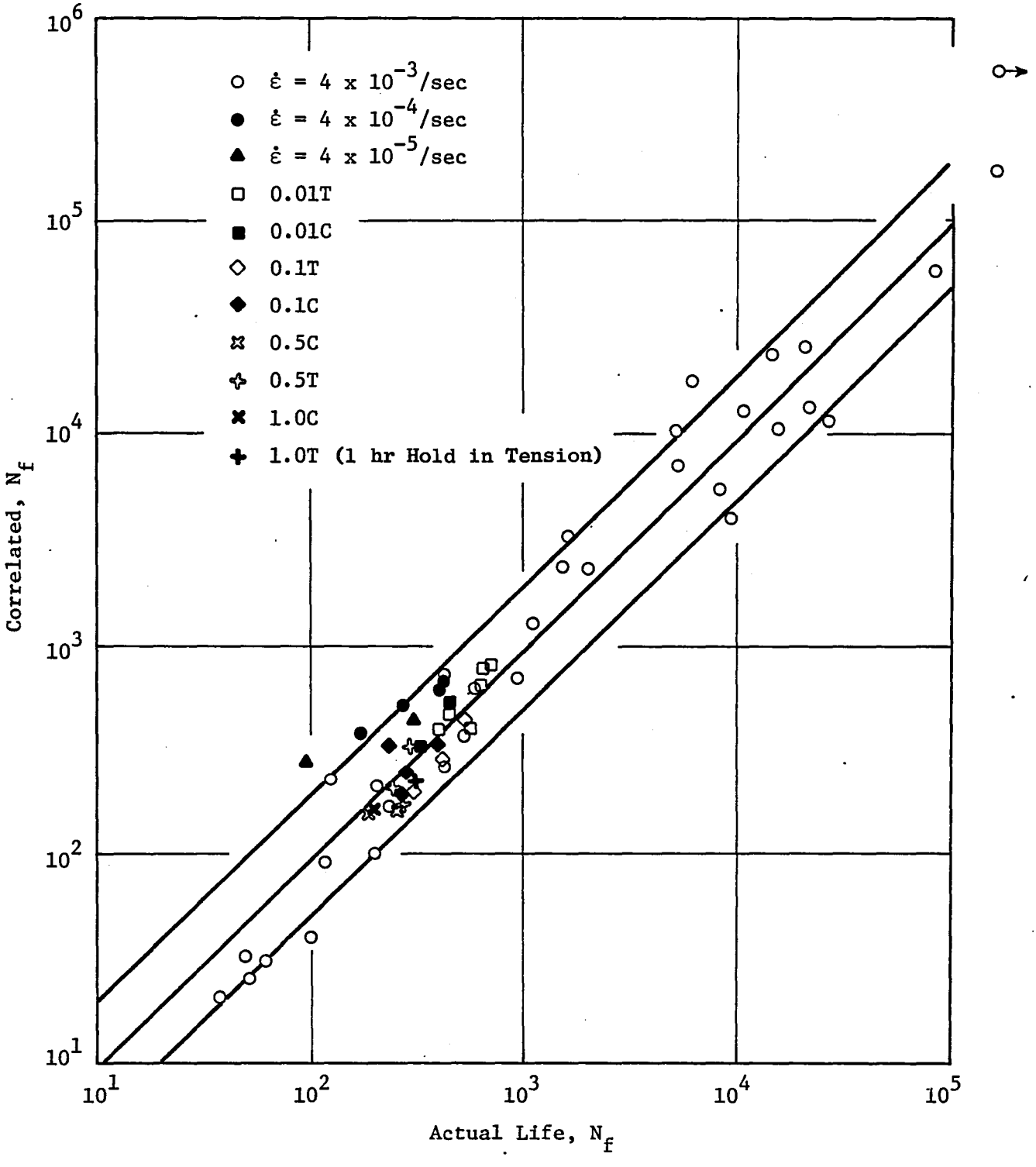

Figure E-13. Inconel 718, 649° C, Reference 4.

These regimes can be examined via the Ostergren parameter. Rearranging Equation 1, gives

$$\frac{N_f(\nu)}{N_f(\nu = 20)} = \left(\frac{20}{\nu}\right)^{b/c} \left[\frac{D(\nu)}{D(20)}\right]^{1/c} \tag{2}$$

where $N_f(\nu)$ is the cyclic life for a given cyclic period, $1/\nu$, and $D(\nu)$ is the value of $\sigma_t \Delta\epsilon_p$ for that frequency. Equation 2 is normalized by the corresponding values for a cyclic frequency of 20 cpm which is a typical laboratory testing rate. Figure E-14 shows the prediction of Equation 2 assuming that

$$\frac{D(\nu)}{D(20)} = 1.0 \tag{3}$$

Considering the case of a tensile hold time with constant strain control, this assumption is equivalent to assuming that the drop in tensile stress due to relaxation is exactly balanced by the increase in inelastic strain induced by the hold time such that Equation 3 is valid. This assumption might reflect what would happen in low cycle fatigue where there is a large portion of inelastic strain. Note that this is the typical test regime for hold time tests due to the higher costs of the longer tests.

Next, consider the case where the strain is predominantly elastic (beyond the transition fatigue life); the main effect of the hold time might be to reduce the tensile stress. Assuming that the cyclic inelastic strain range is independent of the cyclic frequency in this regime then

$$\frac{D(\nu)}{D(20)} = \frac{\sigma_t(\nu)}{\sigma_t(20)} \leq 1.0$$

Figure E-15 simulates this assumption based on Equation 2 for a tension hold time of 20 minutes. As expected, the lower the value of $\sigma_t(\nu)$, the less is the effect of the increased cyclic period. The important point is that critical hot section components are most likely designed in this regime beyond the transition lifetime where such effects might be manifested. Thus it appears that experimental work is needed in this regime to verify these results. In addition, since the magnitude of the effect that is predicted in Figure E-15 depends on the extent of tensile stress decrease induced by the hold period, accurate accounting of the time-dependent deformation response would be required in actual component analyses. This would require accurate constitutive equations. It should be noted that the predictions in Figure E-15 are for tension hold times; if the hold time were in compression, it would be expected that

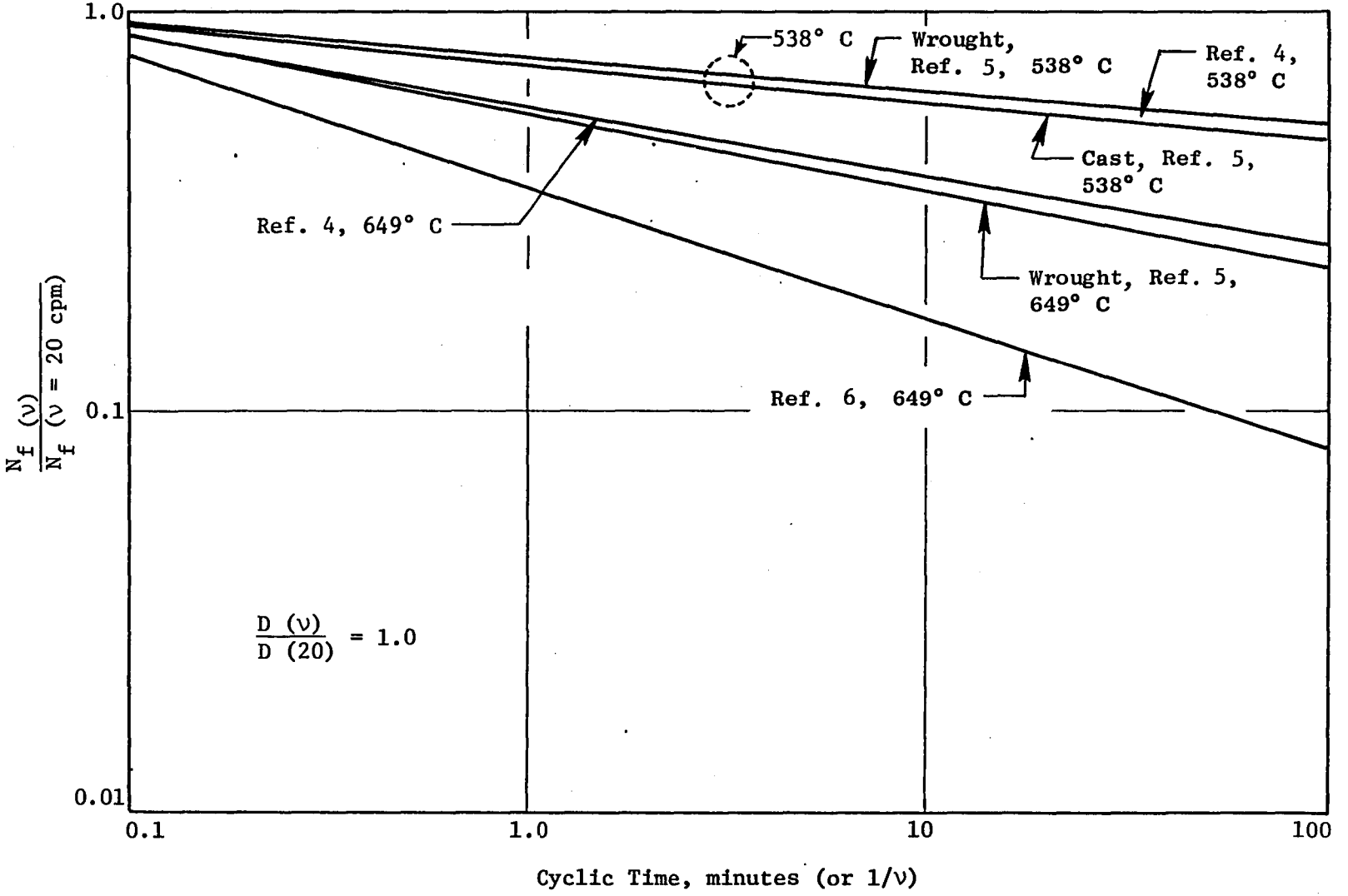

Figure E-14. Predicted Effect of Cyclic Period, Assuming That the Damage Parameter Does Not Change With Hold Time.

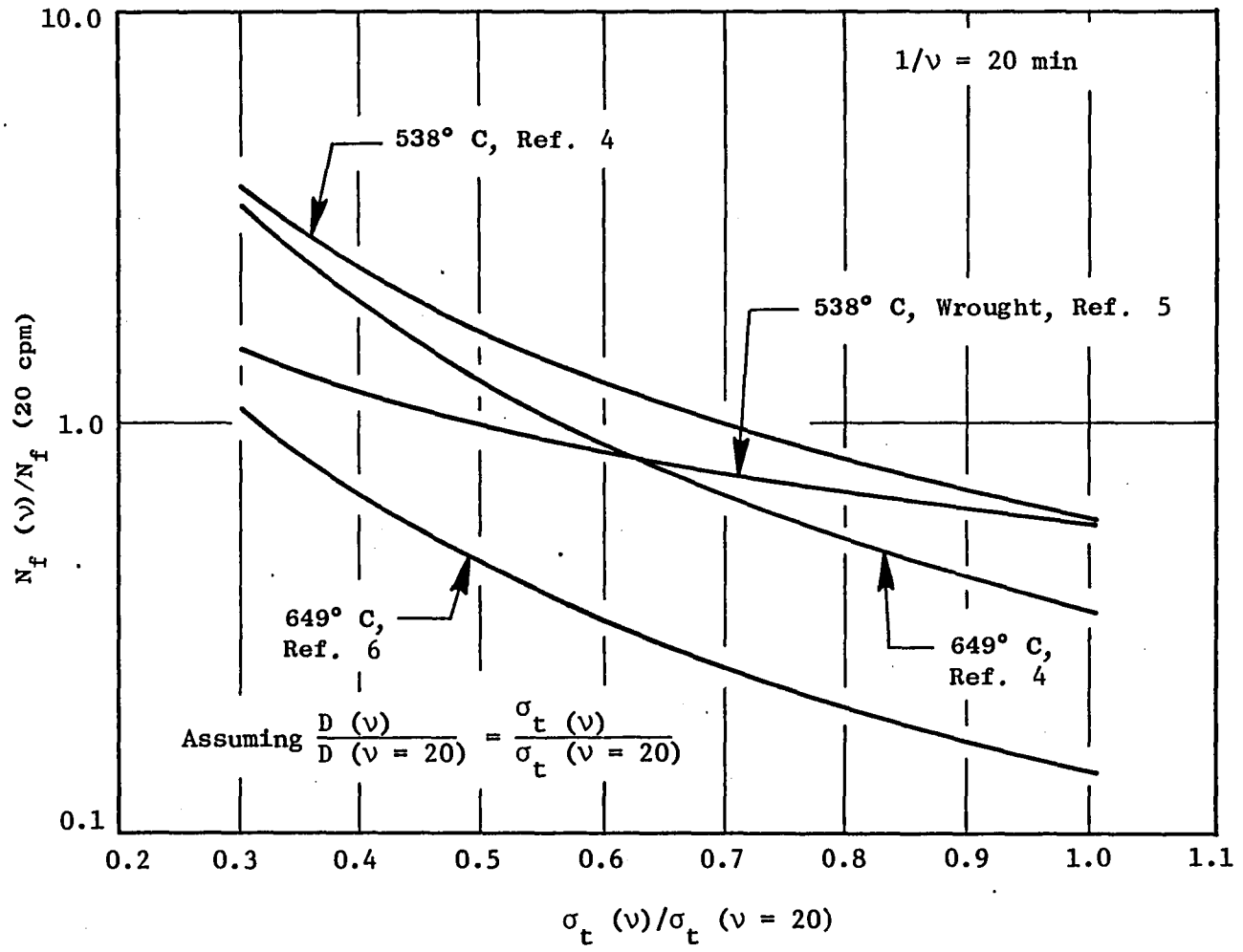

Figure E-15. Predicted Effect of Tensile Hold Time Assuming That Inelastic Strain Range is Not Changed by Increased Cyclic Period (Tension Hold Time is Assumed).

$$\frac{\sigma_t\ (\nu)}{\sigma_t\ (20)} > 1.0$$

and the effect of the maximum stress would lead to reduced life.

Application of Mean Stress Theories at High Temperature

The preceding discussion has applied a time-dependent model to nickel-base superalloy data generated at moderate temperatures. Data generated on a different superalloy, René 80, at a much higher temperature, 980° C, provides an opportunity to examine a different model. Unlike the Inconel data just discussed, the René 80 data include three R_ε ratios, ∞, 0, -1, as well as three strain rates. The high temperature at which these specimens were tested means that there are significant creep effects, with the result that the mean stress is virtually zero (±28 MPa compared to a minimum stress range of 262 MPa) for all the data. However, due to the variation in strain rate, there is a significant change in maximum stress for the same strain range. Figures E-16, E-17, and E-18 show the cyclic stress-strain curves for the three strain rates; the lines are described subsequently. Note that the data trends do not show a discernible dependence on the R ratio, but that there is substantial scatter in the data. Careful examination of these figures shows that the data tend to merge at the two higher rates at strain ranges greater than about 1%; this observation is confounded by the scatter, however.

The reason for the stress range scatter is unclear. However, it is noted that René 80 is a cast alloy with relatively large grains. The effect of these large grains was such that Coffin found a marked variation in the diametral strain range in testing hourglass specimens, depending upon the angular location of the extensometer at the minimum section. It might be that the stress range scatter is a manifestation of the large grain nature of René 80. In any event, it seems clear that such large scatter in stress range could present problems for maximum stress crack initiation models. On the other hand, if such models accurately reflect the materials innate capabilities, then it could be argued that maximum stress models should reduce the scatter when compared to other models.

The analysis of these data considered the theories of Leis, Ostergren, Walker, Cruse and Meyer, and Coffin. Coffin's frequency modified (FM) approach was included as an alternative interpretation of these data, as it included no stress level measure (e.g., mean or maximum stress) and utilized only strain range; however, it did consider a rate-dependent effect through the use of frequency. Since the other theories have been considered in other sections, only Coffin's theory is detailed here.

The FM equations are given by

$$\Delta\varepsilon = \frac{A'}{E} N_i^{-\beta'} \nu^{K_1'} + C_2 N_i^{-\beta_\nu \beta(1-K)}, \qquad (4)$$

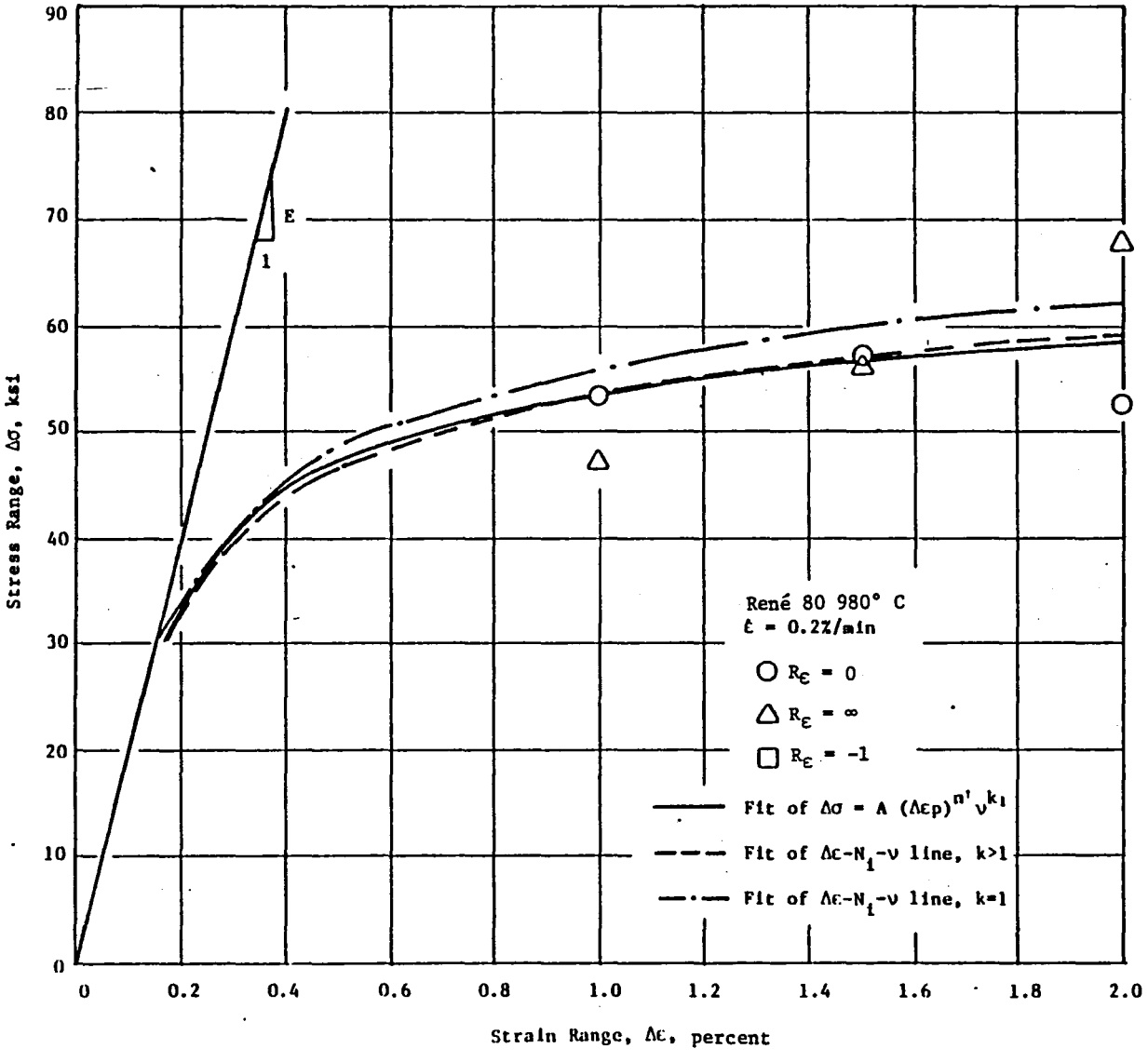

Figure E-16. Cyclic Stress/Strain Curves for a Strain Rate of $\dot{\varepsilon}$ = 0.2%/Minute.

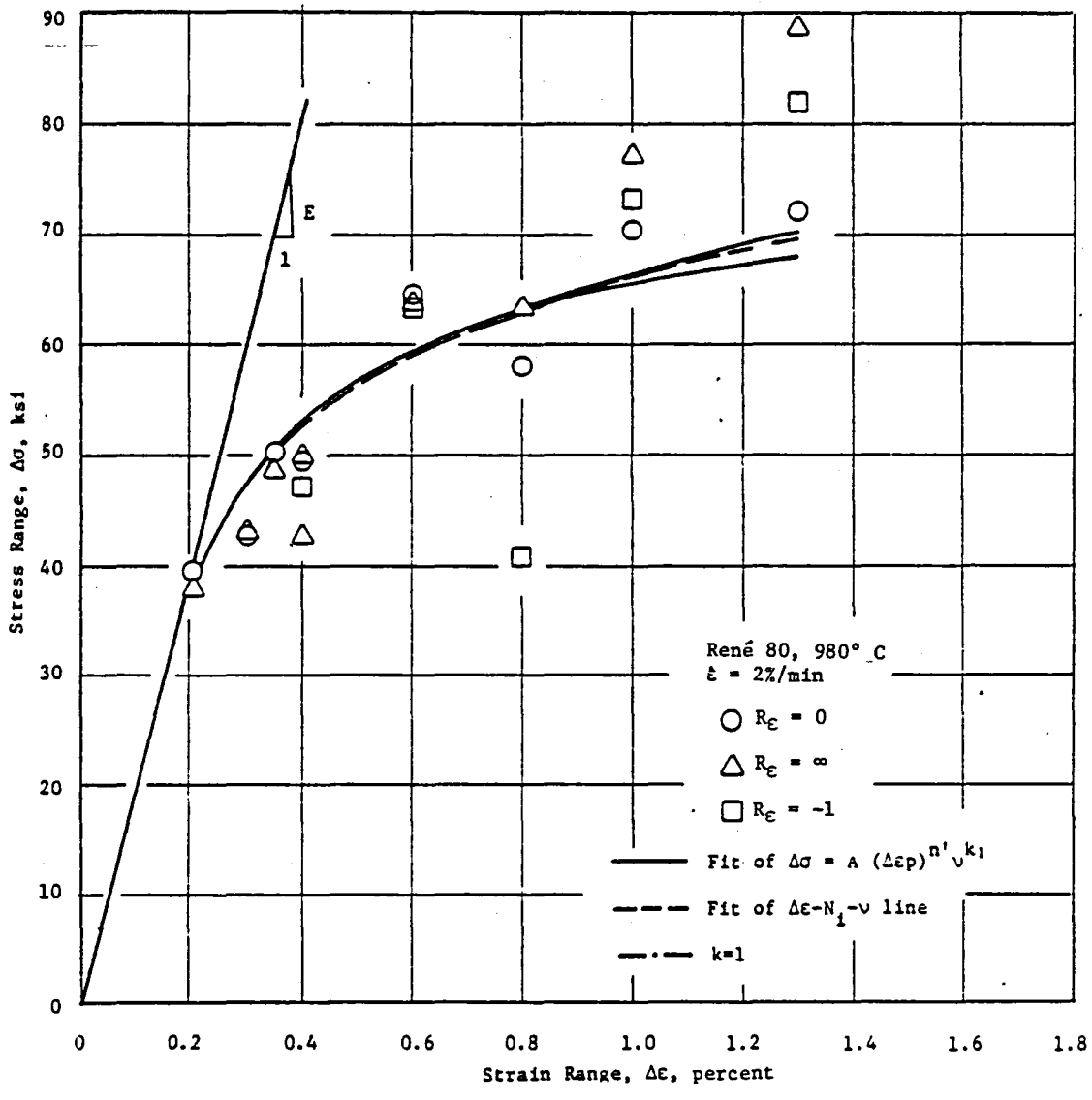

Figure E-17. Cyclic Stress/Strain Curves for a Strain Rate of $\dot{\varepsilon}$ = 2%/Minute.

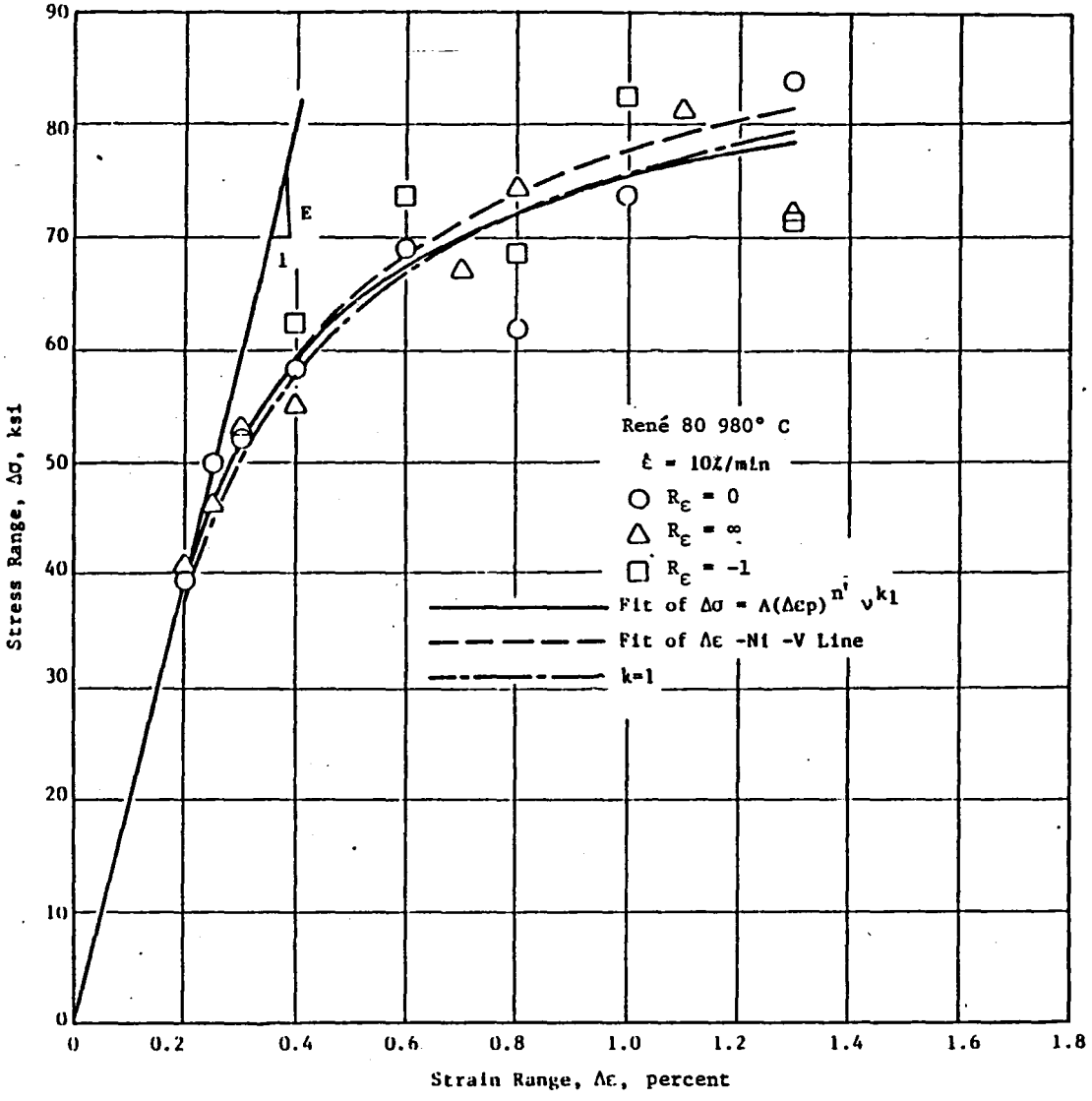

Figure E-18. Cyclic Stress/Strain Curves for a Strain Rate of $\dot{\varepsilon}$ = 10%/Minute.

where E is Young's modulus and A', β', K_1', C_2, β, and K are independent constants from which all subsequent equations can be derived. The first term on the right-hand side of Equation 4 represents the elastic strain range ($\Delta\varepsilon_e = \Delta\sigma/E$), while the second term represents the plastic strain range ($\Delta\varepsilon_p$). Eliminating the cycles to crack initiation, N_i, between these two terms, an equation for the cyclic stress-strain curve appears:

$$\Delta\sigma = A(\Delta\varepsilon_p)^{n'\nu K_1}, \qquad (5)$$

where

$$n' = \beta'/\beta, \quad A' = A\,C_2^{n'}, \text{ and } K_1 = K_1' + \beta'(K-1).$$

Equation 5 was fitted to all of the Rene 80 980° C (1800° F) data by using a standard linear regression technique. The results were as shown in Figure E-19 where the line was obtained from the resulting regression analysis with A = 486 MPa (70.4 ksi), n' = 0.183, and K_1 = 0.0951. As was observed, there appeared to be considerable scatter in the stress response when plotted on the basis of frequency. The cyclic stress-strain curve defined by the above-noted range quantities was assumed not to be a function of the R_ε ratio. The solid lines in Figures E-16 through E-18 were generated using this fit to describe the plastic strain-stress-frequency relationship.

The rest of the constants for Equation 4 were determined by linearly regressing the $\Delta\varepsilon_p$ line as a function of ν and N_i. These data were fitted several ways, as summarized in Table E-I. Many different approaches were used in this regression analysis because K was greater than unity. Although this was consistent with the results presented by Coffin for Rene 80 at 870° C (1600° F), it indicated a reverse frequency effect such that the predicted life was longer as frequency was reduced at short lives (Figures E-20 and E-21). Since the resulting elastic lines were as expected, the trend reversed at longer lives such that raising the frequency increased the life. These results were found for the total data set, for the $R_\varepsilon = 0$ data, and for the $R_\varepsilon = \infty$ data. The $R_\varepsilon = -1$ data showed $K < 1$, but were based on fewer data, and only the two higher strain rates were used in the experiments. Consequently, two sets of analyses were used: (1) K was assumed to be unity and the data were fit this way; and (2) K was allowed to be greater than unity. Both analyses were based on all the data and the results are given in Table E-I.

As an alternative to this approach, linear regression can be applied directly to the elastic strain range-frequency-Ni data to determine the constants A', β', and K_1'. The cyclic stress-strain curve can then be predicted by combining the fits of the elastic strain and plastic strain constants as is indicated below Equation 5. The constants determined by such a regression analysis are given at the end of Table E-I; the resulting cyclic, stress-strain curves are given in Figures E-16 through E-18 by the dashed lines for $K > 1$ and $K = 1$. As is shown by the comparisons in Figures E-16 through E-18,

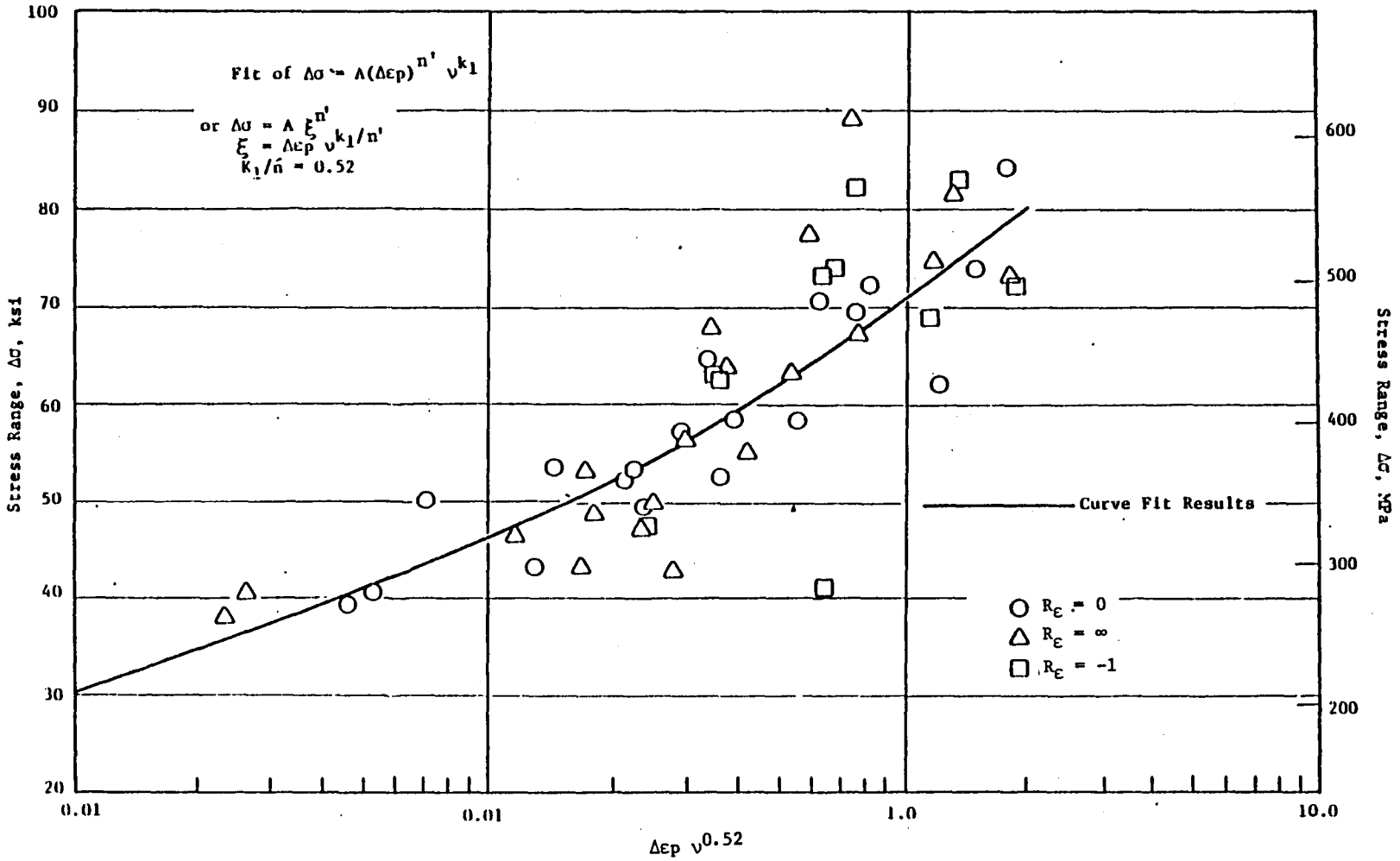

Figure E-19. Fit of Equation 5 to All of the René 80, 980° C Data Using a Standard Linear Regression Technique.

Table E-I. Results of FM Regression Analyses Fit of 980° C Rene 80 Data (ν in CPM, and ϵ in Percent).

Fit of Plastic Data

Method	C_2	β	K
$A_\epsilon = \infty$ Data Only	14.825	0.6773	0.919
$A_\epsilon = +1$ Data Only	10.878	0.604	1.156
$A_\epsilon = -1$ Data Only	12.658	0.6116	1.229
All Data	12.17	0.614	1.169
All Data (K = 1)	15.34	0.666	1.0

Resulting Elastic Fit

Method	A' (MPa/ksi)	β'	K_1'
All Data	767.5/111.2	0.112	0.0761
All Data (K = 1)	800.63/116.03	0.122	0.0951

Fit of Elastic Line

A' (MPa/ksi)	β'	K_1'
837.2/121.32	0.27	0.0836

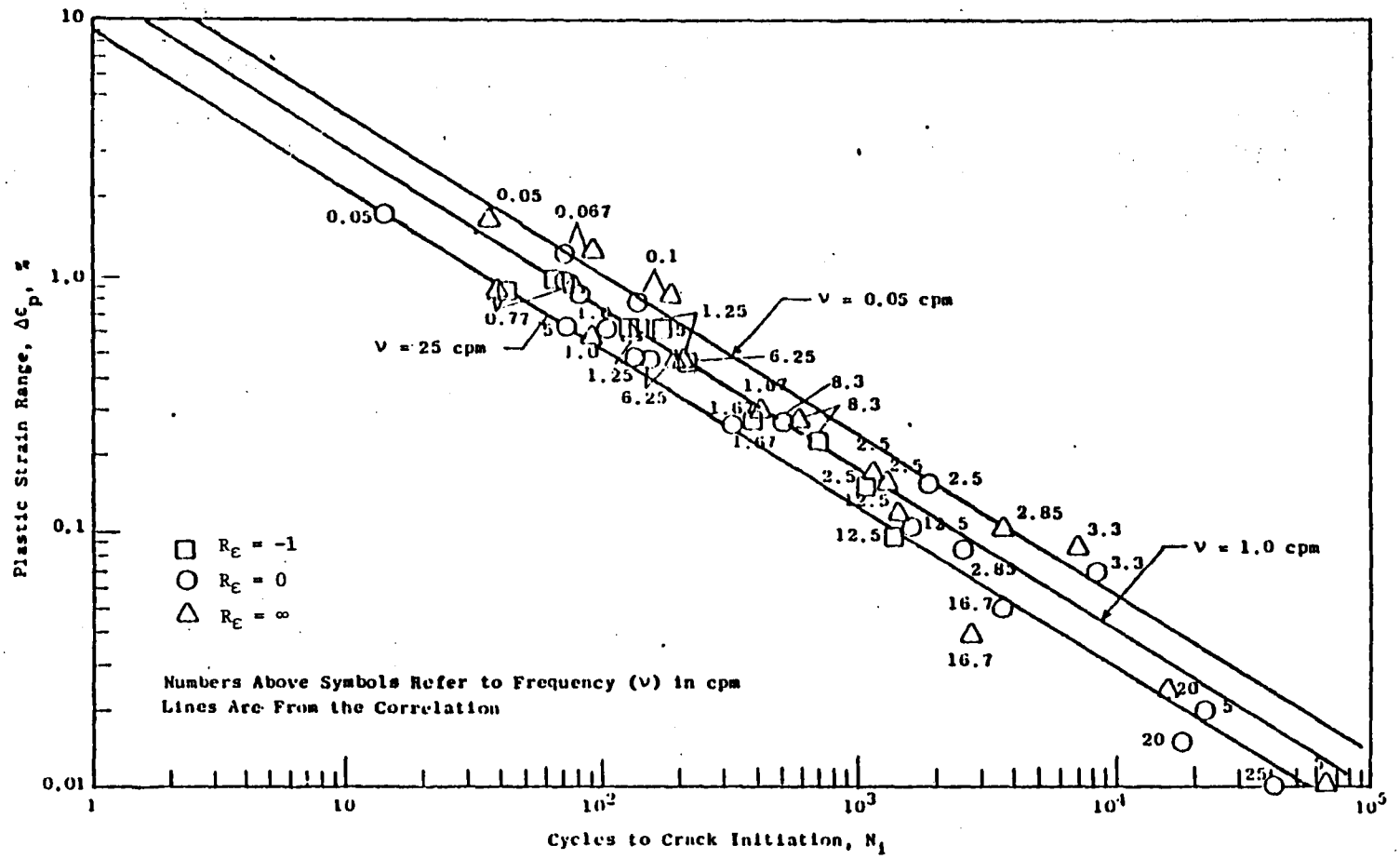

Figure E-20. Full FM Method - René 80, 980° C.

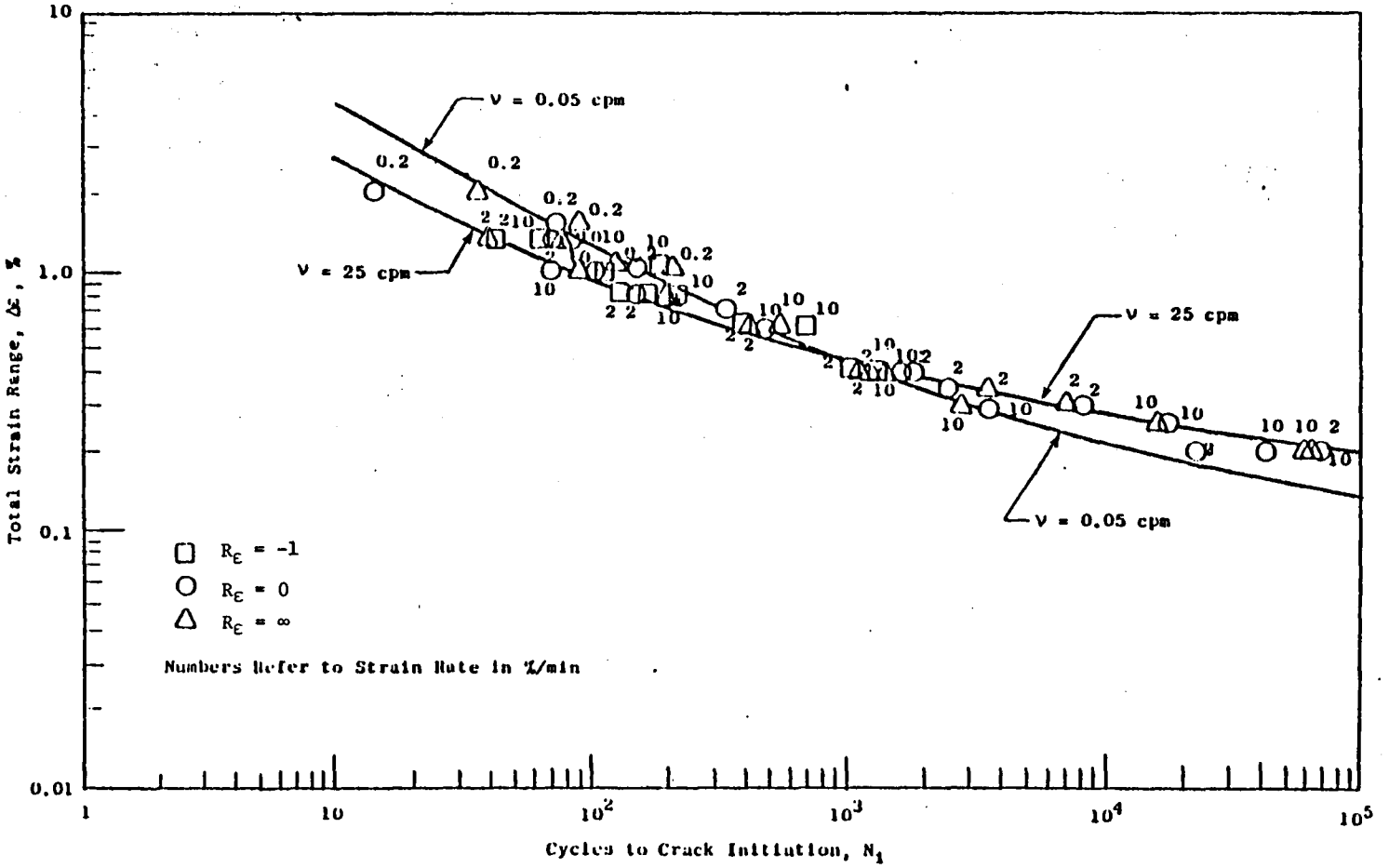

Figure E-21. Full FM Method - René 80, 980° C.

there is little difference in these various methods of deriving the cyclic stress-strain curve, particularly when one considers the data scatter. However, comparing the average error of the subsequent fatigue life predictions shows that there is about 10% difference between the average life predictions yielded by the various fitting methods.

Table E-II compares the various life correlating schemes on the basis of an average error measure, E, and a measure of the standard deviation, σ, which are more fully described in the Appendix on mean stress,

$$E^2 = \frac{1}{n} \sum_{j=1}^{n} (1-\beta_j)^2,$$

$$\sigma^2 = \frac{1}{n} \sum_{j=1}^{n} [\ell n\ \beta_j]^2,$$

where

$$\beta_j = \frac{N_i\ (\text{Pred.})_j}{N_i\ (\text{Act.})_j},$$

and $N_i\ (\text{Pred.})_j$ and $N_i\ (\text{Act.})_j$ are the predicted and actual cycles to crack initiation for the jth data point, respectively. In the last column of this table, a factor is given which would be applied to the average life to predict the -3 standard deviation life assuming that the data are described by a log-normal distribution.

Several points can be made through a discussion of these results. In Appendix C, it is shown that both E and σ should be close in numerical value (omitting the factor of 100% which is applied to E) if the data are such that $\ell n\beta$ is approximated by the first term of Taylor's series expansion. This is the case for errors of up to about 20%. If the values of E and σ are different, then a certain skewness in the data can be inferred depending on which measure is larger. Comparing the numerical values of E and σ in Table E-II, it is seen that near equality is observed in several cases, but that the Leis parameter shows a gross discrepancy of E = 76.9% compared to σ = 0.497. In this case, the reason for this difference was one data point where N_i(Pred.)/ N_i(Act.) = 4.8. If this one data point is removed from the data set, then the value of E drops by about 50% whereas the σ value changes by only about 10% (note that there are 50 data points). Thus on the surface of it, it appears that this one data point is weighted too heavily in the E value. However, as shown in Figure E-22, there are several points which are significant on either side of the determined trend lines by various order polynomials (particularly when compared to the plot of strain range in Figure E-21).

Table E-II. Theory Comparison for René 80 Data at 980° C.

Theory	E %	σ	$e^{-3\sigma}$
Leis	110.47 (76.9)(1)	(0.497)(1)	(0.225)
ε eq.	46.13 (37.78)(1)	(0.3327)(1)	(0.368)
Cruse and Meyer	53.23	0.521	(0.209)
Ostergren	53.85	0.407	(0.294)
Coffin (K = 1)	50.07 (40.26)(2)	0.419 (0.381)(2)	0.285 (0.319)
Coffin (K > 1)	54.3 (44.32)(2)	0.411 (0.372)(2)	0.291 (0.327)
Strain Range	48.3 (37.78)(1)	(0.3327)(1)	(0.368)

(1)Error is defined by a regression curve fit of the form

$$\ln N_i = \sum_{i=1}^{P} a_i \, x^{i-1}$$

where x is a function of one of the various parameters. The first number in the table assumes that x is just the parameter, while the number in parentheses corresponds to the function of the parameter being logarithmic.

(2)The first number corresponds to fitting the cyclic stress strain curve first, while the number in parentheses corresponds to regressing the elastic strain-frequency-N_i line.

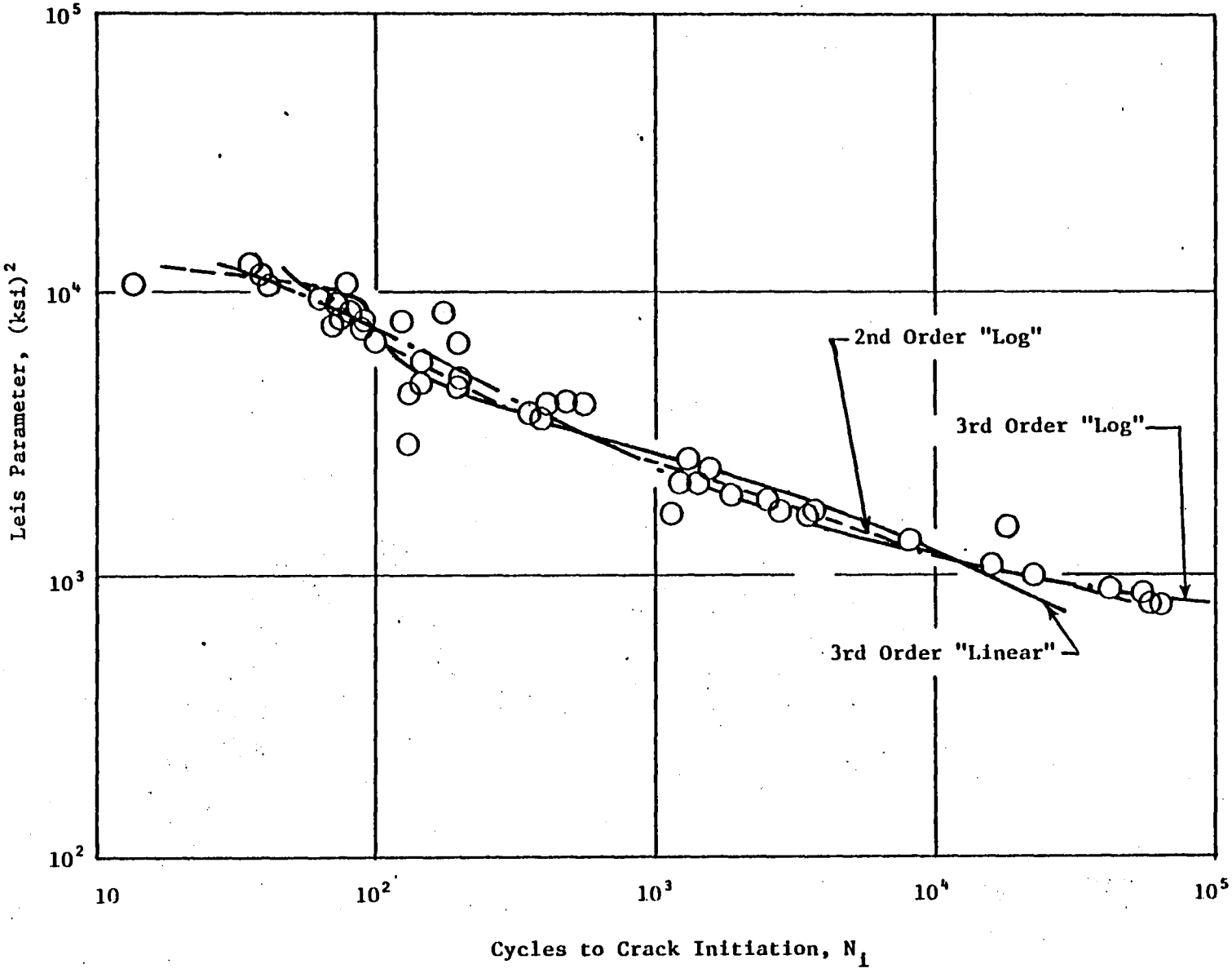

Figure E-22. René 80, 980° C Data Correlation by the Leis Parameter.

Recalling that the Leis parameter is the product of a stress value multiplied by strain range, it appears that the reason for the increased scatter in this case is due to the scatter in the stress range as is found in Figures E-16 through E-18. The fact that the Leis model does not improve the correlation compared to strain range could imply that stress measures may not be a major consideration in model construction for this alloy.

Nevertheless, it is observed that the Ostergren parameter (which uses the product of maximum stress and plastic strain range in combination with cyclic frequency) does a significantly better job in correlating the data. On the basis of the σ measure, it is comparable with the FM approach which is the best of the more exotic models. Since the Leis model showed promise in the Inconel 718 data comparisons, it seems clear that the most viable method of correlating fatigue data will depend on material as well as temperature and other test parameters. Note that in Table E-II, strain range (or, as it turns out, equivalent strain) is the best parameter in this data comparison. However, as shown in the previous section, approaches such as Ostergren or the FM (as well as many other time-dependent methods) should be capable of predicting hold time effects. Thus there is conjecture that had hold time tests been included in this data set these data would have been better correlated by one of these methods than by strain range alone. Nevertheless, it would appear that while more confidence exists in extrapolating these results to other time-dependent models, it also appears that the standard deviation could be affected by the scatter in the stress behavior in this alloy. behavior in this alloy.

Application of a Mean Stress Theory to a Thermal-Mechanical Fatigue Problem

It should be noted that all of the comparisons of mean stress theories with data discussed thus far, whether high temperature or low temperature, with or without hold times, were isothermal. To be applicable to hot section components of aircraft gas turbine engines, such mean stress theories must offer correlative ability to components which undergo simultaneous variations in temperature and strain in a thermal-mechanical fatigue (TMF) experiment. In such uniaxial TMF cycles, the sense of the mean stress depends upon the variation in temperature and strain as functions of time employed in a particular experiment. Essentially, for a given strain and strain history, the stress level which will satisfy these strain conditions will depend upon the temperature. For instance, in a so-called in-phase cycle, the temperature and strain reach their maximum value at the same time. This is illustrated in Figure E-23(a) wherein a negative mean stress is shown. Conversely, when the phasing of the temperature and strain are reversed (a so-called out-of-phase cycle), the mean stress becomes tensile as shown schematically in Figure E-23(b). The figure shows only possible results; the exact shape of the hysteresis hoop will depend upon material, maximum temperature, temperature range, and the phasing of strain and temperature as primary variables. In any event, it seems clear that the sense of the mean stress will depend upon the phasing of

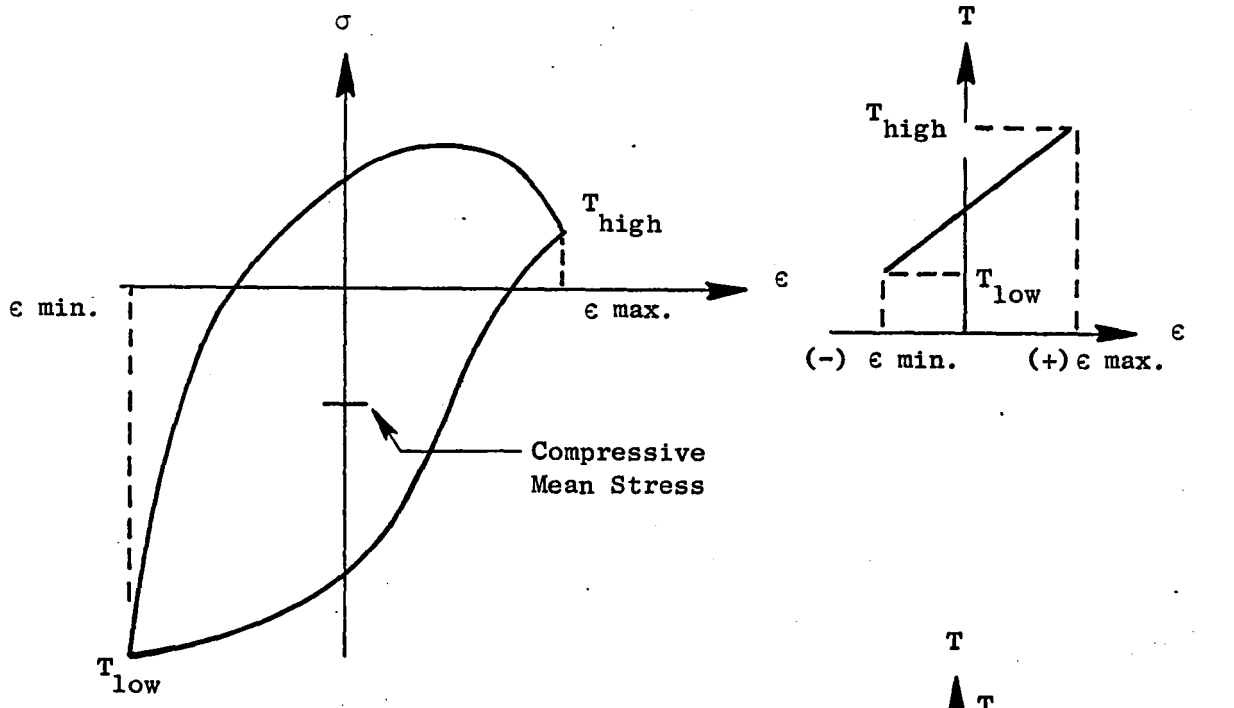

(a) In-Phase TMF Hysteresis Loop

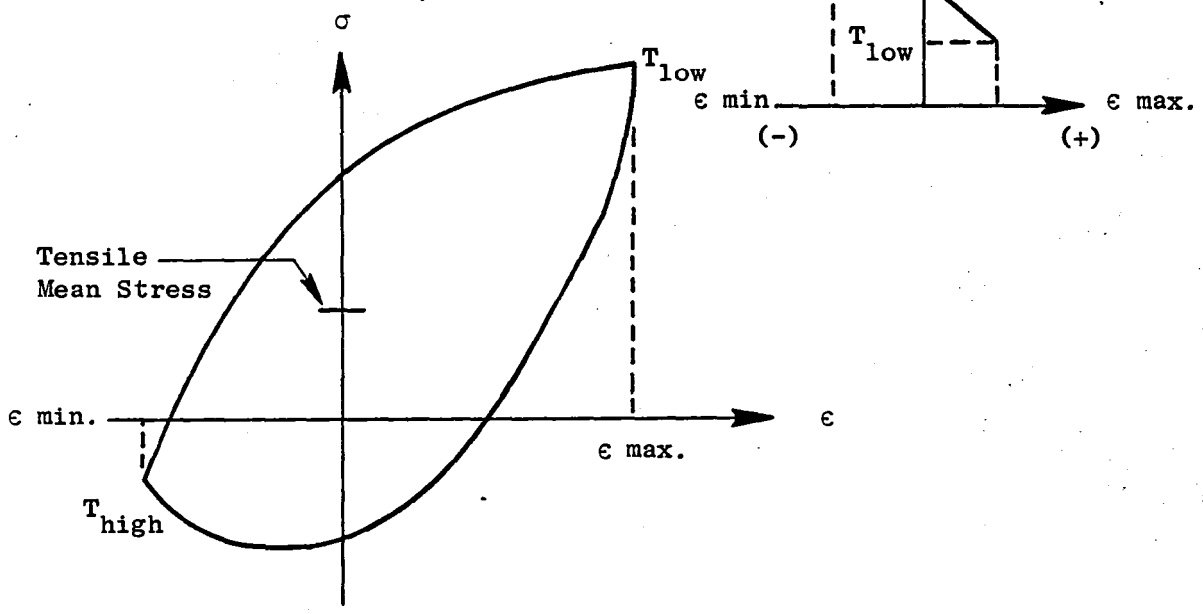

(b) Out-of-Phase TMF Hysteresis Loop

Figure E-23. Schematic Illustration of Loop Shapes Under Two TMF Cycles.

the temperature and strain. An essential question for mean stress theories which are based on isothermal data consolidation is how can they be successfully applied in TMF where the inherent strength of the material changes (with temperature) throughout the cycle. One example is briefly discussed below (Reference 7).

The temperature and strain phasing of typical fatigue critical location in hot path components is normally out-of-phase. One experimental example which models the strain-temperature-time profile of the critical region of a turbine blade tip is described in Figures E-24 and E-25. Note that a substantial positive mean stress is developed. In Reference 7, the fatigue life of this blade tip region was predicted by several schemes; one was the Smith-Watson-Topper (SWT) mean stress model described in Appendix C. This approach was based on the results of Jaske (Reference 8) who showed that for AISI 1010 steel his TMF data correlated with the SWT approach by using isothermal data at the maximum temperature of the TMF cycle. The SWT parameter is given as

$$P = E\sigma_{max}\Delta\varepsilon \qquad (6)$$

Several sets of René 80 data were analyzed (including the 980° C data discussed in the previous section) in this manner giving the results that are shown in Figure E-26. The data at 980° C (1800° F) collapse reasonably well considering the scatter in stress response for René 80 at this temperature. Note, too, that the parameter is a strong function of temperature, although the 1100° C (2000° F) data agree reasonably well with the 980° C data.

Using this approach to analyze the blade tip required a definition of the modulus. Using the one at 980° C (1800° F) (the lower the temperature the higher is the value of P), the number of predicted cycles to failure for the TMF cycle described in Figures E-24 and E-25 was approximately 225 cycles based on the 980° C data. None of the test specimens in Reference 7 were tested to failure; however, the longest tested specimen had 135 cycles and showed coating cracking when examined with a fluorescent penetrant. The factory test experience of this blade tip region was that 3.8 mm long cracks were found at the inspection interval of 3000 equivalent cycles.

Note that all of the variables (E, σ_{max}, and $\Delta\varepsilon$) in Equation 6 increase in value as temperature decreases. That is, for example, the fatigue resistance to a given strain range, $\Delta\varepsilon$, increases as temperature decreases. Also note that the TMF data in Figure E-26 do not necessarily agree with the maximum isothermal temperature. Indeed, if a lower temperature isothermal curve is used, the predicted life is greater than 1000 cycles for the blade tip region. Ideally, all the data would fall on one curve, thereby removing any ambiguity. This particular example used only one mean stress theory (and apparently better isothermal theories for this class of alloys were discussed elsewhere in this report) which was developed for low temperature applications; it incorporates no measure of elevated temperature damage (as does Ostergren's method). It is clear that additional work is required to evaluate the utlity of isothermal mean stress theories for predicting TMF conditions.

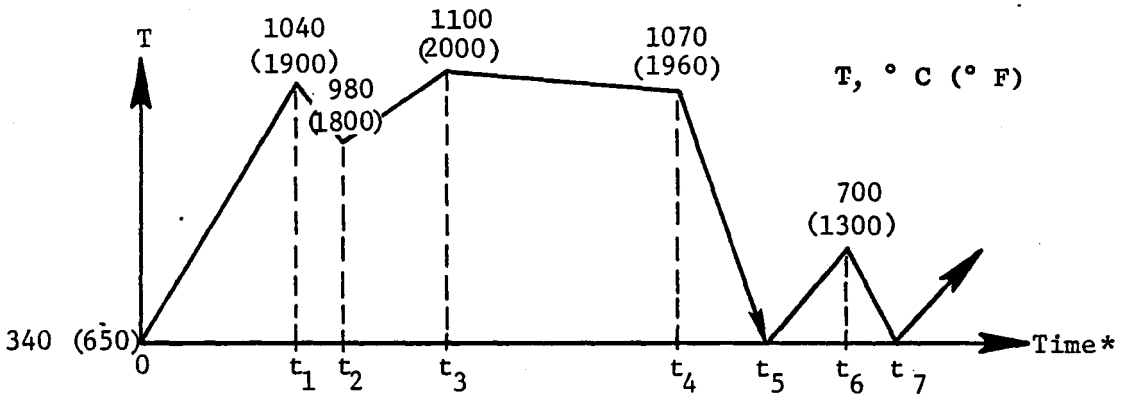

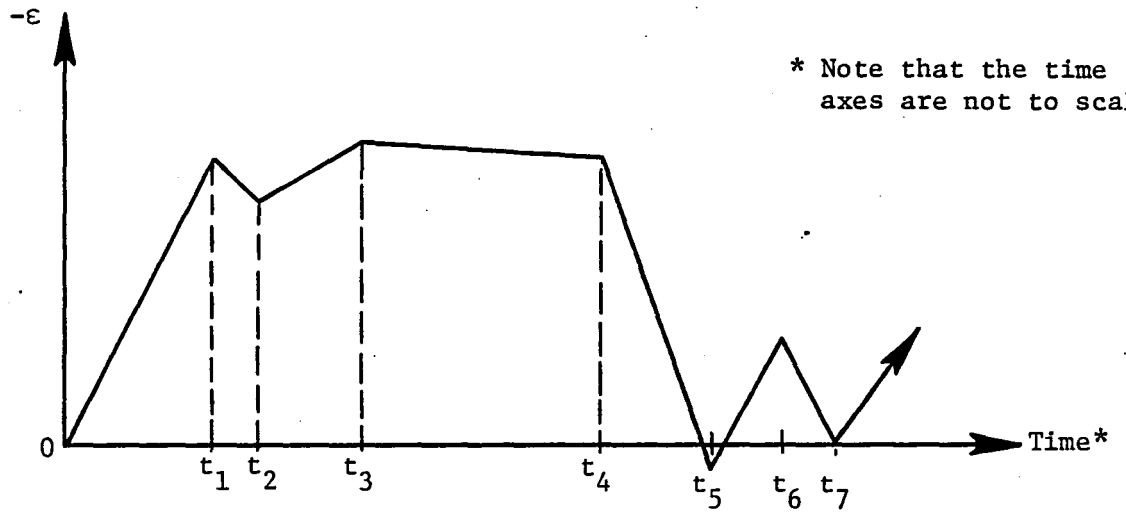

Point	Blade Time/Test Time (sec)	Blade Strain/Test Strain (%)
1	6.7/75	-0.285/-0.33
2	6.9/84	-0.255/-0.295
3	45/126	-0.293/-0.333
4	200/327	-0.28 /-0.32
5	203.5/672	+0.025/+0.02
6	220/891	-0.06 /-0.07
7	226/1116 (18.6 min)	0/0

Figure E-24. Schematic of the Imposed Temperature and Strain History for Test I.

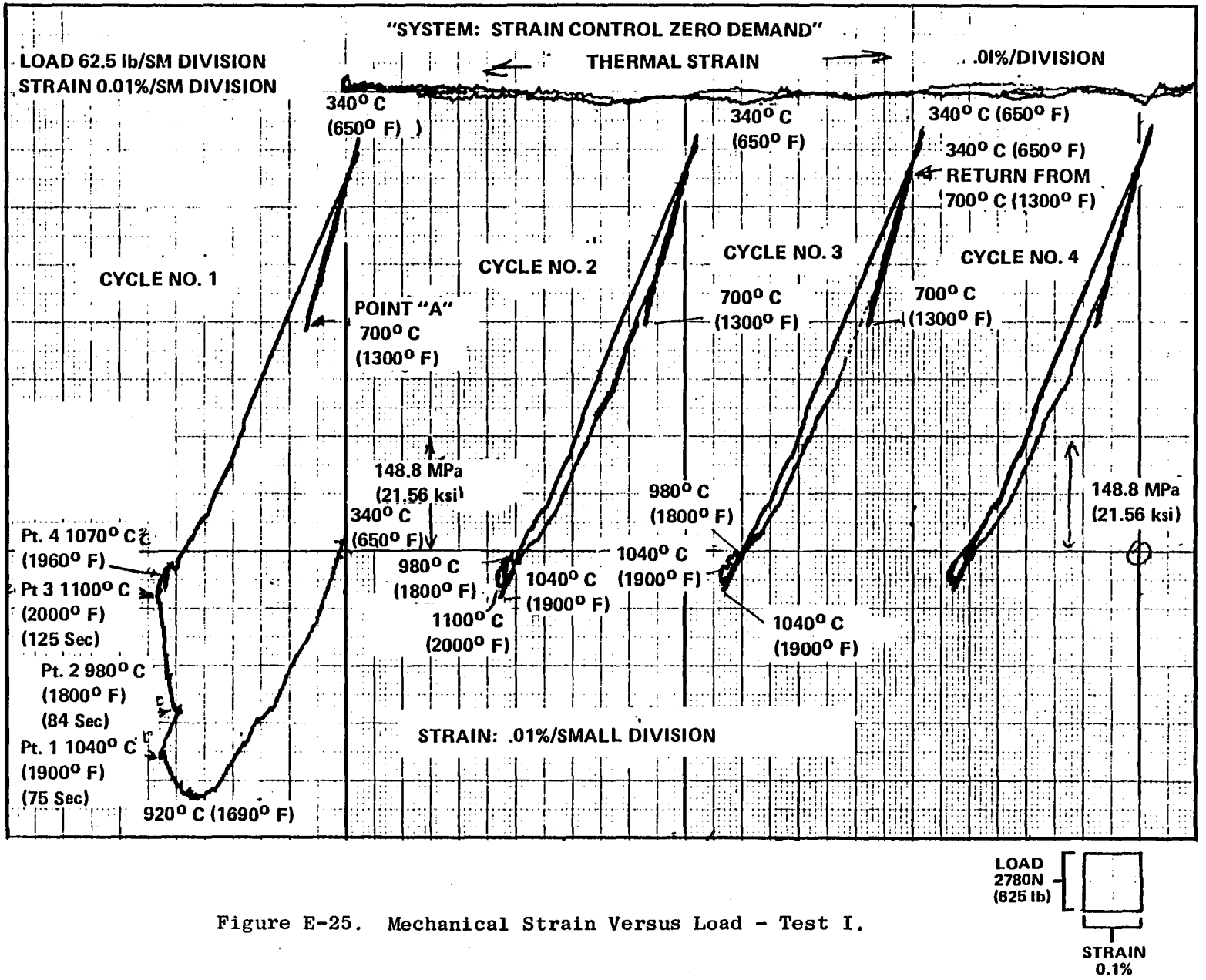

Figure E-25. Mechanical Strain Versus Load - Test I.

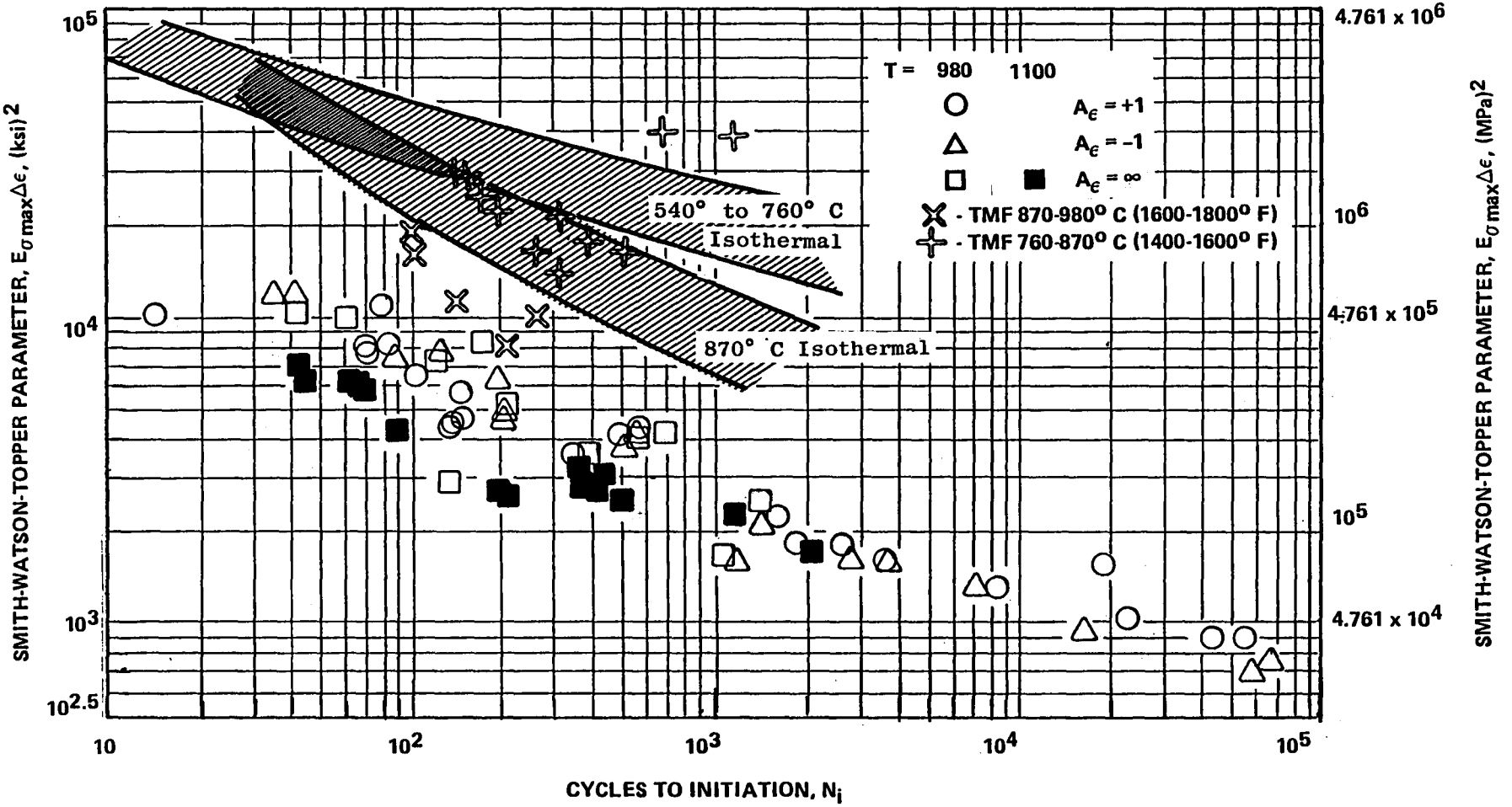

Figure E-26. SWT Analysis - René 80.

APPENDIX E - REFERENCES

1. Walker, K., "The Effect of Stress Ratio During Crack Propagation and Fatigue for 2024-T3 and 7075-T6 Aluminum," Effects of Environment and Complex Load History on Farigue Life, ASTM STP 462, ASTM, 1970, pp. 1-14.

2. Cook, T.S., "Cyclic Stress Strain Behavior of Inconel 718," Mechanical Testing for Deformation Model Development, ASTM STP 765, 1982, pp. 269-283.

3. Ostergren, W.J., "Correlation of Hold Time Effects in Elevated Temperature Low Cycle Fatigue Using a Frequency Modified Damage Function," 1976 ASME-MPC Symposium on Creep-Fatigue Interaction, MPC-3, December 1976, pp. 179-202.

4. Brinkman, C.R. and Korth, G.W., "Strain Fatigue and Tensile Behavior of Inconel 718 from Room Temperature to 650° C," J. Testing and Evaluation, JTEVA, Vol. 2, No. 4 (July 1974) pp. 249-259.

5. Embley, G.T., "Low Cycle Fatigue Behavior of Wrought and Cast Alloy 718," Report No. 80 GTD-045, Class I, General Electric Co., Schenectady, N.Y., August 4, 1980.

6. Shahani, V. and Popp, H.G., "Evaluation of Cyclic Behavior of Aircraft Turbine Disk Alloys," National Aeronautics and Space Administration, NASA CR-159433, June 1978.

7. McKnight, R.L., Laflen, J.H., and Spamer, G.T., "Turbine Blade Tip Durability Analysis," NASA CR-164268, February 1981.

8. Jaske, C.E., "Thermal-Mechanical Low-Cycle Fatigue of AISI 1010 Steel," Thermal Fatigue of Materials and Components, ASTM STP 612, D.A. Spera and D.F. Mowbray (Editors), ASTM, 1976, pp. 170-198.

End of Document